

Appendix C – Stress Intensity Factor Equations and Tables

Sections in this Appendix:

- Introduction
- C1: Through Cracks
- C2: Corner Cracks
- C3: Embedded Cracks
- C4: Surface Cracks
- C5: Standard Specimens
- C6: Polynomial Series
- C7: Tabular Data
- C8: Boundary Element Solutions
- C9: Hybrid Cracks
- C10: Weight Function Solution Options
- C11: Compounding
- C12: Pin Load Options
- C13: Sign-Independent Load Approximation
- C14: Surface Crack Closure Correction Factor
- C15: References

Introduction

This appendix contains the normalized mode-I stress intensity factors for various crack geometries available in NASGRO. Quantities F_0, F_1, F_2, F_3, F_4 used in eqn. 2.2 of the main reference manual are defined in this appendix.

This page lists common symbols for all crack cases. Some of these may be redefined for individual cases. Variables such as a, c, t, W, D are shown in the figures for crack geometries in the GUI and in the main reference manual.

$$u = c / D$$

$$v = a / t$$

$$w = c / W$$

$$x = a / c$$

$$y = D / W$$

$$f_x = \begin{cases} [1 + 1.464x^{1.65}]^{-1/2} & \text{for } x \leq 1 \\ [1 + 1.464x^{-1.65}]^{-1/2} & \text{for } x > 1 \end{cases}$$

$$\sqrt{Q} = 1/f_x$$

$$f_0(z) = 0.7071 + 0.7548z + 0.3415z^2 + 0.642z^3 + 0.9196z^4$$

$$f_1(z) = 0.078z + 0.7588z^2 - 0.4293z^3 + 0.0644z^4 + 0.651z^5$$

$$f_\phi = \begin{cases} [(x \cos \phi)^2 + \sin^2 \phi]^{1/4} & \text{for } x \leq 1 \\ [\cos^2 \phi + (x^{-1} \sin \phi)^2]^{1/4} & \text{for } x > 1 \end{cases}$$

$$H_c = H_1 + (H_2 - H_1) \sin^p \phi$$

$$I = 1 - \sin \phi$$

$$J = 1 - \cos \phi$$

$$M_0 = M_1 + M_2 v^2 + M_3 v^4$$

Note that for a few crack cases, full details of tabular solutions are not shown for proprietary reasons.

Section C1: Through Cracks

TC01 – Through Crack at the Center of a Plate

$$F_0 = (\sec \pi w)^{1/2}, \quad F_1 = F_0 / 2$$

References: Combination of [C1], [C2], and [C21]

TC02 – Through Crack at the Edge of a Plate

$$F_0 = Y \left[0.752 + 2.02w + 0.37(1 - \sin \beta)^3 \right]$$

$$F_1 = F_0 / 2$$

$$F_2 = Y \left[0.923 + 0.199(1 - \sin \beta)^4 \right]$$

$$Y = \sec \beta \left[(\tan \beta) / \beta \right]^{1/2}$$

$$\beta = \pi w / 2$$

Reference: [C3]

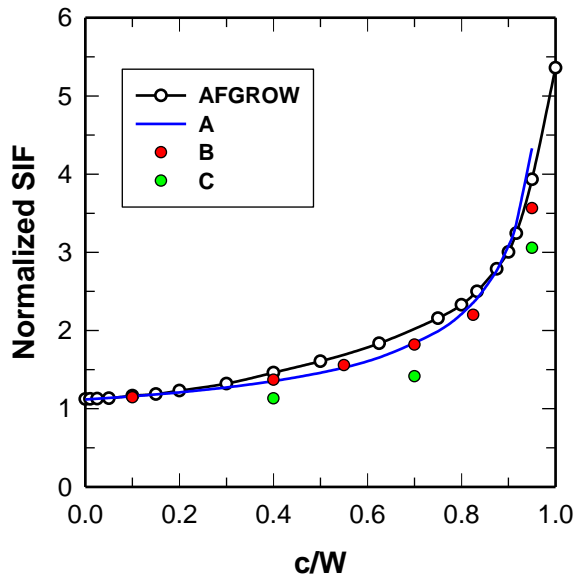
TC02 – Supplement for Bending Constraints at Remote Ends

The SIF results for a TC02 crack subjected to bending constraints at remote ends are derived from tabulated pairs of normalized crack depth and SIF provided in AFGROW Users Guide and Technical Manual [C62] and independently verified at SwRI using the finite element method. The tabulated data is shown in the following, where the column on the left is the normalized crack depth with respect to the width of the plate, and the column on the right is the normalized SIF.

c/W	$K/(\sigma_{\infty} \sqrt{\pi c})$
0	1.122
0.01	1.124
0.025	1.127
0.05	1.132
0.1	1.165
0.15	1.185
0.2	1.23
0.3	1.32
0.4	1.46
0.5	1.606
0.625	1.835
0.75	2.156
0.8	2.327
0.8333	2.499
0.875	2.789
0.9	3.005

0.916667	3.244
0.95	3.933
1	5.36

The verification done at SwRI can be found in the following figure. It contains four sets of numerical data. The first plot with black solid line and black hollow circle symbol is based on the above tabulated data pairs from AFGROW. The second with blue line and denoted by A is from Compendium of Stress Intensity Factors by Rooke and Cartwright [C70]. The last two plots are results from SwRI using 2D FE analysis with constraint boundary. The difference in these two plots is in the aspect ratio designating the slenderness of the plate defined by the ratio of the height (H) over the width (W). The plot with red solid circle is based on H/W=10 and the one with green solid circle has a shorter height, H/W=3. The definition for the abscissa and ordinate of the figure is the same as those used in the above table.



TC03 – Through Crack from an Offset Hole in a Plate

$$F_0 = G_0 f_{w0}, \quad F_1 = F_0 / 2, \quad F_3 = (G_0 y / 2 + G_1) f_{w3}$$

$$G_0 = f_0(z), \quad G_1 = f_1(z) \quad \text{where} \quad z = (1 + 2u)^{-1}$$

The values of f_{w0} , f_{w3} and F_2 are obtained from solutions listed in tables C1, C2 and C3 generated using the boundary element method.

References: [C4], [C7]

Table C1: Normalized Stress Intensity Factors f_{w0} : Tension

	c/(B-D/2)	D/2B=.05	D/2B=0.1	D/2B=0.3	D/2B=0.5	D/2B=0.7	D/2B=0.8	D/2B=0.9
2B/W=.1	0.00	1.094	1.134	1.183	1.257	1.734	2.090	3.062
	0.02	0.999	0.990	1.083	1.245	1.708	2.076	3.035
	0.05	0.975	0.990	1.063	1.239	1.673	2.060	3.005
	0.10	0.976	0.987	1.063	1.232	1.635	2.046	2.983
	0.20	0.949	0.996	1.077	1.240	1.643	2.074	3.051
	0.30	0.923	1.012	1.093	1.230	1.664	2.117	3.181
	0.50	0.877	1.056	1.147	1.282	1.703	2.193	3.321
	0.70	0.877	1.161	1.258	1.390	1.751	2.207	3.481
	0.90	1.103	1.528	1.656	1.749	2.014	2.361	3.637
	0.95	1.372	1.873	2.046	2.126	2.241	2.728	3.907
	0.98	1.902	2.526	2.800	2.846	3.170	3.752	5.116
	1.00	2.256	2.963	3.309	3.337	3.800	4.446	5.929
2B/W=.2	0.00	0.987	1.006	1.051	1.247	1.770	2.269	3.708
	0.02	0.991	0.995	1.053	1.233	1.757	2.251	3.598
	0.05	1.000	1.002	1.058	1.214	1.742	2.229	3.466
	0.10	1.002	0.979	1.061	1.193	1.725	2.209	3.335
	0.20	1.009	1.009	1.077	1.231	1.736	2.238	3.421
	0.30	1.017	1.024	1.099	1.260	1.766	2.294	3.563
	0.50	1.052	1.067	1.164	1.340	1.820	2.393	3.760
	0.70	1.144	1.170	1.297	1.485	1.886	2.427	3.962
	0.90	1.502	1.550	1.717	1.913	2.206	2.638	4.161
	0.95	1.771	1.877	2.059	2.266	2.462	3.063	4.499
	0.98	2.086	2.219	2.369	2.732	3.514	4.203	5.913
	1.00	2.296	2.449	2.578	3.049	4.229	4.974	6.865
2B/W=.5	0.00	0.976	1.006	1.094	1.366	2.109	2.923	5.247
	0.02	0.994	0.999	1.083	1.352	2.093	2.905	5.198
	0.05	1.001	1.006	1.089	1.333	2.075	2.885	5.146
	0.10	1.004	0.983	1.093	1.313	2.059	2.873	5.115
	0.20	1.011	1.016	1.115	1.361	2.096	2.939	5.279
	0.30	1.024	1.036	1.146	1.403	2.164	3.054	5.576
	0.50	1.073	1.095	1.244	1.530	2.333	3.331	6.307
	0.70	1.197	1.233	1.444	1.781	2.571	3.605	6.983
	0.90	1.657	1.734	2.053	2.486	3.296	4.288	7.710
	0.95	2.096	2.203	2.631	3.176	3.761	5.134	8.884
	0.98	2.771	2.940	3.316	4.019	5.654	7.283	11.942
	1.00	3.222	3.434	3.779	4.590	6.940	8.737	13.999
2B/W=.7	0.00	0.985	1.016	1.105	1.393	2.160	3.286	6.294
	0.02	0.985	0.987	1.095	1.369	2.148	3.266	6.242
	0.05	1.002	1.007	1.101	1.380	2.135	3.245	6.190
	0.10	1.005	0.985	1.090	1.351	2.127	3.236	6.172
	0.20	1.014	1.019	1.127	1.407	2.174	3.328	6.405
	0.30	1.027	1.040	1.165	1.460	2.260	3.496	6.826
	0.50	1.082	1.108	1.281	1.625	2.487	3.942	7.978
	0.70	1.225	1.270	1.520	1.955	2.836	4.504	9.396
	0.90	1.767	1.857	2.274	2.840	3.850	5.843	11.335
	0.95	2.149	2.260	2.811	3.540	4.875	7.249	13.610
	0.98	2.736	2.880	3.702	4.601	6.207	10.703	18.433
	1.00	3.128	3.295	4.304	5.321	7.112	13.042	21.679
2B/W=1.	0.00	0.998	1.029	1.127	1.446	2.191	3.422	6.709
	0.02	0.995	1.002	1.113	1.423	2.179	3.316	6.450
	0.05	1.003	1.010	1.119	1.432	2.166	3.187	6.140
	0.10	1.006	0.987	1.108	1.401	2.158	3.056	5.835
	0.20	1.014	1.022	1.145	1.461	2.208	3.139	6.054
	0.30	1.028	1.044	1.185	1.520	2.298	3.295	6.459
	0.50	1.087	1.117	1.309	1.694	2.555	3.725	7.614
	0.70	1.248	1.299	1.570	2.035	2.982	4.309	9.173
	0.90	1.916	2.023	2.533	3.249	4.286	5.781	11.502
	0.95	2.593	2.765	3.522	4.478	5.617	7.316	14.088
	0.98	3.825	4.116	5.343	6.819	8.460	11.063	19.823
	1.00	4.648	5.021	6.572	8.410	10.392	13.601	23.681

Table C2: Normalized Stress Intensity Factors f_{w3} : Pin Loading

	c/(B-D/2)	D/2B=.05	D/2B=.1	D/2B=.3	D/2B=.5	D/2B=.7	D/2B=.8	D/2B=.9
2B/W=.1	0.00	0.829	0.850	0.997	1.271	1.992	2.742	4.753
	0.02	0.908	0.853	1.000	1.278	1.987	2.739	4.723
	0.05	0.956	0.935	1.022	1.293	1.986	2.742	4.700
	0.10	1.059	1.000	1.085	1.333	2.002	2.771	4.727
	0.20	1.159	1.078	1.210	1.451	2.124	2.929	5.039
	0.30	1.247	1.170	1.324	1.545	2.272	3.132	5.431
	0.50	1.282	1.379	1.574	1.828	2.599	3.559	6.054
	0.70	1.501	1.859	1.944	2.225	2.989	3.967	6.873
	0.90	1.863	2.358	2.864	3.140	3.911	4.825	7.971
	0.95	2.027	3.136	3.625	3.950	4.557	5.807	9.136
	0.98	2.179	4.701	5.025	5.350	6.584	8.231	12.360
	1.00	2.287	5.797	6.003	6.322	7.979	9.887	14.540
2B/W=.2	0.00	0.836	0.878	1.063	1.401	2.338	3.281	5.851
	0.02	0.920	0.906	1.063	1.408	2.331	3.274	5.777
	0.05	1.015	0.995	1.106	1.419	2.336	3.273	5.700
	0.10	1.090	1.026	1.176	1.446	2.356	3.299	5.665
	0.20	1.215	1.169	1.316	1.600	2.492	3.469	5.966
	0.30	1.340	1.288	1.448	1.746	2.659	3.694	6.381
	0.50	1.769	1.611	1.741	2.093	3.020	4.167	7.169
	0.70	2.026	1.965	2.194	2.575	3.449	4.598	8.025
	0.90	2.989	2.940	3.255	3.696	4.488	5.545	9.161
	0.95	3.610	3.604	4.001	4.488	5.214	6.659	10.413
	0.98	4.313	4.472	4.537	5.377	7.505	9.365	14.061
	1.00	4.793	5.075	4.908	5.923	9.079	11.212	16.526
2B/W=.5	0.00	0.845	0.887	1.123	1.581	2.780	4.170	8.082
	0.02	0.923	0.916	1.116	1.568	2.809	4.161	8.043
	0.05	1.018	1.004	1.159	1.604	2.790	4.159	8.015
	0.10	1.092	1.035	1.218	1.617	2.823	4.191	8.051
	0.20	1.216	1.178	1.375	1.786	2.983	4.405	8.449
	0.30	1.336	1.312	1.517	1.951	3.198	4.703	9.076
	0.50	1.605	1.635	1.854	2.353	3.707	5.421	10.637
	0.70	2.033	2.104	2.405	2.997	4.383	6.209	12.222
	0.90	3.114	3.300	3.778	4.548	6.059	7.885	14.145
	0.95	4.014	4.276	4.945	5.937	7.104	9.630	16.675
	0.98	5.301	5.773	6.314	7.598	10.740	13.858	22.705
	1.00	6.179	6.798	7.256	8.742	13.231	16.738	26.775
2B/W=.7	0.00	0.835	0.868	1.066	1.478	2.568	4.099	8.411
	0.02	0.906	0.890	1.057	1.459	2.567	3.994	8.363
	0.05	0.991	0.968	1.094	1.493	2.573	3.884	8.326
	0.10	1.050	0.989	1.137	1.508	2.601	3.841	8.359
	0.20	1.139	1.110	1.272	1.660	2.752	4.342	8.799
	0.30	1.225	1.220	1.401	1.815	2.956	4.671	9.510
	0.50	1.389	1.445	1.689	2.155	3.471	5.523	11.454
	0.70	1.700	1.808	2.136	2.763	4.215	6.618	13.888
	0.90	2.709	2.966	3.655	4.498	6.104	9.057	17.377
	0.95	3.483	3.770	4.477	5.450	7.866	11.410	21.207
	0.98	4.458	4.935	5.923	7.632	10.183	17.013	29.583
	1.00	5.118	5.728	6.916	9.131	11.767	20.827	35.234
2B/W=1.	0.00	0.828	0.846	0.986	1.319	2.130	3.414	7.149
	0.02	0.890	0.863	0.977	1.301	2.128	3.341	6.929
	0.05	0.964	0.931	1.004	1.324	2.130	3.255	6.673
	0.10	1.002	0.937	1.033	1.324	2.149	3.182	6.444
	0.20	1.044	1.018	1.132	1.441	2.259	3.336	6.775
	0.30	1.072	1.078	1.220	1.558	2.416	3.576	7.324
	0.50	1.149	1.215	1.432	1.850	2.832	4.216	8.880
	0.70	1.361	1.480	1.813	2.348	3.476	5.091	11.000
	0.90	2.146	2.394	3.075	3.954	5.257	7.162	14.274
	0.95	2.921	3.298	4.329	5.490	6.310	9.186	17.764
	0.98	4.325	4.930	6.276	8.424	10.599	14.029	25.195
	1.00	5.277	6.040	7.609	10.436	13.532	17.322	30.207

Table C3: Stress Intensity Correction Factors $F_2 = K / (S_2 \sqrt{\pi a})$: In-plane Bending

	c/(B-D/2)	D/2B=.05	D/2B=.10	D/2B=.30	D/2B=.50	D/2B=.70	D/2B=.80	D/2B=.90
2B/W=.10 (D=2.0)	.00	2.693	2.859	3.218	4.031	5.386	6.717	9.765
	.02	1.779	2.274	3.048	3.781	5.210	6.516	9.449
	.05	1.212	1.662	2.651	3.510	4.918	6.394	9.394
	.10	0.930	1.254	2.234	3.179	4.734	6.202	9.292
	.20	0.768	0.989	1.779	2.758	4.394	5.950	9.299
	.30	0.766	0.903	1.531	2.475	4.165	5.818	9.465
	.50	0.638	0.858	1.330	2.127	3.756	5.526	9.486
	.70	0.627	0.903	1.308	1.978	3.480	5.167	9.547
	.90	0.782	1.164	1.611	2.275	3.682	5.188	9.624
	.95	0.974	1.423	1.967	2.716	4.242	5.859	10.223
	.98	1.358	1.921	2.676	3.608	5.650	7.942	13.387
	1.0	1.615	2.252	3.148	4.202	6.588	9.331	15.497
2B/W=.20 (D=2.0)	.00	2.468	2.807	2.998	3.603	5.226	6.783	10.854
	.02	1.567	1.976	2.734	3.424	5.060	6.540	10.175
	.05	1.049	1.522	2.431	3.156	4.795	6.394	9.727
	.10	0.855	1.116	2.059	2.910	4.666	6.205	9.672
	.20	0.748	0.937	1.649	2.576	4.336	5.997	9.704
	.30	0.751	0.831	1.420	2.323	4.102	5.880	9.889
	.50	0.722	0.806	1.247	2.064	3.754	5.638	10.022
	.70	0.788	0.853	1.265	1.975	3.516	5.319	10.155
	.90	1.053	1.137	1.592	2.321	3.811	5.427	10.287
	.95	1.216	1.384	1.899	2.774	4.438	6.225	11.039
	.98	1.475	1.616	2.224	3.232	5.915	8.471	14.490
	1.00	1.647	1.771	2.441	3.537	6.899	9.969	16.791
2B/W=.50 (D=2.0)	.00	1.697	1.824	2.264	2.904	4.643	6.580	11.659
	.02	0.991	1.320	1.995	2.753	4.478	6.393	11.016
	.05	0.704	0.993	1.766	2.609	4.317	6.197	10.953
	.10	0.574	0.762	1.510	2.387	4.189	6.102	11.069
	.20	0.524	0.643	1.236	2.128	3.968	5.962	11.252
	.30	0.526	0.616	1.105	1.959	3.831	5.937	11.641
	.50	0.576	0.649	1.049	1.804	3.689	5.995	12.655
	.70	0.681	0.753	1.142	1.879	3.712	6.056	13.483
	.90	0.993	1.094	1.595	2.450	4.450	6.802	14.403
	.95	1.266	1.399	2.015	3.110	5.404	8.048	16.485
	.98	1.702	1.874	2.562	3.899	7.475	11.353	22.090
	1.00	1.993	2.190	2.926	4.425	8.855	13.556	25.827
2B/W=.70 (D=2.0)	.00	1.065	1.212	1.589	2.264	3.814	5.785	11.009
	.02	0.630	0.862	1.444	2.136	3.720	5.631	10.227
	.05	0.457	0.653	1.294	2.036	3.528	5.485	10.226
	.10	0.385	0.525	1.115	1.889	3.442	5.384	10.234
	.20	0.373	0.463	0.939	1.692	3.282	5.304	10.779
	.30	0.395	0.468	0.867	1.582	3.205	5.350	11.258
	.50	0.473	0.534	0.869	1.328	3.180	5.600	12.662
	.70	0.599	0.664	1.009	1.693	3.347	6.002	14.378
	.90	0.944	1.039	1.512	2.342	4.280	7.385	16.785
	.95	1.170	1.279	1.863	2.910	5.368	9.062	20.022
	.98	1.532	1.642	2.484	3.767	6.767	13.325	27.048
	1.00	1.774	1.883	2.899	4.339	7.699	16.166	31.732
2B/W=1.0 (D=2.0)	.00	0.165	0.202	0.693	1.240	2.390	3.849	7.353
	.02	0.079	0.178	0.632	1.201	2.360	3.658	7.045
	.05	0.077	0.151	0.573	1.140	2.236	3.584	7.121
	.10	0.100	0.156	0.515	1.069	2.194	3.538	7.295
	.20	0.148	0.195	0.481	0.996	2.133	3.522	7.486
	.30	0.200	0.243	0.491	0.972	2.127	3.595	7.874
	.50	0.314	0.354	0.574	1.024	2.221	3.881	9.060
	.70	0.468	0.513	0.746	1.221	2.496	4.343	10.682
	.90	0.849	0.923	1.280	1.974	3.544	5.746	13.222
	.95	1.183	1.287	1.878	2.763	4.656	7.277	16.259
	.98	1.786	1.949	2.764	4.181	7.034	11.047	22.911
	1.00	2.188	2.391	3.354	5.127	8.619	13.561	27.345

TC04 – Through Crack from Hole in a Lug

$$\begin{aligned}
 F_3 &= (G_0 y / 2 + G_1) G_w G_L G_2 \\
 G_0 &= f_0(z), G_1 = f_1(z) \text{ where } z = (1 + 2u)^{-1} \\
 G_L &= [\sec(\pi y / 2)]^{1/2}, G_w = (\sec \lambda)^{1/2} \\
 G_2 &= C_1 + C_2(c/b) + C_3(c/b)^2 + C_4(c/b)^3 \\
 \lambda &= (\pi/2)(1+u)/(W/D-u), b = (W-D)/2 \\
 C_1 &= 0.688 + 0.772y + 0.613y^2 \\
 C_2 &= 4.948 - 17.318y + 16.785y^2 \\
 C_3 &= -14.297 + 62.994y - 69.818y^2 \\
 C_4 &= 12.35 - 58.644y + 66.387y^2
 \end{aligned}$$

References: Combination and empirical fits of [C4] and [C5], and unpublished boundary integral analysis at NASA Langley.

TC05 – Through Crack from Hole in a Plate with a Row of Holes

Nondimensional factors F_0, F_3 for tension and pin load respectively were computed using the boundary element method. For a single crack from one of the holes, the results are listed in tables C4, C5 and for two equal cracks from one hole, the results are given in tables C6, C7. The factors for the case of two equal cracks from each of the holes are listed in tables C8, C9. The correction factor for lateral tensile loading F_4 is given below in the form of a series solution:

$$\begin{aligned}
 F_4 &= \sum_{m=0}^8 B_{0,m} f^m + \sum_{n=1}^4 \sum_{m=0}^8 B_{n,m} h_4^n f^m \\
 f &= (D/H)^{1+n/4} \quad (H \text{ is hole spacing}) \\
 h_4 &= \tan[\pi(\beta - k_4)/2k_4] \\
 k_4 &= 0.51, \beta = (D/2 + c)/H
 \end{aligned}$$

Table C10 lists values of coefficients $B_{n,m}$.

Table C4: Stress Intensity Correction Factors (Tension, One Crack, $.0055 \leq D/B \leq .1$)

c/(H-D)--	0.0	.01	.05	.1	.15	.2	.4	.6	.8	.9	0.95	0.99
>												
D/H												
0.05	2.858	1.782	1.043	.8898	.8338	.8058	.7648	.7581	.7681	.7876	.8244	1.065
0.10	2.921	2.195	1.327	1.065	.9595	.9054	.8222	.8017	.8122	.8514	.9296	1.333
0.20	2.965	2.574	1.793	1.410	1.230	1.126	.9590	.9141	.9386	1.033	1.197	1.828
0.30	3.101	2.796	2.167	1.761	1.534	1.391	1.141	1.074	1.126	1.281	1.516	2.366
0.40	3.219	3.009	2.520	2.134	1.888	1.719	1.395	1.308	1.399	1.617	1.922	2.940
0.50	3.474	3.299	2.922	2.575	2.328	2.145	1.765	1.664	1.809	2.111	2.538	3.656
0.60	3.886	3.786	3.461	3.162	2.933	2.752	2.342	2.238	2.443	2.858	3.424	4.550
0.70	4.878	4.585	4.344	4.091	3.899	3.735	3.343	3.260	3.561	4.153	4.906	5.932
0.75	5.331	5.272	5.056	4.852	4.663	4.523	4.170	4.118	4.501	5.251	6.108	7.054
0.80	6.382	6.335	6.182	5.934	5.798	5.690	5.429	5.432	5.947	6.850	7.720	8.517
0.85	8.265	8.202	8.036	7.776	7.678	7.619	7.513	7.671	8.353	9.392	10.11	10.66
0.90	11.78	11.54	11.45	11.17	11.10	11.10	11.49	12.12	13.38	14.36	14.61	14.90

Table C5: Stress Intensity Correction Factors (Pin Loading, One Crack , D/B = .1)

- c/(H-D)-->	0.0	.01	.05	.1	.15	.2	.4	.6	.8	.9	0.95	0.99
D/H												
0.05	.9805	.4358	.1353	.0721	.0521	.0425	.0297	.0275	.0292	.0331	.0402	.0755
0.10	1.062	.6693	.2793	.1657	.1220	.0994	.0671	.0592	.0607	.0706	.0886	.1657
0.20	1.243	.9904	.5774	.3898	.3016	.2512	.1701	.1480	.1548	.1860	.2362	.4063
0.30	1.455	1.275	.8898	.6604	.5349	.4568	.3199	.2816	.3005	.3618	.4502	.7480
0.40	1.733	1.589	1.242	.9926	.8388	.7350	.5372	.4812	.5212	.6225	.7614	1.205
0.50	2.089	1.971	1.670	1.420	1.248	1.124	.8648	.7917	.8661	1.033	1.295	1.845
0.60	2.609	2.542	2.251	2.015	1.836	1.701	1.391	1.307	1.432	1.693	2.042	2.734
0.70	3.522	3.412	3.175	2.962	2.793	2.657	2.329	2.250	2.461	2.883	3.416	4.145
0.75	4.188	4.096	3.895	3.696	3.553	3.426	3.118	3.059	3.345	3.912	4.559	5.265
0.80	5.214	5.209	5.003	4.803	4.676	4.574	4.330	4.315	4.721	5.444	6.143	6.783
0.85	7.085	7.042	6.889	6.642	6.540	6.481	6.392	6.507	7.161	8.069	8.685	9.029
0.90	10.53	10.35	10.29	10.23	10.14	10.15	10.47	11.05	12.21	13.10	13.52	14.01

Table C6: Stress Intensity Correction Factors (Tension, Two Cracks, $.0055 \leq D/B \leq .1$)

c/(H-D)->	0.0	.01	.05	.1	.15	.2	.4	.6	.8	.9	0.95	0.99
D/H												
0.05	2.858	1.854	1.247	1.131	1.093	1.075	1.068	1.101	1.174	1.245	1.332	1.760
0.10	2.921	2.229	1.476	1.267	1.189	1.151	1.110	1.136	1.215	1.382	1.476	2.172
0.20	2.965	2.583	1.871	1.554	1.411	1.332	1.227	1.238	1.350	1.548	1.844	2.923
0.30	3.101	2.800	2.213	1.861	1.673	1.562	1.392	1.396	1.566	1.864	2.279	3.734
0.40	3.219	3.029	2.557	2.204	1.996	1.859	1.633	1.637	1.884	2.291	2.831	4.592
0.50	3.474	3.319	2.939	2.623	2.411	2.262	1.995	2.013	2.362	2.919	3.660	5.656
0.60	3.886	3.783	3.470	3.199	2.999	2.849	2.571	2.624	3.107	3.858	4.843	7.087
0.70	4.878	4.619	4.348	4.126	3.954	3.823	3.584	3.714	4.409	5.480	6.815	8.878
0.75	5.331	5.267	5.096	4.864	4.713	4.608	4.428	4.635	5.505	6.856	8.417	10.46
0.80	6.382	6.375	6.202	5.963	5.844	5.776	5.709	6.032	7.170	8.833	10.50	12.38
0.85	8.265	8.215	8.048	7.806	7.730	7.709	7.834	8.415	9.924	11.61	13.52	15.20
0.90	11.78	11.58	11.44	11.21	11.15	11.18	11.85	13.09	15.62	17.89	19.08	20.53

Table C7: Stress Intensity Correction Factors (Pin Loading, Two Cracks , D/B =.1)

c/(H-D)> D/H	0.0	.01	.05	.1	.15	.2	.4	.6	.8	.9	0.95	0.99
0.05	.9805	.4561	.1712	.1093	.0871	.0764	.0651	.0683	.0760	.0833	.0957	.1464
0.10	1.062	.6789	.3178	.2105	.1670	.1437	.1100	.1034	.1088.	.1236	.1484	.2555
0.20	1.243	.9941	.6056	.4355	.3553	.3090	.2337	.2169	.2362	.2583	.3598	.6158
0.30	1.455	1.278	.9093	.7004	.5889	.5204	.4036	.3812	.4299	.5310	.6719	1.148
0.40	1.733	1.592	1.255	1.026	.8893	.7994	.6391	.6155	.7128	.8867	1.117	1.854
0.50	2.089	1.980	1.680	1.447	1.294	1.186	.9839	.9673	1.141	1.432	1.815	2.836
0.60	2.609	2.534	2.258	2.038	1.879	1.761	1.532	1.539	1.828	2.289	2.888	4.165
0.70	3.522	3.411	3.174	2.984	2.830	2.717	2.499	2.570	3.054	3.810	4.751	6.208
0.75	4.188	4.089	3.928	3.730	3.593	3.492	3.313	3.447	4.097	5.113	6.293	7.832
0.80	5.214	5.202	5.022	4.828	4.720	4.643	4.557	4.797	5.699	7.028	8.366	9.877
0.85	7.085	7.048	6.895	6.664	6.589	6.556	6.666	7.145	8.529	10.28	11.67	12.85
0.90	10.53	10.29	10.30	10.27	10.20	10.22	10.81	11.95	14.30	16.44	17.82	19.68

Table C8: Stress Intensity Correction Factors (Tension, Two Cracks at each Hole, $.0055 \leq D/B \leq .1$)

$2c/(H-D)$	0.0	.02	.05	.1	.15	.2	.4	.6	.8	.9	0.95	0.99
D/H												
0.05	2.890	1.851	1.452	1.254	1.184	1.154	1.155	1.263	1.526	1.807	2.552	5.124
0.10	2.895	2.238	1.789	1.488	1.362	1.298	1.250	1.372	1.711	2.246	2.980	5.750
0.20	2.957	2.575	2.220	1.881	1.697	1.594	1.450	1.509	1.809	2.355	3.225	6.303
0.30	3.051	2.809	2.528	2.260	2.023	1.893	1.693	1.735	2.115	2.812	3.858	8.310
0.40	3.216	3.024	2.822	2.550	2.360	2.226	1.987	2.040	2.596	3.438	4.611	9.664
0.50	3.483	3.310	3.157	2.942	2.779	2.642	2.417	2.496	3.040	3.931	5.470	11.05
0.60	3.864	3.760	3.629	3.452	3.295	3.184	2.970	3.107	3.879	5.190	7.204	13.41
0.70	4.658	4.556	4.514	4.367	4.160	4.066	3.902	4.134	5.178	6.973	9.601	16.88
0.75	5.305	5.223	5.158	5.021	4.881	4.771	4.643	4.942	6.207	8.384	11.37	20.47
0.80	6.494	6.387	6.363	6.136	6.053	5.948	5.788	6.156	7.515	9.734	13.07	25.28
0.85	8.523	8.348	8.124	7.925	7.901	7.723	7.634	8.526	10.65	14.25	19.55	41.29
0.90	12.50	11.88	11.69	11.56	11.37	11.28	11.69	12.67	15.77	20.51	27.60	56.99

Table C9: Stress Intensity Correction Factors (Pin Loading, Two Cracks at each Hole , D/B = .1)

2c/(H-D)	0.0	.02	.05	.1	.15	.2	.4	.6	.8	.9	0.95	0.99
D/H												
0.05	.9945	.4588	.2724	.1730	.1328	.1113	.0795	.0739	.0857	.1125	.1530	.3326
0.10	1.068	.6795	.4652	.3202	.2534	.2156	.1568	.1488	.1781	.2358	.3220	.6715
0.20	1.259	.9958	.7936	.6112	.5116	.4492	.3447	.3328	.3995	.5278	.7261	1.413
0.30	1.471	1.279	1.103	.9158	.7991	.7202	.5790	.5655	.6798	.9013	1.233	2.654
0.40	1.730	1.599	1.410	1.261	1.139	1.049	.8780	0.870	1.069	1.411	1.886	3.956
0.50	2.104	1.983	1.848	1.684	1.563	1.469	1.283	1.291	1.565	2.040	2.716	5.354
0.60	2.596	2.530	2.408	2.249	2.131	2.044	1.853	1.910	2.361	3.152	4.370	8.127
0.70	3.487	3.394	3.329	3.178	3.036	2.954	2.794	2.928	3.652	4.827	5.901	11.22
0.75	4.116	4.084	4.007	3.876	3.761	3.677	3.538	3.743	4.685	6.311	8.401	13.35
0.80	5.283	5.214	5.185	5.010	4.866	4.764	4.607	4.841	5.884	7.580	11.11	19.28
0.85	7.208	6.988	6.880	6.750	6.665	6.583	6.598	7.165	8.934	11.96	16.41	34.76
0.90	11.11	10.75	10.53	10.39	10.22	10.14	10.40	11.24	13.99	18.20	24.50	50.57

Table C10 : Values of Coefficients $B_{n,m}$

m	$B_{0,m}$	$B_{1,m}$	$B_{2,m}$	$B_{3,m}$	$B_{4,m}$
0	6.2909E-3	-4.2720E-4	-8.4488E-4	-2.1989E-4	9.3740E-5
1	-3.7092E-2	6.5214E-2	6.7469E-2	2.4756E-2	-1.8505E-2
2	9.1764E-1	-9.7885E-1	-9.3965E-1	3.3014E0	-3.6289E0
3	-9.5339E-1	1.3252E1	-6.4009E0	-1.5032E1	4.2827E0
4	-5.7380E0	-5.5698E1	1.5976E1	3.4969E1	3.8805E1
5	2.1452E1	1.3165E2	-1.6777E1	-5.5679E1	-1.6295E2
6	-3.6137E1	-1.8986E2	-1.5827E0	2.7062E1	4.3705E2
7	3.0526E1	1.4719E2	5.3097E1	4.5520E1	-5.5017E2
8	-1.0024E1	-4.5487E1	-4.7418E1	-4.2747E1	2.2008E2

Reference: [C8]

TC06 – Through Crack in a Sphere

$$F_0 = (1 + 3\lambda^{1.9})^{0.4}, \quad \lambda = c / \sqrt{Rt} \leq 3$$

Reference: [C20]

TC07 – Through Crack in Cylinder in Longitudinal Direction

$$F_0 = (1 + 0.52\lambda + 1.29\lambda^2 - 0.074\lambda^3)^{1/2}$$

$$\lambda = a / \sqrt{Rt} \leq 10$$

Reference: [C9]

TC08 – Through Crack in Cylinder in Circumferential Direction

$$F_0 = (I_0 / 2\pi\alpha)^{1/2}, \quad F_1 = (I_1 / 2\pi\alpha)^{1/2}$$

$$I_0 = [\sqrt{8}(f^2 - 1) + \pi\beta^2 / b]\alpha^2 / k, \quad I_1 = [\sqrt{8}(g^2 - 1) + \pi\beta^2 / b]\alpha^2 / k$$

$$f = 1 + h(1 - \alpha \cot \alpha) / 2\alpha$$

$$g = [1 + h(\alpha + \alpha \cot^2 \alpha - \cot \alpha) / 4](\sin \alpha) / \alpha$$

$$h = \sqrt{2} / (\cot[(\pi - \alpha) / \sqrt{2}] + \sqrt{2} \cot \alpha)$$

$$b = \alpha / 2k, \quad k = \sqrt{t / R} [12(1 - v^2)]^{-1/4}$$

$$\beta = 1 + (\pi / 16)b^2 - 0.0293b^3 \quad \text{for } b \leq 1$$

$$= (\sqrt{8}b / \pi)^{0.5} + (0.179 / b)^{0.885} \quad \text{for } b > 1$$

Reference: [C10]

TC09 – Through Crack from Hole in a Plate under Combined Loading

$$F_0 = \sum_{n=0}^4 [A_n(1+B) + B_n]b^n, \quad F_1 = 1.6[(1+u)b]^{3/2}(1+v)/(3+v)$$

$$F_2 = (D / 3X) \sum_{n=0}^5 C_n b^n, \quad F_3 = \sum_{n=0}^5 D_n b^n$$

$$b = 1 / (1 + 2u)$$

Table C11 : Values of Coefficients A_n , B_n , C_n , and D_n

n	A_n	B_n	C_n	D_n
0	-0.00074	0.70920	0.7968	0
1	0.06391	0.68902	0.5326	0.0780
2	-0.10113	0.52270	0.2767	0.7588
3	-0.29411	0.65768	0.0630	-0.4293
4	-0.79179	1.91920	-0.0166	0.0644
5	–	–	1.7197	0.6510

References: [C4], [C11], [C12], [C21] and [C22]

TC10 – Through Crack from Hole in a Cylinder under Tension or Pin Loading

The correction factors F_0 and f_3 are listed in tables 2 to 7 of reference [C31] for $R/t = 30$. For other R/t values, correction factors given in table 9 of the same report are to be multiplied into F_0 . $F_3 = f_3 nr / \pi R$ relates f_3 and F_3 . n is the no. of holes, r is the hole radius and R is the cylinder mean radius. Correction to F_0 is done only if the crack is longer than the hole radius. Correction due to finite edge distance is same as that for TC05. More details are given in [C32].

References: [C31, C32]

TC11 – Through Crack in a Plate –Nonlinear Stress

Crack case TC11 is a weight function solution for a through-the-thickness crack in a plate of finite width subjected to loadings resulting in a general nonlinear stress distribution. The crack can be offset from the plate center. The stress can be defined along the crack plane in the corresponding uncracked body by either a sixth-order polynomial or a stress array defined in terms of the coordinates varying along the net section. The specification of stressing is always in reference to a global coordinate system where its origin is at the center of the plate, its x -direction is along the net section, and the y -axis is normal to the crack plane and parallel to the loading direction.

Two sets of crack configuration were included: 1) a symmetric configuration in which the crack is at the center of the plate and the stressing is symmetric with respect to the y -axis and 2) a non-symmetric configuration that may include cases such as a non-symmetric crack subjected to symmetric stressing or a symmetric crack subjected to non-symmetric stressing. In all cases, the specification of stress variations in terms of either polynomial or stress array uses one-half of the plate width ($W_d=W/2$) as the normalization length. The only difference is the referred coordinate range along the x -axis. The symmetric configuration makes use of positive x -axis only, while the non-symmetric configuration uses the full range of x -axis. In other words, for stressing in terms of a six-order polynomial defined as follows

$$\sigma(x) = \sum_{i=0}^6 a_i \left(\frac{x}{W_d} \right)^i$$

the x coordinates vary from 0 to W_d for the symmetric configuration and from $-W_d$ to W_d for the non-symmetric configuration. Similarly, for stressing in terms of stress array, the normalized coordinates for the symmetric configuration vary from 0 to 1, while for the non-symmetric configuration they vary from -1 to 1.

The solution schemes for polynomial stress variations provide a very fast method for stress intensity factors. For highly nonlinear stress distributions where polynomial forms are not applicable, the solution schemes using stress arrays are suggested.

The geometry validity ranges for TC11 are described as follows:

$$0 \leq \frac{a}{\text{Min}(B, W - B)} \leq 0.99$$

$$0.01 \leq \frac{2B}{W} \leq 1.99$$

where W is the plate width, a is one-half of the crack length, and B is the offset of the crack center from one side of the plate. The first requirement defines the valid crack length, which can extend up to 99% of the smaller net section. The second requirement defines the valid offset range of the crack center from the side surface.

The weight function for TC11 is analytically derived, and is based on a six-terms expansion around the crack tip location. The stress intensity factor for is given by [Ref. C33].

$$K_I^A = \int_{-a}^a \sigma(x) \left(\frac{m_1^A}{\sqrt{a-x}} + m_2^A \right) dx$$

where

$$\begin{aligned} m_1^A &= \sqrt{\frac{1+\frac{x}{a}}{\pi}} \left[\beta_1^A \left(1 - \frac{x}{a} \right) + \beta_2^A \left(1 + \frac{x}{a} \right) \right] \\ m_2^A &= \frac{1}{\sqrt{\pi a}} \left\{ \left[\beta_3^A + \beta_4^A \left(1 - \frac{x}{a} \right) + \beta_5^A \left(1 + \frac{x}{a} \right) \right] \sqrt{1 - \left(\frac{x}{a} \right)^2} + \beta_6^A \left[1 - \left(\frac{x}{a} \right)^2 \right]^{\frac{3}{2}} \right\} \end{aligned}$$

where the coefficients of the weight functions (β 's) are determined through interpolation from tabulated data for any given a/B .

For stress variations that are in terms of polynomial, the SIF solutions are determined by simple summation over the analytically-derived terms that were hard-coded in the routine for fast computing. For stress variations defined by the stress array, the integration is performed numerically using the Gauss-Chebyshev quadrature with convergence check.

TC12 – Edge Through Crack in a Plate – Nonlinear Stress

Crack case TC12 is a weight function solution for an edge through crack in a finite plate subjected to loadings resulting in a general nonlinear stress distribution. The stress can be defined in terms of more general in-plane nonlinear stress distributions on the crack plane in the corresponding uncracked body. It can be described by either a pre-defined sixth-order polynomial or a stress array defined at the position coordinates varying from the location where the crack emanates extending across the whole plate width. The sixth-order polynomial applicable to represent the stress variation consists of the linear combination of various terms of

normalized coordinate with different exponents; $\sigma(x) = \sum_{i=0}^6 \alpha_i (x/W)^i$. The normalization is with respect to the plate width.

The solution scheme for polynomial stress variations provides a very fast computational tool for stress intensity factors where stress variations can be best represented by the pre-defined polynomial. For highly nonlinear stress distributions where polynomial forms are not applicable, it is suggested using the solution scheme utilizing the stress array.

The geometry validity range for TC12 is as follows:

$$0 \leq \frac{a}{W} \leq 0.9$$

where a denotes the crack length, and W is the plate width.

The weight function for TC12 is analytically derived. The weight function is based on a five-terms expansion around the crack tip location. The stress intensity factor for the crack tip is thus given by

$$K_I = f \sqrt{\pi a}$$

where

$$f = \frac{1}{\sqrt{2\pi}\tilde{a}} \int_0^{\tilde{a}} \sigma(\tilde{x}) \left[\sum_{i=1}^5 \beta_i \left(1 - \frac{\tilde{x}}{\tilde{a}}\right)^{\frac{i-3}{2}} \right] d\tilde{x}$$

where \tilde{a} and \tilde{x} are normalized crack length and coordinate with respect to the plate width W , and the coefficients of the weight functions (β 's) are determined through interpolation from tabulated data for given a/W ratios. For stress variations that can be represented by the pre-defined polynomial, the solution has been pre-integrated analytically and hard-coded into the routine for fast computing. For stress variations defined by the stress array, the integration is performed numerically using the Gauss-Chebyshev quadrature with convergence check.

The crack case does not yet check for failure due to net-section stress.

Reference: [C34]

TC13 – Through Crack (or Twin Cracks) at an Off-Center Hole in a Plate– Nonlinear Stress

Crack case TC13 is a weight function solution for a through surface crack at an off-center hole in a finite width plate with a general nonlinear stress distribution. It has nominally the same geometry as TC03. The crack is assumed to propagate along the smaller net section of the two formed by

the off-center through-thickness hole in the plate. The difference between TC03 and TC13 is that TC03 is defined in terms of remote loads, moments, and pin loads, while TC13 is a weight function solution defined in terms of general nonlinear stress distributions on the crack plane in the corresponding uncracked body. The TC03 solution scheme is thus restricted by these three specific loading conditions, whereas TC13 is a more powerful analysis tool for analyzing cracked components subjected to any complex loadings where stress variations along the crack plane in the uncracked body are available. The derivation of the TC13 weight functions is based on the TC03 solutions for a plate subjected to remote uniform tension, and hence the two solutions are consistent for uniform remote tension. The new TC13 solution does not yet check for failure due to net-section yield. For this and other legacy reasons, TC03 is still retained. Crack case TC13 [from NASGRO 6.0 onwards] includes a symmetric geometry (with twin cracks) loaded symmetrically.

Crack case TC13 provides consistent stress intensity factor solutions for stresses in two different input forms:

1. The fundamental weight function solution permits direct input of the principal normal stresses on the crack plane as pairs of $[(x/t)_i, S_i]$, where the x -axis originates from the root of the hole and extends along the smaller net section of the two formed by the through-thickness hole in the plate.
2. The user can alternatively input a combination of tension and bending applied at the remote ends of the plate. The tension is simply denoted by uniform tensile stress, while the remote bending is required to result in an in-plane linear stress variation and thus anti-symmetric variation is expected. The individual magnitudes of the remote loads can be specified in the GUI for load block definition. The fracture mechanics module internally estimates the local stress variations on the crack plane (in the corresponding uncracked body) along the net section and then invokes the same weight function formulation as above.

The geometry validity range for all TC13 solutions is as follows:

$$\begin{aligned} 0.1 &\leq 2B/W \leq 1.0 \\ 0.05 &\leq D/(2B) \leq 0.9 \\ 0.001 &\leq a/(B-D/2) \leq 0.999 \end{aligned}$$

The weight function for a through crack at an off-center hole in a finite plate is analytically derived. The formulation is based on the stress variation along the net section formed by a through-thickness hole in a plate subjected to remote tension, and the tabulated stress intensity factors for TC03 (See Table C1). The net section stress variation is designated as the reference stress and was determined using two-dimensional finite element analysis. The stress variation can be simplified as a two-terms product; net section stress as a function of $2B/W$ and $D/(2B)$, and normalized stress variation as a function of $D/(2B)$ and normalized coordinate $x/(B-D/2)$, or equivalently,

$$\sigma(x) = \sigma_{net} \left(\frac{2B}{W}, \frac{D}{2B} \right) \cdot \bar{\sigma} \left(\frac{D}{2B}, \frac{x}{B-D/2} \right)$$

where σ_{net} is the net section stress, and $\bar{\sigma}$ the normalized stress variation whose profile is dictated by the ratio of the hole radius to the offset only.

Using the tabulated stress intensity factors for TC03 as the reference solutions, the weight function for a through surface crack at an off-center hole in a finite plate is given by

$$w_c\left(\tilde{x}, \xi; \frac{2B}{W}, \frac{D}{2B}\right) = \frac{1}{\sqrt{2\pi\xi}} \sum_{i=1}^5 \beta_i \left(\xi; \frac{2B}{W}, \frac{D}{2B}\right) \left(1 - \frac{\tilde{x}}{\xi}\right)^{\frac{i-3}{2}}$$

where i varies from 1 to 5, ξ symbolizes the normalized crack length $a/(B-D/2)$, and \tilde{x} the normalized coordinate varying from 0 to ξ . The coefficients β_i 's are tabulated as a function of normalized crack depth ξ , and normalized plate dimensions, $2B/W$ and $D/(2B)$. For a general stress variation $\sigma(x)$, the SIF can thus be expressed in terms of an integral over the whole crack depth:

$$K\left(\xi; \frac{2B}{W}, \frac{D}{2B}\right) = \sqrt{R} \cdot \int_0^\xi \sigma(\tilde{x}) w_c\left(\tilde{x}, \xi; \frac{2B}{W}, \frac{D}{2B}\right) d\tilde{x}$$

The integration is carried out numerically using Gauss-Chebyshev quadrature with convergence check.

TC14 – Through-crack at edge of plate, subjected to remote displacement

Highlights:

- Two types of remote displacement input:
 - Displacement field derived from remote tension and remote in-plane bending
 - User-specified remote displacement (tabular input)
- Two displacement constraint types at the remote end
 - Type I: no constraint for displacements in the x-direction, displacement in the y-direction is user-defined
 - Type II: fixed constraint for displacements in x-directions, displacement in the y-direction is user-defined
- Requires user to provide Young's modulus and Poisson's ratio

TC14 is a new through-crack geometry allowing for user-specified remote displacements instead of applied loads or stresses. The coordinate system used to define TC14 is shown in the figure in the GUI. The user-defined displacement is defined by providing a displacement value (in the y-direction) as a function of x, $D(x)$. Two types of displacement constraints are available at the remote ends: Type I and Type II. Type I constraint designates that the remote ends are free to expand and contract along the x-direction, but are specified by the user as $D(x)$ in the y-direction. Type II constraint fixes the displacement in the x direction ($u(x) = 0$) and uses the user-specified displacement in the y-direction ($v(x) = D(x)$). Additionally, the user must specify the state of stress for the analysis: plane stress or plane strain. The scale factor for the displacement

solutions work in exactly the same fashion as with standard stress solutions; the scale factor multiplies (scales) the entire user-specified displacement gradient.

TC15 – Through-crack at edge of variable-thickness plate, weight function solution

Highlights:

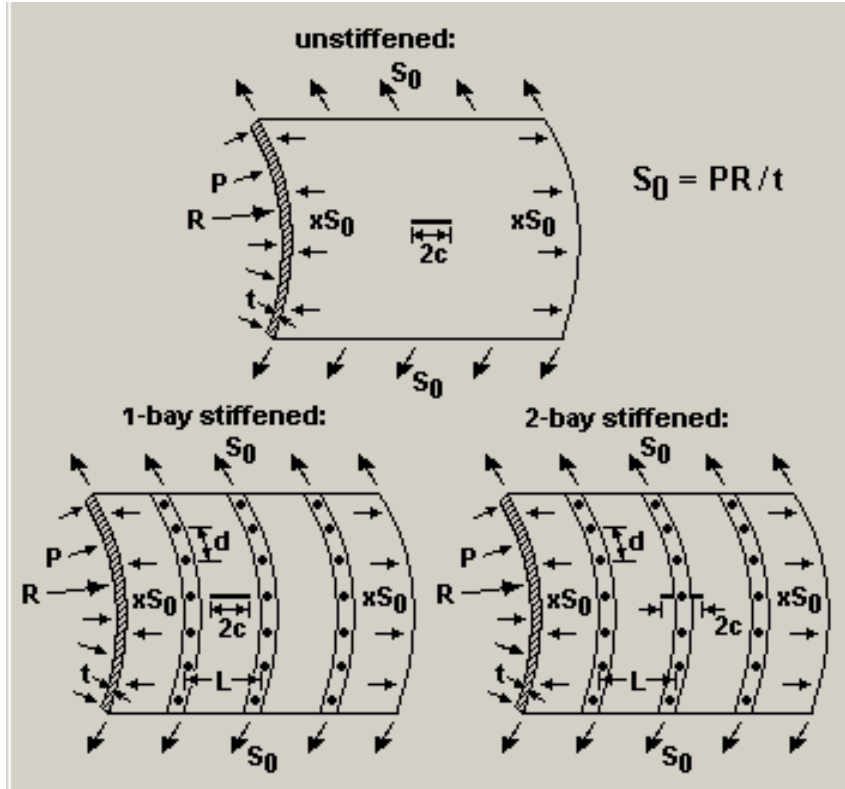
- Variable-thickness plate (symmetric about center of plate), with thickness varying smoothly with position
- Weight function solution, up to 4 stress distributions
- User-specified stress gradient entry

TC15 is a new through-crack geometry allowing for variable thickness as a function of x (along the width direction) and with a univariant nonlinear stress distribution (also as a function of x). A schematic of the TC15 geometry is shown in the figure in the GUI when TC15 is selected as the geometry for analysis.

The origin of the coordinate system defined for TC15 is placed at the intersection of the edge crack with the left surface at the center of the plate thickness (please see figure in the GUI). The x coordinate is the direction of crack propagation and is used to specify the variation of both the user-specified stress distribution and the thickness variation of the plate. The user-specified stress distribution can be defined in terms of any (user-specified) point spacing during stress gradient entry. The thickness variation in the plate is required to be symmetric about the central plane of the plate. Two options are provided for user input of the plate thickness variation: linear interpolation or hermite interpolation. For both options, a table is provided in the GUI (similar to the stress input table) for the user to define thickness as a function of non-dimensional position. If linear interpolation is selected, the analysis will use piecewise-linear interpolation of the thickness as a function of position. If hermite interpolation is selected, the analysis will use hermite polynomials to interpolate thickness as a function of position.

TC16 - Through Crack in Curved Panel with Bulging

Crack case TC16 accounts for nonlinear out-of-plane deformations (“bulging”) of the crack surfaces resulting from complex stress and displacement fields in pressurized fuselages. The crack case configurations include cracks in unstiffened fuselages as well as cracks in stiffened fuselages. The cracks in stiffened fuselages can be bay-centered (that is, wholly-contained within a panel bounded by stiffeners, also called 1-bay cracks) or frame-centered (that is, growing out of a stiffener between two panels, also called 2-bay cracks). The central stiffener for 2-bay cracks can be intact or broken.



Enhancements introduced in NASGRO v6.1:

- Swift bulge factor for 1-bay cracks
- Option for broken stiffeners for Swift and Chen-Schijve bulge factors for 2-bay cracks
- Nonzero biaxial load ratio enabled in Chen-Schijve model when compounded with the Rooke and Cartwright stiffened flat plate correction factor
- Damping factor F (to model incomplete damping due to the presence of particular types of stiffeners) added to the Chen-Schijve models

Enhancements introduced in NASGRO v6.2:

- Interpolation between the three Rooke and Cartwright ratios of rivet spacing to stiffener spacing

Aircraft companies typically account for bulging in curved fuselage panels by using a bulge factor to serve as a “correction” factor on the comparable K for a flat sheet of the same material, thickness, and crack size:

$$K = \beta_{\text{bulge}} \beta \sigma \sqrt{\pi c} \quad (1)$$

where K is the SIF for the curved fuselage panel, β_{bulge} is the bulge factor, and β is the usual geometric correction factor. For stiffened fuselage panels, β also contains information on the stiffener geometry. All loading is assumed to stem from the internal pressure, and while both hoop and longitudinal stress are accounted for in the bulge factors expressions (via a stress biaxiality

ratio for those bulge factor expressions where stress biaxiality features), only the hoop stress (S_0) is available as input for NASGRO's fracture and crack growth equations.

Two bulge factor models are implemented in TC16: the Swift empirical model (developed largely for the DC-10) and the Chen-Schijve semi-empirical model (applicable to geometries ranging from commuter to large transport aircraft). Each bulge factor model can be applied to unstiffened panels, 1-bay stiffened panels, 2-bay stiffened panel with intact central stiffener, and 2-bay stiffened panel with broken central stiffener.

For stiffened panel configurations the bulge factors can be optionally compounded by the Rooke-Cartwright stiffened flat sheet correction factor.

Notes and Limitations of the Bulge and Correction Factors

Crack size limits (L is the stiffener spacing):

- a) $c \geq 0$ for cracks in unstiffened panels.
- b) $0 \leq c \leq L/2$ for one-bay cracks.
- c) $0 \leq c \leq L$ for two-bay cracks.

Limitations of the Bulge Factor solutions:

- a) The Swift model:
 - i) Stiffeners should be at least 20" apart.
 - ii) Users have reported unconservative results for large crack sizes.
- b) The Chen and Schijve model:
 - i) Fuselage radius ranging from 60" to 120".
 - ii) Pressure ranging from 1.4psi to 14.7psi. Note that the solution is well-behaved outside of this range except at $P=0$, where it is singular. NASGRO allows computations to continue for $P > 14.7$ and for $0 \leq P < 1.4$. To evaluate $P=0$ (a realistic case), NASGRO uses $P=1e-6$ as a limiting value instead.
 - iii) Skin thickness ranging from 0.025" to 0.1".
- c) Effects of longerons are not considered.

Limitations of the Rooke and Cartwright stiffened sheet correction factors:

- a) Rooke and Cartwright cite studies showing that correction factors are insensitive to a value of the ratio of rivet diameter to rivet spacing of less than 0.25; their correction factor development assumes a "typical aerospace structures" value of 0.25 for this ratio.
- b) Correction factor curves are published for
 - i) 3 values of d/L , the ratio of rivet spacing to stiffener spacing: 1/3, 1/6, 1/12; starting with version 6.2, NASGRO accepts any user-supplied value of d/L between (and including) 1/3 and 1/12 and interpolates the correction factor.
 - ii) 4 values of μ , the ratio of stiffener stiffness to combined stiffness of the stiffener and sheet: 0.1, 0.2, 0.3, 0.5.
 - iii) c/L , the ratio of half crack size to stiffener spacing, ranging from 0.05 to 1.45 for the intact stiffener case.
 - iv) c/L ranging from 0.02 to 1.45 (exception: 0.06 to 1.45 for the $\mu=0.5$ and $d/L=1/12$ curve) for the broken stiffener case.

- v) Although the upper limit is 1.45 on the Rooke and Cartwright published curves, NASGRO uses an upper limit of 1 to match the range of validity of the bulge factor models.
- c) Users have reported that the lower limits of the c/L range of the Rooke and Cartwright curves are too high for realistic analyses; NASGRO extrapolates these curves back to $c/L=0$ using the following rationale:
 - i) For intact stiffeners, the correction factors approach 1 asymptotically as c/L approaches 0; this allows simple extrapolation to $c/L=0$ without concern.
 - ii) For broken stiffeners, the correction factors increase rapidly as c/L approaches 0 for some of the curves. NASGRO extrapolates these curves to approximate finite values at $c/L=0$. These values are thought to be reasonable and are based on user experience; however, they have not been rigorously tested by the NASGRO team.
- d) Since the Rooke and Cartwright curves were derived for uniaxial tension only, NASGRO's original implementation forced the biaxial load ratio to 0 in the Chen-Schijve model if it was compounded with the Rooke and Cartwright correction factor. However, some NASGRO users have found that allowing nonzero biaxial load ratios can bring the analysis more in line with test results, although it reduces the conservatism resulting from a zero load ratio. Starting in NASGRO 6.1, users may specify a nonzero biaxial load ratio when the Chen-Schijve model is compounded with the Rooke-Cartwright correction factor.

The Swift Bulge Factor Model

The basis for Swift's bulge factors is Kuhn's commonly-used empirical bulge factor for unstiffened cylinders

$$\beta_{bulge} = 1 + 5 \left(\frac{2c}{R} \right) \quad (2)$$

where c is the half crack length and R is the cylinder radius.

For stiffened shells Swift introduced a cosine function to account for the bulging effects damping out as the crack tip nears a stiffener. For 1-bay cracks this takes the form

$$\beta_b = 1 + 5 \left(\frac{2c}{R} \right) \left[\cos\left(\frac{\pi c}{L}\right) + F \left\{ 1 - \cos\left(\frac{\pi c}{L}\right) \right\} \right] \quad (3)$$

where F is the ratio of bulging at the stiffener to maximum bulging at mid-bay and accounts for incomplete damping. For example, when stiffening includes a substantial frame member reinforced by a crack stopper strap, bulging is completely damped ($F=0$); this may not be the case for a lighter stiffener or in absence of a strap. F is assumed to be known by the analyst; NASGRO provides a default value of 0.

Swift noted that maximum bulging for 2-bay cracks with intact stiffeners occurs when crack tips are halfway between stiffeners, especially when stiffener spacing L is at least 20". He found that the magnitude of the bulging effect could be estimated by evaluating the unstiffened equation (Eq.

2) at mid-bay (note that for purposes of scaling the bulging effect only, equation 2 is evaluated using a half-crack length of $2c$ -- the rest of the bulge factor development assumes a half crack length of c):

$$\beta_{bulge} = 1 + 5 \left(\frac{L/2}{R} \right) \left[\frac{1 + \cos(2\pi x/L)}{2} + F \frac{1 - \cos(2\pi x/L)}{2} \right] \quad (4)$$

where x is the distance from mid-bay to crack tip (measured positively from mid-bay to the outer stiffener: $x = c - L/2$).

Since a broken central stiffener does not contribute significantly to bulging, it is common practice to assume that the 2-bay broken stiffener solution is essentially the same as the 1-bay solution, albeit with twice the stiffener spacing:

$$\beta_b = 1 + 5 \left(\frac{2c}{R} \right) \left[\cos\left(\frac{\pi c}{2L}\right) + F \left\{ 1 - \cos\left(\frac{\pi c}{2L}\right) \right\} \right] \quad (5)$$

Note that the Swift models neglect nonlinear effects due to internal pressure and can thereby overestimate the bulge factor.

The Chen-Schijve Bulge Factor Model

Noting that simple expressions such as Swift's can overestimate the bulge factor because they ignore the nonlinear effects due to internal pressure, Chen and Schijve (1990) combined empirical and analytical approaches to derive the following expression for the bulge factor for an unstiffened curved panel:

$$\beta_{bulge} = \sqrt{1 + M} \quad (6)$$

where

$$M = \frac{5}{3\pi} \frac{Etc}{R^2 P} \frac{0.316}{\sqrt{1+18\chi}} \tanh \left[0.06 \left(\frac{R}{t} \right) \sqrt{\frac{Pc}{Et}} \right] \quad (7)$$

and E = skin elastic modulus, t = skin thickness, c = half crack length, R = fuselage radius, P = pressure, and χ = stress biaxiality ratio ($\sigma_{long}/\sigma_{hoop}$).

Drawing upon Tom Swift's observation that the bulging effect is damped out as the crack tips approach stiffeners, equation (6) was extended to stiffened panels by applying a damping function D similar to Swift's damping function:

$$\beta_{bulge} = \sqrt{1 + MD} \quad (8)$$

Chen and Schijve's damping function did not include an "incomplete damping" factor similar to Swift's F (to model incomplete damping due to the presence of particular types of stiffeners),

however it can be argued that since Chen and Schijve drew inspiration for their damping function from Swift, they could easily have included F in their formulation but chose not to. In addition, NASGRO users have found that inclusion of incomplete damping brings analysis more in line with test results. It is proposed to implement these requests as described below:

For a 1-bay crack of half crack length c , M is given by equation (7) and D was originally given by Chen and Schijve as

$$D = \frac{1 + \cos(2\pi c/L)}{2} \quad (9a)$$

Starting with NASGRO 6.1, this was modified to

$$D = \frac{1 + \cos(2\pi c/L)}{2} + F \frac{1 - \cos(2\pi c/L)}{2} \quad (9b)$$

For a 2-bay crack of half crack length c with an intact stiffener, M is given by

$$M = \frac{5}{12\pi} \frac{EtL}{R^2 P} \frac{0.316}{\sqrt{1+18\chi}} \tanh \left[0.06 \left(\frac{R}{t} \right) \sqrt{\frac{PL}{4Et}} \right] \quad (10)$$

and D , originally given by

$$D = \frac{1 - \cos(2\pi c/L)}{2} \quad (11a)$$

was modified, starting with NASGRO 6.1 to

$$D = \frac{1 - \cos(2\pi c/L)}{2} + F \frac{1 + \cos(2\pi c/L)}{2} \quad (11b)$$

where equation (10) reflects the bulging effect reaching a maximum at mid-bay and follows Swift's method of using a half crack length of $2c$ to scale the bulge factor magnitude.

Chen and Schijve did not discuss a formulation for 2-bay cracks with broken central stiffeners, but the NASGRO team feels confident that Swift's rationale for extending his 1-bay model to this configuration can be applied to the Chen and Schijve model as well. Thus M is given by equation (7) and D can be derived from equation (9b) by simply using twice the stiffener spacing

$$D = \frac{1 + \cos(\pi c/L)}{2} + F \frac{1 - \cos(\pi c/L)}{2} \quad (12)$$

Note that while this is thought to be a reasonable extension of the Chen and Schijve model, it has not been verified experimentally.

The Rooke-Cartwright Correction Factor for Stiffened Sheets

This solution models an infinite flat sheet reinforced by a periodic set of stiffeners attached at discrete intervals by a single row of rigid fasteners.

In the derivation each stiffener is represented as a distribution of point forces where the distribution is determined so that compatibility of displacements and equilibrium of forces between the sheet and stiffeners are satisfied.

The forces at the points of attachment (the rivet locations) are obtained by solving a set of simultaneous equations arising from the compatibility conditions. The load concentration in each stiffener is obtained by summing the point forces and adding this to the uniform end load on the stiffener.

The stress intensity factor is then obtained by summing the effects of these forces and using a Green's function for a single force, and adding the result to that for a crack in a uniformly loaded sheet.

Rooke and Cartwright published their results as a series of curves of correction factors ($\beta = K_I / \sigma\sqrt{\pi c}$) as a function of the ratio of half crack size c to stiffener spacing L for the following parameter variations:

- The ratio of rivet spacing d to stiffener spacing L : $d/L = 1/3, 1/6, 1/12$.
- The ratio of the stiffness of the stiffeners to the stiffness of the stiffeners and sheet combined: $\mu = 0.1, 0.2, 0.3, 0.5$, where $\mu = A_s E_s / (A_s E_s + L t E)$, A_s and E_s are the cross-sectional area and the stiffness of the stiffener, respectively, and t and E are the thickness and the stiffness of the sheet, respectively.

The NASGRO team has digitized these curves (with the caveat regarding extrapolation to $c/L=0$ noted in the Limitations section above) in the tables below.

Table I: Rooke-Cartwright Factors for One-Bay Cracks

c/L	d/L=1/3				d/L=1/6				d/L=1/12			
	$\mu=0.1$	$\mu=0.2$	$\mu=0.3$	$\mu=0.5$	$\mu=0.1$	$\mu=0.2$	$\mu=0.3$	$\mu=0.5$	$\mu=0.1$	$\mu=0.2$	$\mu=0.3$	$\mu=0.5$
0.0	1.0	1.0	1.0	1.0	1.0	1.0	1.0	1.0	1.0	1.0	1.0	1.0
0.25	0.99	0.98	0.97	0.958	0.992	0.98	0.972	0.955	0.989	0.98	0.97	0.95
0.275	0.988	0.978	0.961	0.945	0.991	0.97	0.963	0.94	0.985	0.976	0.964	0.942
0.3	0.98	0.97	0.956	0.932	0.983	0.968	0.955	0.93	0.982	0.97	0.958	0.932
0.325	0.977	0.961	0.94	0.918	0.979	0.96	0.944	0.915	0.979	0.961	0.945	0.918
0.35	0.97	0.955	0.93	0.9	0.974	0.948	0.93	0.898	0.973	0.95	0.935	0.9
0.375	0.962	0.94	0.912	0.878	0.964	0.938	0.911	0.871	0.964	0.936	0.915	0.875
0.4	0.955	0.925	0.895	0.85	0.954	0.918	0.882	0.84	0.953	0.916	0.884	0.84
0.425	0.941	0.908	0.875	0.82	0.936	0.888	0.849	0.798	0.936	0.881	0.852	0.8
0.45	0.933	0.89	0.855	0.79	0.908	0.855	0.805	0.742	0.905	0.843	0.798	0.733

0.475	0.92	0.862	0.825	0.755	0.875	0.81	0.752	0.681	0.844	0.76	0.7	0.625
0.5	0.905	0.84	0.8	0.72	0.835	0.75	0.69	0.606	0.75	0.638	0.58	0.5
0.55	0.88	0.795	0.742	0.66	0.754	0.64	0.57	0.488	0.572	0.456	0.395	0.33
0.6	0.85	0.76	0.7	0.605	0.7	0.572	0.503	0.423	0.542	0.44	0.384	0.32
0.65	0.825	0.725	0.66	0.565	0.674	0.555	0.486	0.41	0.562	0.462	0.412	0.356
0.7	0.81	0.7	0.63	0.54	0.67	0.558	0.493	0.42	0.581	0.487	0.442	0.385
0.75	0.795	0.685	0.618	0.53	0.677	0.57	0.507	0.44	0.599	0.51	0.464	0.412
0.8	0.787	0.678	0.608	0.525	0.68	0.58	0.518	0.457	0.61	0.528	0.481	0.433
0.85	0.78	0.675	0.605	0.524	0.687	0.592	0.53	0.47	0.62	0.542	0.5	0.45
0.9	0.775	0.672	0.61	0.53	0.692	0.6	0.542	0.48	0.63	0.556	0.515	0.46
0.95	0.772	0.674	0.618	0.535	0.696	0.603	0.554	0.49	0.638	0.564	0.523	0.478
1	0.77	0.675	0.63	0.54	0.699	0.61	0.558	0.499	0.645	0.575	0.535	0.49

Table II: Rooke-Cartwright Factors for Two-Bay Cracks, Intact Central Stiffener

c/L	d/L=1/3				d/L=1/6				d/L=1/12			
	$\mu=0.1$	$\mu=0.2$	$\mu=0.3$	$\mu=0.5$	$\mu=0.1$	$\mu=0.2$	$\mu=0.3$	$\mu=0.5$	$\mu=0.1$	$\mu=0.2$	$\mu=0.3$	$\mu=0.5$
0.0	1.0	1.0	1.0	1.0	1.0	1.0	1.0	1.0	1.0	1.0	1.0	1.0
0.05	0.994	0.988	0.98	0.973	0.96	0.94	0.925	0.912	0.87	0.84	0.82	0.79
0.1	0.978	0.963	0.95	0.934	0.908	0.87	0.84	0.809	0.792	0.742	0.72	0.683
0.15	0.959	0.935	0.91	0.882	0.867	0.814	0.77	0.745	0.773	0.72	0.693	0.665
0.2	0.938	0.901	0.87	0.83	0.842	0.784	0.747	0.71	0.77	0.72	0.686	0.663
0.25	0.922	0.876	0.84	0.793	0.837	0.772	0.741	0.698	0.776	0.722	0.689	0.662
0.3	0.91	0.857	0.82	0.768	0.832	0.768	0.735	0.69	0.78	0.727	0.693	0.661
0.35	0.902	0.842	0.805	0.75	0.83	0.766	0.731	0.686	0.781	0.732	0.698	0.662
0.4	0.898	0.834	0.795	0.736	0.829	0.766	0.73	0.685	0.784	0.736	0.7	0.665
0.45	0.892	0.824	0.783	0.724	0.828	0.765	0.73	0.683	0.788	0.738	0.702	0.667
0.5	0.886	0.822	0.777	0.718	0.827	0.765	0.73	0.682	0.791	0.739	0.705	0.669
0.55	0.878	0.82	0.77	0.71	0.826	0.765	0.729	0.68	0.796	0.7395	0.709	0.667
0.6	0.877	0.817	0.765	0.703	0.826	0.765	0.727	0.678	0.798	0.74	0.71	0.664
0.65	0.876	0.81	0.76	0.7	0.825	0.764	0.725	0.678	0.796	0.739	0.708	0.665
0.7	0.875	0.802	0.757	0.697	0.825	0.763	0.722	0.676	0.792	0.738	0.705	0.66
0.75	0.869	0.797	0.748	0.688	0.824	0.758	0.715	0.665	0.79	0.735	0.702	0.655
0.8	0.861	0.782	0.738	0.674	0.82	0.75	0.705	0.65	0.782	0.727	0.698	0.645
0.85	0.858	0.774	0.72	0.652	0.812	0.737	0.69	0.626	0.778	0.715	0.678	0.622
0.9	0.846	0.759	0.697	0.62	0.793	0.712	0.663	0.595	0.764	0.692	0.652	0.59
0.95	0.83	0.73	0.665	0.582	0.767	0.672	0.615	0.535	0.73	0.642	0.59	0.523
1	0.805	0.696	0.628	0.54	0.7	0.592	0.52	0.44	0.6	0.48	0.42	0.36

Table III: Rooke-Cartwright Factors for Two-Bay Cracks, Broken Central Stiffener

c/L	d/L=1/3				d/L=1/6				d/L=1/12			
	$\mu=0.1$	$\mu=0.2$	$\mu=0.3$	$\mu=0.5$	$\mu=0.1$	$\mu=0.2$	$\mu=0.3$	$\mu=0.5$	$\mu=0.1$	$\mu=0.2$	$\mu=0.3$	$\mu=0.5$
0.0	1.17	1.36	1.56	2.16	1.34	1.65	2.07	3.25	2	3	4	10
0.02	1.16	1.35	1.558	2.15	1.31	1.625	2.025	3.07	1.74	2.46	3.245	-
0.04	1.155	1.335	1.545	2.125	1.285	1.58	1.938	2.86	1.54	2.05	2.49	-
0.06	1.15	1.32	1.53	2.098	1.26	1.538	1.87	2.7	1.4	1.79	2.175	3.5
0.08	1.145	1.31	1.515	2.06	1.235	1.482	1.788	2.545	1.3	1.63	1.97	2.985

0.1	1.135	1.292	1.494	2.02	1.21	1.442	1.73	2.4	1.235	1.52	1.81	2.67
0.15	1.119	1.262	1.44	1.91	1.152	1.345	1.57	2.09	1.13	1.34	1.57	2.185
0.2	1.102	1.237	1.39	1.79	1.12	1.28	1.458	1.89	1.1	1.27	1.43	1.9
0.25	1.085	1.205	1.33	1.687	1.086	1.22	1.36	1.73	1.098	1.22	1.35	1.75
0.3	1.075	1.175	1.285	1.593	1.07	1.18	1.292	1.612	1.095	1.19	1.293	1.625
0.35	1.068	1.15	1.242	1.505	1.065	1.15	1.242	1.515	1.094	1.163	1.257	1.54
0.4	1.058	1.13	1.21	1.439	1.06	1.13	1.212	1.44	1.092	1.145	1.215	1.475
0.45	1.047	1.108	1.176	1.38	1.05	1.11	1.18	1.38	1.073	1.12	1.196	1.422
0.5	1.04	1.09	1.157	1.334	1.048	1.098	1.162	1.337	1.065	1.105	1.17	1.38
0.55	1.035	1.075	1.135	1.285	1.0375	1.08	1.145	1.292	1.06	1.1	1.135	1.325
0.6	1.027	1.065	1.118	1.248	1.028	1.06	1.12	1.251	1.05	1.096	1.1	1.292
0.65	1.018	1.05	1.1	1.203	1.02	1.052	1.099	1.22	1.04	1.07	1.07	1.24
0.7	1.01	1.04	1.08	1.168	1.015	1.05	1.08	1.18	1.035	1.065	1.065	1.2
0.75	1.004	1.022	1.055	1.123	1.005	1.048	1.05	1.13	1.02	1.05	1.05	1.155
0.8	1.002	1.005	1.0275	1.082	1	1.03	1.01	1.08	1.01	1.02	1.02	1.085
0.85	0.99	0.985	0.985	1.025	0.991	0.991	0.95	1.015	1	1	1	1.01
0.9	0.97	0.95	0.94	0.95	0.96	0.94	0.88	0.925	0.945	0.965	0.935	0.9
0.95	0.946	0.91	0.88	0.86	0.915	0.87	0.8	0.81	0.88	0.86	0.8	0.745
1	0.915	0.86	0.825	0.77	0.85	0.7825	0.72	0.69	0.75	0.7	0.65	0.58

References: [C50, C51, C52, C53, C54]

TC17 – Through Crack at Edge Notch in Plate – Univariant WF

The TC17 crack case is for a through-thickness crack at the tip of an edge notch in a plate. The SIF solution is based on the weight function formulation for crack case TC12. The generality of the weight function formulation is valid for a crack at the tip of an edge notch of arbitrary shape. Nevertheless, for user convenience, only two common types of notch shape are supported in the GUI. Respectively, they are angular straight-edge notch and elliptical notch that are defined by their own unique sets of geometric parameters.

The formulation requires specification of the variation of the stress component normal to the net section plane in an uncracked plate. The user-specified load types can be in terms of either global loading applied remotely (tension-bend) or local stressing on the crack plane along the net section resulting from the edge notch. Crack case TC17 provides consistent stress intensity factor results between these two load specifications. The following describes each stress input form:

1. The loading applied at the remote ends is to be represented by two stress components: uniform tension and linear in-plane bending, with individual magnitudes specified in the GUI for load block definition. The fracture mechanics module computes the net section stress variations internally through interpolation. The weight function formulation is then utilized to calculate the stress intensity factor. For this load type, the shakedown option is provided as a result of alleviated stress gradient near the notch tip.
2. The loading specified in terms of stress variations on the crack plane along the net section can be expressed either by polynomial function or in tabulated form. However, only the tabulated stress form has the shakedown option. The polynomial is expressed mathematically by a six-order function in terms of normalized parameter x/b , where x is measured from the notch tip and b is the width of the net section, and the variation is

given by $\sigma(x) = \sum_{j=0}^6 C_j \cdot (x/b)^j$ with coefficients C_j 's provided by the user. For specifying stress variations in tabulated form, the user is required to specify the stress variation as a function of normalized coordinate using data pairs of $[(x/b)_i, S_i]$, where S_i is the stress at $x = x_i$ with x -coordinate originating from the notch tip. Note the data arrangement needs to be sorted in advance in ascending order.

Since the weight function formulation for this crack case is the same as the one developed for an edge crack – crack case TC12, a similar geometry validity range is available. Respectively, depending on the edge notch shape, the validity range is listed as follows. For schematics, please refer to the bitmap depicted in Geometry GUI tab for crack case TC17.

- Angular notch

$$0 \leq \theta \leq 75^\circ$$

$$0 \leq \frac{d+r}{W} \leq 0.75$$

$$0 \leq \frac{d}{r} \leq 24$$

$$\frac{c}{W-d-r} \leq 0.9$$

where θ is the angle enclosed by the straight edges of the notch, d is the nominal depth of the notch measured from the edge surface of the plate to the center of the root radius of the notch, r is the root radius of the curvature at the notch tip, W is the width of the plate, and c is the crack depth originating from the notch tip. Note that the solution is independent of the angle θ over the range specified, and therefore input of θ is not solicited.

- Elliptical notch

$$0.2 \leq \frac{e_1}{e_2} \leq 5$$

$$0 \leq \frac{e_1 - B}{W} \leq 0.75$$

$$\frac{c}{W + B - e_1} \leq 0.9$$

$$0 \leq B < e_1$$

where e_1 and e_2 define the long and the short axes of the elliptical perimeter of the notch, B is the offset of the ellipse away from the edge surface of the plate, W is the width of the plate, and c is the crack depth emanating from the notch tip. The offset of the ellipse B is always assumed away from the edge surface of the plate instead of into the plate.

The weight function is expressed by a five-term series expansion around the crack tip location at $\tilde{x} = \tilde{c}$, and the stress intensity factor derived from weight function formulation is defined by

$$K_I = f\sqrt{\pi c}$$

where the factor f is defined by

$$f = \frac{1}{\sqrt{2\pi}\tilde{c}} \int_0^{\tilde{c}} \sigma(\tilde{x}) \left[\sum_{i=1}^5 \beta_i \left(1 - \frac{\tilde{x}}{\tilde{c}}\right)^{i-\frac{3}{2}} \right] d\tilde{x}$$

The symbols with tilde denote normalized parameters by the net section width b ; i.e., $\tilde{c} = c/b$ and $\tilde{x} = x/b$, and the coefficients in the weight function, β_i 's are the same as those for crack case TC12. Since the formulation requires the stress to be defined locally; i.e., along the net section plane, the variation of stress component normal to the net section plane for loading applied remotely needs to be determined internally. This conversion is performed internally in the program through interpolation among reference net section stress solutions associated with discrete geometric parameters. The reference net section stress solutions are tabulated and stored in the program, and the reference stresses for determining the reference net section stresses are unit remote tension and bending.

TC18 – Through Crack(s) at (Offset) Embedded Slot or Elliptical Hole in Plate - Univariant WF

The TC18 crack case is for a through-thickness crack (or two symmetrical through-thickness cracks) at the notch tip(s) of an (offset) embedded slot or elliptical hole in a plate. The SIF solution is based on the same weight function formulation developed for crack case TC13. This crack case is based on certain assumptions on the geometries of the hole and the crack. To be specific, they are listed as follows:

- The shape of the embedded hole is assumed to be symmetrical to its own vertical and horizontal axes.
- The hole is located at the horizontal symmetric axis of the plate.
- For the one-crack configuration, the crack is required to be located at the notch tip of the embedded hole associated with the smaller net section, or the tip closer to the edge surface of the plate.
- For the two-crack configuration, the symmetry in geometry and loading needs to be preserved to ensure two cracks of equal depths. This imposes two requirements on applying this configuration: (1) the embedded hole is required to be at the center of the plate, and (2) the loading needs to be symmetric to the central vertical axis of the plate.

The weight function formulation requires to be specified the variation of stress component normal to the net section plane in an uncracked plate. For the one-crack configuration where the crack is located at the notch tip closer to the edge surface of the plate, the stress variation is the one along the smaller net section. For the two-crack configuration, the stress variation at either net section is applicable on account of the symmetric conditions. The applied loads for this crack case are therefore always converted to the “local” stress variations along the net section even for loading applied remotely.

The user-specified load types can be in terms of either remote loading or local stressing on the crack plane along the net section resulting from the embedded hole. Crack case TC18 provides consistent stress intensity factor solutions between these load specifications. In the following each stress input form is described.

1. The loading applied at the remote ends is resolved into uniform tension and linear in-plane bending. Their individual magnitudes are specified in the GUI for load block definition. The remote loading is converted to net section stress variations internally in the program. The weight function formulation is then utilized to compute the stress intensity factors. The shakedown option is provided as a result of alleviated stress gradient near the notch tip.
2. The loading specified along the net section can be expressed either by polynomial function or in tabulated form. However, only the tabulated stress form has the shakedown option. The polynomial is expressed mathematically by a six-order function in terms of normalized parameter x/b , where x is measured from the notch tip and b is the width of the net section. The equation form is given by $\sigma(x) = \sum_{j=0}^6 C_j (x/b)^j$ with coefficients C_j 's provided by the user. Note the reference net section is always the one associated with the crack. For specifying stress variations in tabulated form, the user is required to provide the data pairs of $[(x/b)_i, S_i]$ to describe the stress variation, where S_i is the stress at $x = x_i$ with x -coordinate originating from the notch tip. Note the data arrangement needs to be sorted in advance in ascending order.

As indicated the weight function formulation for this crack case is the same as the one developed for crack case TC13, a similar geometry validity range is available. Respectively, depending on the shape of the embedded hole; i.e., embedded straight-edge slot or elliptical hole, the validity range is listed as follows. For schematics, please refer to the bitmap depicted in Geometry GUI tab for crack case TC18.

- Straight-edge embedded slot

$$0.1 \leq \frac{2B}{W} \leq 1$$

$$0 \leq \frac{d+r}{B} \leq 0.75$$

$$0 \leq \frac{d}{r} \leq 24$$

$$\frac{c}{B-d-r} \leq 0.99$$

where B is the offset of the slot measured from the edge surface of the plate, W is the width of the plate, d is one half of the nominal length of the slot, r is the root radius of the curvature at the notch tip, and c is the crack depth. The nominal length $2d$ defines the distance from one center of root radius to the other center, and thus $2(d+r)$ is the distance between two notch tips.

- Elliptical embedded hole

$$0.2 \leq \frac{e_1}{e_2} \leq 5$$

$$0.1 \leq \frac{2B}{W} \leq 1$$

$$B > e_1$$

$$0 \leq \frac{e_1}{B} \leq 0.75$$

$$\frac{c}{B - e_1} \leq 0.99$$

where e_1 and e_2 define the long and the short axes of the elliptical shape of the hole, B is the offset of the hole measured from the center to the edge surface of the plate, W is the width of the plate, and c is the crack depth emanating from the notch tip.

The same weight function formulation for TC13 is used. The stress intensity factor solution for a general stress variation is thus defined by

$$K_I \left(\tilde{c}; \frac{2B}{W}, \frac{D}{2B} \right) = \sqrt{R} \int_0^{\tilde{c}} \sigma(\tilde{x}) w_c \left(\tilde{x}, \tilde{c}; \frac{2B}{W}, \frac{D}{2B} \right) d\tilde{x}$$

where the weight function is

$$w_c \left(\tilde{x}, \tilde{c}; \frac{2B}{W}, \frac{D}{2B} \right) = \frac{1}{\sqrt{2\pi\tilde{c}}} \sum_{i=1}^5 \beta_i \left(\tilde{c}; \frac{2B}{W}, \frac{D}{2B} \right) \left(1 - \frac{\tilde{x}}{\tilde{c}} \right)^{i-\frac{3}{2}}$$

The symbols with tilde denote normalized parameters by the net section width b ; i.e., $\tilde{c} = c/b$ and $\tilde{x} = x/b$. The coefficients of the weight function w_c are designated by β_i 's. They are identical to those used in crack case TC13 and are a function of normalized crack depth \tilde{c} , normalized offset $\tilde{B} = B/(W/2)$ and normalized radius $\tilde{R} = (D/2)/B$ of the hole. The definition of D depends on the shape of the embedded hole. For an embedded straight-edge slot, $D = 2(d + r)$. For an elliptical hole, $D = 2e_1$. Accordingly the definition for the net section width also alternates according to the shape of the embedded hole. Respectively, the reference width is $b = B - d - r$ for a straight-edge slot, and $b = B - e_1$ for an elliptical hole.

For loading applied remotely, the variation of stress component normal to the net section plane is estimated internally. This conversion is performed in the program through interpolation among reference net section stress solutions associated with discrete geometric parameters. The reference net section stress solutions are determined and stored inside the program. They are in reference to two reference stresses: unit remote tension and bending.

TC19 – Through crack at hole (offset) in plate with broken ligament – univariant WF

The TC19 crack case is for a through-thickness crack at a hole in a plate with one of the net sections completely broken through. The crack should be at the exact opposite side of the hole with respect to the broken ligament. It is treated as one of the special configurations in crack case TC17 in view of the very minimum effect of notch opening to the net section stress variation. This crack case can be used to describe the continuous damage scenario after the smaller net section in TC13 crack case is broken through and a through-thickness crack initiates at the opposite side of the hole. The broken ligament is represented by two parallel edge surfaces with

an infinitesimal gap. For a cracked configuration with an edge notch such as this crack case, the distance of the gap does not play a role in affecting the SIF solutions as long as this distance is smaller than the diameter of the hole. The key geometric parameters are the offset of the hole and the diameter of the hole. The offset can be determined as the sum of the broken net section and the radius of the hole. The crack length at the notch tip is designated by c and is always measured from the bore surface. The loading can be specified as a result of remote simple tension and in-plane bending, or crack opening stress variations in reference to uncracked configuration across the net section. Note the sign for in-plane bending is designated as positive at the edge surface with broken ligament ensuring the crack at the notch tip remains open.

As indicated, the user-specified loading can be in terms of either remote loading or local stressing along the remaining net section. Crack case TC19 provides consistent stress intensity factor solution among these load specifications. The following describes each stress input form:

1. The loading applied at the remote ends is resolved into uniform tension and linear in-plane bending. Their individual magnitudes are specified in the GUI for load block definition. The remote loading is converted to net section stress variations internally in the program. The weight function formulation is then utilized to compute the stress intensity factors. The shakedown option is also provided as a result of alleviated stress gradient near the notch tip.
2. The loading specified along the net section can be in terms of either polynomial function or data pairs in tabulated form. However, only the tabulated stress form has the shakedown option. The polynomial is expressed mathematically by a six-order function with normalized parameter x/b , where x is measured from the notch tip and b is the width of the remaining net section. The stress variation is thus defined by $\sigma(x) = \sum_{j=0}^6 C_j (x/b)^j$ with coefficients C_j 's provided by the user. For specifying stress variations in tabulated form, the user is required to provide the variations of stress component normal to the crack plane as a function of normalized coordinate; i.e., pairs of $[(x/b)_i, S_i]$, where S_i is the stress at the x_i -coordinate originating from the notch tip. Note the data arrangement needs to be sorted in advance in ascending order.

The similar geometry validity limits to those for TC12 are used. Respectively, they are listed in the following. For schematics, please refer to the bitmap depicted in Geometry GUI tab for crack case TC19.

$$0 \leq \frac{B + D/2}{W} \leq 0.75$$

$$0 \leq \frac{2B}{D} \leq 24$$

$$\frac{c}{W - B - \frac{D}{2}} \leq 0.9$$

where D is the diameter of the hole, B is the offset of the hole encompassing the broken ligament, and W is the width of the plate.

The stress intensity factor solutions with stress variation across the net section $\sigma(x)$ is given by

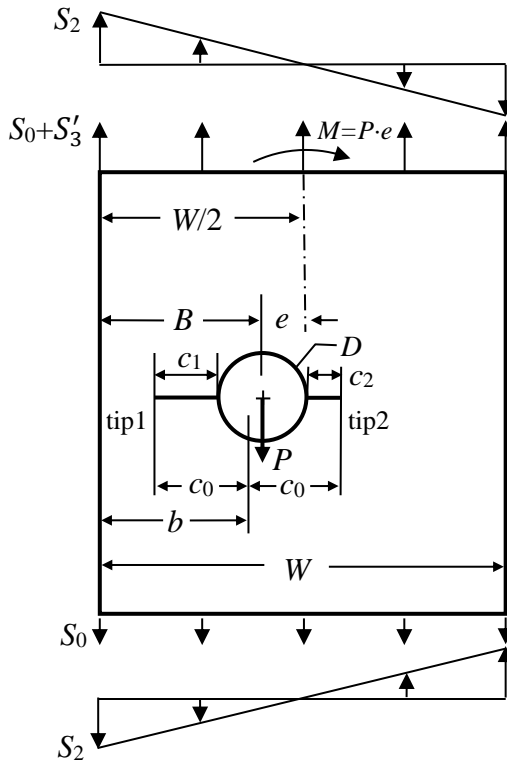
$$K_I = f \sqrt{\pi c}$$

where the factor f is defined by

$$f = \frac{1}{\sqrt{2}\pi\tilde{c}} \int_0^{\tilde{c}} \sigma(\tilde{x}) \left[\sum_{i=1}^5 \beta_i \left(1 - \frac{\tilde{x}}{\tilde{c}}\right)^{i-\frac{3}{2}} \right] d\tilde{x}$$

The normalized parameters are with respect to the remaining net section width $b = W - B - D/2$; i.e., $\tilde{c} = c/b$ and $\tilde{x} = x/b$, and the coefficients of the weight function, β_i 's are the same as those for crack case TC12. For loading applied remotely, the variation of stress component normal to the net section plane is determined internally. Please refer to the description in the section for crack case TC17 for more detail.

TC23 – Unequal Straight Through Cracks at an Offset Hole



Configuration of TC23

- Load condition:
Remote tension (S_0), in-plane bending (S_2), and pin-load (P): $S_3 = P/(Dt)$ or $S'_3 = P/(Wt)$. P is positive if it tends to make the crack open. Pin load options are described in Section C11.
- Geometric dimensions:
Thickness: t
Width: W
Hole diameter: $D = 2R$
Distance from the hole center to the plate edge: B
- Cracks:

Diametric cracks with sizes c_1 and c_2 measured from hole edges. The solution also works for radial crack, i.e. either c_1 or c_2 can be zero.

- Derived dimensions:

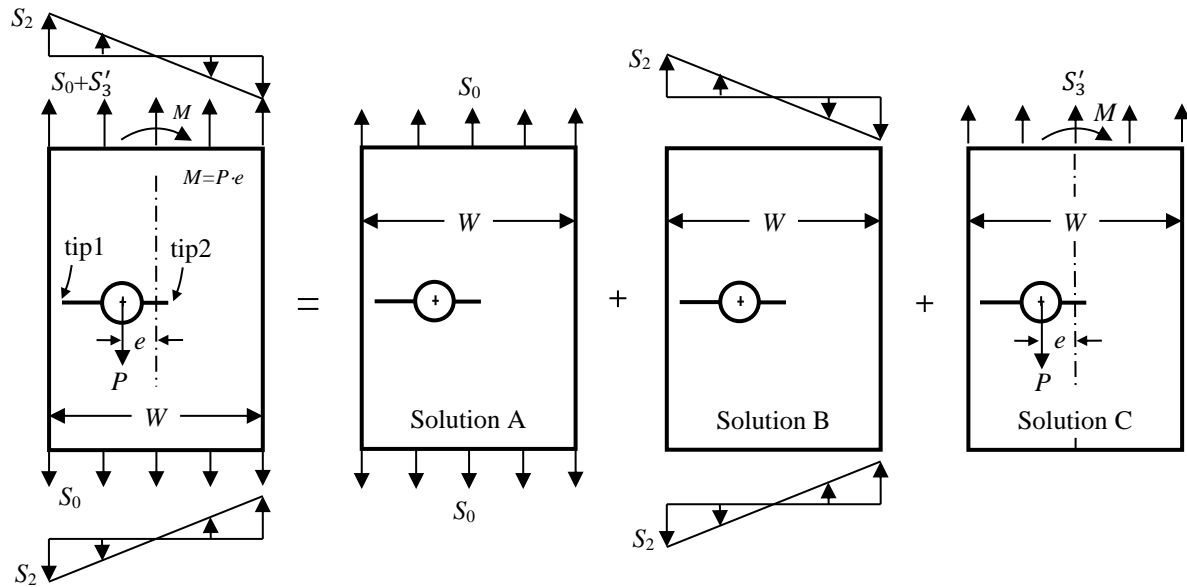
$$\text{Hole center offset: } e = W/2 - B$$

$$\text{Half crack length from tip to tip: } c_0 = (c_1 + D + c_2)/2$$

$$\text{Distance from the center of the overall flaw to the plate edge: } b = B + (c_2 - c_1)/2.$$

STRESS INTENSITY FACTORS

The stress intensity factors of the crack case are obtained by the principle of superposition:



$$K_i = K_i^A + K_i^B + K_i^C$$

where i is crack tip index ($i=1$ for crack tip 1, and 2 for crack tip 2). K_i^A is the stress intensity factor under remote tension (solution A). K_i^B is the stress intensity factor under in-plane bending (solution B). K_i^C is the stress intensity factor under pin-load (solution C).

- Solution A

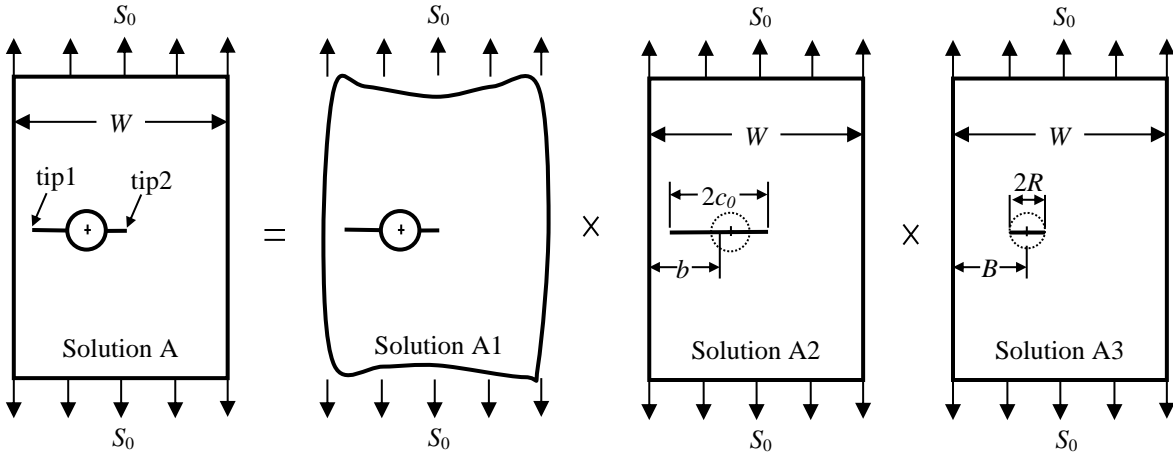
The stress intensity factors under remote tension (S_0) are calculated by

$$K_i^A = \beta_i^A S_0 \sqrt{\pi c_i}$$

The beta factors (β_i^A) are obtained by the compounding scheme shown below.

$$\beta_i^A = \prod_{j=1}^3 \beta_i^{A_j}$$

where j is sub-solution index. Closed-form solutions are available for the beta factors ($\beta_i^{A_j}$).



- Solution A1: unequal cracks at a hole in an infinite plate under tension.

The solution was derived by Tweed and Rooke [C57], which requires solving coupled singular integral equations by numerical method, and is computationally intensive. The NRC of Canada developed several closed-form solutions to approximate the solution. The latest one is given as follows [C58]:

$$\beta_1^{A_1} = \frac{K_1^{A_1}}{S_0 \sqrt{\pi c_1}} = \beta_r(\rho_1) \beta_u(\gamma_2, \gamma_1) \sqrt{\frac{2c_0}{c_1 + D}}$$

$$\beta_2^{A_1} = \frac{K_2^{A_1}}{S_0 \sqrt{\pi c_2}} = \beta_r(\rho_2) \beta_u(\gamma_1, \gamma_2) \sqrt{\frac{2c_0}{c_2 + D}}$$

$$\gamma_i = \frac{c_i}{R} \quad i = 1, 2$$

$$\rho_i = \frac{c_i}{c_i + R} = \frac{\gamma_i}{\gamma_i + 1} \quad i = 1, 2$$

$$\beta_\gamma(\rho_i) = \sum_{k=0}^6 R_k \rho_i^k$$

$$\beta_u(\gamma_a, \gamma_b) = \frac{D_0 + D_1 \gamma_a + D_2 \gamma_a^2 + D_3 \gamma_b + D_4 \gamma_b^2 + D_5 \gamma_a \gamma_b + D_6 \gamma_a^2 \gamma_b + D_7 \gamma_a \gamma_b^2}{1 + D_8 \gamma_a + D_9 \gamma_a^2 + D_{10} \gamma_b + D_{11} \gamma_b^2 + D_{12} \gamma_a \gamma_b + D_{13} \gamma_a^2 \gamma_b + D_{14} \gamma_a \gamma_b^2}$$

k	R_k	D_k
0	3.364500	1.00000000
1	-7.209304	0.98654553
2	8.230965	0.03673931
3	-3.500286	0.90111374
4	-2.923363	-0.01711464
5	4.306705	2.26550938

6	-1.562110	0.08639597
7	-	3.52048868
8	-	1.12869498
9	-	0.05132827
10	-	0.90257160
11	-	-0.01714307
12	-	2.34770606
13	-	0.08386375
14	-	3.52544398

The error of the above closed-form solution is less than 1% for any $c/R \leq 500$, 1.3% for any $c/R \leq 1000$, and 2.7% for any $c/R \leq 6400$ according to reference [C56].

- Solutions A2 and A3 are finite width corrections accounting for the interaction between plate edge and the crack, and the interaction between plate edge and the hole. They are given by

$$\text{If } b \leq W/2: \quad \beta_1^{A_2} = \phi_1(c_0, b), \quad \beta_2^{A_2} = \phi_2(c_0, b)$$

$$\text{If } b > W/2: \quad \beta_1^{A_2} = \phi_2(c_0, W-b), \quad \beta_2^{A_2} = \phi_1(c_0, W-b)$$

$$\text{If } B \leq W/2: \quad \beta_1^{A_3} = \phi_1(R, B), \quad \beta_2^{A_3} = \phi_2(R, B)$$

$$\text{If } B > W/2: \quad \beta_1^{A_3} = \phi_2(R, W-B), \quad \beta_2^{A_3} = \phi_1(R, W-B)$$

$$\phi_1(\mu, \omega) = \left[\lambda_s + \frac{1 - \lambda_s}{4} (1 + \cos^{0.25}(\lambda_1))^2 \right] \sqrt{\sec(\lambda_1)}$$

$$\phi_2(\mu, \omega) = 1 + \frac{\sqrt{\sec(\lambda_{12})} - 1}{1 + 0.21 \sin \left(8 \arctan \left(\left(\frac{\lambda_1 - \lambda_2}{\lambda_1 + \lambda_2} \right)^{0.9} \right) \right)}$$

$$\lambda_1(\mu, \omega) = \frac{\pi\mu}{2\omega}$$

$$\lambda_2(\mu, \omega) = \frac{\pi\mu}{2W - 2\omega}$$

$$\lambda_{12}(\mu, \omega) = \frac{4}{7}\lambda_1 + \frac{3}{7}\lambda_2$$

$$\lambda_s(\mu, \omega) = \sin \left(\frac{\pi\lambda_2}{\lambda_1 + \lambda_2} \right)$$

- Solution B:

The stress intensity factors subjected to in-plane bending (S_2) are calculated by

$$K_i^B = \beta_i^B S_2 \sqrt{\pi c_i}$$

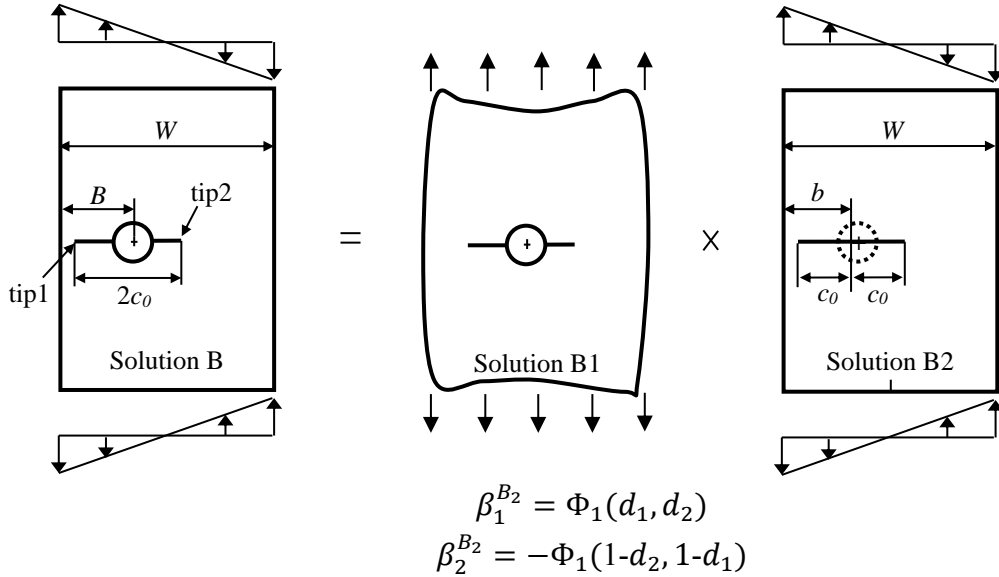
The beta factors (β_i^B) are obtained by the compounding scheme shown on next page,

$$\beta_i^B = \beta_i^{B_1} \cdot \beta_i^{B_2}$$

- Solution B1 accounts for the effect of the hole,

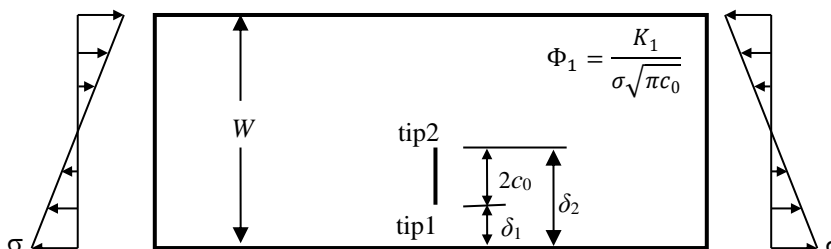
$$\beta_i^{B_1} = \beta_i^{A_1}$$

- $\beta_l^{B_2}$ is the beta factor of the overall crack of size $2c_0$ under bending, calculated by interpolating the benchmark beta factors obtained by the FEM, given in tabular form as a function of the two crack tip positions.



where $d_1 = (b-c_0)/W$ and $d_2 = (b+c_0)/W$ are the normalized distances from the left edge of the plate to crack tip 1 and tip 2, respectively. The benchmark beta factors (Φ_1) are obtained by the finite element method, and listed in the following table.

The benchmark beta factors (Φ_1) of a crack in a finite plate under in-plane bending at tip 1 as a function of crack tip locations obtained by the finite element method



δ_1/W	0.01	0.03	0.05	0.10	0.15	0.20	0.25	0.30	0.35	0.40	0.45	0.50
δ_2/W	0.01	1.003	1.016	1.007	0.980	0.946	0.908	0.865	0.816	0.759	0.694	0.619
0.03	1.059	0.940	0.924	0.900	0.866	0.827	0.782	0.731	0.674	0.611	0.542	0.465
0.05	1.158	0.947	0.900	0.850	0.809	0.764	0.714	0.660	0.600	0.535	0.465	0.389
0.10	1.353	1.013	0.909	0.800	0.735	0.677	0.619	0.558	0.495	0.428	0.357	0.283
0.15	1.508	1.084	0.942	0.787	0.700	0.630	0.564	0.499	0.433	0.364	0.293	0.220
0.20	1.645	1.149	0.977	0.785	0.681	0.600	0.528	0.458	0.389	0.319	0.247	0.174
0.25	1.774	1.209	1.011	0.788	0.668	0.578	0.500	0.427	0.355	0.283	0.211	0.137
0.30	1.897	1.264	1.042	0.791	0.658	0.560	0.477	0.400	0.326	0.253	0.179	0.106
0.35	2.014	1.312	1.068	0.792	0.647	0.543	0.456	0.376	0.300	0.226	0.151	0.077
0.40	2.122	1.353	1.087	0.790	0.636	0.526	0.435	0.353	0.276	0.200	0.125	0.051
0.45	2.217	1.384	1.100	0.784	0.622	0.508	0.414	0.330	0.250	0.175	0.100	0.025
0.50	2.296	1.405	1.104	0.773	0.605	0.488	0.392	0.307	0.228	0.151	0.075	0.000
0.55	2.354	1.413	1.099	0.757	0.585	0.465	0.369	0.283	0.203	0.126	0.050	-0.025
0.60	2.389	1.408	1.085	0.736	0.561	0.441	0.344	0.258	0.177	0.100	0.024	-0.051
0.65	2.398	1.391	1.062	0.710	0.535	0.415	0.317	0.231	0.151	0.073	-0.003	-0.077
0.70	2.381	1.361	1.031	0.680	0.506	0.386	0.288	0.202	0.122	0.045	-0.031	-0.106
0.75	2.339	1.320	0.993	0.646	0.474	0.354	0.257	0.171	0.091	0.013	-0.063	-0.137
0.80	2.274	1.270	0.949	0.608	0.438	0.320	0.223	0.136	0.055	-0.023	-0.099	-0.174

0.85	2.190	1.211	0.899	0.566	0.399	0.280	0.183	0.095	0.013	-0.067	-0.144	-0.220
0.90	2.091	1.146	0.844	0.519	0.352	0.232	0.133	0.042	-0.044	-0.126	-0.206	-0.283
0.95	1.977	1.070	0.778	0.457	0.287	0.162	0.055	-0.043	-0.136	-0.224	-0.309	-0.389
0.97	1.927	1.304	0.743	0.420	0.245	0.114	0.000	-0.104	-0.202	-0.295	-0.383	-0.465
0.99	1.867	0.983	0.689	0.352	0.162	0.015	-0.114	-0.231	-0.340	-0.442	-0.535	-0.619

$\frac{\delta_1}{W}$ $\frac{\delta_2}{W}$	0.55	0.60	0.65	0.70	0.75	0.80	0.85	0.90	0.95	0.97	0.99
0.01	0.535	0.442	0.340	0.231	0.114	-0.015	-0.162	-0.352	-0.689	-0.983	-1.867
0.03	0.383	0.295	0.202	0.104	0.000	-0.114	-0.245	-0.420	-0.743	-1.034	-1.927
0.05	0.309	0.224	0.136	0.043	-0.055	-0.162	-0.287	-0.457	-0.778	-1.070	-1.977
0.10	0.206	0.126	0.044	-0.042	-0.133	-0.232	-0.352	-0.519	-0.844	-1.146	-2.091
0.15	0.144	0.067	-0.013	-0.095	-0.183	-0.280	-0.399	-0.566	-0.899	-1.211	-2.190
0.20	0.099	0.023	-0.055	-0.136	-0.223	-0.320	-0.438	-0.608	-0.949	-1.270	-2.274
0.25	0.063	-0.013	-0.091	-0.171	-0.257	-0.354	-0.474	-0.646	-0.993	-1.320	-2.339
0.30	0.031	-0.045	-0.122	-0.202	-0.288	-0.386	-0.506	-0.680	-1.031	-1.361	-2.381
0.35	0.003	-0.073	-0.151	-0.231	-0.317	-0.415	-0.535	-0.710	-1.062	-1.391	-2.398
0.40	-0.024	-0.100	-0.177	-0.258	-0.344	-0.441	-0.561	-0.736	-1.085	-1.408	-2.389
0.45	-0.050	-0.126	-0.203	-0.283	-0.369	-0.465	-0.585	-0.757	-1.099	-1.413	-2.354
0.50	-0.075	-0.151	-0.228	-0.307	-0.392	-0.488	-0.605	-0.773	-1.104	-1.405	-2.296
0.55	-0.100	-0.175	-0.252	-0.330	-0.414	-0.508	-0.622	-0.784	-1.100	-1.384	-2.217
0.60	-0.125	-0.200	-0.276	-0.353	-0.435	-0.526	-0.636	-0.790	-1.087	-1.353	-2.122
0.65	-0.151	-0.226	-0.300	-0.376	-0.456	-0.543	-0.647	-0.792	-1.068	-1.312	-2.014
0.70	-0.179	-0.253	-0.326	-0.400	-0.477	-0.560	-0.658	-0.791	-1.042	-1.264	-1.897
0.75	-0.211	-0.283	-0.355	-0.427	-0.500	-0.578	-0.668	-0.788	-1.011	-1.209	-1.774
0.80	-0.247	-0.319	-0.389	-0.458	-0.528	-0.600	-0.681	-0.785	-0.977	-1.149	-1.645
0.85	-0.293	-0.364	-0.433	-0.499	-0.564	-0.630	-0.700	-0.787	-0.942	-1.084	-1.508
0.90	-0.357	-0.428	-0.495	-0.558	-0.619	-0.677	-0.735	-0.800	-0.909	-1.013	-1.353
0.95	-0.465	-0.535	-0.600	-0.660	-0.714	-0.764	-0.809	-0.850	-0.900	-0.947	-1.158
0.97	-0.542	-0.611	-0.674	-0.731	-0.782	-0.827	-0.866	-0.900	-0.924	-0.940	-1.059
0.99	-0.694	-0.759	-0.816	-0.865	-0.908	-0.946	-0.980	-1.007	-1.016	-1.003	-0.980

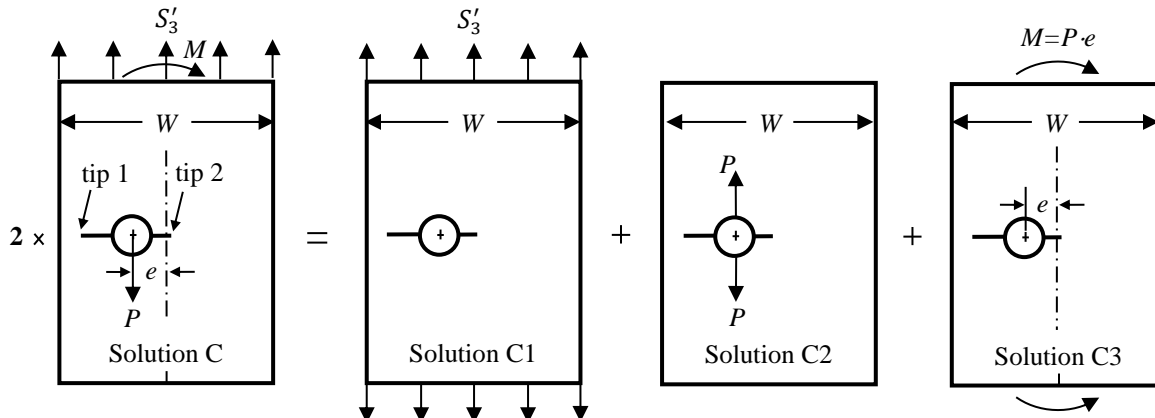
- Solution C:

The stress intensity factors subjected to pin-load in terms of S'_3 are calculated by

$$K_i^C = \beta_i^C S'_3 \sqrt{\pi c_i}$$

The beta factors (β_i^C) are obtained by the principle of superposition shown below.

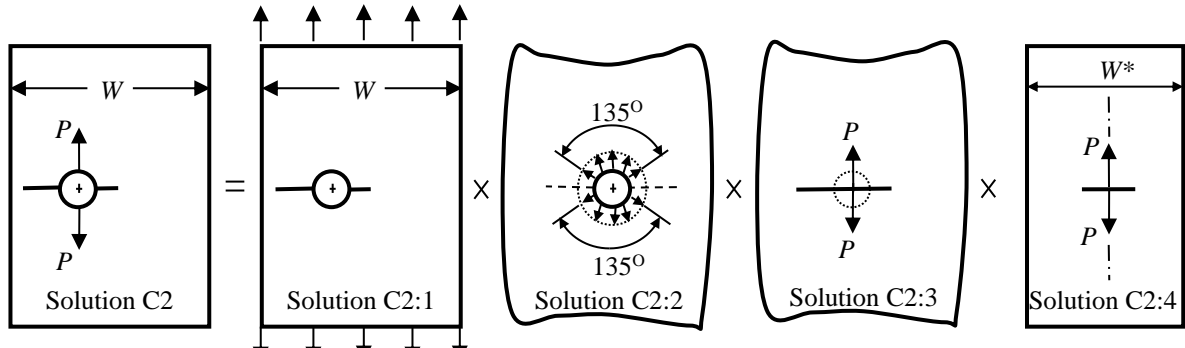
$$\beta_i^C = \frac{1}{2} \left(\sum_{j=1}^3 \beta_i^{C_j} \right)$$



- Solution C1 = solution A, i.e.

$$\beta_i^{C_1} = \beta_i^A$$

- Solution C2 is obtained by the compounding scheme shown below.



$$\beta_i^{C_2} = \beta_i^{C_{2:1}} \cdot \beta_i^{C_{2:2}} \cdot \beta_i^{C_{2:3}} \cdot \beta_i^{C_{2:4}}$$

and

$$\beta_i^{C_{2:1}} = \beta_i^A$$

$$\beta_i^{C_{2:2}} = e^{0.15(\rho_i^2 - 1)}$$

$$\beta_1^{C_{2:3}} = \frac{W}{\pi c_0} \sqrt{\frac{c_0 - \zeta}{c_0 + \zeta}}$$

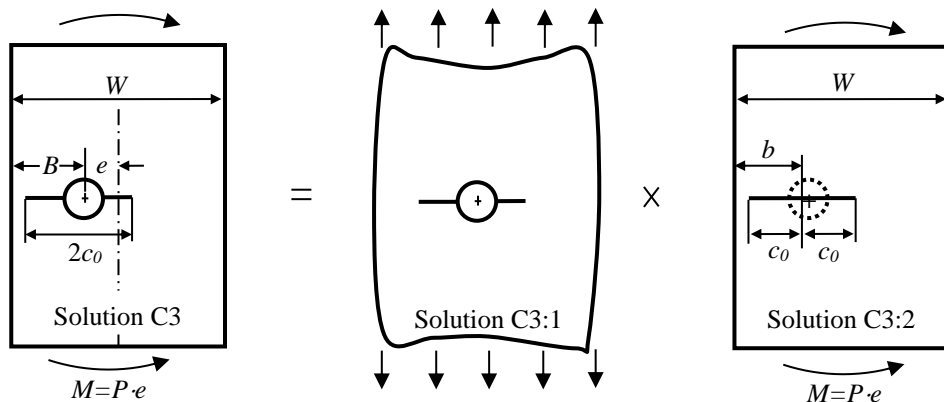
$$\beta_2^{C_{2:3}} = \frac{W}{\pi c_0} \sqrt{\frac{c_0 + \zeta}{c_0 - \zeta}}$$

$$\zeta = (c_1 - c_2)/2$$

$$\text{If } b \leq \frac{W}{2}: \quad \beta_1^{C_{2:4}} = \frac{\lambda_1(c_0, b)}{\sin[\lambda_1(c_0, b)]}, \quad \beta_2^{C_{2:4}} = \frac{\lambda_{12}(c_0, b)}{\sin[\lambda_{12}(c_0, b)]}$$

$$\text{If } b > \frac{W}{2}: \quad \beta_1^{C_{2:4}} = \frac{\lambda_{12}(c_0, W-b)}{\sin[\lambda_{12}(c_0, W-b)]}, \quad \beta_2^{C_{2:4}} = \frac{\lambda_1(c_0, W-b)}{\sin[\lambda_1(c_0, W-b)]}$$

- Solution C3 is obtained by using the same compounding scheme in solution B.



$$\beta_i^{C_3} = \beta_i^{C_{3:1}} \cdot \beta_i^{C_{3:2}} = \frac{6e}{W} \beta_i^{B_1} \cdot \beta_i^{B_2}$$

The factor $(6e/W)$ is present in the above equation because $\beta_i^{C_3}$ is the geometry factor in terms of pin-load stress S'_3 .

- Total stress intensity factors:

The total stress intensity factors are the sum of the three sub-solutions under remote tension, in-plane bending, and pin-load, i.e.

$$K_i = \left(\beta_i^A S_0 + \beta_i^B S_2 + \frac{D}{W} \beta_i^C \bar{S}_3 \right) \sqrt{\pi c_i}$$

where c_i is the crack size at crack tip i ($i=1, 2$). S_0 and S_2 are the applied remote tension and in-plane bending stress, respectively. \bar{S}_3 is the effective pin-load stress value,

$$\bar{S}_3 = \begin{cases} \max\{S_3, 0\} & \text{for compression clipping} \\ S_3 & \text{for full range} \end{cases}$$

and $S_3 = P/(Dt)$ is the applied pin-load stress defined in NASGRO.

The SIF geometry factors of TC23 are defined as:

$$F_i = \frac{K}{S_i \sqrt{\pi c_1}} \quad \text{at } c_1\text{-tip}$$

$$F_i = \frac{K}{S_i \sqrt{\pi c_2}} \quad \text{at } c_2\text{-tip}$$

Where $i = 0$ for remote tension, 2 for in-plane bending, and 3 for pin-load.

References: [C55], [C56], [C57], [C58]

TC24 – Through crack at center of plate, subjected to remote displacement

Stress intensity factors for a through-thickness crack at the center of a plate subjected to remote displacement boundary conditions were numerically determined following a procedure similar to that used for the TC14 crack model. The database consisting of discrete sets of SIF tables is used to compute the solutions with user-specified geometric dimensions. The solutions can accommodate the following types of displacements, constraints and stress states:

- Two types of remote displacement definition:
 - Displacement field derived from remote tension
 - User-specified remote displacement (tabular input)
- Two displacement constraint types at the remote end:
 - Type I: no constraint for displacements in the x-direction, displacement in the y-direction is user-defined
 - Type II: fixed constraint for displacements in x-directions, displacement in the y-direction is user-defined
- Two stress states:
 - Plane stress

- Plane strain

Since the loading is displacement controlled, the crack model requires users to provide Young's modulus and Poisson's ratio.

This crack model is a new through-thickness crack geometry where the remote loading is in terms of displacements instead of loads or stresses. Due to the condition of symmetry, the origin of the coordinate system is at the center of the plate as depicted in the GUI bitmap. The symmetric displacement condition is thus enforced requiring the users to define displacement variation $D_i(x)$ in reference to the origin.

Two types of displacement constraints are available at the remote ends: Type I and Type II. Type I constraint designates that the remote ends are free to expand and contract along the x-direction, but are specified by the user as $D(x)$ in the y-direction. Type II constraint fixes the displacement in the x direction; *i.e.*, $u(x) = 0$, and utilizes the user-specified displacement in the y-direction $D_i(x)$.

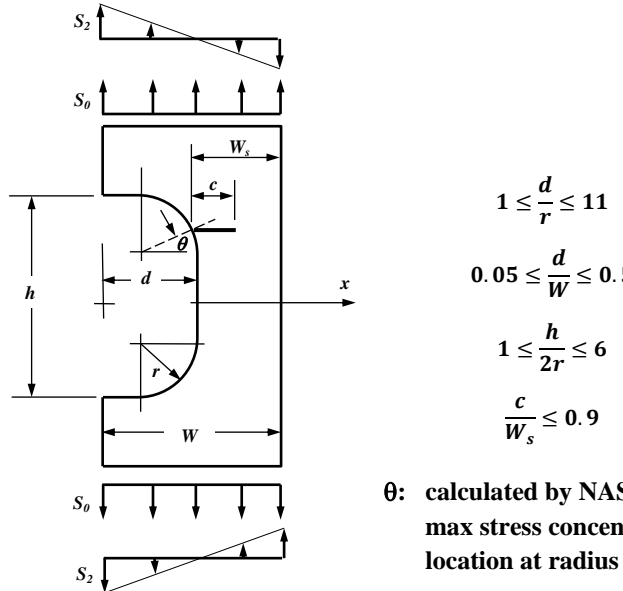
The scale factor for the displacement solutions work in exactly the same fashion as with standard stress solutions; the scale factor multiplies (scales) the entire user-specified displacement gradient. The number of quantities depends on the displacement definition. For remote tensile displacement, only one scaling factor D_0 is involved. For tabulated displacement definition, up to four displacement distributions can be defined and as a result, up to four scale factors require specification by user.

The user-specified displacement distribution is always (as in TC14) decomposed into four displacement components represented by the first four shifted Chebyshev polynomials. The coefficients with individual polynomial functions can be determined analytically through orthogonality condition. The reference solutions in reference to the four Chebyshev polynomials are then used in combination with the determined coefficients to finalize the SIF values corresponding to the user-specified displacement distribution.

Reference: [C67]

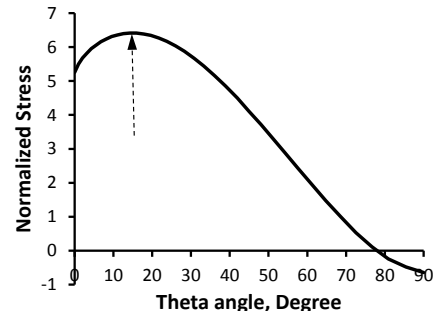
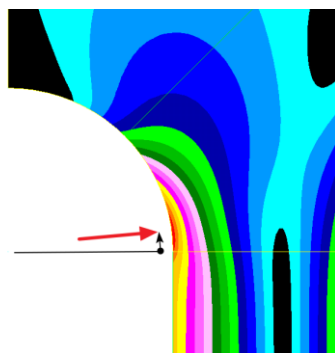
TC25 – Through Crack at Edge Rectangular Cutout with Rounded Corners

This crack model is a weight function solution for an edge through-thickness crack at an edge rectangular cutout with rounded corners. A schematic describing this crack model is given in the following figure. It's the same as the one in GUI bitmap. The key geometric parameters defining this crack model are the plate width (W), the height (h), the depth (d) and the radius (r). The loading is in terms of remote tension (S_0) and in-plane bending (S_2). The crack initiation site, designated by θ measured from the geometric transition region where the rounded corner merges to the flat side surface of the net section, is predicted by NASGRO. In reference to this crack initiation site, the crack plane is defined and as well the net section width (W_s). The solution limits of this fracture mechanics module are also listed in the same figure. Note the depth of the cutout cannot be more than 50% of the width of the plate.



Geometric and loading parameters applicable to TC25 crack model

The location of stress concentration can be illustrated by von Mises stress contours as shown in the following figure. The actual location of this initiation site is determined by the maximum surface stress along the rounded corner¹ as illustrated in figure by the surface stress variation as a function of angle, where the dash arrow designates the angle with maximum stress. This angle is determined by NASGRO through interpolation among reference solutions, of which detail is described in the later sections.



Stress concentration identified at the rounded corners and the surface stress variation along the rounded corner in terms of angular location

Two sets of reference stress solutions were generated using finite element method in reference to discrete geometric ratios and two reference stresses: remote tension and bending. The solutions are the variations of stress component with the loading direction along the net section defined at the crack initiation site. Each reference solution has its own θ designating the crack initiation site. For a combination of remote tension and bending with their respective scaling factors, the predicted θ angle is computed through interpolation. Assuming the stress scaling factors for S_0 and S_2 are f_T and f_M , the net section stress resulting from tension and bend combination is then

¹ It can be slightly different from the one from maximum von Mises stress.

given by $f_T\sigma_T(x) + f_M\sigma_M(x)$ where $\sigma_T(x)$ and $\sigma_M(x)$ are net section stress variations with remote tension S_0 and bend S_2 . For specified edge cutout geometry, both stress variations are determined through interpolation among the two sets of reference stress solutions.

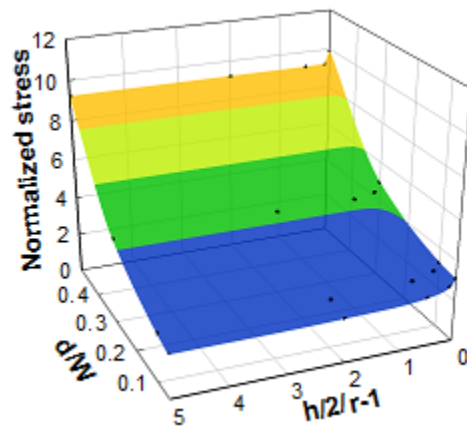
For the angle designated with the crack initiation site, its numerical value is predicted by

$$\theta = \theta_T \xi_T + \theta_M \xi_M$$

where the ratios ξ_T and ξ_M are defined by $\xi_T = f_T/(f_T + f_M)$, $\xi_M = f_M/(f_T + f_M)$ and θ_T and θ_M are the angles interpolated among the angular values with reference stress solutions.

The weight function used for this crack model is the same one used by TC12. The net section described in GUI bitmap with the crack initiation site is used as the plate width with the TC12 crack model. Since the stress gradient is determined through interpolation, NASGRO only makes use of the stress pairs analysis option with OPS enabled when utilizing the TC12 fracture mechanics module.

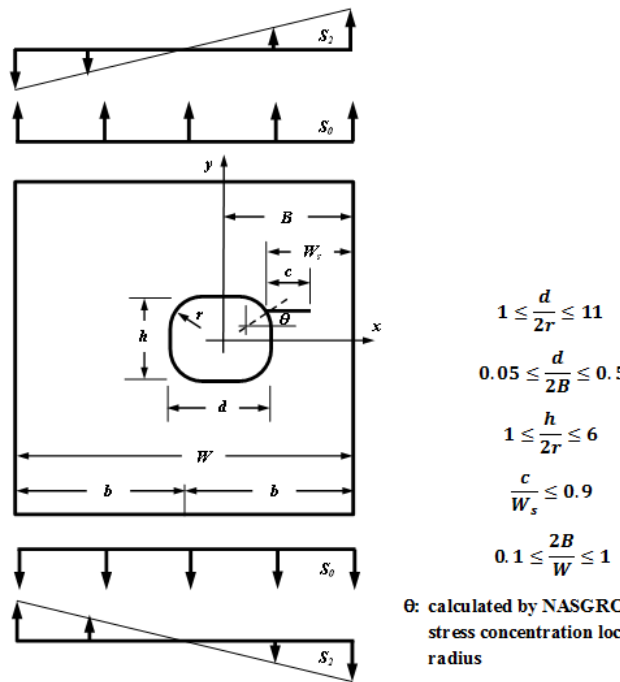
For some extreme usage leading to elongated cutouts; either in the longitudinal or net section direction, that are outside the validity limits; e.g., $h/(2r) > 6$ (from: $h/(2r) - 1 > 5$) or $d/W < 0.05$, it is suggested the users change the cutout dimensions to match the geometric dimensional ratios at the solution limits. For example, if the original dimensions lead to $h/(2r) = 3$ and $d/W = 0.02$, the solution with $h/(2r) = 3$ and $d/W = 0.05$ can be used. The stress solution using these limits generally provides more conservative assessment. An exemplary mesh plot is shown as follows where the variation of concentrated stress is expressed as a function of $h/(2r) - 1$ and d/W at $d/r = 1$. The values along $h/(2r) = 6$ and $d/W = 0.05$ provide the upper bound results.



A sample plot showing the variation of concentrated stress expressed as a function of $h/(2r) - 1$ and d/W at $d/r = 1$

TC26 – Through Crack at Offset Internal Rectangular Cutout with Rounded Corners

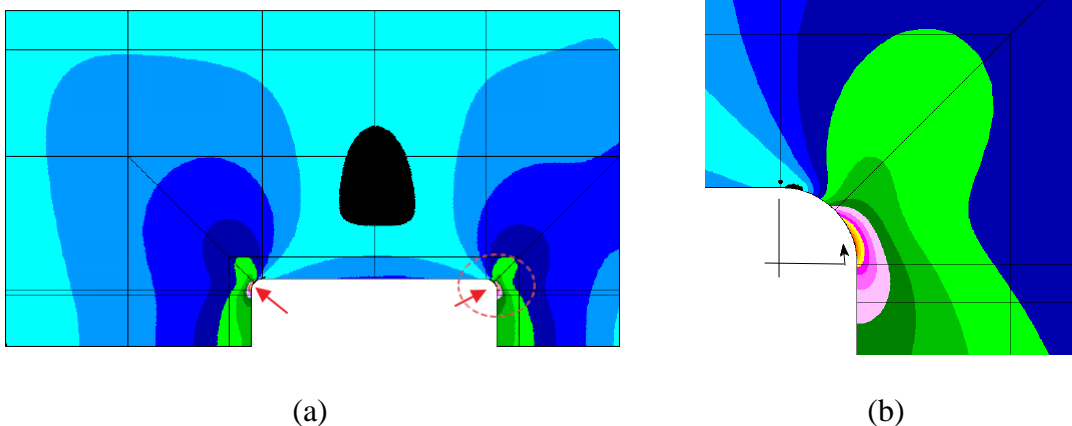
This crack model is a weight function solution for a through-thickness crack at the rounded corners of an offset internal rectangular cutout. A schematic similar to the bitmap in GUI is shown as follows. Geometric parameters involved in defining this crack model are the plate width ($W=2b$), the cutout height (h), the cutout width (d), the radius (r), and the offset of the cutout (B). The loading allowed for user's specification can be a combination of remote tension (S_0) and bending (S_2) with their respective stress scaling factors. The crack initiation site, designated by the crack initiation angle θ measured from the geometric transition from rounded corners to the flat side surface of the net section, is predicted by NASGRO. The net section with this crack initiation site W_s is defined perpendicular to the loading direction. Since the angle θ can be a couple of degrees, W_s is generally larger than the net section at the symmetric plane ($B - d/2$); the exception is when $h=2r$ with $\theta=0$ where $W_s = B - d/2$. The solution limits of this crack model depend on the range of reference stress solutions being generated. The right column of the figure lists the solution limits with this fracture mechanics module. For practical usage, the minimum net section at the symmetric plane is required to be at least one-half of the cutout width.



Geometric and loading parameters applicable to TC26 crack model

The location of stress concentration can be illustrated by the von Mises stress contours depicted in the following figure. The one on the left; i.e., (a), shows a plate with a slightly offset cutout subjected to uniform tension loaded remotely. The analytical model describes one-half of the plate as a result of symmetric condition. The stress contours indicate two highly stress concentrated regions at the rounded corners. The specific location of interest is with the narrower net section and is magnified and plotted in (b). The crack initiation site is close to this stress

concentration region and is determined by the maximum surface stress along the rounded corner². The determination is numerically searching the angle with the maximum surface stress along the rounded corner. NASGRO TC26 crack model calculates this angle for the combined tension and bend through interpolation among the crack initiation angles in reference stress solutions. The details will be described in the later sections.



Contours of von Mises stress used to depict the stress concentration regions: (a) contours from plate with slightly offset internal cutout subjected to remote tension and (b) magnified view at rounded corner with narrower net section

The reference stress solutions were generated using the centered internal cutout configuration. The net section stress variation in reference to the crack initiation site were extracted with discrete specification of geometric ratios. Two reference stresses: tension and bend, were applied remotely. Thus, each reference stress solution has association with its own definition of geometric dimensional ratios, crack initiation angle, net section width, stress variation and loading conditions.

To determine the net sectional stress variation in reference to the predicted crack initiation site for user-specified stress scaling factor f_0 and f_2 with S_0 and S_2 , the discrete reference stress solutions are used for further interpolation. With $\sigma_T(x)$ denoting the net sectional stress interpolated in reference to remote tension and $\sigma_M(x)$ the stress with remote bend, the net sectional stress for user-specified combined loading is given by

$$\sigma(x) = F_T \sigma_T(x) + F_M \sigma_M(x)$$

The ratios F_T and F_M are used to relate the stress scaling factors and the offset to conversion from centered configuration to offset application. They are given by

$$F_T = f_0 + f_2 \left(1 - \frac{B}{b}\right), \quad F_M = f_2 \frac{B}{b}$$

² It can be slight different from the one determined by maximum von Mises stress.

The crack initiation angle predicted by TC26 is also in terms of the above two ratios and is given by

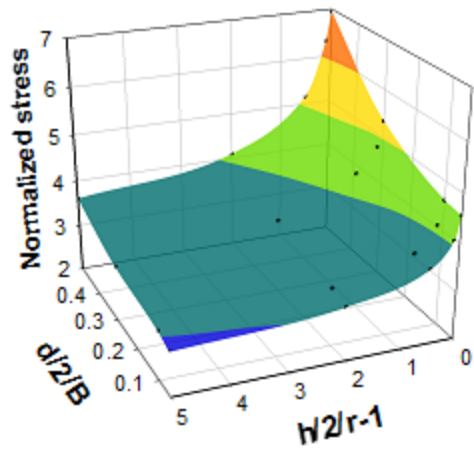
$$\theta = \theta_T \xi_T + \theta_M \xi_M$$

where the ratios ξ_T and ξ_M are defined by $\xi_T = F_T/(F_T + F_M)$ and $\xi_M = F_M/(F_T + F_M)$, and θ_T and θ_M are the crack initiation angles interpolated among the angular values with reference stress solutions.

The weight function approach for this crack model is similar to the one for TC18 but with slight modifications after calibrated against finite element solutions. To start with, the basic weight function is the one for TC13 – through cracks at holes. The first screening checks if the offset of the cutout is less than 80% and if $h \leq d$ or not. If it's valid, the plate width and the offset are modified and the TC13 SIF solution with this 80% offset is used. The second screening is towards the elongated cutout in the longitudinal (loading) direction where $h > d$. If it's valid, two major axes e_1 and e_2 corresponding to an approximate elliptical cutout are defined. The TC18 SIF solution for an elliptical hole with additional correction factored in from the offset is then used. The detailed steps are described as follows for this specific application:

- Step 1: Determine the TC13 SIF solution: K_{TC13} , with the hole radius given by $B - W_s$.
- Step 2: Determine the TC12 SIF solution using the plate width given by W_s
- Step 3: Determine an interpolated SIF solution: $K_{TC18}^{(0)}$, between the TC12 and TC13 SIF solutions following the same approach used by TC18 for elliptical slots.
- Step 4: Scale the $K_{TC18}^{(0)}$ SIF solution as a result of the relative net section ratio: e_1/W_s . The new SIF solution denoted by $K_{TC18}^{(1)}$ is given by $K_{TC18}^{(1)} = (K_{TC18}^{(0)} - K_{TC13}) \cdot e_1/W_s + K_{TC13}$.
- Step 5: Apply the correction factor by multiplication resulting from the offset: B/b . The final SIF solution is given by $K_{TC26} = [0.9 \cdot (B/b - 1) + 1] \cdot (K_{TC18}^{(1)} - K_{TC13}) + K_{TC13}$.

For elongated cutouts of which geometric ratios outside of the solution limits, it is suggested that the users change the cutout dimension to match the geometric dimensional ratios at the solution limits. For example, if the original dimensions lead to $h/(2r) = 3$ and $d/(2B) = 0.02$, the solution with $h/(2r) = 3$ and $d/(2B) = 0.05$ can be used. The predicted stress at the solution limits generally provides a more conservative assessment as depicted in the following figure. The trend in this bi-variable variation indicates as $h/(2r) - 1 > 5$ and $d/(2B) < 0.05$ the stress values are less than the values at the closest solution limits.



A sample plot showing the variation of concentrated stress expressed as a function of $h/(2r) - 1$ and $d/(2B)$ at $d/(2r) = 3$

TC27 – Through crack at hole in lug – univariant WF

Crack case TC27 represents a through-thickness edge crack initiated at the hole of a straight lug under pin-loading. Nominally, TC27 has the same geometry and loading as TC04. However, TC27 employs the weight function solution TC13 and the nonlinear stress variation for an uncracked lug. Consequently, TC27 represents a more powerful analysis tool, e.g., it can handle residual stresses. TC27 has a larger range of geometric parameters, e.g., $W/D \geq 1.25$ for TC27 but $W/D \geq 2$ for TC04. Finally, comparisons between TC04/TC27 and benchmark results (obtained from finite element analyses) demonstrate that TC27 is more accurate than TC04. Crack case TC27 provides stress intensity factor solutions input as values of the pin-loading ($S_3 = P/Dt$). Individual magnitudes of the pin-loading are specified through the GUI for load block definitions. The fracture mechanics module internally estimates the local stress variations on the crack plane (in the corresponding uncracked body) along the net section and then invokes TC13.

Nonlinear stress variations along the crack plane were computed using the following assumptions:

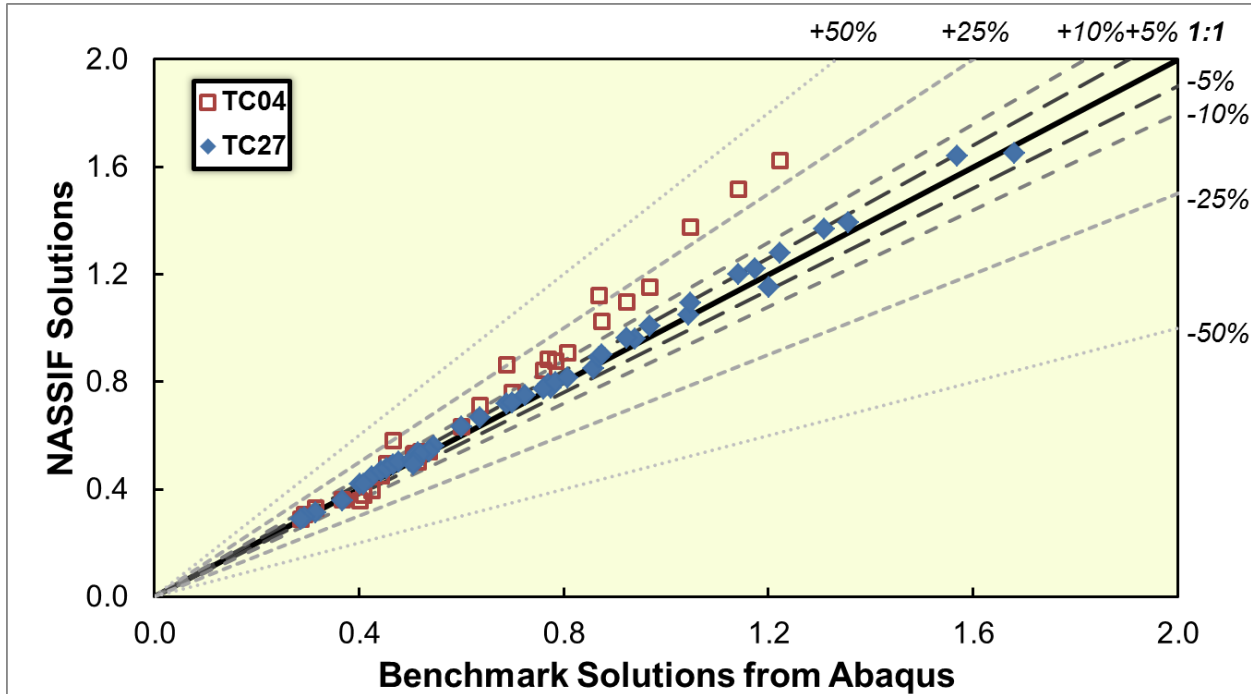
- Fixed boundary conditions prevent movement of the lug's surface. Uniform tractions along the lug surface are not physically realistic when the pin-hole's diameter (D) is large relative to the lug's width (W), except for long lugs where the height (H) is much greater than the width. Finite element analyses used to compute reference stresses set the height of the lug equal to its width.
- The loading (P) remains normal to the fixed surface. This loading direction is considered the 0° orientation. Body forces applied to the pin's volume supplies the driving force for crack growth. We fix the crack plane normal to the applied loading (90°) and allow the crack to propagate over the remaining ligament of the lug. The 90° assumption minimizes the crack ligament and facilitates the development of numerical models to support verification studies.
- The friction coefficient relates the normal stress to the shear stress at all points in the pin-lug interface. Higher values of μ lead to more load transferred from the pin to the lug by shear. Parametric studies examined values of $\mu = 0.01, 0.3, 0.6$, and 1.0 and indicate that the effect of friction varies with W/D on the 90° stress plane. The complicated relationship between the friction coefficient and the stress profile lead us to include a small friction coefficient ($\mu = 0.3$) in computations of reference stresses. This value is thought to be physically realistic. Friction coefficients may not be known with certainty in practice.
- A steel pin loads a steel lug. Different combinations of materials (e.g., a steel pin loading an aluminum lug) lead to slightly different stress profiles (on the order of 1 – 2%). The case where a steel pin loads a steel lug was found to be conservative.
- The pin fits neatly into the lug hole. That is, the diameter of the lug's hole exactly equals the diameter of the pin.

TC27 has the same geometric validity ranges as TC13, except for the additional constraint that $W/D \geq 1.25$. This ratio represents a lower limit for most straight lug geometries. The limits are:

$$1.25 \leq \frac{W}{D} \leq 10$$

$$0 \leq \frac{c}{W - D} \leq 0.4995$$

Please refer to TC13 for additional information on integration of the weight functions.



Verification of TC27 and comparison with TC04

The previous figure shows verification studies of TC27. Values of stress intensity factors from detailed finite element analyses (using Abaqus 6.12-1) provide the benchmark data. Almost all stress intensity factors computed with TC27 have less than 10% error in comparison with the benchmark data. Error with TC04 may exceed 25%. For both crack cases, the error tends to be conservative (i.e., driving increased crack advance). This figure also highlights the increased range of geometries in TC27 vs. TC04; several computed values of TC27 do not have corresponding values of TC04 since the input geometry lies outside of the range of TC04 solutions.

Calculation of stress intensity factors for two symmetric through cracks

For two symmetric through cracks, stress intensity factors may be computed based on a correction of the stress intensity factor of a single, non-symmetric crack. Verification studies of the two crack solution using finite element simulations lead to the following relationship:

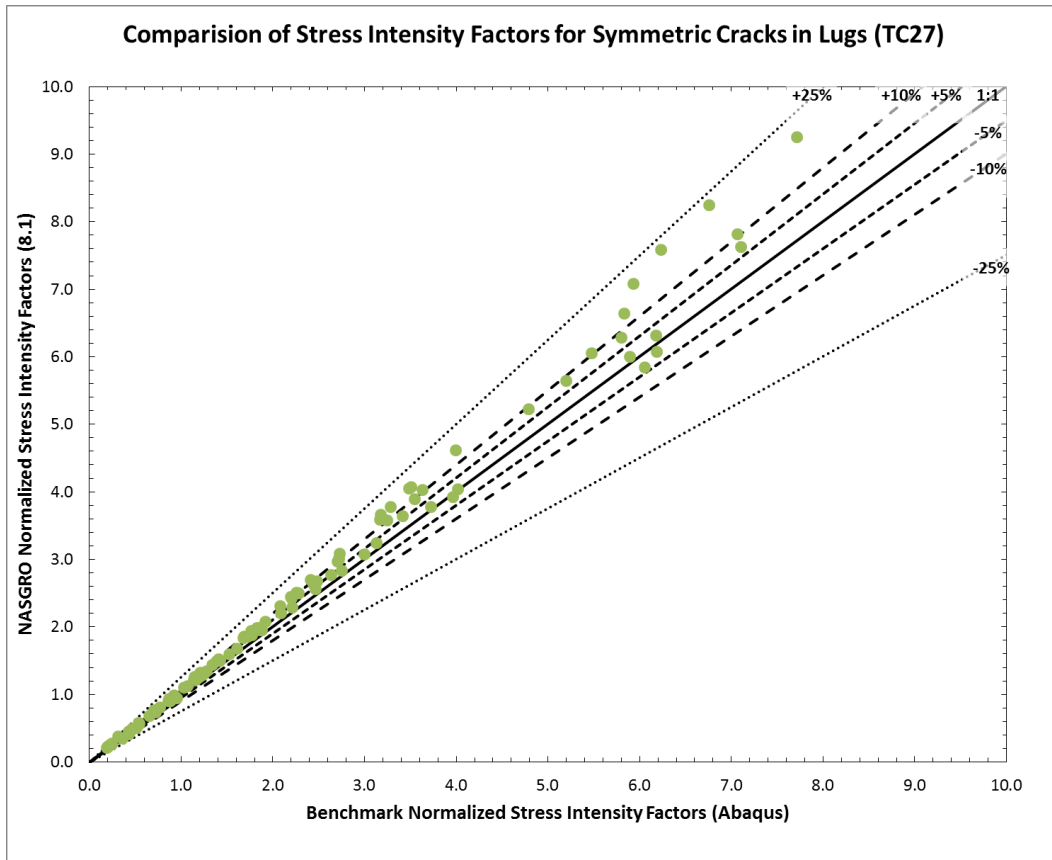
$$K_{2crks} = \max \left(1, \frac{1}{F_{Shah} \times F_{FW}} \right) \times K_{1crk}$$

$$F_{Shah} = \sqrt{\frac{D + c}{D + 2c}}$$

$$F_{FW} = \sqrt{\frac{D + 0.05 \times (W - D)}{D + c}}$$

Here, F_{Shah} represents the Shah correction factor. The F_{FW} factor prevents non-conservative stress intensity factor solutions for short, straight lugs when the crack is large relative to the hole diameter.

The figure below highlights key results from the verification studies. It compares stress intensity factors (normalized by $S_3 \times \sqrt{\pi c}$) for two symmetric cracks computed using benchmark Abaqus solutions to results from NASGRO. For most cases, stress intensity factors are within 10% of the benchmark solution.



TC28 – Curved Through Crack at Edge of Plate

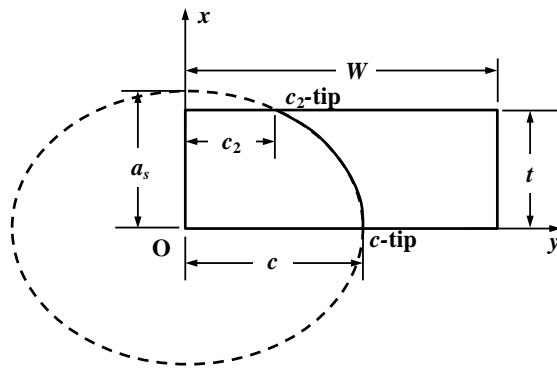
The TC28 crack model assumes that the through crack breaks through the thickness resulting in two surface tips, one each at the front and the back surfaces of the plate. The two tips, respectively denoted by c -tip at the front surface and c_2 -tip at the back surface, are assumed along a crack tip perimeter described by an elliptical equation (see the figure below). The equation has its center at the bottom-left corner of the rectangular cross section and the crack front is governed by

$$\frac{y^2}{c^2} + \frac{x^2}{a_s^2} = 1$$

Note the radius along x -axis a_s is an artificial length parameter given by

$$a_s = \frac{c}{\sqrt{1 - \left(\frac{c_2}{c}\right)^2}}$$

where c and c_2 are the observed surface crack lengths from the left side of the cross section.



The crack model can be subjected to load combinations resulting in a stress gradient varying along the thickness direction, a univariant crack opening stress variation originating from the front surface. The stress intensity factors at both surface tips are determined by weight function formulation. The approximate weight functions near singularity are given by

$$W_{c_2}(a, x; M_{1a}, M_{2a}, M_{3a}) = \frac{2}{\sqrt{2\pi(a-x)}} \left[1 + M_{1a} \sqrt{1 - \frac{x}{a}} + M_{2a} \left(1 - \frac{x}{a} \right) + M_{3a} \left(1 - \frac{x}{a} \right)^{\frac{3}{2}} \right]$$

$$W_c(a, x; M_{1c}, M_{2c}, M_{3c}) = \frac{2}{\sqrt{\pi x}} \left[1 + M_{1c} \sqrt{\frac{x}{a}} + M_{2c} \frac{x}{a} + M_{3c} \left(\frac{x}{a} \right)^{\frac{3}{2}} \right]$$

where the coefficients M_1 's, M_2 's and M_3 's are determined by reference solutions with three linearly independent reference stresses: $\sigma_1 = 1$, $\sigma_2 = 1 - x/a$, and $\sigma_3 = (1 - x/a)^3$. The

reference solutions designating the c - and c_2 -tips are taken at a very small fraction of the thickness inside both front and back surfaces.

The stress intensity factors are determined by integration of the product of crack opening stress and weight function over the crack depth.

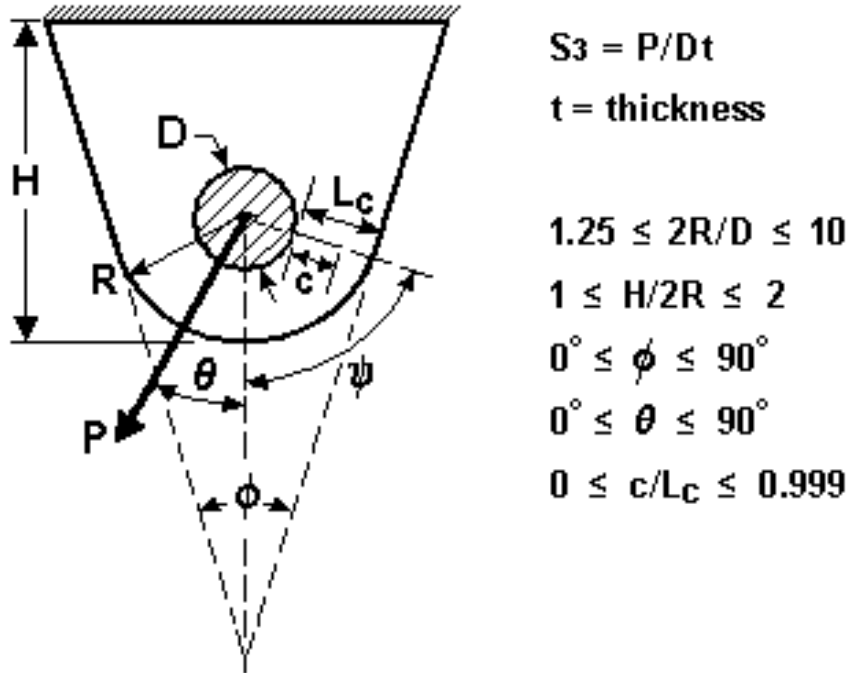
$$K_{a,c} = \int_0^a \sigma(x) W_{a,c} dx$$

The length parameter a in the weight functions is defined as a depth slightly smaller than the thickness by a fraction.

The solution limits are in terms of geometric ratios and are given in the following with W denoting the width of the plate and t the thickness. The original development restricted the crack length ratio c_2/c up to 1. The extension from 1 to 5 was achieved by flipping both geometric configuration and stress gradient. In that case, the virtual ellipse is centered at the top left corner of the plate, such that the c_2 length (on the back surface) is longer than the c length (on the front surface).

$$\begin{aligned} 0.2 &\leq \frac{c_2}{c} \leq 5 \\ 0 &\leq \frac{c}{W} \leq 0.9 \\ 1 &\leq \frac{W}{t} \leq 20 \end{aligned}$$

TC30 – Through Crack at Hole in Obliquely Loaded and Tapered Lug – Univariant WF



Configuration of crack case TC30

Crack case TC30 represents a through-thickness edge crack initiated at the hole of a symmetric tapered lug under oblique pin-loading. It is a new solution that is distinct and separate from earlier lug solutions that assumed straight, short lugs under vertical loading. Straight means that the lug geometry has no taper. Short implies that these lugs have height equal to their width. Vertical loading restricts loads to a constant angle. TC30 supports a much larger range of geometries and loadings for pin-loaded holes in lugs as indicated by the previous figure:

$$\begin{aligned}
 1.25 &\leq \frac{2R}{D} \leq 10 \\
 1 &\leq \frac{H}{2R} \leq 2 \\
 0^\circ &\leq \phi \leq 90^\circ \\
 0^\circ &\leq \theta \leq 90^\circ \\
 0 &\leq \frac{c}{L_c} \leq 0.999
 \end{aligned}$$

Here, the ratio $2R/D$ provides the ratio of the lug's outer radius (R) to its pin-hole diameter (D). The limits range from a very large hole ($2R/D = 1.25$) to a very small hole ($2R/D = 10$) and can cover earlier solutions for straight, short lugs under normal loading (TC27). The lug's heel-to-toe height (H) is variable in TC30 with limits for a short lug ($H = 2R$) to a much longer lug ($H = 4R$). TC30 supports symmetrically tapered lugs with symmetric taper angle (ϕ) that supports straight lugs ($\phi = 0^\circ$) to right-angled tapers ($\phi = 90^\circ$). The oblique loading angle (θ) varies from perpendicular to the base ($\theta = 0^\circ$) to parallel to the base ($\theta = 90^\circ$).

The geometric parameters (R, D, H, ϕ) and loading angle (θ) establish the crack angle (ψ). In an uncracked lug, there are two local minima of opening-stress values ($\sigma_{\theta\theta}$). The crack angle matches the angle of one of these local maxima on the inner lug surface. To determine the appropriate maxima, we selected the crack angle to coincide with the minimum crack ligament. Generally, the crack angle (ψ) is not normal to the loading angle θ as is usually assumed. Recall that the crack angle is set based on local stress maxima – these locations are different for different geometries and loading angles. NASGRO sets the crack angle for a user-defined geometry by interpolation over a table of known crack angle values.

The crack path (L_c) is radial to the pin-hole's center. Its location depends on the crack angle. The geometry resulting from the crack angle, taper angle, and height leads to a complicated relationship for L_c that is computed internally by NASGRO. Users may assume a minimum value of $L_c = R - 0.5 \times D$ to ensure that their cracks lie within the geometry.

The crack path is not allowed to curve (“kink”) during crack propagation. This radial crack path minimizes the distance between the pin-hole surface and outer lug surface. In reality, the crack path may deviate from a radial path when there is mixed-mode loading, *i.e.*, non-zero values of $\frac{K_{II}}{K_I}$. Most radial crack paths (72%) in tapered lugs lead to a ratio of $K_{II}/K_I \leq 0.1$ and will likely not deviate significantly from a straight radial crack path. Almost all radial crack paths (>95%) have mixed mode ratio $K_{II}/K_I \leq 0.2$. However, certain geometric configurations may lead higher mixed mode ratios. These crack paths may deviate towards the taper edge when crack tips encounter the straight taper edge at a shallow angle, *i.e.*, $\phi \geq 90^\circ - \psi$. These conditions may arise when $\phi > 25^\circ$ and $\theta < 10^\circ$. In these cases, TC30 produces non-conservative SIF solutions when the crack becomes large relative to the remaining ligament, *i.e.*, $c/L_c > 0.5$. However, the geometries where non-conservatism develops tend to promote long ligaments (L_c) that may fracture before mixed mode loading issues develop.

Crack case TC30 provides SIF solutions input as values of the pin-loading ($S_3=P/Dt$). Individual magnitudes of the pin-loading are specified through the GUI for load block definitions. The fracture mechanics module internally estimates the local stress variations on the crack plane (in the corresponding uncracked body) along the net section and then integrates these stresses with the weight function TC13 over the crack face.

The stress gradient routines for TC30 are based on opening-mode stress gradient solutions from 336 geometric and loading combinations: 8 relative pin sizes ($2R/D$), 7 loading angles (θ), 3 taper angles (ϕ), and 2 height ratios ($H/2R$). These routines interpolate over the range of geometric parameters for the appropriate crack angle and stress gradients. Verification indicates that 99% of computed crack angles are within 3% of benchmark crack angles. Verification also indicates that 99% of crack plane forces are within 4% of benchmark forces. (The crack plane force equals the area under the stress gradient curve).

Nonlinear stress variations along the crack plane were computed using the following assumptions:

- Fixed boundary conditions prevent movement of the lug's base. Uniform tractions along the lug surface are not physically realistic when the pin-hole's diameter (D) is large

relative to the lug's radius (R), except for long lugs where the height (H) is much greater than the width.

- The loading (P) remains fixed at angle θ . Variable loading angles (θ) lead to indeterminate crack angles that would not be tractable as a simple input solution. Consequently, the loading angle cannot vary over the loading history in TC30 solutions. Body forces applied to the pin's volume transfer load from the external geometry to the pin, which transfers forces to the cracked lug.
- The friction coefficient relates the normal stress to the shear stress at all points in the pin-lug interface. Higher values of μ lead to more load transferred from the pin to the lug by shear. Parametric studies examined values of $\mu=0.1, 0.3$, and 0.9 and indicate that the effect of friction varies with the geometric configuration and loading angle. The complicated relationship between the friction coefficient and the stress profile lead us to include a small friction coefficient ($\mu=0.3$) in computations of reference stresses. This value is thought to be physically realistic. Friction coefficients may not be known with certainty in practice.
- A steel pin loads a steel lug. Different combinations of materials (e.g., a steel pin loading an aluminum lug) lead to slightly different stress profiles (on the order of 1–2%). The case where a steel pin loads a steel lug was found to be conservative to the case of a steel pin loading an aluminum lug.
- The pin fits neatly into the lug hole. That is, the diameter of the lug's hole exactly equals the diameter of the pin.

A few notes on stresses from the new parameters:

- Over the range of examined geometries, oblique loads between $\theta = 30^\circ - 60^\circ$ generate higher stresses than oblique loads at other angles. Most stresses peak at loading angles near $\theta = 45^\circ$. The loading angle becomes more significant as relative pin-hole size ($2R/D$) decreases.
- Height varies in these solutions, in contrast to earlier solutions such as TC04 and TC27. Height has little impact on the solution for vertically loaded pins ($\theta = 0^\circ$). Height has a more pronounced effect on stresses when the loading angle is almost horizontal ($\theta \rightarrow 90^\circ$). Longer lugs generate increased stresses along the crack path under horizontal loading.
- Tapering drives down stresses near the pin-hole and increases the crack path. Both effects should increase the lives of tapered lugs relative to non-tapered lugs.

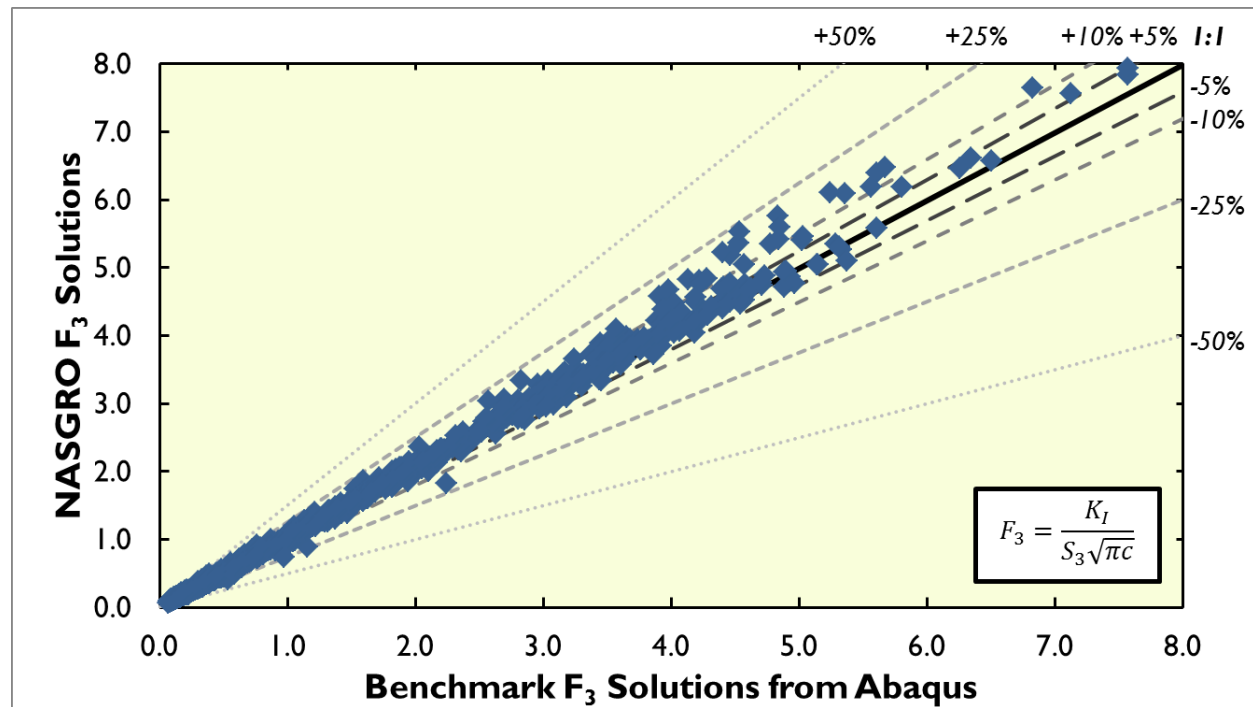
TC30 has the same geometric validity ranges as TC13, except for the additional constraint that $2R/D \geq 1.25$. This ratio represents a lower limit for most lug geometries. This ratio matches the lower limit for lug geometries in TC27.

Please refer to TC13 for additional information on integration of the weight functions.

TC30 supports residual stresses along the crack path – that is, from $0 \leq X/L_c \leq 1$ at the angle ψ . Residual stresses will not alter the crack path. Consequently, a user may execute a NASFLA analysis to obtain ψ and then pick out the residual stress along the crack path.

TC30 supports negative pin-loading options: compression clipping or full range. Please refer to the appropriate documentation for more information.

The following figure summarizes verification studies of TC30. Values of SIFs from detailed finite element analyses (using Abaqus 6.12-1) provide the benchmark SIFs from crack geometries. Most SIFs computed with TC30 have less than 10% error in comparison with the benchmark data. Excessive error tends to be conservative (i.e., driving increased crack advance), though there are a few outliers where the error is non-conservative. These outliers represent geometries that have crack tips intersecting the straight taper edge at an angle.

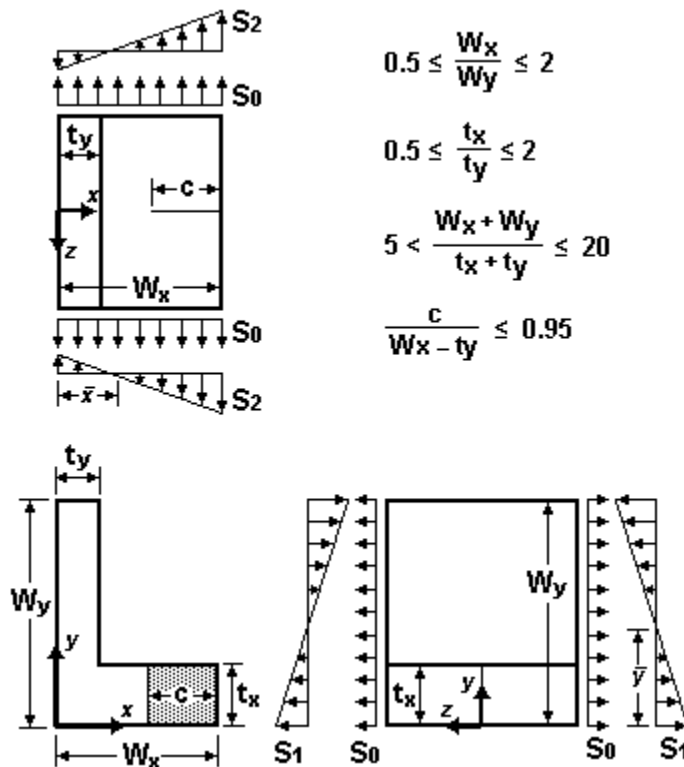


Verification of TC30 with Abaqus benchmark solutions.

TC30 represents a more powerful analysis tool than TC27, which is limited to straight, short lugs under normal loading. Both analyses are based on the same weight function solution, TC13. The main differences between TC27 and TC30 are the crack angle and stress gradient set. TC27 sets a constant crack angle that is perpendicular to the loading, whereas TC30 sets the crack angle based on the geometry and loading. TC27 also uses a different set of stress gradient solutions. While TC30 may be set to the same geometry as TC27 ($W = 2R$; $H = 2R$; $\phi = 0^\circ$; $\theta = 0^\circ$), TC30 is intended to span the range of tapered and obliquely-loaded lug geometries that exist on aerospace platforms. TC27 is intended as a replacement for TC04. The differing assumptions of TC27 and TC30 lead to different SIFs over the solution space. Direct comparisons between TC27 and TC30 reveal that SIF solutions from TC30 are mostly within 1% of TC27 for holes with $2R/D \geq 2$. The impact on fatigue crack growth lives is complicated. SIFs from TC30 may

be above SIFs from TC27 for smaller cracks and below SIFs from TC27 for larger cracks. Furthermore, TC27 sets a minimum crack ligament, whereas TC30 may have a longer crack path than the minimum possible ligament.

TC31 – Through Crack in L-section under Remote Loading – Pre-Corner



L-section parameters and loadings for TC31

The TC31 solution features a through crack in one leg of an L-section under remote stresses. TC31 places the through crack on the cross section and normal to the axial length of the structural member. TC31 restricts the through crack to be straight and normal to free surfaces. TC31 contains stress intensity factor (SIF) solutions for cracks under remotely applied uniform stresses and univariant stress gradients. TC31 limits the crack to one leg of the L-section, i.e., it does not turn the corner of the section. At this time, TC31 does not restrain bending.

The SIF (stress intensity factor) solution is based on the Herrmann-Bažant-Dunn (HBD) method to compute SIFs. Herrmann and co-workers [RF1,RF2] originally developed the HBD method using elementary beam theory to relate the energy release by crack extension to energy release by crack widening. Bažant [RF3] added a correction factor to the original equations. For I-sections, Dunn et al [RF4] demonstrated a method to calibrate Bažant's correction factor using results from finite element analysis results. The HBD method features SIF equations for cracks under remote axial loads (P), moments (M), and torque (T) in plane-stress conditions:

$$K_P = P \times \sqrt{\frac{\beta_P}{t} \times \left(\frac{1}{A^*} - \frac{1}{A} \right)}$$

$$K_M = M \times \sqrt{\frac{\beta_M}{t} \times \left(\frac{1}{I^*} - \frac{1}{I} \right)}$$

$$K_T = T \times \sqrt{\frac{\beta_T}{t} \times \left(\frac{1}{J^*} - \frac{1}{J} \right)}$$

Here, K_P , K_M , and K_T provide SIFs (stress intensity factors) for cracks under axial loads, moments, and torque respectively. The HBD method employs the area (A), second moment of area (I), and polar moment of area (J) of the cross section. Starred quantities (A^* , I^* , and J^*) reflect counterparts of the previous terms without contributions from cracked regions. Consequently, starred quantities will always be less than unstarred quantities whenever there is a crack. The variable t indicates the thickness spanned by the local crack front. The non-dimensional correction factors β_P , β_M , and β_T (for P , M , and T respectively) relate energy released by a widening notch ($\partial U / \partial h$) to energy released by a growing crack ($\partial U / \partial c$) through the relationship:

$$\frac{\partial U}{\partial c} = -2\beta \frac{\partial U}{\partial h}$$

The correction factors depend on the loading, geometric configuration, and crack length. That is, the correction factors for a constant thickness section will differ from the correction factors for a variable thickness section in general. These correction factors need to be calibrated before use in the HBD method.

The previous figure of the TC31 solution shows the parameterization of the L-section and the available stress gradients. L-sections in TC31 have five geometric parameters: widths of the X and Y legs (W_x and W_y); thicknesses of the X and Y legs (t_x and t_y); and the crack length (c). TC31 does not support rounded corners or tapering of the thickness along the legs. TC31 supports loading of the L-section by uniform stresses (S_0), linear stresses varying along the Y axis (S_1), and linear stresses varying along the X axis (S_2).

Using the given geometry and loading, stresses (S_{zz}) at any part of the uncracked cross-section may be determined using the expression:

$$S_{zz}(x, y) = S_0 + S_1 \times \frac{(\bar{y} - y)}{\bar{y}} + S_2 \times \frac{(x - \bar{x})}{(W_x - \bar{x})}$$

These stresses (S_{zz}) are normal to the cross section. TC31 does not support remote shear or remote torsional stresses on the cross-section. Definitions of S_1 and S_2 have been aligned in TC31, TC32, and TC02. The quantities \bar{x} and \bar{y} refer to the cross-sectional centroid locations. Users may determine the values of S_0 , S_1 , and S_2 based on the following equations. Let $S_c = S_{zz}(0,0)$, $S_x = S_{zz}(W_x, 0)$, and $S_y = S_{zz}(0, W_y)$. These outside surface stresses refer to stresses

at the corner (S_c), horizontal leg (S_x), and vertical leg (S_y). For any set of these stresses, the following equations may be used to determine the appropriate values for TC31:

$$\begin{aligned} S_0 &= S_c + (S_x - S_c) \left(\frac{\bar{x}}{W_x} \right) + (S_y - S_c) \left(\frac{\bar{y}}{W_y} \right) \\ S_1 &= -(S_y - S_c) \left(\frac{\bar{y}}{W_y} \right) \\ S_2 &= (S_x - S_c) \left(1 - \frac{\bar{x}}{W_x} \right) \end{aligned}$$

The stress multipliers may also be related to the axial load P , the moment about the X-axis M_x , and the moment about the Y-axis M_y through the following equations:

$$\begin{aligned} S_0 &= \frac{P}{A} \\ S_1 &= -\frac{M_x \times I_{yy} + M_y \times I_{xy}}{I_{xx} \times I_{yy} - I_{xy}^2} \times \bar{y} \\ S_2 &= -\frac{M_y \times I_{xx} + M_x \times I_{xy}}{I_{xx} \times I_{yy} - I_{xy}^2} \times (W_x - \bar{x}) \end{aligned}$$

The above equations are defined using counter-clockwise positive moments on the far end where $z>0$. Moments are assumed to be applied at the centroid (\bar{x}, \bar{y}) of the section. For an L-section, moments about the X and Y axes produce bivariant stress gradients in general. That is, a moment about the X-axis will produce S_1 and S_2 stresses.

Geometric variables referenced in the earlier equations are defined for an L-section as follows:

$$\begin{aligned} A &= t_x(-t_y + W_x) + t_y W_y \\ \bar{x} &= \frac{t_x W_x^2 + t_y^2(-t_x + W_y)}{2(t_x(-t_y + W_x) + t_y W_y)} \\ \bar{y} &= \frac{t_x^2(t_y - W_x) - t_y W_y^2}{2t_x(t_y - W_x) - 2t_y W_y} \\ I_{xx} &= \frac{-t_x^4(t_y - W_x)^2 + 4t_x^3 t_y(t_y - W_x)W_y + 6t_x^2 t_y(-t_y + W_x)W_y^2 + 4t_x t_y(t_y - W_x)W_y^3 - t_y^2 W_y^4}{12(t_x(t_y - W_x) - t_y W_y)} \\ I_{yy} &= -\frac{t_x^2(t_y - W_x)^4 - 2t_x t_y(t_y - W_x)(t_y^2 - t_y W_x + 2W_x^2)W_y + t_y^4 W_y^2}{12(t_x(t_y - W_x) - t_y W_y)} \\ I_{xy} &= \frac{t_x t_y(t_y - W_x)W_x(t_x - W_y)W_y}{4t_x(t_y - W_x) - 4t_y W_y} \end{aligned}$$

All second moments of area (I_{xx} , I_{yy} , and I_{xy}) are referenced to the centroid (\bar{x}, \bar{y}) of the section. The value of I_{xy} may be positive or negative depending on the size and shape of the cross section.

NASGRO employs beta factors (β_P , β_{M_x} , and β_{M_y}) calibrated from 3D finite element analyses of the cracked L-section. These analyses place a straight through crack in an L-section that matches the TC31 geometry. Analyses set the out-of-plane length (along the Z-axis) equal to three times the longest leg's width and impose remote stress gradients of S_0 , S_1 , and S_2 .

These finite element analyses determine the SIF variation along the crack thickness – along the Y-axis. For S_0 and S_2 loadings, SIFs remain relatively constant over the bulk of the section and decrease near the free surface. For S_1 loadings, SIFs peak as $y \rightarrow 0$ just inside of the free surface. For all loadings, SIFs peak near the sharp corner ($y \rightarrow t_x$) for long crack fronts, *i.e.*, as $c \rightarrow W_x - t_y$. For simplicity, SIFs used in the calibration process and verification studies set an averaged SIF for S_0 and S_2 loading and a peak SIF for S_1 loading.

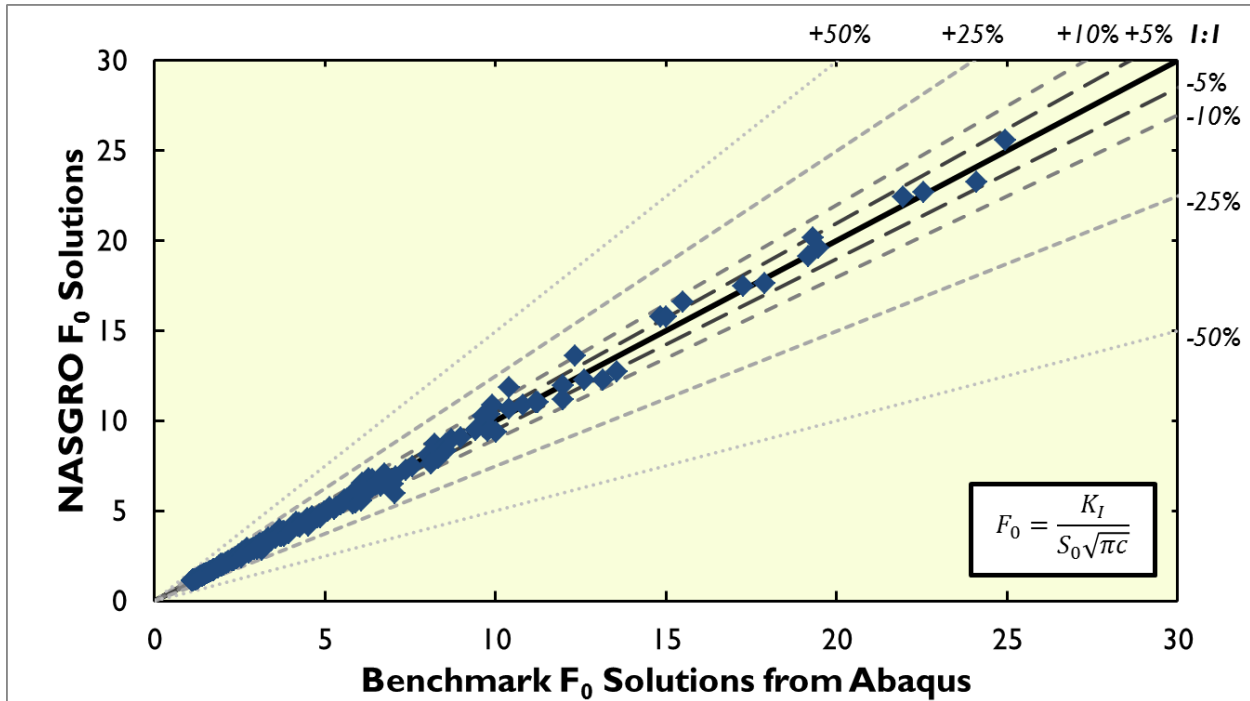
TC31 assumes simple bending to relate the imposed stresses to equivalent moments acting on the crack front. For example, an imposed stress S_2 produces an equivalent moment $\bar{M}_y = S_2 I_{yy} / (W_x - \bar{x})$. That is, the equivalent model \bar{M}_y represents the moment that would be generated on a rectangular section with second moment of area of I_{yy} and applied stress gradient S_2 . The equivalent moment does not match the actual moment for an L-section geometry due to non-zero values of I_{xy} . The HBD method employs the equivalent moment in its SIF calculations. In the calibration process, a known SIF from the FEA is normalized to an appropriate β -factor. Every finite element analysis in the calibration process provides one set of β -factors for the three remote stress gradients (S_0 , S_1 , and S_2). TC31 contains 240 calibrated β -factors per stress gradient. β -factors vary with the cross-section's width skew, slenderness, and crack length parameters over the following ranges:

$$\begin{aligned} \frac{1}{2} &\leq \frac{W_x}{W_y} \leq 2 \\ 5 &\leq \frac{W_x + W_y}{t_x + t_y} \leq 20 \\ \frac{c}{W_x - t_y} &\leq 0.95 \end{aligned}$$

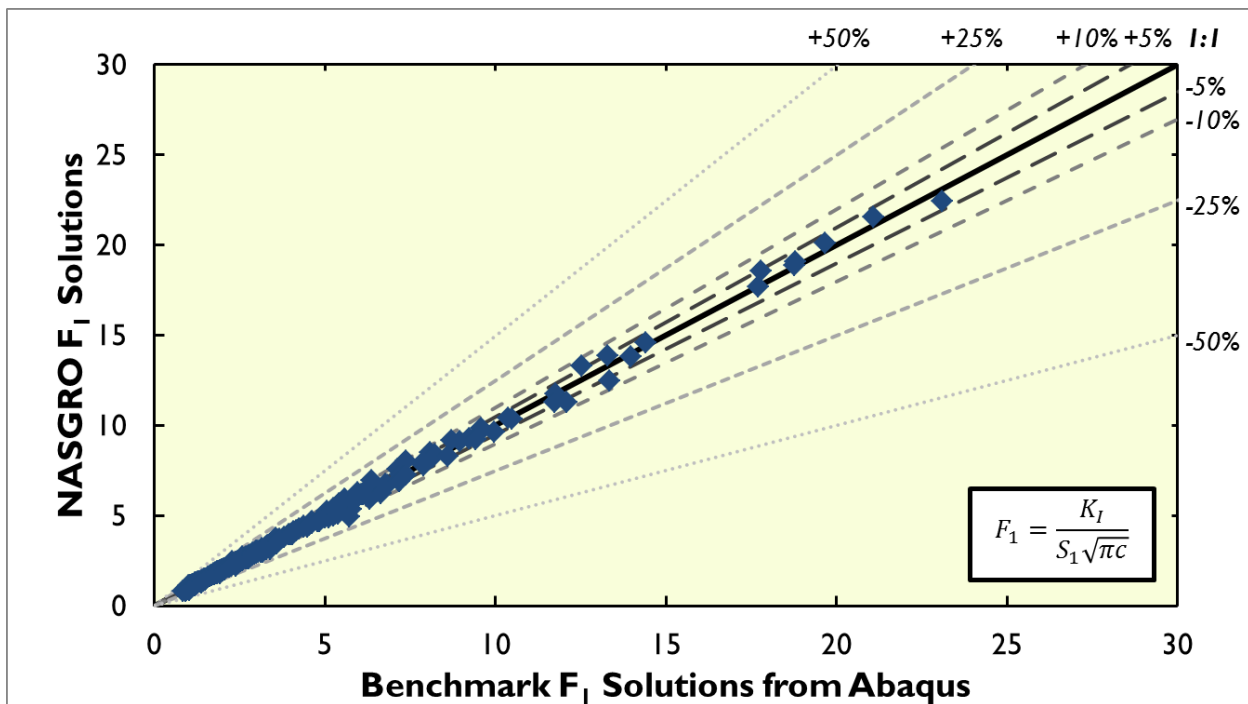
TC31 interpolates over the set of β -factors to determine β -factors appropriate to the user defined geometry. TC31 does not include thickness skew correction (t_x/t_y) in the table of β -factors. Instead, we correct for different thicknesses ($t_x \neq t_y$) using a thickness correction factor and the thickness differences built into the HBD method. This correction enables us to support the following thickness skew limits:

$$\frac{1}{2} \leq \frac{t_x}{t_y} \leq 2$$

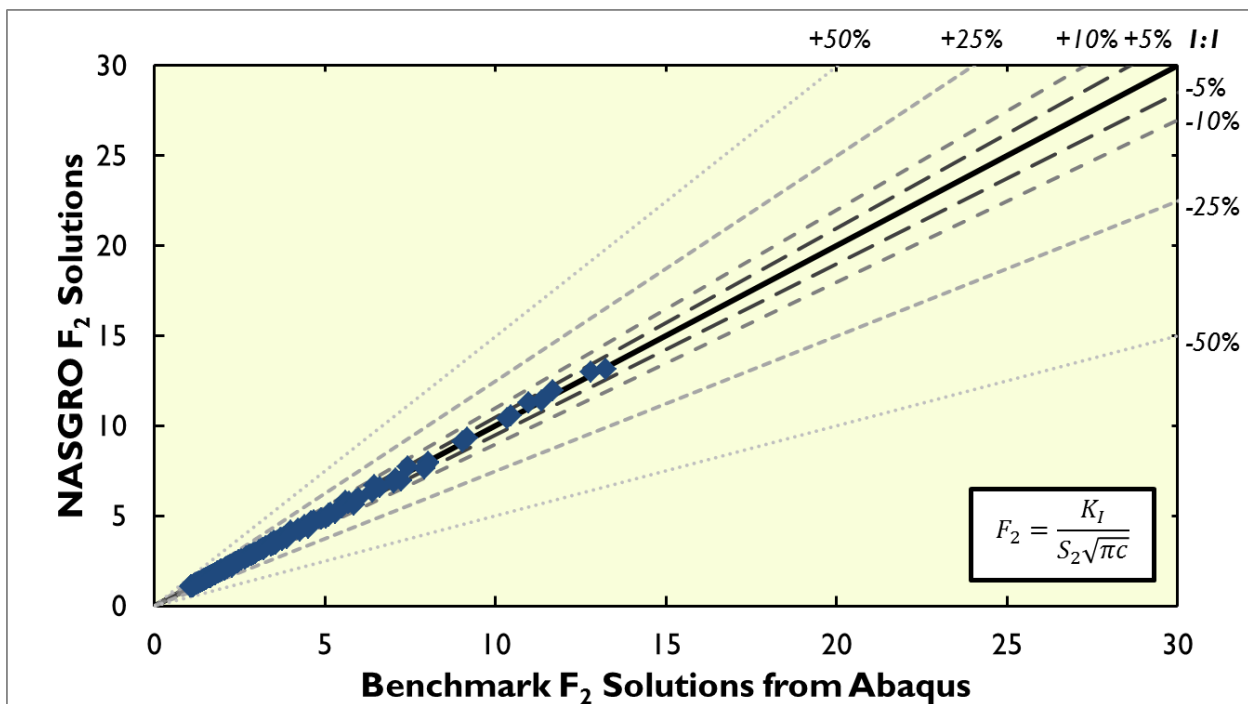
TC31 is not a weight function solution. It cannot accommodate residual stresses. TC31 transitions to TC32 in one cycle when the crack length (c) reaches $0.95 \times (W_x - t_y)$. TC32 is a similar solution to TC31. Please refer to the TC32 documentation for additional information. The following three figures show verification studies of TC31. Geometry correction factors (F) from independent finite element analyses (using Abaqus 6.12-1) provide the benchmark solutions. Each figure shows results from verification analyses generated using a Latin Hypercube Sampling method to fill the solution space. These solutions include different thickness (e.g., in the two legs) to illustrate the thickness skew correction factor. Almost all SIFs computed with TC31 have less than 10% error in comparison with the benchmark data. Studies of the L-section geometry and loading using TC02 as an alternative method indicate increased error over the solutions space. TC02 becomes increasingly inaccurate for this geometry as the crack approaches the corner of the solution.



Verification of TC31 under S_0 loading

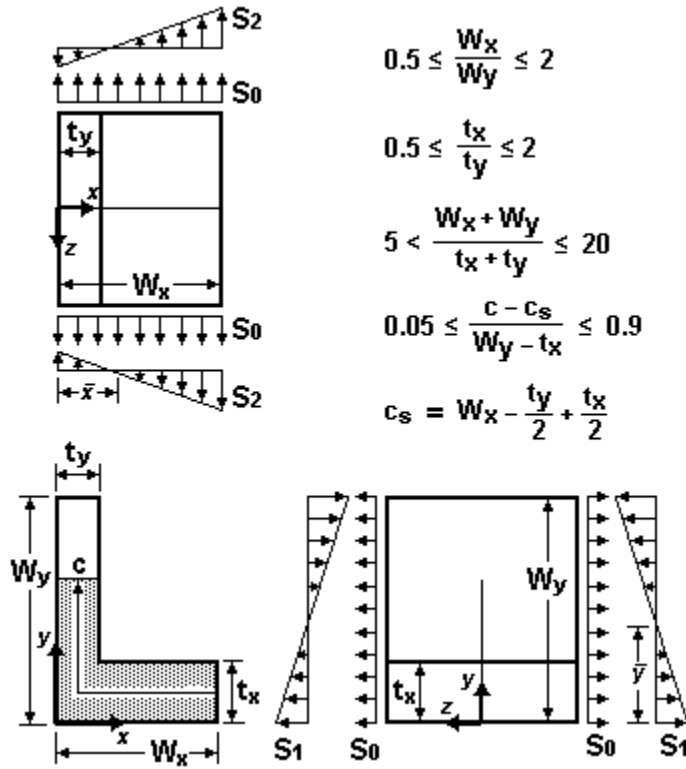


Verification of TC31 under S_1 loading



Verification of TC31 under S_2 loading

TC32 – Through Crack in L-section under Remote Loading – Post-Corner



L-section parameters and loadings for TC32

The TC32 solution features a through crack in two legs of an L-section under remote stresses. TC32 places the through crack on the cross section and normal to the axial length of the structural member. TC32 restricts the through crack to be straight and normal to free surfaces. TC32 contains stress intensity factor (SIF) solutions for cracks under remotely applied uniform stresses and univariant stress gradients. TC32 limits the crack to two legs of the L-section, i.e., it has already turned the corner of the section. At this time, TC32 does not restrain bending. The SIF (stress intensity factor) solution is based on the Herrmann-Bažant-Dunn (HBD) method to compute SIFs. Please refer to TC31 for additional information on this solution method. The previous figure of the TC32 solution shows the parameterization of the L-section and the available stress gradients. L-sections in TC32 have five geometric parameters: widths of the X and Y legs (W_x and W_y); thicknesses of the X and Y legs (t_x and t_y); and the crack length (c). TC32 does not support rounded corners or tapering of the thickness along the legs. TC32 supports loading of the L-section by uniform stresses (S_0), linear stresses varying along the Y axis (S_1), and linear stresses varying along the X axis (S_2). Please refer to TC31 for the extensive relationships to convert S_0 , S_1 , and S_2 to axial loads and moments.

NASGRO employs beta factors (β_P , β_{M_x} , and β_{M_y}) calibrated from 3D finite element analyses of the cracked L-section. These analyses place a straight through crack in an L-section that matches the TC32 geometry. Analyses set the out-of-plane length (along the Z-axis) equal to three times the longest leg's width and impose remote stress gradients of S_0 , S_1 , and S_2 .

Finite element analyses in the post-corner configuration are significantly more complicated than analyses in the pre-corner configuration. Sections with post-corner cracks warp – twist in and out of plane – under remote stress gradients of S_0 , S_1 , and S_2 . Consequently, regions of the crack plane self-contact itself at an angle. Sections with post-corner cracks were modeled using analytically rigid surfaces tied to the deformable section. These sections require several time increments before achieving a stable response (where SIFs increase linearly with loads) using the Augmented Lagrangian method in Abaqus. We assume no friction between the self-contacting surfaces.

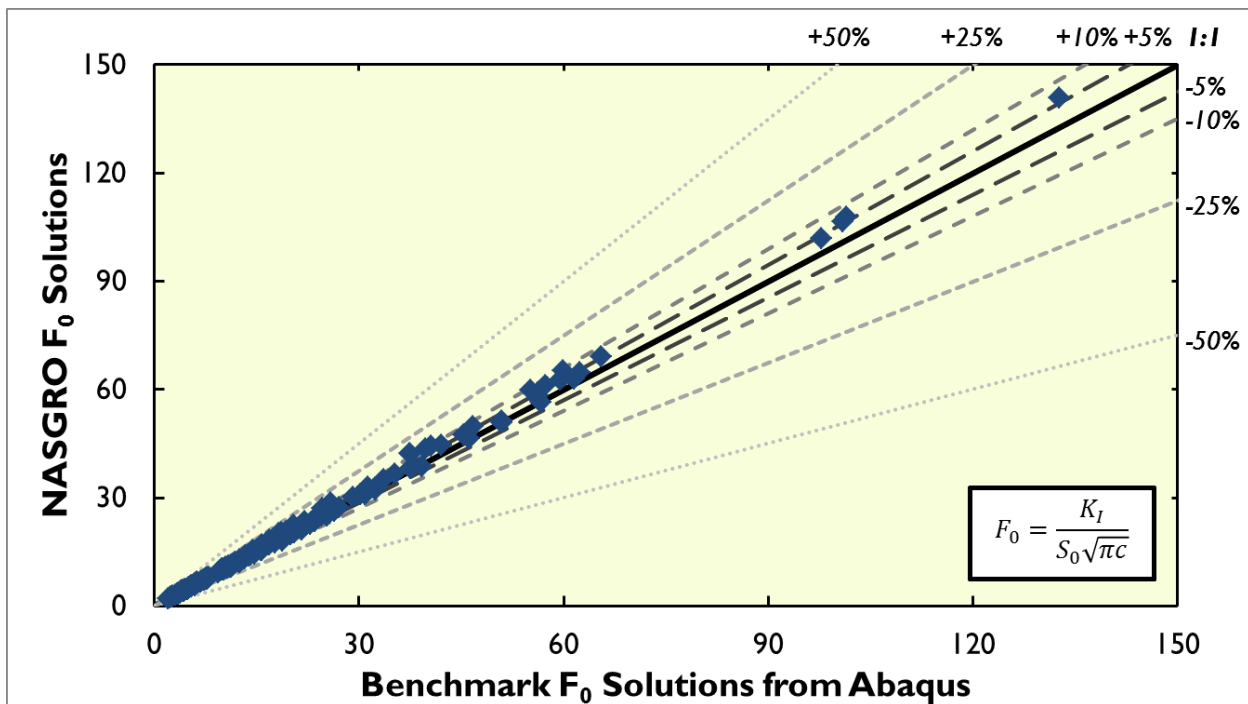
These finite element analyses determine the SIF variation along the crack thickness – along the X-axis. SIFs peak as $x \rightarrow t_y$, near the free surface, and on the corner side of the leg. SIFs become undefined as $x \rightarrow 0$ due to self-contact between the cracked faces. For simplicity, SIFs used in the calibration process and verification studies set an peak SIFs for all loading cases.

TC32 assumes simple bending to relate the imposed stresses to equivalent moments acting on the crack front. For example, an imposed stress S_2 produces an equivalent moment $\bar{M}_y = S_2 I_{yy} / (W_x - \bar{x})$. That is, the equivalent model \bar{M}_y represents the moment that would be generated on a rectangular section with second moment of area of I_{yy} and applied stress gradient S_2 . The equivalent moment does not match the actual moment for an L-section geometry due to non-zero values of I_{xy} . The HBD method employs the equivalent moment in its SIF calculations. In the calibration process, a known SIF from the FEA is normalized to an appropriate β -factor. Every finite element analysis in the calibration process provides one set of β -factors for the three remote stress gradients (S_0 , S_1 , and S_2). TC32 contains 360 calibrated β -factors per stress gradient. β -factors vary with the cross-section's width skew, thickness skew, slenderness, and crack length parameters over the following ranges:

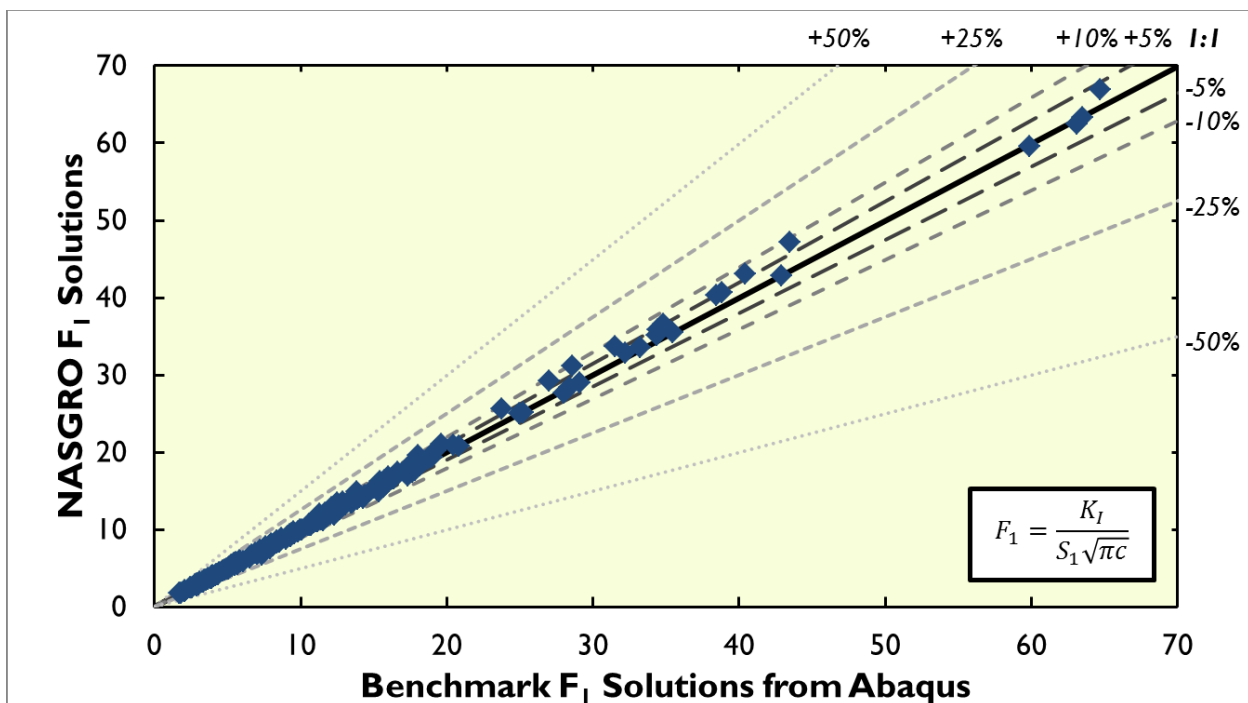
$$\begin{aligned} \frac{1}{2} &\leq \frac{W_x}{W_y} \leq 2 \\ \frac{1}{2} &\leq \frac{t_x}{t_y} \leq 2 \\ 5 &\leq \frac{W_x + W_y}{t_x + t_y} \leq 20 \\ 0.05 &\leq \frac{\frac{c - c_s}{W_y - t_x}}{t_x} \leq 0.95 \end{aligned}$$

TC32 interpolates over the set of β -factors to determine β -factors appropriate to the user defined geometry.

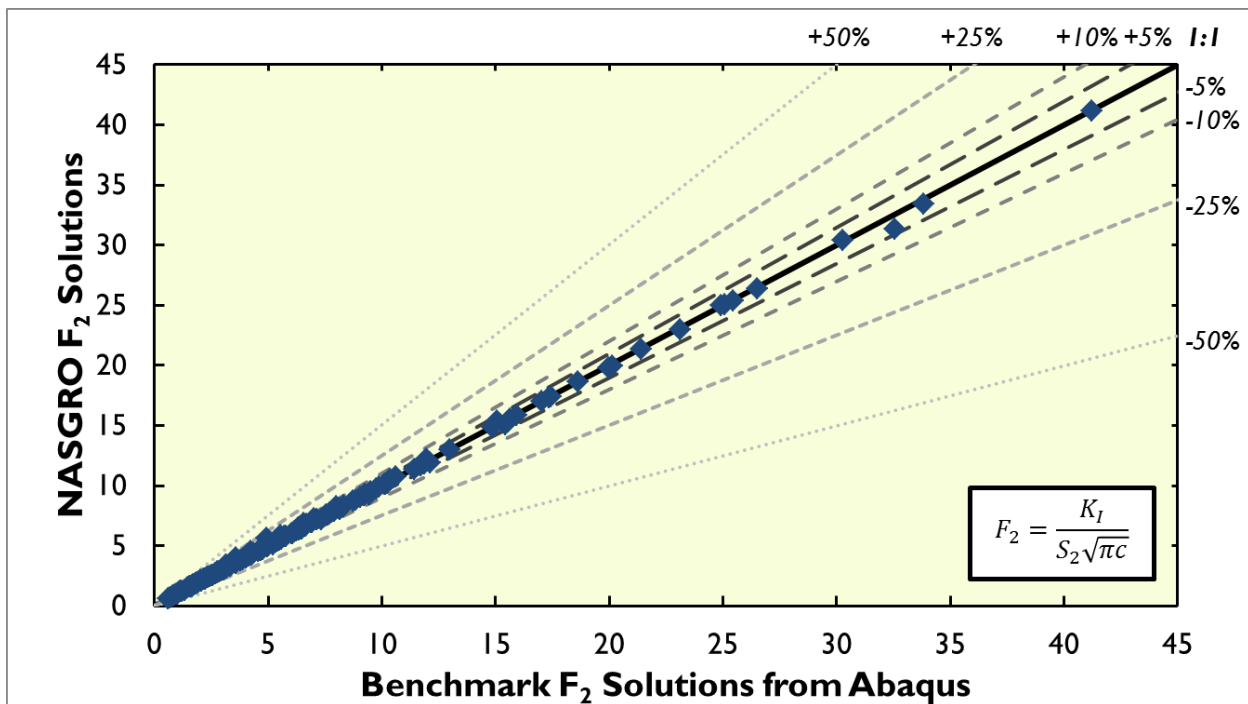
The following three figures show verification studies of TC32. Geometry correction factors (F) from independent finite element analyses (using Abaqus 6.12-1) provide the benchmark solutions. Each figure shows results from verification analyses generated using a Latin Hypercube Sampling method to fill the solution space. Almost all SIFs computed with TC32 have less than 10% error in comparison with the benchmark data.



Verification of TC32 under S_0 loading



Verification of TC32 under S_1 loading



Verification of TC32 under S_2 loading

Section C2: Corner Cracks

CC01 – Corner Crack in a Plate or Bar

$$F_i = f_x f_\phi f_a f_i, \quad i = 0,1,2$$

$$f_a = 1 \quad \text{for } a/c \leq 1$$

$$= \sqrt{c/a} \quad \text{for } a/c > 1$$

$f_i(a/c, a/t, c/W)$ are obtained from interpolating in f_0, f_1 , and f_2 tables (tables C12, C13, C14) as follows:

1) Four data points, $f_i\left(\left(a/c\right)_j, a/t, c/W\right)\Big|_{j=1,2,3,4}$, are calculated using cubic spline interpolation, where $(a/c)_j$ are listed tabular values of 0.0, 0.2, 0.4, 0.5, 1.0, 2.0, 2.5, 5.0, and ∞ ,

and, in general,

$$(a/c)_{j=1,2} < a/c \text{ and } (a/c)_{j=3,4} > a/c.$$

2) $f_i(a/c)$ are then calculated from the above four data points using piecewise Hermite polynomial interpolation

For extension of f_i tables to $1 < a/c \leq \infty$,

$$f_{0,a}(\lambda, \beta)\Big|_{a/c} = f_{0,c}(\beta, \lambda)\Big|_{c/a}$$

$$f_{0,c}(\lambda, \beta)\Big|_{a/c} = f_{0,a}(\beta, \lambda)\Big|_{c/a}$$

$$f_{1,a}(\lambda, \beta)\Big|_{a/c} = f_{2,c}(\beta, \lambda)\Big|_{c/a}$$

$$f_{1,c}(\lambda, \beta)\Big|_{a/c} = f_{2,a}(\beta, \lambda)\Big|_{c/a}$$

$$f_{2,a}(\lambda, \beta)\Big|_{a/c} = f_{1,c}(\beta, \lambda)\Big|_{c/a}$$

$$f_{2,c}(\lambda, \beta)\Big|_{a/c} = f_{1,a}(\beta, \lambda)\Big|_{c/a}$$

where $\lambda = a/t$, $\beta = c/W$,

$f_{i,a}$ is value for $\phi = 90 \text{ deg}$ (a -tip), and

$f_{i,c}$ is value for $\phi = 0 \text{ deg}$ (c -tip).

Reference: Curve fit, interpolation and extrapolation of [C23] numerical results.

Table C12 : Table of f_0 values

a/c	A/t	$c/W =$ $a\text{-tip}$	0.0 $c\text{-tip}$	$c/W =$ $a\text{-tip}$	0.1 $c\text{-tip}$	$c/W =$ $a\text{-tip}$	0.2 $c\text{-tip}$	$c/W =$ $a\text{-tip}$	0.5 $c\text{-tip}$	$c/W =$ $a\text{-tip}$	0.8 $c\text{-tip}$	$c/W =$ $a\text{-tip}$	1.0 $c\text{-tip}$
0.0	0.0	0.996	1.931	1.000	2.024	0.996	1.907	1.003	1.906	1.000	1.870	1.004	1.846
	0.1	1.062	1.930	1.068	1.973	1.069	1.924	1.069	1.795	1.057	1.705	1.055	1.645
	0.2	1.191	2.009	1.196	2.021	1.200	2.005	1.191	1.914	1.182	1.854	1.174	1.814
	0.5	1.766	2.817	1.786	2.874	1.816	2.909	1.935	3.034	2.070	3.171	2.187	3.278
	0.8	2.524	4.427	2.606	5.038	2.715	5.389	3.291	6.605	4.126	7.951	4.832	8.979
	1.0	3.140	5.955	3.278	7.366	3.471	8.289	4.635	11.871	6.432	15.372	7.925	17.706
0.2	0.0	1.037	1.280	1.041	1.285	1.043	1.291	1.070	1.330	1.102	1.390	1.128	1.441
	0.1	1.078	1.311	1.083	1.318	1.087	1.322	1.116	1.355	1.145	1.406	1.169	1.452
	0.2	1.157	1.374	1.161	1.380	1.169	1.388	1.207	1.420	1.240	1.470	1.268	1.513
	0.5	1.515	1.752	1.536	1.787	1.571	1.833	1.732	1.993	1.944	2.243	2.124	2.448
	0.8	2.031	2.498	2.098	2.663	2.196	2.832	2.749	3.528	3.623	4.603	4.378	5.491
	1.0	2.475	3.286	2.578	3.585	2.749	3.931	3.790	5.340	5.523	7.514	7.026	9.311
0.4	0.0	1.073	1.173	1.077	1.177	1.082	1.183	1.130	1.244	1.201	1.314	1.254	1.365
	0.1	1.094	1.196	1.097	1.201	1.104	1.206	1.161	1.267	1.233	1.343	1.289	1.398
	0.2	1.131	1.241	1.135	1.246	1.147	1.257	1.227	1.337	1.306	1.417	1.375	1.488
	0.5	1.317	1.488	1.339	1.521	1.378	1.567	1.577	1.749	1.865	2.072	2.117	2.349
	0.8	1.636	1.985	1.691	2.069	1.780	2.198	2.318	2.781	3.239	3.816	4.066	4.723
	1.0	1.941	2.504	2.015	2.638	2.167	2.861	3.111	3.972	4.813	5.875	6.355	7.559
0.5	0.0	1.086	1.158	1.090	1.160	1.097	1.165	1.150	1.220	1.235	1.302	1.308	1.381
	0.1	1.102	1.179	1.106	1.180	1.113	1.185	1.178	1.245	1.271	1.339	1.350	1.424
	0.2	1.130	1.211	1.134	1.217	1.147	1.228	1.238	1.310	1.345	1.417	1.439	1.511
	0.5	1.272	1.414	1.294	1.446	1.335	1.492	1.550	1.684	1.879	2.045	2.161	2.355
	0.8	1.546	1.827	1.596	1.899	1.684	2.018	2.224	2.574	3.169	3.609	4.010	4.516
	1.0	1.801	2.260	1.871	2.368	2.021	2.558	2.931	3.568	4.595	5.380	6.163	7.059
1.0	0.0	1.138	1.138	1.142	1.141	1.145	1.144	1.236	1.192	1.416	1.343	1.601	1.523
	0.1	1.141	1.142	1.144	1.144	1.154	1.152	1.261	1.220	1.470	1.399	1.683	1.609
	0.2	1.144	1.145	1.152	1.154	1.172	1.172	1.309	1.267	1.565	1.486	1.801	1.685
	0.5	1.198	1.232	1.220	1.261	1.267	1.309	1.547	1.547	2.075	2.056	2.555	2.514
	0.8	1.364	1.413	1.399	1.470	1.486	1.565	2.056	2.075	3.171	3.171	4.196	4.162
	1.0	1.481	1.615	1.545	1.686	1.685	1.801	2.514	2.555	4.162	4.190	5.977	5.977

Table C13 : Table of f_i values

a/c	a/t	$c/W =$ $a\text{-tip}$	0.0 $c\text{-tip}$	$c/W =$ $a\text{-tip}$	0.1 $c\text{-tip}$	$c/W =$ $a\text{-tip}$	0.2 $c\text{-tip}$	$c/W =$ $a\text{-tip}$	0.5 $c\text{-tip}$	$c/W =$ $a\text{-tip}$	0.8 $c\text{-tip}$	$c/W =$ $a\text{-tip}$	1.0 $c\text{-tip}$
0.0	0.0	0.996	1.868	1.000	1.877	0.996	1.893	1.003	1.930	1.000	1.967	1.004	1.992
	0.1	0.934	2.010	0.935	1.969	0.931	1.928	0.934	1.805	0.957	1.682	0.970	1.600
	0.2	0.900	1.994	0.906	1.947	0.904	1.976	0.916	1.936	0.968	1.909	0.930	1.891
	0.5	0.882	2.686	0.878	2.680	0.879	2.751	0.979	2.726	1.068	3.045	1.147	3.100
	0.8	0.631	3.499	0.685	3.745	0.736	4.148	1.022	4.503	1.427	5.294	1.819	5.677
	1.0	0.148	4.255	0.216	4.769	0.315	5.473	0.827	6.231	1.548	7.526	2.076	8.286
0.2	0.0	1.037	1.280	1.041	1.285	1.043	1.291	1.070	1.330	1.102	1.390	1.128	1.441
	0.1	0.939	1.287	0.940	1.289	0.945	1.294	0.975	1.336	1.029	1.400	1.077	1.458
	0.2	0.855	1.295	0.862	1.296	0.870	1.302	0.910	1.360	0.972	1.435	1.025	1.510
	0.5	0.683	1.475	0.689	1.486	0.706	1.520	0.820	1.632	0.956	1.829	1.070	1.990
	0.8	0.392	1.762	0.428	1.811	0.469	1.896	0.730	2.231	1.135	2.811	1.494	3.204
	1.0	0.056	2.050	0.093	2.129	0.165	2.266	0.572	2.793	1.264	3.745	1.883	4.577
0.4	0.0	1.073	1.173	1.077	1.177	1.082	1.183	1.130	1.244	1.201	1.314	1.254	1.365
	0.1	0.941	1.152	0.943	1.100	0.956	1.170	1.015	1.214	1.067	1.307	1.188	1.396
	0.2	0.820	1.148	0.828	1.157	0.842	1.168	0.911	1.212	0.997	1.333	1.124	1.455
	0.5	0.515	1.195	0.538	1.210	0.562	1.236	0.694	1.378	0.877	1.603	1.027	1.807
	0.8	0.194	1.340	0.217	1.360	0.247	1.400	0.488	1.705	0.903	2.243	1.255	2.739
	1.0	-0.026	1.490	-0.018	1.503	0.035	1.573	0.357	2.044	1.028	2.857	1.696	3.599
0.5	0.0	1.086	1.158	1.090	1.160	1.097	1.165	1.150	1.220	1.235	1.302	1.308	1.381
	0.1	0.946	1.130	0.952	1.139	0.965	1.148	1.027	1.192	1.117	1.297	1.233	1.417
	0.2	0.808	1.114	0.820	1.126	0.840	1.140	0.915	1.183	1.019	1.320	1.167	1.482
	0.5	0.475	1.124	0.490	1.140	0.526	1.164	0.660	1.313	0.873	1.573	1.055	1.831
	0.8	0.129	1.223	0.150	1.243	0.184	1.281	0.422	1.570	0.838	2.099	1.197	2.654
	1.0	-0.094	1.334	-0.079	1.343	-0.032	1.407	0.274	1.854	0.934	2.594	1.600	3.375
1.0	0.0	1.138	1.136	1.142	1.141	1.145	1.144	1.236	1.192	1.416	1.343	1.601	1.523
	0.1	0.965	1.087	0.977	1.097	0.993	1.111	1.094	1.176	1.288	1.348	1.488	1.573
	0.2	0.785	1.047	0.810	1.080	0.838	1.080	0.960	1.167	1.180	1.368	1.406	1.650
	0.5	0.345	0.962	0.375	1.000	0.419	1.033	0.590	1.194	0.942	1.574	1.270	2.012
	0.8	-0.070	0.961	-0.043	0.983	-0.006	1.031	0.228	1.230	0.698	1.831	1.189	2.551
	1.0	-0.352	0.964	-0.323	0.990	-0.279	1.043	-0.005	1.407	0.637	2.028	1.154	2.992

Table C14 : Table of f_2 values

a/c	a/t	$c/W =$ $a\text{-tip}$	0.0 $c\text{-tip}$	$c/W =$ $a\text{-tip}$	0.1 $c\text{-tip}$	$c/W =$ $a\text{-tip}$	0.2 $c\text{-tip}$	$c/W =$ $a\text{-tip}$	0.5 $c\text{-tip}$	$c/W =$ $a\text{-tip}$	0.8 $c\text{-tip}$	$c/W =$ $a\text{-tip}$	1.0 $c\text{-tip}$
0.0	0.0	0.997	1.904	0.958	1.162	0.934	1.027	0.861	-0.390	0.765	-1.705	0.727	-2.582
	0.1	1.061	1.930	1.029	1.371	1.002	1.082	0.947	-0.235	0.871	-1.507	0.826	-2.355
	0.2	1.191	1.986	1.144	1.553	1.114	1.159	1.085	-0.087	1.004	-1.328	0.938	-2.155
	0.5	1.764	2.843	1.706	2.300	1.652	1.832	1.598	0.332	1.479	-1.156	1.419	-2.133
	0.8	2.521	4.436	2.458	4.117	2.457	3.814	2.564	2.400	2.582	0.421	2.723	-1.210
	1.0	3.150	5.951	3.087	6.411	3.191	6.273	3.480	4.114	4.004	1.609	4.383	-0.654
0.2	0.0	1.037	1.280	1.006	1.054	0.976	0.822	0.900	0.138	0.800	-0.566	0.740	-1.033
	0.1	1.078	1.311	1.050	1.080	1.020	0.848	0.955	0.150	0.866	-0.550	0.805	-1.018
	0.2	1.157	1.374	1.119	1.123	1.090	0.896	1.039	0.190	0.952	-0.522	0.885	-0.996
	0.5	1.515	1.752	1.469	1.492	1.440	1.259	1.400	0.530	1.313	-0.276	1.250	-0.814
	0.8	2.031	2.498	1.997	2.282	2.009	2.081	2.124	1.447	2.200	0.614	2.300	0.058
	1.0	2.475	3.286	2.470	3.085	2.558	2.967	2.873	2.536	3.320	1.821	3.700	1.347
0.4	0.0	1.070	1.175	1.050	1.000	1.010	0.796	0.940	0.215	0.845	-0.335	0.769	-0.714
	0.1	1.095	1.198	1.070	1.015	1.037	0.812	0.970	0.242	0.875	-0.324	0.806	-0.700
	0.2	1.131	1.241	1.100	1.039	1.074	0.852	1.010	0.276	0.922	-0.284	0.859	-0.658
	0.5	1.317	1.488	1.281	1.288	1.271	1.112	1.250	0.563	1.196	-0.045	1.150	-0.419
	0.8	1.630	1.985	1.629	1.798	1.652	1.635	1.772	1.199	1.912	0.649	1.998	0.282
	1.0	1.941	2.504	1.970	2.318	2.044	2.167	2.376	1.861	2.778	1.548	3.177	1.194
0.5	0.0	1.086	1.158	1.055	0.989	1.020	0.789	0.942	0.244	0.854	-0.269	0.792	-0.625
	0.1	1.102	1.179	1.074	1.000	1.040	0.809	0.968	0.272	0.884	-0.255	0.825	-0.603
	0.2	1.130	1.211	1.100	1.025	1.070	0.846	1.004	0.310	0.930	-0.212	0.878	-0.561
	0.5	1.272	1.414	1.241	1.230	1.234	1.067	1.216	0.566	1.187	0.025	1.157	-0.311
	0.8	1.546	1.827	1.538	1.649	1.560	1.502	1.701	1.123	1.851	0.652	1.938	0.362
	1.0	1.801	2.260	1.851	2.075	1.926	1.939	2.271	1.685	2.680	1.435	3.068	1.132
1.0	0.0	1.138	1.138	1.087	0.965	1.047	0.785	0.962	0.345	0.961	-0.070	0.964	-0.352
	0.1	1.141	1.142	1.097	0.977	1.060	0.810	1.000	0.375	0.983	-0.043	0.990	-0.323
	0.2	1.144	1.145	1.111	0.993	1.080	0.838	1.033	0.419	1.031	-0.006	1.043	-0.279
	0.5	1.192	1.236	1.176	1.094	1.167	0.980	1.194	0.590	1.280	0.228	1.407	-0.005
	0.8	1.343	1.416	1.348	1.288	1.368	1.180	1.574	0.942	1.831	0.698	2.028	0.637
	1.0	1.523	1.601	1.573	1.488	1.650	1.408	2.012	1.270	2.551	1.189	2.992	1.154

CC02 – Corner Crack from Hole in a Plate

$$F_0 = G_0 G_{w0}, \quad F_3 = [G_0 y/2 + G_3] G_{w3}, \quad F_1 = C_r C_f G_1 G_{w1} H_c$$

$$G_0 = f_0(z_0)/d_0, \quad G_3 = f_1(z_0)(g_p/d_0), \quad G_1 = f_0(z_2)/d_2,$$

$$G_{w0} = M_0 g_1 g_3 g_4 f_{w0} f_\phi f_x, \quad G_{w1} = G_{w3} = M_0 g_1 g_3 g_4 f_w f_\phi f_x$$

$$\text{where } z_{0,2} = [1 + 2(c/D)\cos(\mu_{0,2}\phi)]^{-1}$$

$$d_{0,2} = 1 + 0.13z_{0,2}^2, \mu_0 = 0.85, \mu_2 = 0.85 - 0.25v^{1/4}$$

$$g_p = [(1+y)/(1-y)]^{1/2}$$

$$f_w = [(1/\beta) \sin \beta \sec \lambda \sec(\pi y/2)]^{1/2}$$

$$\lambda = (\pi/2)\sqrt{v}[(D+c)/(W-c)], \quad \beta = D/B - 2y$$

f_{w0} are correction factors for finite width effects obtained from

the solution for a through crack from an offset hole in a plate listed in table C1.

$$H_1 = 1 + G_{11}v + G_{12}v^2 + G_{13}v^3, H_2 = 1 + G_{21}v + G_{22}v^2 + G_{23}v^3$$

C_r is the stress concentration factor from Reissner[C25]

C_f is an empirical correction factor given in[C24]

$$C_f = 0.637 - \frac{0.24(D/t)}{\sqrt{19.51 + (D/t)^2}}$$

For $a \leq c$:

$$M_0 = [1.13 - 0.09x] + [-0.54 + 0.89/(0.2+x)]v^2 + [0.5 - 1/(0.65+x) + 14(1-x)^{24}]v^4$$

$$g_1 = 1 + (0.1 + 0.35v^2)I^2, g_3 = (1 + 0.04x)(1 + 0.1J^2)(0.85 + 0.15v^{1/4})$$

$$g_4 = 1 - 0.7(1-v)(x-0.2)(1-x)$$

$$p = 0.1 + 1.3v + 1.1x - 0.7xv$$

$$G_{11} = -0.43 - 0.74x - 0.84x^2, G_{12} = 1.25 - 1.19x + 4.39x^2$$

$$G_{13} = -1.94 + 4.22x - 5.51x^2, G_{21} = -1.5 - 0.04x - 1.73x^2$$

$$G_{22} = 1.71 - 3.17x + 6.84x^2, G_{23} = -1.28 + 2.71x - 5.22x^2$$

For $a>c$:

$$\begin{aligned}
 M_0 &= (1 + 0.04/x) / \sqrt{x} + 0.2v^2 / x^4 - 0.11v^4 / x^4 \\
 g_1 &= 1 + (0.1 + 0.35v^2 / x)I^2 \\
 g_3 &= (1.13 - 0.09/x)(1 + 0.1J^2)(0.85 + 0.15v^{1/4}) \\
 g_4 &= 1, \quad p = 0.2 + 1/x + 0.6v \\
 G_{11} &= -2.07 + 0.06/x, \quad G_{12} = 4.35 + 0.16/x, \quad G_{13} = -2.93 - 0.3/x \\
 G_{21} &= -3.64 + 0.37/x, \quad G_{22} = 5.87 - 0.49/x, \quad G_{23} = -4.32 + 0.53/x \\
 \phi &= 0^\circ \text{ for } dc/dN \\
 &= 80^\circ \text{ for } da/dN
 \end{aligned}$$

The above values of ϕ apply for all values of a/c .

The ranges of applicability of the solution are:
 $0.2 \leq a/c \leq 2$, $1 \leq D/t \leq 4$, and $(D/2+c)/B < 0.5$.

References: [C4], [C6], [C13], [C24] and [C25].

CC03 – Corner Crack from Hole in a Lug

$$\begin{aligned}
 F_3 &= (G_0y/2 + G_3)G_w \\
 G_0 &= f_0(z)/d_0, \quad G_3 = f_1(z)(g_p/d_0) \\
 \text{where } z &= [1 + 2(c/D)\cos(0.85\phi)]^{-1} \\
 d_0 &= 1 + 0.13z^2 \\
 g_p &= [(1+y)/(1-y)]^{1/2} \\
 G_w &= M_0 g_1 g_3 f_\phi f_w f_x \\
 \text{for } a/c < 1 \\
 M_0 &= [1.13 - 0.09x] + [-0.54 + 0.89/(0.2+x)]v^2 + [0.5 - 1/(0.65+x) + 14(1-x)^{24}]v^4 \\
 g_1 &= 1 + (0.1 + 0.35v^2)I^2, \\
 g_3 &= (1 + 0.04x)(1 + 0.1J^2)(0.85 + 0.15v^{1/4})
 \end{aligned}$$

for $a/c > 1$

$$\begin{aligned}
 M_0 &= (1 + 0.04/x) / \sqrt{x} + 0.2v^2 / x^4 - 0.11v^4 / x^4 \\
 g_1 &= 1 + (0.1 + 0.35v^2 / x)I^2 \\
 g_3 &= (1.13 - 0.09/x)(1 + 0.1J^2)(0.85 + 0.15v^{1/4}) \\
 f_w &= [\sec \lambda \sec(\pi y/2)]^{1/2} \\
 \lambda &= (\pi/2)\sqrt{v}[(D+c)/(W-c)] \\
 \phi &= 0^\circ \text{ for } dc/dN \\
 &= 80^\circ \text{ for } da/dN
 \end{aligned}$$

The above values of ϕ apply for all values of a/c .

Reference: [C13] and [C24]

CC04 – Corner Cracks (one or two) from Hole in a Plate

For the case of one crack, the solutions for CC02 are used with the hole-center to edge distance B set equal to half the plate width W.

For two cracks, the following equations are used:

$$F_o = G_o G_w, \quad F_3 = [G_o y / 2 + G_3] G_w, \quad F_1 = C_r C_f G_1 G_w H_c$$

$$G_o = f_o(z_o) / d_o, \quad G_3 = f_1(z_o)(g_p / d_o) \quad G_1 = f_o(z_2) / d_2, \quad G_w = M_o g_1 g_3 g_4 f_w f_\phi f_x$$

$$\text{where } z_{o,2} = [1 + 2(c/D) \cos(\mu_{o,2}\phi)]^{-1}$$

$$d_{o,2} = 1 + 0.13z_{o,2}^2, \mu_o = 0.85, \mu_2 = 0.85 - 0.25v^{1/4}$$

$$g_p = [(1+y)/(1-y)]^{1/2}$$

$$f_w = [\sec \lambda \sec(\pi y/2)]^{1/2}$$

$$\lambda = (\pi/2)\sqrt{v}[(D+Nc)/((W-2c)+Nc)],$$

$$H_1 = 1 + G_{11}v + G_{12}v^2 + G_{13}v^3, H_2 = 1 + G_{21}v + G_{22}v^2 + G_{23}v^3$$

C_r is the stress concentration factor given in [C25]

$$C_f = 0.637 - \frac{0.24(D/t)}{\sqrt{19.51 + (D/t)^2}} \text{ is an empirical correction factor given in [C24]}$$

$$f_o(z) = 1 + 0.358z + 1.425z^2 - 1.578z^3 + 2.156z^4$$

$$f_1(z) = 0.00982278 + 0.0502815z + 1.83559z^2 - 3.27483z^3 + 2.49104z^4$$

For $a \leq c$:

$$M_o = [1.13 - 0.09x] + [-0.54 + 0.89/(0.2+x)]v^2 + [0.5 - 1/(.65+x) + 14(1-x)^{24}]v^4$$

$$g_1 = 1 + (0.1 + 0.35v^2)I^2, \quad g_3 = (1 + 0.04x)(1 + 0.1J^2)(0.85 + 0.15v^{1/4})$$

$$g_4 = 1 - 0.7(1-v)(x-0.2)(1-x)$$

$$p = 0.1 + 1.3v + 1.1x - 0.7xv$$

$$G_{11} = -0.43 - 0.74x - 0.84x^2, \quad G_{12} = 1.25 - 1.19x + 4.39x^2$$

$$G_{13} = -1.94 + 4.22x - 5.51x^2, \quad G_{21} = -1.5 - 0.04x - 1.73x^2$$

$$G_{22} = 1.71 - 3.17x + 6.84x^2, \quad G_{23} = -1.28 + 2.71x - 5.22x^2$$

For $a/c > 1$

$$M_o = [1 + 0.04/x]/\sqrt{x} + 0.2v^2/x^4 - 0.11v^4/x^4$$

$$g_1 = 1 + (0.1 + 0.35v^2/x)I^2, \quad g_3 = (1.13 - 0.09/x)(1 + 0.1J^2)(0.85 + 0.15v^{1/4})$$

$$g_4 = 1$$

$$p = 0.2 + 1/x + 0.6v$$

$$G_{11} = -2.07 + 0.06/x, \quad G_{12} = 4.35 + 0.16/x \quad G_{13} = -2.93 - 0.3/x$$

$$G_{21} = -3.64 + 0.37/x \quad G_{22} = 5.87 - 0.49/x, \quad G_{23} = -4.32 + 0.53/x$$

$$\phi = 0 \quad \text{for } dc/dN$$

$$= 80^\circ \quad \text{for } da/dN$$

The above values of ϕ apply for all values of a/c .

The ranges of applicability of the solution are:

$0.2 \leq a/c \leq 2$, $1 \leq D/t \leq 4$, and $(D/2+c)/(W/2) < 0.5$.

References: [C4], [C6], [C13], [C24] and [C25]

CC05 – Corner Crack in a Plate – 2D Nonlinear Stress

(CC05 is a first generation bivariant solution with accuracy limitations, which has been superseded by crack case CC09. During execution, CC05 is not available within the set of *Corner Cracks*, but is displayed instead in the list of *Superseded Solutions*.)

The loading is very general, i.e., stress variation in both the width(x-axis) and thickness(y-axis) directions can be taken into account. The stresses are to be input via a file containing the coordinates and stress values. A sample file is shown below. The stress intensity correction factors for this case are computed using a 3D weight function method developed by Fujimoto [C36.]. The method requires a reference solution for the geometry under consideration. The current NASGRO solution, for a corner crack in a plate subjected to uniform tension, as shown Tables C12, C13, C14 is used as the reference solution.

Sample Bi-varient Stress input file

```
6      6  No. of points in x, y directions (at least: [3 3], max: [20 20])
0.0    Coordinates along x-direction
0.2
0.4
0.6
0.8
1.0
0.0  1.0  Y-coordinate, stress value for the first x-coord.
0.1  1.0
0.2  1.0
0.5  1.0
0.8  1.0
1.0  1.0
0.0  1.0  Y-coordinate, stress value for the second x-coord.
0.1  1.0
0.2  1.0
0.5  1.0
0.8  1.0
1.0  1.0
0.0  1.0  Y-coordinate, stress value for the third x-coord.
0.1  1.0
0.2  1.0
0.5  1.0
0.8  1.0
1.0  1.0
0.0  1.0  Y-coordinate, stress value for the fourth x-coord.
0.1  1.0
0.2  1.0
0.5  1.0
0.8  1.0
1.0  1.0
0.0  1.0  Y-coordinate, stress value for the fifth x-coord.
0.1  1.0
0.2  1.0
0.5  1.0
0.8  1.0
1.0  1.0
0.0  1.0  Y-coordinate, stress value for the sixth x-coord.
```

0.1	1.0
0.2	1.0
0.5	1.0
0.8	1.0
1.0	1.0

References: [C36] and [C37]

CC06 – Corner Crack from Hole in a Plate – 2D Nonlinear Stress (not active)

The loading can be bivariant as in the case of CC05, i.e., stress variation in both the width (x-axis) and thickness (y-axis) directions is allowed. The stresses are to be input via a file containing the coordinates and stress values. A sample file has been shown above. The stress intensity correction factors for this case are also computed using the 3D weight function method developed by Fujimoto [C36.]. The method requires a reference solution for the geometry under consideration. The reference solution for this case is still under development. Hence this case has been temporarily disabled in this version.

References: [C36] and [C37]

CC07 – Corner Cracks (one or two) from Hole in a Plate – New 3-D soln for one crack

For the case of two cracks, for all three loading conditions, the solutions for CC04 are used. For the case of one crack under bending load, the same solution as in cc04 is used.

For the case of one crack under tension or pin load, completely new solutions were obtained using FRANC3D software package. The solutions are listed in the table C15 below. Numerical interpolation was used to compute the factor for intermediate geometrical values. The new solution extends the validity to $D/t = 0.5$.

The ranges of applicability for CC07:

For two corner cracks:

$$0.2 \leq a/c \leq 2, \quad 1 \leq D/t \leq 4, \quad (D/2+c)/(W/2) < 0.5.$$

For one corner crack:

If it is subjected to tension and/or pin load only,

$$0.1 \leq a/c \leq 2, \quad 0.5 \leq D/t \leq 4.$$

Otherwise,

$$0.2 \leq a/c \leq 2, \quad 1 \leq D/t \leq 4, \quad (D/2+c)/(W/2) < 0.5.$$

Table C15: CC07 (one crack) - SIF Correction Factors by BEM Analysis (FRANC3D)

*R/t⇒	a/c	a/t	Tensile loading						Pin loading					
			a-tip			c-tip			a-tip			c-tip		
			0.25	0.5	2.0	0.25	0.5	2.0	0.25	0.5	2.0	0.25	0.5	2.0
$F_0 = K / S_0 \sqrt{\pi a}$												$F_3 = K / S_3 \sqrt{\pi a}$		
0.1	0	0	2.37	2.6	3.3	0.115	0.375	0.75	0.608	0.75	1.2	0.003	0.023	0.135
	0.1	0.1	2.1825	2.4978	3.3149	0.1817	0.3925	0.6780	0.5135	0.6726	1.1597	0.0038	0.02141	0.1178
	0.3	0.3	1.8282	2.3073	3.3518	0.3205	0.4326	0.5315	0.3234	0.5160	1.0733	0.0051	0.0185	0.0845
	0.7	0.7	1.6212	2.1781	3.9597	0.3815	0.5260	0.7553	0.2179	0.3982	1.1828	0.0057	0.0202	0.1092
	0.9	0.9	1.5307	2.0113	4.1749	0.7191	0.8326	1.0229	0.1892	0.3586	1.2132	0.0139	0.03271	0.1392
0.5	0	0	2.31	2.34	3.1	0.93	1.2	2.04	0.58	0.615	1.07	0.15	0.23	0.665
	0.1	0.1	2.1005	2.2302	2.9831	0.8995	1.1151	1.8912	0.5172	0.5798	1.0170	0.1198	0.1945	0.5888
	0.3	0.3	1.6425	2.0395	2.7709	0.8318	0.9374	1.5842	0.3664	0.5068	0.9229	0.0590	0.1195	0.4470
	0.7	0.7	1.2970	1.7600	2.7891	0.9942	1.0418	1.7411	0.2460	0.3979	0.8928	0.0477	0.0964	0.4424
	0.9	0.9	1.2490	1.7247	2.9498	1.0320	1.1478	1.8912	0.2325	0.3895	0.9254	0.0416	0.0952	0.4591
1.0	0	0	2.02	2.15	2.6	1.37	1.775	2.32	0.5512	0.61	0.9	0.26	0.425	0.765
	0.1	0.1	1.8331	2.0303	2.4942	1.2237	1.5665	2.1873	0.4655	0.5566	0.8635	0.2233	0.3497	0.7079
	0.3	0.3	1.4669	1.7769	2.3238	0.9469	1.1536	1.9489	0.3460	0.4625	0.7870	0.1173	0.2060	0.5933
	0.7	0.7	1.1530	1.5280	2.2361	0.9303	1.0897	1.9003	0.2480	0.3803	0.7350	0.0749	0.1484	0.5435
	0.9	0.9	1.1123	1.5343	2.3788	0.8982	1.0836	1.8864	0.2313	0.3776	0.7731	0.0601	0.1332	0.5186
2.0	0	0	1.425	1.58	1.77	1.43	1.72	2.12	0.39	0.455	0.645	0.33	0.44	0.73
	0.1	0.1	1.3562	1.5094	1.7413	1.2754	1.5468	2.0250	0.3614	0.4282	0.6216	0.2739	0.3747	0.6762
	0.3	0.3	1.2047	1.3494	1.6852	0.9585	1.2011	1.8459	0.3030	0.3688	0.5777	0.1646	0.2555	0.5861
	0.7	0.7	0.9336	1.1936	1.5226	0.8221	1.0250	1.7155	0.2205	0.3169	0.5179	0.1025	0.1861	0.5203
	0.9	0.9	0.8831	1.1894	1.6640	0.7851	0.9825	1.6604	0.2010	0.3116	0.5602	0.0854	0.1653	0.4948

CC08 – Corner Crack (or Twin Cracks) at an Off-Center Hole in a Plate –1D Nonlinear Stress

Crack case CC08 is a weight function solution for the corner crack at an off-center hole in a finite width plate with a general nonlinear stress distribution. It is nominally the same geometry as CC02. The difference between CC02 and CC08 is that CC02 is defined in terms of remote loads and moments and pin loads, while CC08 is a weight function solution defined in terms of general nonlinear stress distributions on the crack plane in the corresponding uncracked body. Crack case CC08 [from NASGRO 6.0 onwards] includes a symmetric geometry (with twin cracks) loaded symmetrically.

The new CC08 solution is based on a completely independent set of reference solutions derived using the boundary element computer program FADD-3D [C39, C40], and has no relationship to the original CC02 solution. The new solution provides some improvements in solution accuracy, although a complete comparison of CC02 vs. CC08 has not yet been completed. The previous CC02 solution has been left unchanged for legacy purposes.

Crack case CC08 provides consistent stress intensity factor solutions for stresses in two different input forms:

1. The fundamental weight function solution permits direct input of the principal normal stresses on the crack plane as pairs of $[(x/t)_i, S_i]$, where the x -axis originates from the root of the hole and extends along the width of the plate.
2. The user can alternatively input a uniform remote tension stress on the plate. The code internally calculates the local stresses along the crack plane in the corresponding uncracked body, including the effects of the off-center hole, and then invokes the same weight function solution as above. It is not yet possible to input a uniform remote moment or pin load with this crack case.

The current geometry validity range for all CC08 solutions is as follows:

$$\begin{aligned}0 &\leq c/a \leq 2.0 \\0 &\leq a/t \leq 0.9 \\0.25 &\leq D/(2t) \leq 2.0 \\0.2 &\leq 2B/W \leq 1.0 \\0 &\leq c/[B-(D/2)] \leq 0.8\end{aligned}$$

The reference solutions along the crack perimeter near the two intersections of the corner crack with the surface generally exhibited increasing values approaching the surface and then decreased sharply immediately at the surface. The reference solutions assigned to the surface value (the c -tip or the a -tip) were selected at the maximum value of K near the corresponding surface, which typically occurred about three degrees inside the surface.

The effects of near-surface constraint on the growth of fatigue cracks at holes using this solution are not yet fully understood. At the present time, in order to be conservative, fatigue crack growth calculations in NASGRO do not multiply these near-surface ΔK values by the crack closure factor, β_R .

The CC08 solution uses the approximate weight function proposed by Glinka [C41, C42].

The weight function at the *c*-tip (the tip on the plate surface) is

$$W_c = \frac{2}{\sqrt{2\pi(c-x)}} \left[1 + M_{1c} \sqrt{\frac{c-x}{c}} + M_{2c} \frac{c-x}{c} + M_{3c} \left(\frac{c-x}{c} \right)^{\frac{3}{2}} \right] \quad (1)$$

The weight function at the *a*-tip (the crack tip in the bore of the hole) is

$$W_a = \frac{2}{\sqrt{\pi x}} \left[1 + M_{1a} \sqrt{\frac{x}{c}} + M_{2a} \cdot \frac{x}{c} + M_{3a} \left(\frac{x}{c} \right)^{\frac{3}{2}} \right] \quad (2)$$

The variable *x* is the distance normal to the hole axis measured from the location where the crack emanates (the root of the hole). The parameters M_{1c}, M_{2c}, \dots , etc. depend on the geometrical parameters and are defined by reference solutions.

At the *c*-tip, M_{1c} , M_{2c} , and M_{3c} are defined by

$$\begin{aligned} M_{1c} &= \frac{\pi}{\sqrt{2Q}} (4Y_0 - 6Y_1) - \frac{24}{5} \\ M_{2c} &= 3 \\ M_{3c} &= 2 \left(\frac{\pi}{\sqrt{2Q}} Y_0 - M_{1c} - 4 \right) \end{aligned} \quad (3)$$

and at the *a*-tip, M_{1a} , M_{2a} , and M_{3a} are given by

$$\begin{aligned} M_{1a} &= \frac{\pi}{\sqrt{4Q}} (30F_1 - 18F_0) - 8 \\ M_{2a} &= \frac{\pi}{\sqrt{4Q}} (60F_0 - 90F_1) + 15 \\ M_{3a} &= -(1 + M_{1a} + M_{2a}) \end{aligned} \quad (4)$$

Q is the shape factor for an elliptical crack approximated by

$$Q = \begin{cases} 1 + 1.464(a/c)^{1.65}, & a/c \leq 1 \\ 1 + 1.464(a/c)^{-1.65}, & a/c > 1 \end{cases} \quad (5)$$

and F_0 , F_1 , Y_0 and Y_1 are normalized SIFs or the reference solutions. F_0 , F_1 are obtained at the a -tip, and Y_0 and Y_1 are at the c -tip. The subscripts identify the two associated reference loads on the crack surfaces: 0 denotes uniform tension, and 1 denotes a linearly decreasing bending stress $\sigma_r(x) = -x/c + 1$.

The stress intensity factors at the a - and c -tips, $K_{a,c}$, can thus be determined by direct integration as

$$K_{a,c} = \int_0^c W_{a,c} \sigma(x) dx \quad (6)$$

where $\sigma(x)$ is the univariant stress applied on the crack surface, and the integration is carried out from $x=0$ to $x=c$.

References: [C39], [C40], [C41], [C42]

CC09 – Corner Crack in a Plate – 2D Nonlinear Stress

Crack case CC09 is a weight function solution for the corner crack in a finite plate, which is nominally the same geometry as CC01 and CC05. The difference between CC01 and CC09 is that CC01 is defined in terms of remote tension and bending stresses, while CC09 is a weight function solution defined in terms of general nonlinear bivariant stress distributions on the crack plane in the corresponding uncracked body. CC05 and CC09 have nominally the same capabilities, but CC05 was a first-generation bivariant solution with some accuracy limitations, and CC09 is a second-generation bivariant solution with improved accuracy.

The new CC09 solution is based on a new weight function formulation and an independent set of reference solutions derived using the boundary element computer program FADD-3D [C39, C40], and has no relationship to the original CC01 or CC05 solutions. The new solution provides improvements in solution accuracy in comparison to both CC01 and CC05, although a complete comparison of the three solutions has not yet been completed. Crack case CC01 has been left unchanged for legacy purposes; CC05 has been moved under *Superseded Solutions*.

The stresses are input via a file that contains the coordinates and stress values. This input format is the same as for the CC05 solution (q.v.) except the distribution of coordinates should be uniform.

The current geometry validity range for CC09 solutions is as follows:

$$0.025 \leq a/c \leq 40$$

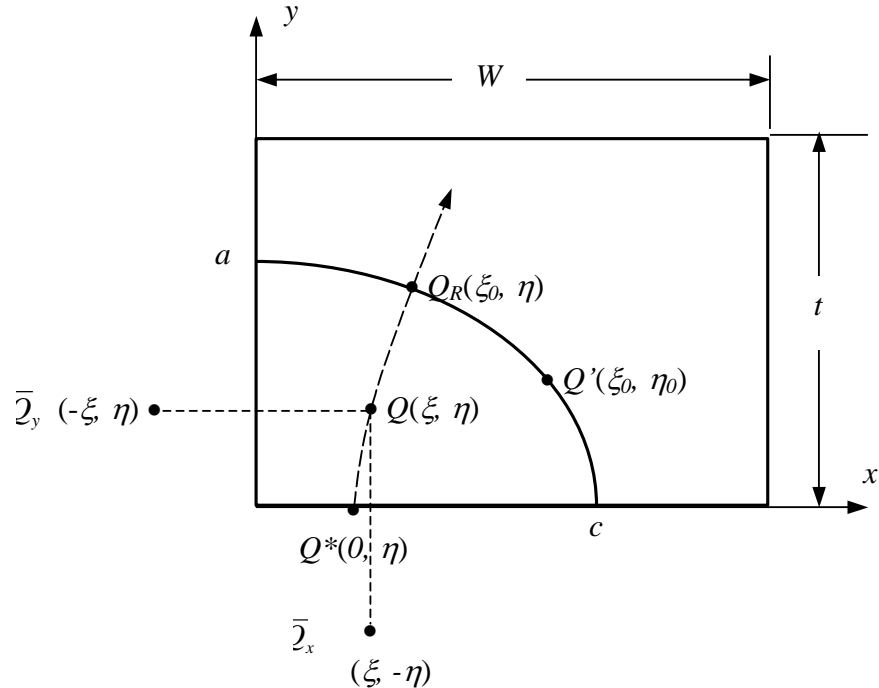
$$0 \leq a/t \leq 0.95$$

$$0 \leq c/W \leq 0.9$$

The reference solutions along the crack perimeter near the two intersections of the corner crack with the surface generally exhibit increasing values approaching the surface and then decrease sharply immediately at the surface. The reference solutions assigned to the surface value (the c -tip or the a -tip) were selected at the maximum value of K near the corresponding surface, which typically occurred about three degrees inside the surface.

The effects of near-surface constraint on the growth of corner fatigue cracks in plates using this solution are not yet fully understood. At the present time, in order to be conservative, fatigue crack growth calculations in NASGRO do not multiply these near-surface ΔK values by the crack closure factor, β_R .

The CC09 solution uses a new bivariant weight function formulation derived by Lee [C44]. The corner crack in a rectangular plate of finite width and thickness is assumed to have a quarter-elliptical shape that can be characterized by two degrees of freedom, the crack dimensions c and a in the width and thickness directions, respectively (in figure below).



Geometry configuration and nomenclature for corner crack in plate.

Due to its simplicity and accuracy, the PWF proposed by Orynyak [C45, C46] for an elliptical crack in an infinite body was used as the basic weight function. This form can be written as

$$W_{QQ'} = \frac{\sqrt{R^2 - r^2}}{\pi \ell_{QQ'}^2 \sqrt{\pi R}} \quad (1)$$

The equation represents the weighting effects on any point Q' along the crack front contributed by a point unit load applied at Q on the elliptical crack surface. Here, R is the distance between Q^* and Q_R , r the distance between Q and Q^* , and $\ell_{\bar{Q}Q'}$ the distance between Q and Q' . The definitions for Q , Q' , Q_R , and Q^* are more concise using elliptical coordinate notation. Respectively, they are given by $Q = (\xi, \eta)$, $Q' = (\xi_0, \eta_0)$, $Q_R = (\xi_0, \eta)$ and $Q^* = (0, \eta)$ where ξ and η are the parameters in the elliptical coordinate system to identify a point along the crack plane with its origin at the center of the crack. It can be seen that Q , Q_R , and Q^* are defined along the same elliptical angle η . ξ_0 is the “elliptical radius” defining the elliptical crack front. This PWF equation is similar to the one for circular cracks derived by Kassir and Sih [C47] as well as Shah and Kobayashi [C48] except for different definitions for the length parameters.

To account for the free boundary correction for a quarter-elliptical corner crack in a quarter-infinite body, Eq. (1) was modified to include two additional length parameters. Now the basic point weight function applicable at Q' for a point unit load applied at Q is given by

$$W_{QQ'} = \frac{\sqrt{R^2 - r^2}}{\pi \ell_{QQ'}^2 \sqrt{\pi R}} \left(1 + \frac{\ell_{QQ'}^2}{\ell_{\bar{Q}_x Q'}^2} + \frac{\ell_{QQ'}^2}{\ell_{\bar{Q}_y Q'}^2} \right) \quad (2)$$

The additional length parameters $\ell_{\bar{Q}_x Q'}$ and $\ell_{\bar{Q}_y Q'}$ correct the free surface effects for a corner crack by assuming a symmetrical stress distribution for an imaginary prolonged crack extending into the other three quadrants. In reference to the figure above, $\ell_{\bar{Q}_x Q'}$ is the distance between \bar{Q}_x and Q' , and $\ell_{\bar{Q}_y Q'}$ the distance between \bar{Q}_y and Q' . The locations, \bar{Q}_x and \bar{Q}_y , are points symmetrical to the location of point load Q with respect to the x - and y -axes.

Additional correction terms are required to account for finite width and thickness effects. Following several exploratory investigations, a formulation was identified with reasonable numerical accuracy and stable convergent approach. The point weight function at Q' for a point unit load applied at Q for a quarter elliptical crack in a finite plate is thus provided by

$$W_{QQ'} = \frac{\sqrt{R^2 - r^2}}{\pi \ell_{QQ'}^2 \sqrt{\pi R}} \left(1 + \frac{\ell_{QQ'}^2}{\ell_{\bar{Q}_x Q'}^2} + \frac{\ell_{QQ'}^2}{\ell_{\bar{Q}_y Q'}^2} \right) \quad (3)$$

$$\left[1 + \Pi_1 \sqrt{1 - \frac{r}{R}} + \Pi_2 \left(1 - \frac{y}{y'} \right) + \Pi_3 \left(1 - \frac{x}{x'} \right) \right]$$

where x and y define the Cartesian coordinates of Q , and $x' = c\sqrt{1-x^2/a^2}$ and $y' = a\sqrt{1-x^2/c^2}$. The SIF can therefore be evaluated by performing surface integration across the crack area. For a given stress distribution $\sigma(x,y)$ applied on the crack plane obtained from an uncracked body subjected to remote loadings, the stress intensity factor is written as

$$K = \int_0^a \int_0^{c\sqrt{1-\frac{y^2}{a^2}}} \sigma(x, y) \cdot W_{QQ'} dx dy \quad (4)$$

The parameters Π_1 , Π_2 , and Π_3 are calibrated by reference solutions at both a - and c -tips to characterize the finite boundary effects. Accordingly, in this approach, three reference stress solutions are required at each tip, and the stress intensity factor at a - and c -tips can be determined by

$$K^{a,c} = \int_0^a \int_0^{c\sqrt{1-\frac{y^2}{a^2}}} \sigma(x, y) \frac{\sqrt{R^2 - r^2}}{\pi \ell^2_{QQ^{a,c}} \sqrt{\pi R}} \left(1 + \frac{\ell^2_{QQ^{a,c}}}{\ell^2_{Q_x Q^{a,c}}} + \frac{\ell^2_{QQ^{a,c}}}{\ell^2_{Q_y Q^{a,c}}} \right) \left[1 + \Pi_1^{a,c} \sqrt{1 - \frac{r}{R}} + \Pi_2^{a,c} \left(1 - \frac{y}{y'} \right) + \Pi_3^{a,c} \left(1 - \frac{x}{x'} \right) \right] dx dy \quad (5)$$

where the superscripts a and c denote parameters associated with a - and c -tips, respectively.

To facilitate the computation, Eq. (5) is preferably written in terms of elliptical coordinate parameters instead of Cartesian. For $\alpha = a/c \leq 1$, the relationships between Cartesian and elliptical coordinates (ξ, η) are as follows:

$$x = b \cosh \xi \cos \eta, \quad y = b \sinh \xi \sin \eta, \quad b = \sqrt{c^2 - a^2} \quad (6)$$

For any point along the crack front, the “elliptical radius” in elliptical coordinate system is the same and is given by

$$\xi_0 = \frac{1}{2} \ln \left(\frac{1+\alpha}{1-\alpha} \right) \quad (7)$$

The above equation is derived by eliminating the dependency on the elliptical angle η among coordinate transformation equations. The Cartesian coordinates for Q , Q_R , Q^* , Q' , \bar{Q}_x , and \bar{Q}_y in terms of elliptical coordinate parameters, are as follows:

$$Q = (b \cosh \xi \cos \eta, b \sinh \xi \sin \eta) \quad (8)$$

$$Q_R = (b \cosh \xi_0 \cos \eta, b \sinh \xi_0 \sin \eta) \quad (9)$$

$$Q^* = (b \cos \eta, 0) \quad (10)$$

$$Q' = (b \cosh \xi_0 \cos \eta, b \sinh \xi_0 \sin \eta) \quad (11)$$

$$\bar{Q}_x = (-b \cosh \xi \cos \eta, b \sinh \xi \sin \eta) \quad (12)$$

$$\bar{Q}_y = (b \cosh \xi \cos \eta, -b \sinh \xi \sin \eta) \quad (13)$$

and the infinitesimal area becomes

$$dxdy = b^2 (\sinh^2 \xi + \sin^2 \eta) d\eta d\xi \quad (14)$$

Furthermore, the integration limits are converted from $y: 0 \rightarrow a\sqrt{1-x^2/c^2}$ and $x: 0 \rightarrow c$ to $\xi: 0 \rightarrow \xi_0$ and $\eta: 0 \rightarrow \pi/2$. The integration sequence is now interchangeable.

Reference Solutions

The weight function method requires an accurate set of reference solutions for a matrix of crack geometries. These reference solutions were numerically generated using the FADD3D fracture mechanics software, a general boundary element code for three-dimensional linear elastic fracture analysis [C39, C40]. Reference solutions were generated at 150 different combinations of geometrical aspect ratios: $a/c=0.1, 0.2, 0.4, 0.6, 0.8, 1.0$; $c/W=0.1, 0.2, 0.5, 0.8, 0.9$; and $a/t=0.1, 0.2, 0.5, 0.8, 0.9$. For a/c and a/t less than 0.1 and approaching zero, reference stress solutions for edge cracks were generated and used [C34]. For a/c larger than 1, the reference solutions were obtained from the corresponding c/a ratios by reversing the stress field and the associated geometry dimensions. As a result, the expanded reference solution matrix constitutes a discrete database covering a complete range of aspect ratio combinations; i.e., a/c from 0 to ∞ , a/t from 0 to 0.9 and c/W from 0 to 0.9. For any arbitrary combination of aspect ratios, the reference solutions are determined from the matrix of specific solutions through Hermite interpolation. Three sets of reference solutions were determined for each crack geometry. These are denoted as solutions for unit tension, unit bending along the x -axis, and unit bending along the y -axis. The solutions were generated by applying the reference stresses on the crack plane in the corresponding uncracked body. The three reference stresses are given by $\sigma_0 = 1$, $\sigma_1 = -y/a + 1$, and $\sigma_2 = -x/c + 1$.

CC10 – Corner Crack at a Hole in a Plate – 2D Nonlinear Stress

Crack case CC10 is a weight function solution for a corner crack at an off-center hole in a finite width plate with a general bivariant stress distribution. The derivation of the weight function methodology used for this crack case is outlined in the discussion of CC09. The stress input format for CC10 is consistent with the other bivariant crack cases (CC05 & CC09) and is detailed in the discussion of CC05.

The current geometry validity range for CC10 is as follows:

$$\begin{aligned} 0.5 &\leq a/c \leq 5 \\ t/2 &\leq D \leq 4t \\ D/2 &< B \leq W/2 \\ 0 &\leq (W-2B)/W \leq 0.8 \end{aligned}$$

CC11: Corner Crack in a Plate with Univariant Stress Gradient

Highlights:

- Weight function solution, up to 4 stress distributions
- User-specified or optimum point spacing stress gradient entry
- Polynomial or tabular input (GUI tables or file input)
- Based on CC09 reference solutions

CC11 is a weight function solution for a corner crack in a plate subjected to a user defined crack plane stress distribution. CC11 is based on the same reference solutions as CC09 (Corner Crack in a Plate with Bivariant Stress Gradient) and give consistent answers with CC09 when a univariant stress distribution is applied. Crack plane stresses can be input in tabular form (via GUI table or file input) or as coefficients of a pre-defined sixth-order polynomial.

CC12 – Quarter-Elliptical Corner Crack at Chamfer in Plate – Bivariant Stressing

The stress intensity factor for a corner crack at a chamfered corner is based on the weight function solutions implemented for crack case CC09. Note that the corner crack must completely span the chamfer, as shown in Figure CC12-1(b). The two chamfer legs d_y and d_x in Figure CC12-1(b) must be equal.

The current geometry validity range for CC12 is as follows:

$$\begin{aligned} 0 \leq (a+d)/t &\leq 0.9 \\ 0 \leq (c+d)/W &\leq 0.9 \end{aligned}$$

To account for the effect of reduction in corner crack area due to chamfering, a multiplication factor was applied to the determined CC09 solutions. This correction factor is based on the ratio of two quarterly infinite domain solutions, as illustrated in Figure CC12-1. One is the bivariant corner crack solution by integrating the weight function over the quarterly elliptical crack surface as shown in 2(a), and the second one is the bivariant corner crack solution by integrating the weight function over the domain confined by the corner crack perimeter and the chamfer as illustrated in Figure CC12-1(b). The weight function in both cases was for the corner crack in a quarterly infinite domain. By designating the first corner crack solution by K_{corner}^∞ and the second one by $K_{chamfer}^\infty$, the stress intensity factor for the cracks at the chamfered corner is defined by

$$K^{CC12} = K_{chamfer} = \frac{K_{chamfer}^\infty}{K_{corner}^\infty} K^{CC09} = C.F. \times K^{CC09}$$

where K^{CC09} is the stress intensity factor computed using the CC09 module for finite dimensions. The correction factor (C.F.) is thus dependent on the stress variation besides the crack tip location and needs to apply to both crack tips separately.

To verify this approach, two sets of stress intensity solutions were determined numerically using the three-dimensional (3D) fracture mechanics program FADD3D. One is for the corner crack in the rectangular plate, and the other is for the corner crack in the chamfered rectangular plate. Two stress variations were applied for validation: one is unit tension $\sigma=1$, and the other is unit bending where $\sigma=1-y/a$ and a is the crack depth along the plate thickness direction — y .

The ratios of the solutions based on these two cracked configurations are corresponding to $K_{chamfer}/K^{CC09}$ and they are used to compare with the above-defined correction factors $K_{chamfer}^\infty/K_{corner}^\infty$. Notice the former is for a finite domain, while the later is for a quarterly infinite domain. The comparison of these factors for both crack tips is displayed in Figure CC12-2(a) for unit tension and in Figure CC12-2(b) for unit bending. The excellent agreement shown in these two figures validates the approach for multiplying the CC09 solution by the correction factor to account for the effect of reduction in crack area due to chamfering.

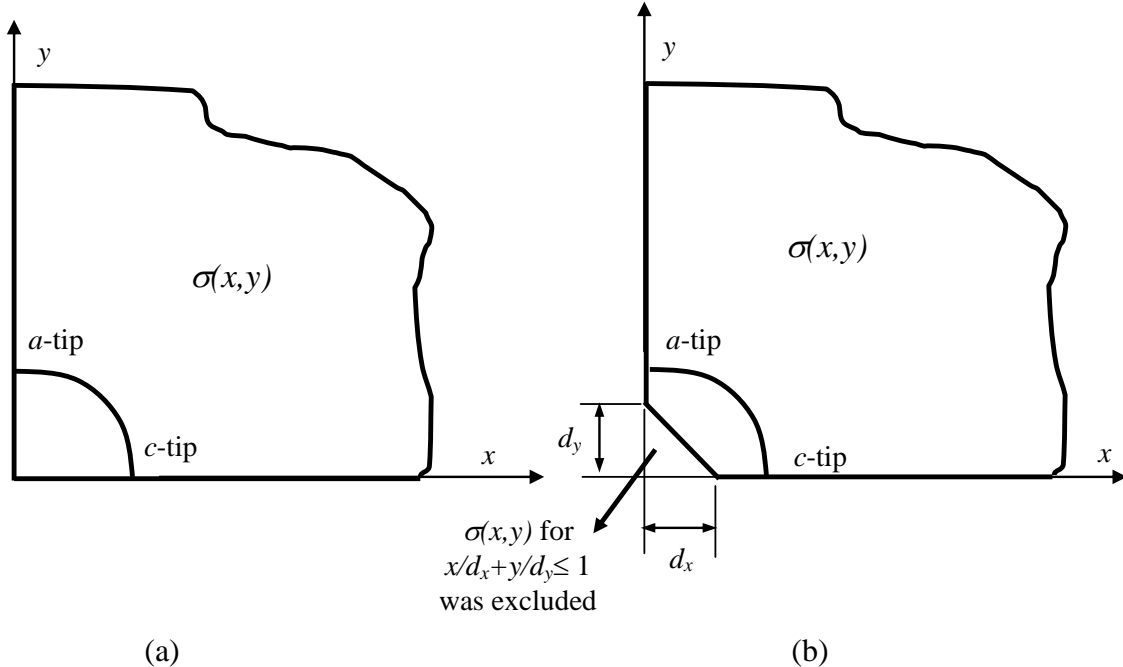


Figure CC12-1. The ratio of two different corner crack solutions was used for determining the stress intensity factors for chamfered corner: (a) the integration for weight function solution over the quarterly elliptical corner crack surface, and (b) the integration over the domain confined by the corner crack perimeter and the chamfer.

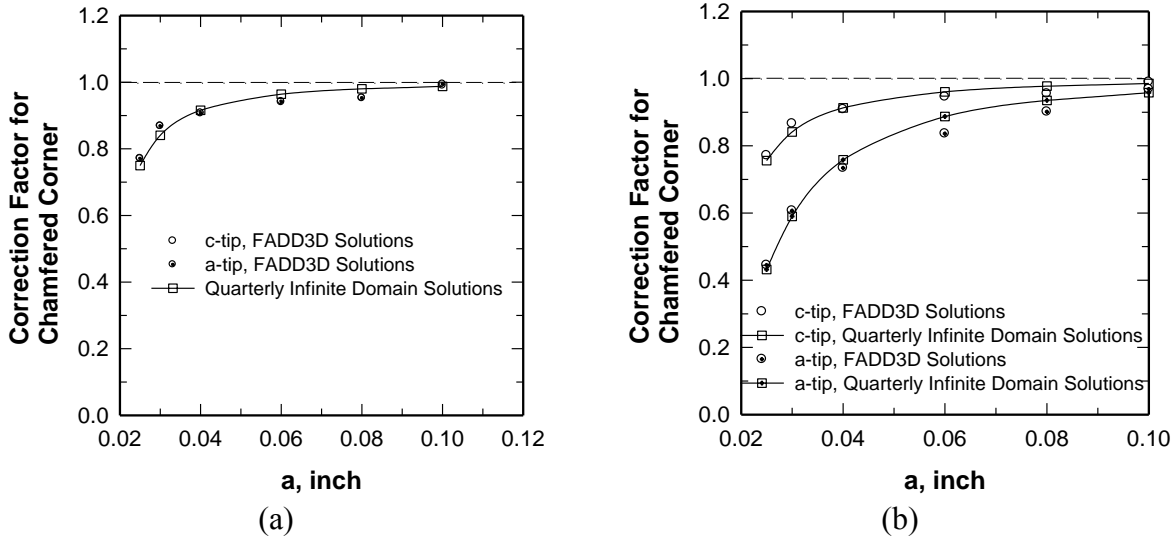


Figure CC12-2. Comparison of correction factors due to chamfering between FADD3D results for finite plate dimensions and weight function solutions for quarterly infinite domain: (a) unit tension and (b) unit bending

CC13 – Quarter-Elliptical Corner Crack at Edge Notch in Plate

The SIF solution for this crack model is based on the same weight function formulation for univariant stresses as that used CC11. The univariant distribution of crack opening stress along the crack growth direction is required along with the weight functions to determine the stress intensity factors at two surface tip locations.

Three types of stress definition can be specified. The simplest one is to apply tension and bending stresses at the remote ends (in contrast to applying stresses on the crack surface). For this stress definition, the CC13 fracture mechanics module internally computes the crack opening stress variation resulting from remote stressing by interpolation among an array of net section stress variations extracted from finite element results at discrete geometric aspect ratios.

The second and the third options for stress definition are provided for users to specify crack opening stress distributions along the crack plane. The second kind describes the stress variation in polynomial function of up to the sixth power expressed in terms of normalized coordinate. The normalized coordinate as the independent variable is with respect to the net section width. The polynomial function is given by

$$\sigma(x) = \sum_{i=0}^{6} a_i \left(\frac{x}{W_{net}} \right)^i$$

where the “effective” sectional width W_{net} is given by $W - (d + r)$ for angular notch or by $W - (e_1 - B)$ for elliptical notch. The length parameters: W , d , r , e_1 , and B , are the width of the plate, the nominal notch depth and the root radius of the angular notch, and the notch depth along the plate width direction and the offset of the ellipse describing the elliptical notch. The

coefficients a_i 's are provided by the user. The coordinate x is measured from the notch tip and across the net section.

The third kind represents the stress variation in tabulated format consisting of stress pairs. The stress pair is in terms of one stress value at one normalized coordinate measured from the notch tip across the net section, W_{net} . All stress pairs are listed row by row according to coordinates in ascending order. By this definition, the normalized coordinates cannot be less than zero or larger than 1.

There are two notch types with this crack model; one is of angular notch type and the other of elliptical notch type. The angular notch is characterized by two straight edges with an enclosed angle θ resulting in a nominal notch depth d and a local root radius r at the notch tip. In contrast, the elliptical notch is fully described by an ellipse of e_1 as the long axis and e_2 as the short axis with an additional offset B . The validity limits of the SIF solutions thus depend on the user-selectable notch shape and are listed in the following. Note the crack length a denotes the crack depth along the root of the notch and the crack length c denotes the crack depth measured on the front surface of the plate and along the plate width direction.

- Angular notch:

$$0^\circ \leq \theta \leq 75^\circ$$

$$0 < \frac{d+r}{W} \leq 0.75$$

$$0 \leq \frac{d}{r} \leq 24$$

$$\frac{c}{W-d-r} \leq 0.95$$

$$\frac{a}{t} \leq 0.95$$

The normalized coordinate is defined by $x/(W - d - r)$. The coordinate x is measured from the notch tip along the crack growth path.

- Elliptical notch:

$$\begin{aligned} 0.2 &\leq \frac{e_1}{e_2} \leq 5 \\ 0 &< \frac{e_1 - B}{W} \leq 0.75 \\ \frac{c}{W + B - e_1} &\leq 0.95 \\ \frac{a}{t} &\leq 0.95 \\ 0 &\leq B \leq e_1 \end{aligned}$$

The normalized coordinate is defined by $x/(W + B - e_1)$. The coordinate x is measured from the notch tip along the crack growth path.

CC14 – Quarter-Elliptical Corner Crack at Offset Embedded Slot or Elliptical Hole in Plate

The SIF solution of this crack model is mostly based on the same weight function formulation as for cracks at a hole subjected to univariant stressing; i.e., the one used by CC08. The only exception is for elliptical holes with $e_2/e_1 > 1$ where additional adjustments by the CC11 SIF solutions are imposed through interpolation. The univariant distribution of crack opening stress along the crack growth direction is required along with the weight functions to determine the stress intensity factors at two surface tip locations.

Two types of stress definition can be specified. The simplest one is to apply tension and bending stresses at remote ends. For this stress definition, the CC14 fracture mechanics module internally computes the crack opening stress variation resulting from remote stressing by interpolation among an array of net section stress variations extracted from finite element results at discrete geometric aspect ratios.

The other stress definition addresses the crack opening stress along the crack plane. The description represents the crack opening stress variation in stress pairs. Only the tabulated option is provided (*i.e.*, no polynomial stress option). The stress pair consists of one normalized coordinate and one stress value. The normalized coordinate is with respect to the smaller net section created by the offset of the hole or the slot B with $B \leq W/2$ and W is the width of the plate. The coordinate x is measured from the notch tip across the net section along which the crack growth path is assumed. By this definition, the variation of normalized coordinate is from 0 to 1.

Most of the CC14 SIF solutions are based on the same weight function approach for CC08 where the radius of the hole characterizing CC08 crack model is replaced by the “effective” notch depth in CC14 crack model. The definition of this “effective” notch depth depends of the type of the slot. For elliptical holes, it is the long axis e_1 while for straight-edge slots, it is the straight edge plus the root radius, $d + r$. For elliptical holes with $e_2/e_1 > 1$, the following interpolation between the SIF results from CC08 and CC11 weight function solutions is used.

$$K^{CC14} = (K^{CC08} - K^{CC11}) \left(\frac{e_1^2}{e_2^2} \right)^{0.2} + K^{CC11}$$

The interpolation ensures when the ratio of short axis to long axis e_2/e_1 equals to 1.0, the SIF solution for CC14 crack model is solely based on the weight function approach used by CC08 crack model; *i.e.*, $K^{CC14} = K^{CC08}$, while when $e_2/e_1 \rightarrow \infty$ or $e_1/e_2 \rightarrow 0$, the SIF solution retreats to the one for CC11 crack model. The interpolative relationship is empirically determined based on finite element results.

There are two types of slot with this crack model; one is straight-edge slots and the other elliptical holes. The straight-edge slot is characterized by two parallel straight edges and two semi-circular notch ends. The straight edge defines the nominal notch depth d and the semi-circular notch tip defines the local root radius r with the notch tip. In contrast, the elliptical hole is described by an ellipse of e_1 as the long axis and e_2 as the short axis. The offset of the slot or

hole from the right side of the plate defines the offset B . The validity limits of SIF solutions depend on the user-selected notch shape and are listed as follows. Note the crack depth along the bore is denoted by a , and the surface crack length along the plate width direction and on the front plate surface is denoted by c .

- Straight-edge slot:

$$0 \leq \frac{d+r}{B} \leq 0.75$$

$$0.25 \leq \frac{d+r}{t} \leq 2$$

$$0 \leq \frac{d}{r} \leq 24$$

$$0.2 \leq \frac{2B}{W} \leq 1$$

$$0 \leq \frac{c}{B-d-r} \leq 0.8$$

$$\frac{a}{c} \geq 0.5$$

$$0 \leq \frac{a}{t} \leq 0.9$$

The normalized coordinate is defined by $x/(B - d - r)$. The coordinate x is measured from the notch tip along the smaller net section.

- Elliptical notch:

$$0 \leq \frac{e_1}{B} \leq 0.75$$

$$0.25 \leq \frac{e_1}{t} \leq 2$$

$$0.2 \leq \frac{e_1}{e_2} \leq 5$$

$$0.2 \leq \frac{2B}{W} \leq 1$$

$$0 \leq \frac{c}{B-e_1} \leq 0.8$$

$$\frac{a}{c} \geq 0.5$$

$$0 \leq \frac{a}{t} \leq 0.9$$

The normalized coordinate is defined by $x/(B - e_1)$. The coordinate x is measured from the tip of the elliptical notch along the smaller net section.

CC15 – Quarter-Elliptical Corner Crack at Offset Hole in Plate with Broken Ligament

The weight function approach for this crack case is identical to the one used by CC13. The univariant distribution of crack opening stress along the net section is required to determine the SIFs at two surface tips; one along the bore and the other at the free surface of the plate.

Provided options to specify stress definition are (1) remote tension/bend, (2) polynomial stressing, and (3) tabulated stress variations. The latest two options are for describing the crack opening stress distributions along the crack plane. For the first stress definition option, the crack opening stresses defined along the net section are computed from the user-specified tension and bending combination at remote ends. The determination is by interpolation among an array of net sections stress variations from finite element results at discrete geometric aspect ratios.

The second stress definition option requires users to provide coefficients a_i 's as defined in the following polynomial stress functions.

$$\sigma(x) = \sum_{i=0}^6 a_i \left(\frac{x}{W_{net}} \right)^i$$

where the “effective” sectional width W_{net} is given by $W - (B + D/2)$. The length parameters: W , D , and B , are the width of the plate, the diameter of the hole, and the offset of the hole from the left side of the plate. Note in this configuration the left one of the two net sections characterized by the hole is broken resulting in the broken ligament. The coordinate x is measured from the root of the hole and along the crack growth plane or the remaining net section on the right.

The third stress definition option, following the NASGRO convention for stress definition, defines the univariant crack opening stress variations by stress pairs consisting of normalized coordinates and associated stress values. The fracture mechanics module will interpolate the intermediate stress value when evaluating the integration for weight function solutions.

To make use of the weight function formulation for CC11 crack model, the following transformations are used: (1) the “effective” sectional width W_{net} of this crack model is used and replaces the “thickness” used by CC11, (2) the surface crack length c along the plate width direction of this crack model replaces the “crack depth” a used by CC11, and (3) the surface crack length a along the bore of this crack model replaces the “surface crack length” c used by CC11. The same univariant stress variations are used and applicable for CC11 crack model.

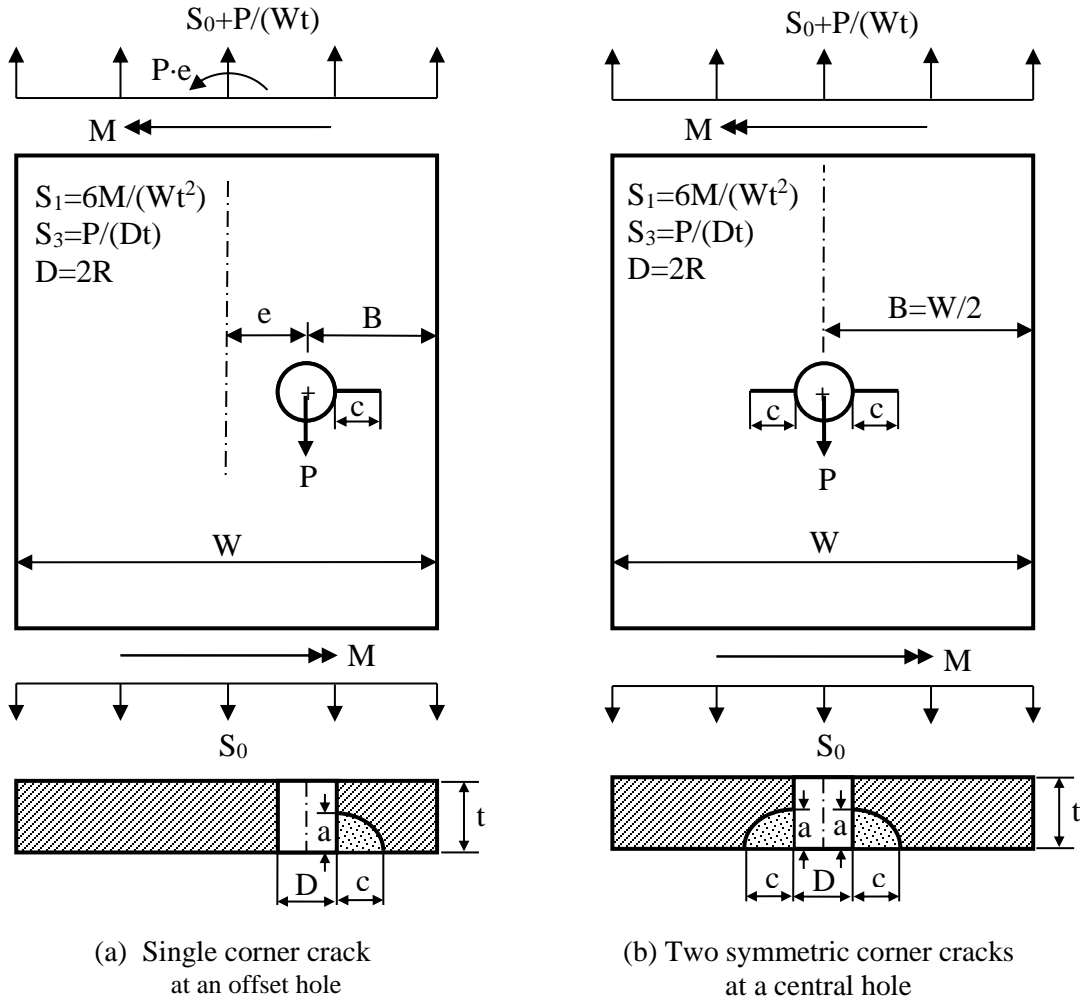
The validity limits are listed as follows:

$$\begin{aligned} 0 &\leq \frac{2B}{D} \leq 24 \\ 0 &\leq \frac{B + \frac{D}{2}}{W} \leq 0.75 \\ \frac{\frac{c}{W} - \frac{B}{2}}{W - B - \frac{D}{2}} &\leq 0.9 \\ \frac{a}{t} &\leq 0.95 \end{aligned}$$

The normalized coordinate is defined by $x/[W - (B + D/2)]$. The coordinate x is measured from the notch tip along the crack growth path.

CC16 - Corner Crack(s) at a Hole Based on Fawaz-Andersson Solution

CC16 is a corner-crack-at-hole solution based on Fawaz-Andersson solution for one corner crack at a hole [C59] and the modified Newman finite width correction equations developed by Guo [C61]. The crack case deals with a single corner crack at an offset hole or two symmetric corner cracks at a central hole in a finite plate subjected to remote tension (S_0), out-of-plane bending (S_1), and pin load (S_3), as shown below, where B can be larger or less than or equal to $W/2$.



Configuration of crack case CC16

The fundamental stress intensity factors of single corner crack

The fundamental stress intensity factors (beta factors) of single corner crack at a hole in an infinite plate, developed by Fawaz and Andersson by using the finite element method, are given on a grid of 25x11x26, i.e., twenty five a/c values, eleven a/t values, and twenty six R/t values.

- The 25 a/c values: 0.1, 0.1111, 0.125, 0.1428, 0.1667, 0.2, 0.25, 0.333, 0.5, 0.667, 0.75, 0.8, 1.0, 1.25, 1.333, 1.5, 2, 3, 4, 5, 6, 7, 8, 9, 10.
 - The 11 a/t values: 0.1, 0.2, 0.3, 0.4, 0.5, 0.6, 0.7, 0.8, 0.9, 0.95, 0.99.

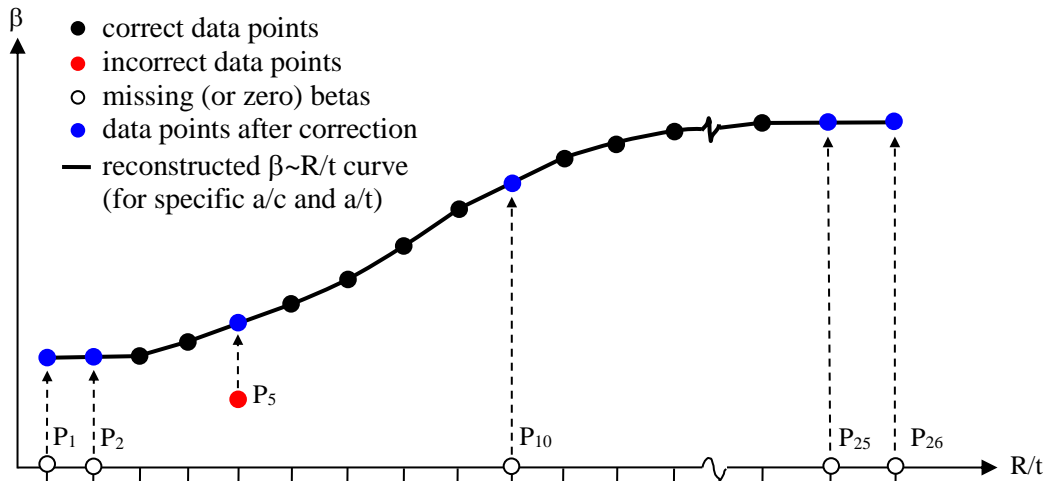
- The 26 R/t values: 0.1, 0.1111, 0.125, 0.1428, 0.1666, 0.2, 0.25, 0.333, 0.5, 0.6666, 0.75, 0.8, 1.0, 1.25, 1.333, 1.5, 1.6666, 2, 3, 4, 5, 6, 7, 8, 9, 10.

The beta factors are available along the whole crack front, but only the data at the vertices (a-tip and c-tip) are needed. The beta factors at the vertices are actually the local maximum beta factors near or at a-tip and c-tip.

The original database of the beta factors has the following problems based on our analysis:

- The database for remote tension (S_0):
 - A number of beta factors are missing near the boundary of the domain.
- The database for out-of-plane bending (S_1):
 - A number of beta factors are missing near the boundary of the domain.
 - The beta factors for $R/t=4, 5, 6, 7$, and 10, as well as the beta factors at $a/c=8$ and 9, $a/t=0.2 \sim 0.99$, and $R/t=0.1428$ do not make sense.
- The database for pin load (S_3):
 - A number of beta factors are missing near the boundary of the domain.
 - The beta factors for $R/t=8$ and 9 are incorrect. A few beta factors under pin load are negative.

Based on our observations, the beta factors are not very sensitive to the change of R/t , especially when R/t reaches a certain high value. The beta factors under bending do not change much for $R/t > 3$. For a specific a/c and a/t , the questionable beta factors (missing betas or incorrect betas) are reconstructed by using the betas at the adjacent valid R/t values as shown in the figure below.



Schematic diagram for reconstructing the F-A database for specific a/c and a/t

- If a questionable beta is at the end, such as P_1 , P_2 , P_{25} , or P_{26} , it is assigned to the valid beta at the boundary.
- If a questionable beta is in the middle, like P_5 or P_{10} , it is replaced by the beta value obtained by linear interpolation from its adjacent points.

There are 25×11 $\beta \sim R/t$ curves for each crack tip under each load condition (tension, bending, or pin load). Each of the $\beta \sim R/t$ curves is reconstructed this way. The database of beta factors are

extended down from $a/t=0.1$ to $a/t=0$, with the betas at $a/t=0$ determined by the K_t -based method proposed by Dr. Yi-Der Lee,

$$\beta = F_{Kt} \cdot \frac{F_{ca}}{E_k} \quad (1)$$

where $F_{Kt} = 1.122K_t$ for tension (S_0) and bending (S_1), and $F_{Kt} = 0.98175$ for pin load (S_3). K_t is the stress concentration factor at the corner of the vanishing crack. $F_{ca}=c/a$ for a-tip and $F_{ca}=1$ for c-tip. E_k is a function of crack aspect ratio,

$$E_k = \begin{cases} \sqrt{1 + 1.464 \left(\frac{c}{a}\right)^{1.65}} & \text{if } \frac{c}{a} \leq 1 \\ \frac{c}{a} \cdot \sqrt{1 + 1.464 \left(\frac{a}{c}\right)^{1.65}} & \text{if } \frac{c}{a} > 1 \end{cases} \quad (2)$$

Calculation of stress intensity factors for single corner crack

The total stress intensity factor for a given crack size “ a ” is calculated by

$$K = \sum F_i \cdot S_i \sqrt{\pi a} = \sum (\beta_i \cdot F_{H,i}) \cdot S_i \sqrt{\pi a} = \sum (\beta_i \cdot F_{W,i} \cdot F_{Off,i}) \cdot S_i \sqrt{\pi a} \quad (3)$$

Where i is the stress quantity index ($i=0$ for tension, 1 for bending, and 3 for pin load). β_i is the beta factor of the corresponding infinite plate. $F_{H,i}$ is the general finite width correction factor. It equals the product of the finite width correction factor ($F_{W,i}$) and the hole offset correction factor ($F_{Off,i}$).

- Calculation of the primary geometry factor (β_i)

The primary geometry factors during crack propagation are obtained by interpolating off the reconstructed F-A database. Since the beta factors in the database are given on a pretty dense grid, linear interpolation is selected. Another consideration on selecting linear interpolation is that we are likely to implement the F-A solution for two unequal corner cracks at a hole in the near future, where 4-D linear interpolation is about to be employed.

For a specific problem, the R/t value is fixed. So the first step is to construct the beta tables as a function of a/c and a/t for the specific R/t value before crack propagation analysis. For each a/c and a/t in the F-A database, the beta factor under the specific R/t is obtained by linear interpolation.

During crack propagation, a/c and a/t are changing. If $a/t \geq 0.1$, the stress intensity factor for the given a/c and a/t values is obtained by 2-D linear interpolation based on the beta tables constructed for the specific R/t value in the above step. If $a/t < 0.1$, Hermite interpolation is employed. Note that the beta factors at c-tip in the F-A database are defined as $K/[\sigma\sqrt{\pi c}]$. In order to be consistent with the definition in NASGRO, i.e. $\beta(\text{c-tip}) = K/[\sigma\sqrt{\pi a}]$, the beta factors at c-tip obtained by interpolation are multiplied by $1/\sqrt{a/c}$.

- Finite width correction factor ($F_{i,W}$) for tension and bending

The Newman finite width correction factor ^[C60] for a central hole in the plate of width “2B” is defined as

$$F_W = \sqrt{\sec\left(\frac{\pi R}{2B}\right) \cdot \sec\left[\frac{(2R+nc)\pi}{4(B-c)+2nc} \sqrt{\frac{a}{t}}\right]} \quad (4)$$

where n is the number of cracks, and $R=D/2$ is the radius of the hole. $n=1$ for single corner crack. Note that the same finite width correction equation is used for both c- and a-tip.

Evaluation ^[C61] on the Newman finite width correction by comparing it with the CC08 solution reveals that:

The original Newman finite width correction equation works well at c-tip for $(R+c)/B$ up to 0.9, but it does a poor job at a-tip. It does not work well for narrow plates either.

The following equations are then developed by Guo ^[C61] for remote tension and bending based on the original Newman finite width correction equation:

$$\bar{F}_W(\text{a-tip}) = G_1 \cdot G_2 \cdot F_W = G_1 \cdot G_2 \sqrt{\sec\left(\frac{\pi R}{2B}\right) \cdot \sec\left[\frac{\pi(2R+nc)}{4(B-c)+2nc} \sqrt{\frac{a}{t}}\right]} \quad (5a)$$

$$\bar{F}_W(\text{c-tip}) = G_1 \sqrt{\sec\left(\frac{\pi R}{2B}\right) \cdot \sec\left[\frac{\pi(2R+nc)}{4(B-c)+2nc} \sqrt{\frac{a}{t}}\right]} \quad (5b)$$

where G_1 is used to fine-tune the correction for narrow plates, and G_2 is used to characterize the different effects on a-tip.

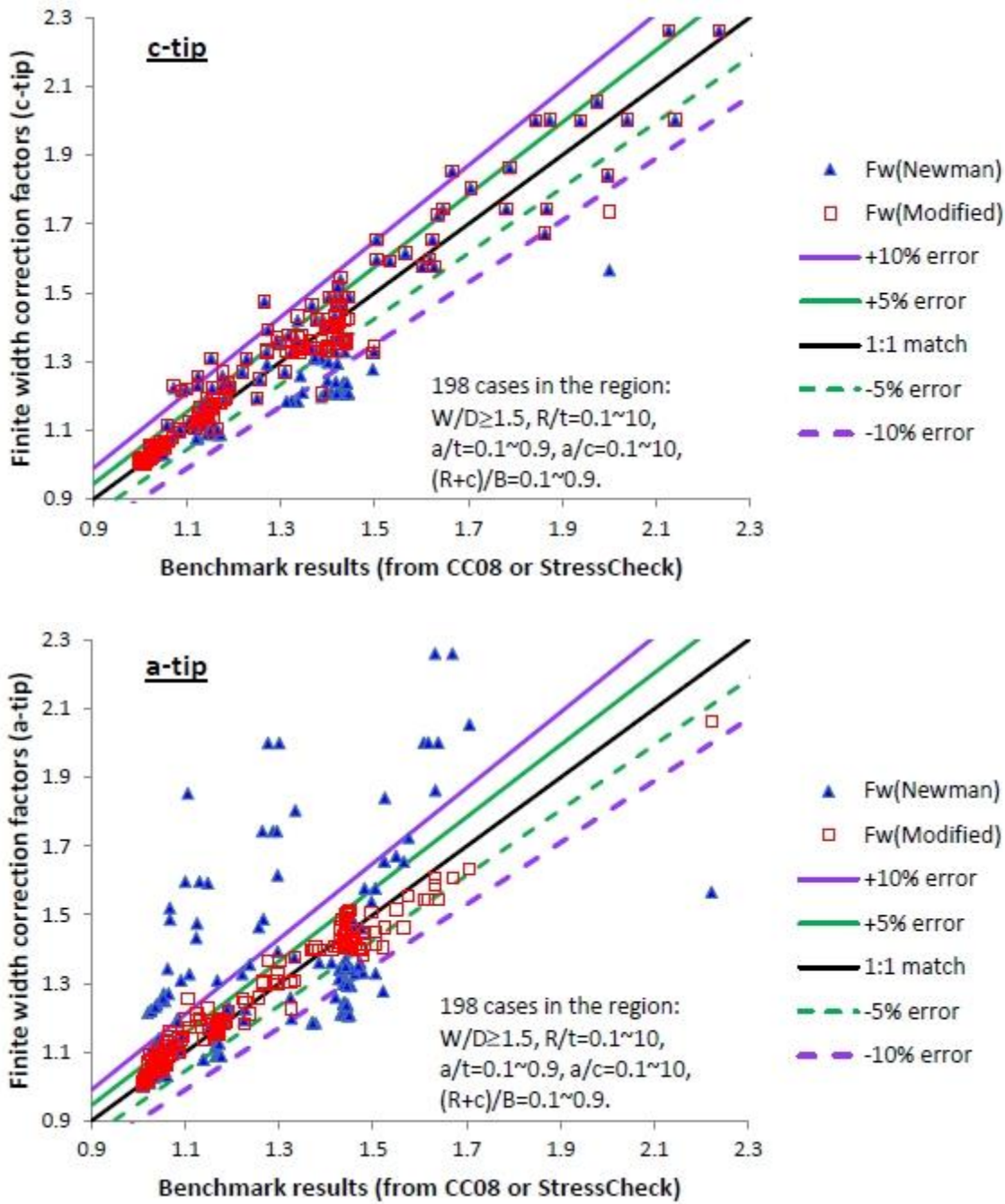
$$G_1 = 1 + \left(\frac{R}{B}\right)^{n_1} \left[\left(1 - \frac{a}{t}\right) \frac{R}{R+c}\right]^{n_2} \quad (6)$$

$$G_2 = \frac{1 + \left(\frac{R}{B}\right)^{n_3}}{1 + \left(\frac{a}{t}\right)^{n_4} \left(\frac{R+c}{B}\right)^{n_5}} \quad (7)$$

The exponents $n_1 \sim n_5$ are obtained by calibrating the solution with the results obtained from CC08 and FEA. Equations (6) and (7) are verified extensively with 198 cases, where 160 cases are within the geometry limits of CC08, and 38 cases are outside the geometry limits of CC08. The benchmark results of finite width correction factors for the 160 cases are calculated by running CC08; the benchmark results of finite width correction factors for the 38 cases outside the geometry limits of CC08 are obtained by the p-version FEA software - StressCheck. The modified finite width correction equations, along with the Newman finite width correction equation, are compared with the benchmark results obtained from CC08 and StressCheck in the following two figures, one for c-tip, and the other for a-tip.

The first figure shows that the Newman and modified finite width correction equations give almost identical results at c-tip except for the narrow plates with small W/D values, where the modified equation gives better results. For a-tip, most of the results given by the modified finite

width correction equation have errors less than 5%. A few data have errors larger than 5% but less than 10%. However, the Newman finite width correction equation gives results with much bigger errors. They can be either over-conservative or non-conservative.



Verification of the modified finite width correction equations under remote tension

The above two figures show that the modified finite width correction equations are valid within the following geometry limits:

$$W/D \geq 2, \quad 0.1 \leq R/t \leq 10, \quad 0.1 \leq a/c \leq 10, \quad (R+c)/B \leq 0.9.$$

- Hole offset correction factor ($F_{i,off}$) for tension and bending

NASGRO borrows the hole offset correction equations used in the AFGROW [C62].

- If $B < W/2$,

$$F_{off} = \frac{\sin\left(\sqrt{\frac{a}{t}} \cdot \frac{D+c}{B-c/2} \cdot \frac{W-2B}{W}\right)}{\sqrt{\frac{a}{t}} \cdot \frac{D+c}{B-c/2} \cdot \frac{W-2B}{W}} F_c \quad (8)$$

where $F_c = \min\{1 - (0.45F_G - 0.021)[c/(B-D/2)]^{16}, 1.0\}$ and $F_G = \min\left\{\frac{2B}{W} + \frac{D}{2B}, 0.7\right\}$.

The above equation is valid for $(D+c)/(2B-c) \leq 0.7$, i.e., $(R+c)/B \leq 0.824 - 0.176R/B$.

Evaluation [C61] on the AFGROW hole offset correction equation for $B < W/2$ by comparing it with CC08 solution reveals that:

- The hole offset effect becomes significant only if the hole is very close to the edge in a wide plate, like $B/R < 2 \sim 2.5$ and $W/B > 5 \sim 10$.
- The agreement between the AFGROW hole offset correction and the CC08 results is not bad within the solution limits of CC08, especially at c-tip. The errors are usually less than 5% at c-tip and 10% at a-tip.
- If $B = W/2$, $F_{off} = 1$.
- If $B > W/2$, the following hole offset correction equation is used in AFGROW:

$$F_{off} = F_A \cdot F_B \quad (9)$$

where

$$F_A = 1 + \frac{\sqrt{\sec\left[\frac{\pi D}{4B}\left(\frac{4}{7} \cdot \frac{B}{W-B} + \frac{3}{7}\right)\right]} - 1}{1 + 0.21 \cdot \sin(8 \cdot \arctan[(2B/W-1)^{0.9}])}$$

and

$$\begin{aligned} F_B &= 1 + F_c \cdot \sin(\pi \cdot \tanh[2\delta^{1.1} + (1.18\delta)^7]) \\ F_c &= \frac{0.5}{\exp(10\gamma + 4.2\gamma^2 + (3\gamma)^{14})} \quad \text{and} \quad \gamma = 1 - B/W \\ \delta &= \frac{D+c}{2B-c} \sqrt{\frac{a}{t}} \end{aligned}$$

The above AFGROW hole offset correction equation for $B > W/2$ gives out $F_{off} = \sqrt{\sec(\frac{\pi D}{4B})}$ when $B \rightarrow W/2$ (a central hole), which does not make sense. The following corrected equation is thus used in NASGRO:

$$\bar{F}_{off} = F_A \cdot F_B \cdot \sqrt{\cos\left(\frac{\pi D}{4B}\right)} \quad (9a)$$

NASGRO team did not perform further evaluation on the AFGROW hole offset correction equation for $B > W/2$.

Note that the same general finite width correction factor ($F_{H,i}$) is used for remote tension and out-of-plane bending.

- **Correction factors for pin loading**

When crack case CC16 was first implemented in NASGRO (starting with v7.1), a new finite width correction factor was derived for remote tension loading, and this same factor was also used for pin loading. Work to develop new (future) pin loading capabilities for weight function crack case CC08 (first implemented in v8.1) demonstrated that the CC16 finite width correction factors for tension loading could be non-conservative when used for pin loading. Therefore, an improved CC16 finite width correction factor for pin loading was developed from the enhanced CC08 solution. This pin-loaded correction factor was first implemented in v8.0 (beginning with the production release) and was also backported to the bug-fix release v7.12.

Further study of this revised solution indicated that, while accurate for narrow plates with centered holes, these values could be over-conservative for narrow plates with holes highly offset from the centerline. Therefore, a second CC16 revision focusing on the hole-offset correction factor was developed, verified, and implemented in v8.1a. Once again, the revised CC16 solution only changed K-values under pin-loading – solutions for tension and out-of-plane bending have been unaffected. These solutions were applied to CC17 starting in 8.01 and 8.1f.

Even further study revealed non-physical oscillations – “peaks” and “troughs” – in the solution introduced by the interpolation process. These “peaks” and “troughs” only influenced relatively small cracks ($a/t \leq 0.2$) at small holes ($D/\min(2B, 2 \times (W - B)) \leq 0.5$). These “peaks” and “troughs” were visible in the stress intensity factors computed with increasing crack depth (a/t). These oscillations were due to the interpolation scheme. In these routines, the pin-loaded correction factor interpolated over the non-dimensional crack length $c/(B^* - D/2)$, where $B^* = \min(B, W - B)$. Varying this parameter has the unintentional consequence of simultaneously varying the relative hole size, $D/2B^*$, which largely controls the geometry correction factor for pin-loaded holes. Consequently, the interpolation process sampled from various ratios of $D/2B^*$ as crack growth progressed and lead to the observed “peaks” and “troughs”.

Several attempts were made to eliminate the non-physical oscillations in the solution. Adding more points to the solution matrix shifted the oscillations to other parts of the solution space, even if the solution matrix tripled in size. Changing the solution space in only the small crack regime ($a/t \leq 0.2$) introduced a discontinuity at the boundary, $a/t = 0.2$. This discontinuity was triggered by differences in the interpolation schemes.

NASGRO 8.2f takes the radical step of changing the entire parameterization for pin-loaded CC16 to eliminate the non-physical oscillations. This approach eliminates the non-physical oscillations and improves the solution quantity. It does not introduce any discontinuities into the solution. The new parameterization scheme interpolates over the relative hole size rather than over the relative crack depth. Consequently, stress intensity factors in NASGRO 8.2f will differ from stress intensity factors in earlier versions of NASGRO. These changes only affect cracks under pin-loading. Again, it is unclear exactly how these changes will impact fatigue crack growth lives overall, but the differences may effectively cancel out in some cases.

Preliminary investigations with these new pin-loaded geometry correction factors have revealed lower lives for: 1) cracks on the long ligament side of highly offset holes as $0.5 \times D/(W - B) > 0.5$ and 2) cracks in thick plates where $D/2t \rightarrow 0.1$. In this second case, additional studies suggest that both the old and new geometry correction factors are systematically conservative.

In the new parameterization, NASGRO defines the plate by the non-dimensional parameters $D/2B^*$, $D/2t$, and $1 - 2B^*/W$. (This last parameter is symmetric for cracks on the short and large ligaments.) The crack can be defined by two of the following three parameters: crack depth (a/t), crack shape (a/c), and crack length ($c/(B^* - D/2)$). NASGRO uses the a/t and a/c . In CC16, allowable combinations of a/t and a/c lead to non-physical cracks, *i.e.*, cracks that are longer than the plate. For example, a deep crack ($a/t = 0.95$) breaks through most plates if the crack has a very low aspect ratio ($a/c = 0.1$). The solution matrix must accommodate this case, even though it is rare in practice. The crack length can be confined to the plate by restricting a/t and a/c . Specifically, if $0 \leq c/(B^* - D/2) \leq 0.9$, then:

$$\left(\frac{a}{c}\right)_{lower} = \max\left(0.1, \frac{10}{9} \times \frac{a}{t} \times \frac{2t}{D} \times \left(\frac{\frac{D}{2B^*}}{1 - \frac{D}{2B^*}}\right)\right) \leq \frac{a}{c} \leq 10 = \left(\frac{a}{c}\right)_{upper}$$

$$\left(\frac{a}{t}\right)_{lower} = 0 \leq \frac{a}{t} \leq \min\left(0.95, 9 \times \frac{D}{2t} \times \left(\frac{1 - \frac{D}{2B^*}}{\frac{D}{2B^*}}\right)\right) = \left(\frac{a}{t}\right)_{upper}$$

These limits only come into effect in certain geometries – usually, the crack is confined by the more restrictive limits of CC08 that have been bolded in the previous equations. The new routines sample and interpolate over the non-dimensional parameters $P_{a/t}$ and $P_{a/c}$ defined over the available range. That is, $P_{a/t} \in [0,1]$ and $P_{a/c} \in [0.1,10]$. For a given geometry, we map a/t to $P_{a/t}$ by first determining the upper bound and then dividing a/t by it. That is, $P_{a/t} = (a/t)/(a/t)_{upper}$. We apply a similar mapping between a/c and $P_{a/c}$.

The improved geometry correction factors for pin-loaded holes employ a look-up table of the appropriate correction factor based on CC08 and have discrete values for the following non-dimensional geometric ratios:

$$\frac{D}{2B^*} = 0.01, 0.05, 0.1, 0.2, 0.3, 0.4, 0.5, 0.6, 0.7, 0.8, 0.9$$

$$\log_{10}\left(\frac{D}{2t}\right) = -1, -0.6, -0.3, 0, +0.3, +0.6, +1$$

$$\log_{10}(P_{a/t}) = -2, -1.6, -1.3, -1, -0.4, -0.1, 0$$

$$\log_{10}(P_{a/c}) = -1, -0.6, -0.3, 0, +0.3, +0.6, +1$$

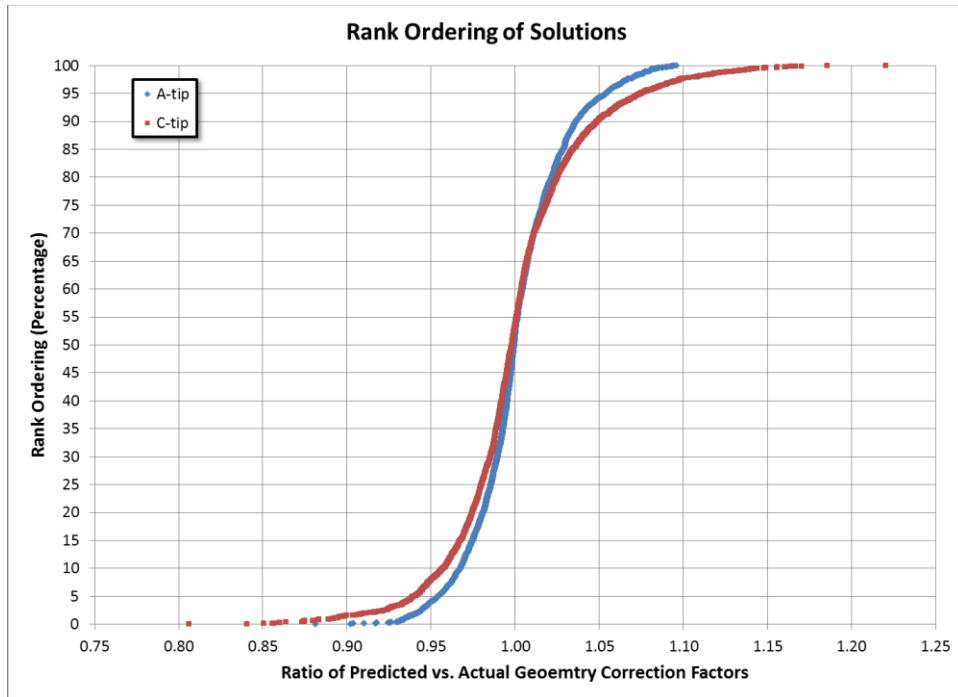
$$1 - \frac{2B^*}{W} = 0, 0.5, 0.7, 0.8$$

The final parameter defines the offset of the hole in the plate. NASGRO distinguishes between the cracks on the short and long ligament of the plate. The total solution matrix contains 52,822

entries. Interpolation with cubic Hermite splines provides correction factors for non-dimensional ratios between known ratios in the look-up table (e.g., $D/2B^* = 0.15$ which is between $D/2B^* = 0.1$ and $D/2B^* = 0.2$). The ratios $D/2t$, $P_{a/c}$, and $P_{a/t}$ are interpolated over log-10 space to minimize oscillations, whereas the other ratios are interpolated in real space. When the input non-dimensional ratio is outside of these limits (e.g., $a/t = 0.99$), the resulting correction factor is set equal to the value at the closest non-dimensional ratio found in the solution matrix (e.g., $a/t = 0.95$). NASGRO 8.2 now outputs a warning message when the crack tip exceeds the bounds of $a/t > 0.95$ and $c/(B^* - 0.5 \times D)$. The geometry correction factor extrapolates for parametric crack depths $P_{a/c} < 0.01$.

The geometry correction factor (for a given set of non-dimensional ratios in this table) equals the ratio of $K_I^{ND}/K_I^{D=0.01W}$, where both values of K_I have been computed using the CC08 weight function solution and the appropriate stress variation along the crack plane. Here, K_I^{ND} reflects K_I for the input non-dimensional ratios, and $K_I^{D=0.01W}$ represents K_I with the same geometric dimensions as K_I^{ND} but with a plate width equal to 100 times the hole diameter.

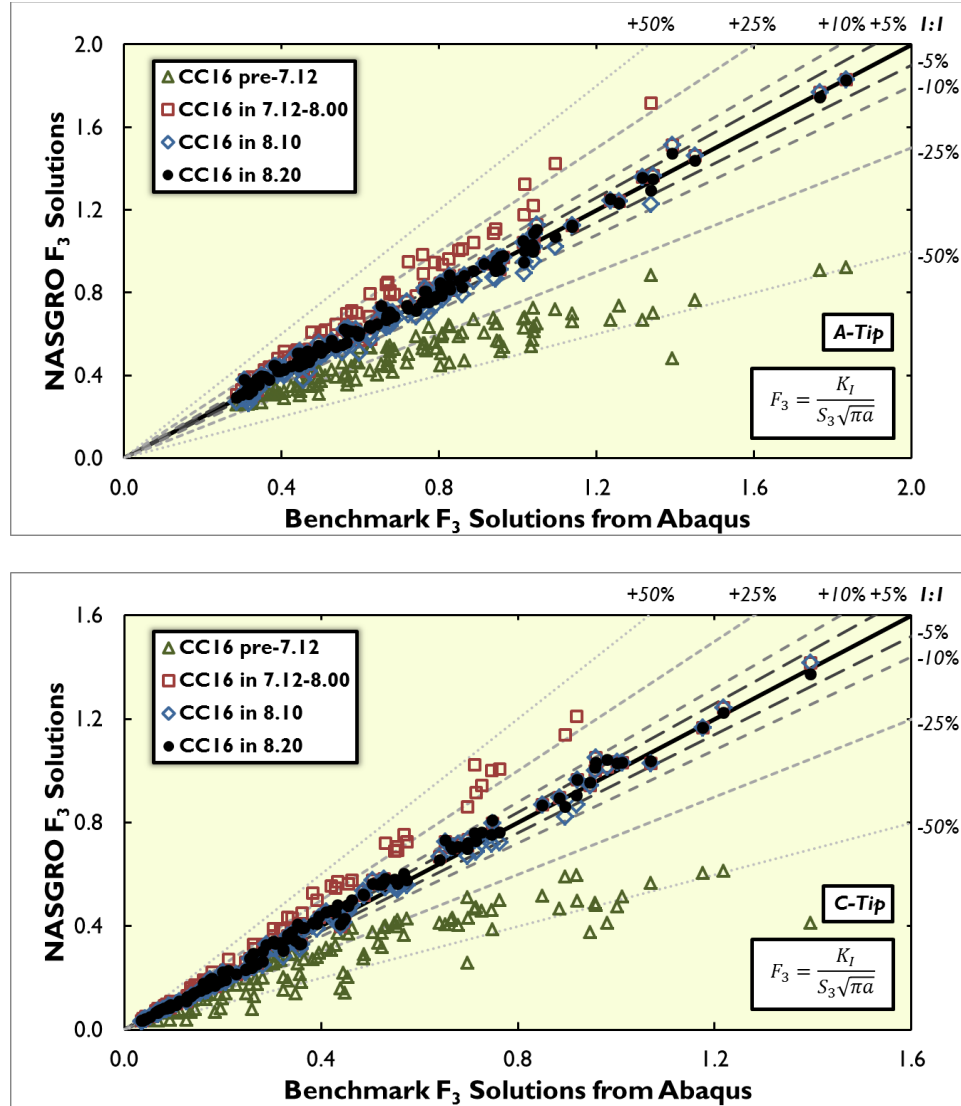
The pin-loaded correction factor was verified against independent correction factors. The verification matrix sampled 2500 geometries (combinations of $D/2t$, a/c , etc...) over the full parametric space using Latin Hypercube Sampling with reduced correlation. These geometries are separate from the geometries that define the solution matrix except by accident. For all geometries, a new correction factor was computed using CC08 and the geometry correction factor was predicted using the new routines. The following figure shows the rank ordering (*i.e.*, the cumulative distribution function) of the results. The horizontal axis shows the ratio of the predicted geometry correction factor vs. independent correction factor. Ratios of one imply that the prediction exactly matches the independent correction factor; ratios above one imply that the predictions are conservative; and ratios below one imply non-conservatism vs. CC08. For a given ratio, the vertical axis provides the percentage of solutions lower than that ratio. The results in this figure suggest good agreement between geometry correction factors computed directly using CC08 and the new parametric factor routines. The a-tip and c-tip both have a median value near unity. There is more scatter in the c-tip solution than in the a-tip solution.



Verification of geometry correction factors for pin-loaded holes against CC08.

The new solution was also examined for oscillations over the parameter space – that is, the “peaks” and “troughs” in the previous correction factor. To do this, the solution was plotted as it varied with each variable over the solution range – *e.g.*, a/t as it varied from ~0.001 to its maximum value while $D/2B^*$, $D/2t$, $1 - 2B^*/W$, and a/c were held constant. These plots were prepared for all 2500 geometries from the LHS described earlier. These plots do not show the earlier non-physical oscillations in the a-tip solutions with respect to a/t . There is a limited set of geometries where the c-tip solution show some non-physical curvature with respect to a/t . These oscillations are confined to thin plates ($D/2t \rightarrow 10$) and crack with low aspect ratios ($a/c \rightarrow 0.1$). This configuration is likely not stable – cracks should grow into a more stable shape where the interpolation is better behaved.

The pin-loaded correction factors were independently verified by comparing them with 162 stress intensity factor solutions calculated using finite element methods (Abaqus) for models containing cracks at pin-loaded holes. Comparisons of the FE verification results against the new CC16 correction factors for pin-loaded holes are shown the figure below. This comparison provides verification for both the new CC16 factor as well as the underlying CC08 model. In general, the geometry correction factor in NASGRO 8.2 is very similar to the geometry correction factor in NASGRO 8.1.



Verification of finite width correction factors for pin-loaded holes. Points shown in these figures have holes centered in the plate (i.e., no offset correction factors).

The beta correction is applied in calculation of the range of stress intensity factors in NASFLA. Suppose the applied maximum and minimum stress intensity factors are K_{max} and K_{min} , respectively. The range of stress intensity factors with the beta correction is,

$$\Delta K = \beta_R \cdot (K_{max} - K_{min}) \quad (10)$$

where

$$\beta_R = \begin{cases} 0.9 + 0.2R^2 - 0.1R^4 & \text{if } R \geq 0 \\ 0.9 & \text{if } R < 0 \end{cases} \quad (11)$$

Note that the original values of K_{max} , K_{min} , and R remain unchanged; only ΔK is changed.

Calculation of stress intensity factors for two symmetric corner cracks

The stress intensity factors of two symmetric corner cracks at a central hole are obtained from the stress intensity factors of the corresponding single corner crack solution and the Shah correction factor (F_{Shah}), i.e.,

$$K_{2\text{crks}} = \frac{K_{1\text{crk}}}{F_{\text{Shah}}} \cdot \frac{\bar{F}_{W,2\text{crks}}}{\bar{F}_{W,1\text{crk}}} \quad (12)$$

where $\bar{F}_{W,1\text{crk}}$ and $\bar{F}_{W,2\text{crks}}$ are the finite width correction factors of one corner crack and two corner cracks, respectively. F_{Shah} is the Shah correction factor [C63],

$$F_{\text{Shah}} = \sqrt{\frac{D + \frac{\pi ac}{4t}}{D + \frac{\pi ac}{2t}}} \quad (13)$$

Solution Limits

The solution limits are determined by the domain of the reconstructed F-A database and the application scopes of the finite width correction and the hole offset correction equations.

- Domain of the reconstructed F-A database (the fundamental beta factors):
 $0.1 \leq R/t \leq 10, 0.1 \leq a/c \leq 10, 0 \leq a/t \leq 0.99$
- Application scope of the NASGRO finite width correction:
 $B/R \geq 2, 0.1 \leq R/t \leq 10, 0.1 \leq a/c \leq 10, (R+c)/B \leq 0.9$
- Application scope of the AFGROW hole offset correction:
If $B < W/2$: $(D+c)/(2B-c) \leq 0.7$, i.e $(R+c)/B \leq 0.824 - 0.176R/B$.
If $B = W/2$: no need to perform hole offset correction.
If $B > W/2$: no application scope is mentioned in AFGROW users manual.

Combining the above three conditions, we have the following solution limits for CC16:

- For single corner crack,
If $B < W/2$: $B/R \geq 2, 0.2 \leq D/t \leq 20, 0.1 \leq a/c \leq 10, 0 \leq a/t \leq 0.99, (D+c)/(2B-c) \leq 0.7$.
If $B \geq W/2$: $B/R \geq 2, 0.2 \leq D/t \leq 20, 0.1 \leq a/c \leq 10, 0 \leq a/t \leq 0.99, (D/2+c)/B \leq 0.9$.
- For two symmetric corner cracks,
 $B/R \geq 2, 0.2 \leq D/t \leq 20, 0.1 \leq a/c \leq 10, 0 \leq a/t \leq 0.99, (D/2+c)/B \leq 0.9$.

References: [C59], [C60], [C61], [C62], [C63]

CC17 - Two unequal corner cracks at a hole in a finite plate

The K-solution of two unequal corner cracks at a hole in a finite plate subjected to remote tension, out-of-plane bending, and pin load (CC17) is based on:

- The reconstructed Fawaz-Andersson (F-A) database of stress intensity factors for two unequal corner cracks at a hole in an infinite plate [C⁶⁴].
- The equivalent hole method (EHM) for finite width correction developed by Guo [C⁶⁵].

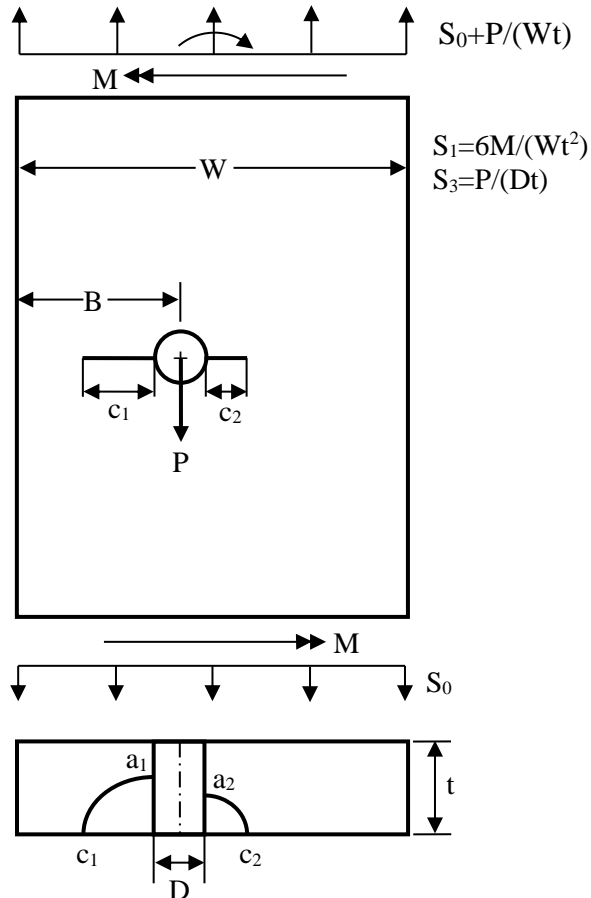


Fig.1 Configuration of crack case CC17

- **The original Fawaz-Andersson (F-A) database of beta factors**

The beta factors in the original F-A database are given on a grid of 25x11x25x11x26, i.e. 25 a_1/c_1 values, 11 a_1/t values, 25 a_2/c_2 values, 11 a_2/t values, and 26 R/t values.

25 a_1/c_1 values: 0.1, 0.111, 0.125, 0.1428, 0.1667, 0.2, 0.25, 0.333, 0.5, 0.667, 0.75, 0.8, 1.0, 1.25, 1.333, 1.5, 2, 3, 4, 5, 6, 7, 8, 9, 10

25 a_2/c_2 values: 0.1, 0.111, 0.125, 0.1428, 0.1667, 0.2, 0.25, 0.333, 0.5, 0.667, 0.75, 0.8, 1.0, 1.25, 1.333, 1.5, 2, 3, 4, 5, 6, 7, 8, 9, 10

11 a_1/t values: 0.1, 0.2, 0.3, 0.4, 0.5, 0.6, 0.7, 0.8, 0.9, 0.95, 0.99

11 a_2/t values: 0.1, 0.2, 0.3, 0.4, 0.5, 0.6, 0.7, 0.8, 0.9, 0.95, 0.99

26 R/t values: 0.1, 0.1111, 0.1250, 0.1428, 0.1666, 0.2, 0.25, 0.3333, 0.5, 0.6666, 0.75, 0.8, 1, 1.2500, 1.3333, 1.5, 1.6666, 2, 3, 4, 5, 6, 7, 8, 9, 10

Domain of the original database is: $R/t \in [0.1, 10]$, $a/c \in [0.1, 10]$, $a/t \in [0.1, 0.99]$. The database contains $3 \times 26 \times 37950 \times 4 = 11,840,400$ beta factors. The total size of the database files is about 330MB.

The following problems have been found with the original F-A database:

Wrong betas:

- Database for tension:
No wrong betas detected.
- Database for bending:
The betas for $R/t=4, 5, 6, 7, 10$ are wrong (negative betas at c1- and c2-tip).
- Database for bearing:
The betas for $R/t=8, 9$ are wrong. They are much smaller than the betas at $R/t=7$ and 10.
Many crack profiles have small negative betas at small R/t values (0.1~0.5).

Missing (zero) betas:

There are 568866 (about 4.8%) missing (zero) betas in the database. The crack profiles with a very big crack on one side and a very small crack on the other side tend to have less valid betas as R/t changes. A crack profile refers to a specific combination of crack sizes (a_1/c_1 , a_1/t , a_2/c_2 , a_2/t).

• Reconstructing the F-A database

To correct the wrong betas or missing (zero) betas, we re-generate the $\beta \sim R/t$ curve for each of the crack profiles (a_1/c_1 , a_1/t , a_2/c_2 , and a_2/t). If a wrong or missing beta is in the middle, it is replaced by the value obtained by linear interpolation for R/t. If it is at the end, it is set to the adjacent valid beta. The quality of the reconstructed $\beta \sim R/t$ curve for a specific crack profile depends on the number of valid betas and the valid end R/t values with valid betas. Because some crack profiles in the original domain have no valid betas at all, we have to reduce the original domain when we reconstruct a valid database. Based on the availability of the valid beta factors in the original F-A database and the needs of engineering application, NASGRO team decided to reconstruct the database in the domain: $a/c \in [0.2, 5]$, $a/t \in [0.1, 0.95]$ and $R/t \in [0.125, 10]$. NASGRO team also extended the lower a/t limit to $a/t=0$. The beta factors at $a_1/t=0$ and/or $a_2/t=0$ are determined by the K_t -based method proposed by Dr. Yi-Der Lee.

$$\beta = \frac{F_{Kt}}{E_k} \cdot F_{ca} \quad (1)$$

where F_{ca} and E_k are two functions of crack aspect ratio of the vanishing crack. F_{Kt} is related to the stress concentration factor (K_t) at the corner of the vanishing crack. Suppose crack 1 is the vanishing crack, as shown in Fig.2. $F_{ca}=c_1/a_1$ for a_1 -tip, and $F_{ca}=1$ for c_1 -tip.

$$E_k = \begin{cases} \sqrt{1 + 1.464 \left(\frac{c_1}{a_1}\right)^{1.65}} & \text{if } \frac{c_1}{a_1} \leq 1 \\ \frac{c_1}{a_1} \sqrt{1 + 1.464 \left(\frac{a_1}{c_1}\right)^{1.65}} & \text{if } \frac{c_1}{a_1} > 1 \end{cases} \quad (2)$$

$F_{Kt} = 1.122K_t$ for S_0 and S_1 , and $F_{Kt} = 0.98175$ for S_3 . K_t is the stress concentration factor at the corner of the vanishing crack, calculated by the following formula proposed by Dr. Shivakumar,

$$K_t = 1 + 2\sqrt{1 + \frac{\pi}{4} \cdot \frac{c_2}{2R} \cdot \frac{a_2}{t}} \quad (3)$$

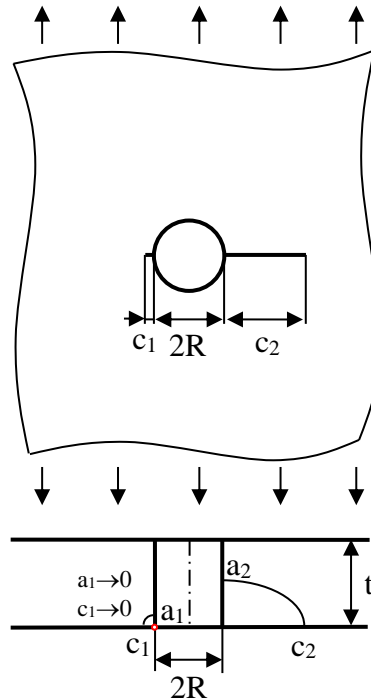


Fig.2 Two unequal corner cracks with a vanishing crack at a hole in an infinite plate

Equation (3) agrees reasonably well with the FEA results. Here are two examples:

$R/t=0.25, a_2/t=0.65, a_2/c_2=1.0: K_t = 3.58$ by eq.(3); $K_t = 3.27$ by FEA (StressCheck).
 $R/t=0.125, a_2/t=0.65, a_2/c_2=0.2: K_t = 6.53$ by eq.(3); $K_t = 6.16$ by FEA (StressCheck).

After extending the database down to $a/t=0$, the domain of the new database is thus: $a/c \in [0.2, 5]$, $a/t \in [0, 0.95]$, and $R/t \in [0.125, 10]$. The new domain contains

15 a_1/c_1 values: 0.2, 0.25, 0.333, 0.5, 0.667, 0.75, 0.8, 1.0, 1.25, 1.333, 1.5, 2, 3, 4, 5.

15 a_2/c_2 values: 0.2, 0.25, 0.333, 0.5, 0.667, 0.75, 0.8, 1.0, 1.25, 1.333, 1.5, 2, 3, 4, 5.

11 a_1/t values: 0.0, 0.1, 0.2, 0.3, 0.4, 0.5, 0.6, 0.7, 0.8, 0.9, 0.95.

11 a_2/t values: 0.0, 0.1, 0.2, 0.3, 0.4, 0.5, 0.6, 0.7, 0.8, 0.9, 0.95.

24 R/t values: 0.125, 0.1428, 0.1666, 0.2, 0.25, 0.3333, 0.5, 0.6666, 0.75,

0.8, 1, 1.25, 1.3333, 1.5, 1.6666, 2, 3, 4, 5, 6, 7, 8, 9, 10.

The beta factors of the reconstructed database are stored in three binary files. The total size of the three files is about 15MB, which is much smaller than the size of the original database (330MB). The following facts contribute to reduction of the database size:

- The original database contains some data we do not need. Each of the data files of the original database contains 16 columns, but only 4 columns are needed.
- The new database has smaller domain. The beta factors in the reconstructed database are given on a grid of 15x11x15x11x24, compared to the grid of 25x11x25x11x26 of the original database.
- The new database is stored in binary files.

- **Calculation of stress intensity factors**

The stress intensity factor at a specific crack tip is calculated by

$$K = \sum_i F_{H,i} \cdot \beta_i \cdot S_i \sqrt{\pi x} \quad (4)$$

Where ‘i’ is stress component index ($i=0$ for tension, 1 for out-of-plane bending, and 3 for pin load). x is the crack size of the crack tip, i.e. $x=a_1$ for a_1 -tip, $x=c_1$ for c_1 -tip, $x=a_2$ for a_2 -tip, and $x=c_2$ for c_2 -tip.

β_i is the beta factors associated to stress S_i for the given geometry and crack sizes. For a given R/t value, the beta tables are generated before crack growth analysis by interpolating off the reconstructed database for R/t , where piece-wise linear interpolation is employed. During crack growth analysis, the beta factors (β_i) for a given crack profile (i.e. a specific combination of a_1/c_1 , a_1/t , a_2/c_2 , and a_2/t) are calculated by interpolating off the beta tables for the given R/t , where four-dimensional piece-wise linear interpolation is employed.

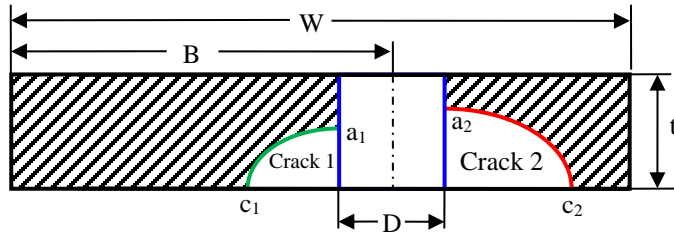
$F_{H,i}$ is the general finite width correction factor at the crack tip for stress S_i . For tension and bending, it is determined by the equivalent hole method (EHM) developed by Guo [C65]. The equivalent hole method, as shown in Fig.3, converts the opposite crack into additional hole, then uses the finite width and hole offset correction equations for one corner crack to perform finite width correction for two unequal corner cracks. For example, if we want to determine the general finite width correction factors of crack 1 in Fig.(3a), we convert crack 2 into additional hole. This way, the two-crack problem becomes a one corner crack problem with a bigger hole (i.e. the equivalent hole). The general finite width correction factors of crack 1 can be calculated by,

$$F_{H,i} = F'_{W,i} \cdot F'_{off,i} \quad (5)$$

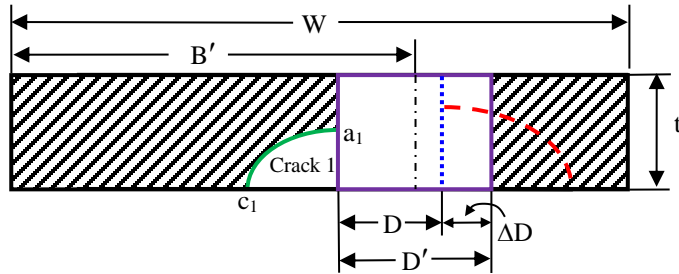
where $F'_{W,i}$ and $F'_{off,i}$ are the finite width correction factor and hole offset correction factor of the corner crack with the equivalent hole, calculated by eqs.(5~9) for one corner crack at a hole (CC16). The diameter of the equivalent hole is D' and the distance from the hole center to the plate edge is B' . $D'=D+2\Delta R$ and $B'=B+\Delta R$, where ΔR is the hole radius increment due to conversion of the opposite crack. It is derived by a semi-empirical method and formulated by

$$\Delta R = \gamma \cdot \frac{\pi c_2}{8} \cdot \sqrt{\frac{a_2}{t}} \cdot \left(\frac{\chi^2}{\chi^2 + 0.25^2} \right)^n \quad \text{and} \quad \chi = \frac{c_1 + R}{c_2 + R} \quad (6)$$

where the coefficient γ and exponent n are obtained by calibrating the FEA results of stress intensity factors.



(a) Two unequal corner cracks at an offset hole (the physical hole)
 Crack 1: a_1, c_1 ; Crack 2: a_2, c_2
 Geometry dimensions: t, W, B, D



(b) Single corner crack with a bigger hole (the equivalent hole)
 Crack 1: a_1, c_1 ; Crack 2: converted into hole
 Geometry dimensions: t, W, B', D'
 where $D' = D + \Delta D = D + 2\Delta R$, and $B' = B + \Delta R$

Fig.3 Schematic diagram showing the equivalent hole method (EHM) for determining the general finite width correction factors of two unequal corner cracks at an offset hole

The general finite width correction factors of crack 2 can be determined by the same method, where crack 1 is converted into hole. The hole radius increment due to conversion of crack 1 is given by

$$\Delta R = \gamma \cdot \frac{\pi c_1}{8} \cdot \sqrt{\frac{a_1}{t}} \cdot \left(\frac{\chi^2}{\chi^2 + 0.25^2} \right)^n \quad \text{and} \quad \chi = \frac{c_2 + R}{c_1 + R} \quad (6a)$$

The equivalent hole method is verified by the FEA in a wide range of geometrical dimensions and crack sizes under tension [C65]. The general finite width correction factors calculated by the EHM agree well with the FEA results, as shown in Fig.4. The errors between the EHM and FEA results are usually less than 8%, and 90% of the data have errors less than 5%.

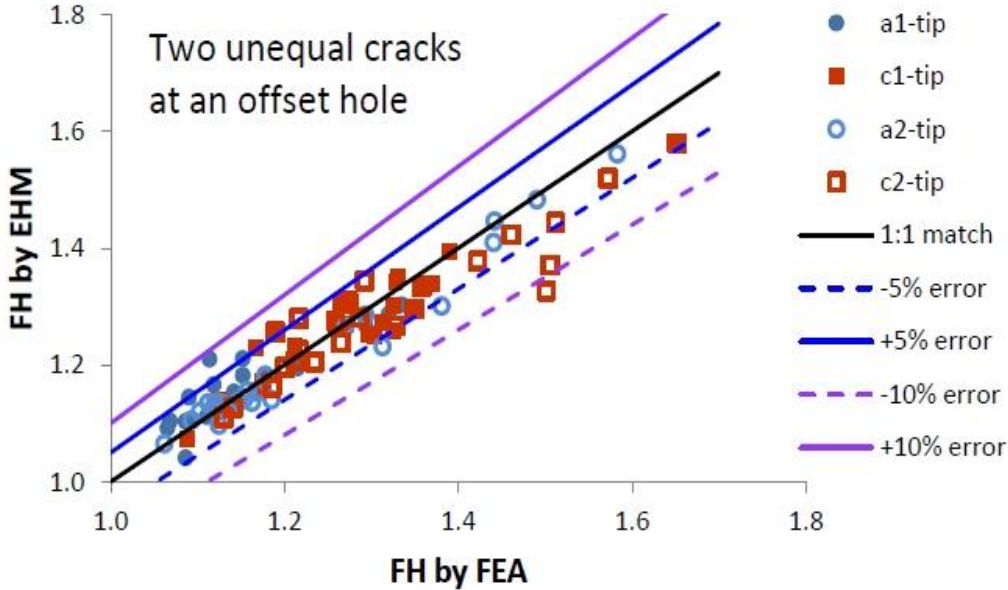


Fig.4 Verification of the equivalent hole method (EHM) under tension

CC17 has the following geometry limit,

$$(D+c)/(2B-c) \leq 0.7 \quad (7)$$

The hole offset correction equation for one corner crack at the equivalent hole is valid if

$$(D'+c)/(2B'-c) \leq 0.7 \quad (8)$$

There is no definition of hole offset correction factors between $(D+c)/(2B-c)$ and $(D'+c)/(2B'-c)$ because Eq.(8) is more stringent than eq.(7). An approximate approach is to use the hole offset correction factor of the physical hole to replace the hole offset correction factor for the equivalent hole. The general finite width correction factor for $B' < W/2$, $(D'+c)/(2B'-c) > 0.7$ and $(D+c)/(2B-c) \leq 0.7$ is thus calculated by

$$F_{H,i} = F'_{W,i} \cdot F_{off,i} \quad (9)$$

where $F_{off,i}$ is the hole offset correction factor of the physical hole.

The correction factor, $F_{H,i}$, in Eqn (4) for pin-loading differs from the tension/bend correction factor starting in version 8.1b. This version replaced the geometry correction factors for tension and bending with geometry correction factors for pin-loading that are identical to the correction factors in CC16. Consequently in all later versions of NASGRO (8.1b+), the pin-loaded solution for CC17 changes whenever the pin-loaded correction factors change in CC16, *e.g.*, the changes in 8.2f documented in the earlier section.

Verification studies of CC17 indicated that for narrow plates, the finite width correction factors derived for tension and bend were usually non-conservative when applied to pin-loading. Instead, CC17 now invokes the combined correction factors for a single corner crack at a pin-loaded hole. These correction factors were originally determined for CC16 (and discussed there) and have been reused in the CC17 routines. These factors correct for finite width and offset effects on the stress intensity factor solutions. Furthermore, the EHM that had been developed to

improve the quality of the tension and bend solutions was found to consistently over-predict the benchmark solutions for pin loading. Therefore, the actual geometric dimensions (unmodified by the EHM) are instead used to evaluate the combined correction for pin loading. Figure 5 shows the comparison of CC17 stress intensity factor solutions under pin-loading against the benchmark FEA solutions. Note that a number of these test cases are for extreme geometries. The CC17 solutions generally agreed with the benchmark verification solutions within 10% for more common configurations.

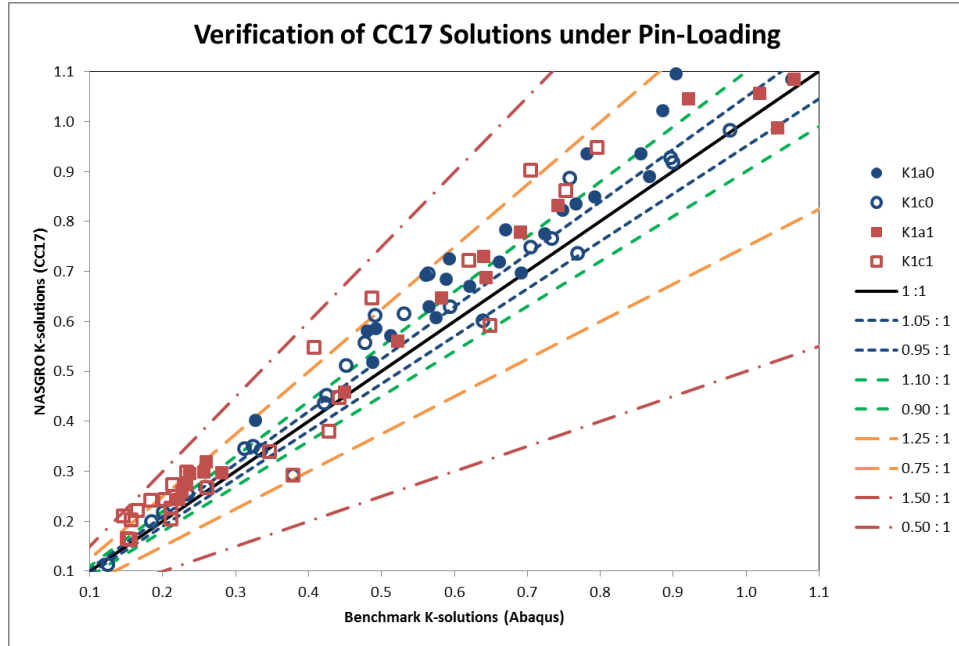


Fig.5 Verification of the CC17 correction factors for pin-loading

The beta correction is applied in calculation of the range of stress intensity factors in NASFLA. Suppose the applied maximum and minimum stress intensity factors are K_{max} and K_{min} , respectively. The range of stress intensity factors with the beta correction is,

$$\Delta K = \beta_R \cdot (K_{max} - K_{min}) \quad (10)$$

where

$$\beta_R = \begin{cases} 0.9 + 0.2R^2 - 0.1R^4 & \text{if } R \geq 0 \\ 0.9 & \text{if } R < 0 \end{cases} \quad (11)$$

Note that the original values of K_{max} , K_{min} , and R remain unchanged; only ΔK is changed.

The SIF geometry factors of CC17 in NASSIF are defined as:

$$F_i = \frac{K}{S_i \sqrt{\pi a_1}} \quad \text{at } a_1\text{-tip and } c_1\text{-tip} \quad (12)$$

$$F_i = \frac{K}{S_i \sqrt{\pi a_2}} \quad \text{at } a_2\text{-tip and } c_2\text{-tip} \quad (13)$$

Where $i = 0$ for remote tension, 1 for out-of-plane bending, and 3 for pin-load.

- **Geometry limits**

The geometry limits of CC17 are controlled by

- The geometry domain of the reconstructed F-A database, i.e.,
$$0.25 \leq D/t \leq 20, \quad 0.2 \leq a_1/c_1 \leq 5, \quad 0 \leq a_1/t \leq 0.95, \quad 0.2 \leq a_2/c_2 \leq 5, \quad 0 \leq a_2/t \leq 0.95$$
- The geometry limits of the finite width and hole offset correction equations for one corner crack at a hole in a finite plate, which are:
$$B/R \geq 2, \quad (W-B)/R \geq 2, \quad 0.2 \leq D/t \leq 20, \quad (D+c)/(2B-c) \leq 0.7, \quad 0.1 \leq a/c \leq 10, \quad 0 \leq a/t \leq 0.99.$$

Combining the above two groups of geometry limits, we have the following geometry limits for the solution of CC17:

$B/R \geq 2$! required by our finite width correction equations
$(W-B)/R \geq 2$! required by our finite width correction equations
$0.25 \leq D/t \leq 20$! domain of the reconstructed F-A database
$0.2 \leq a_1/c_1 \leq 5$! domain of the reconstructed F-A database
$0.2 \leq a_2/c_2 \leq 5$! domain of the reconstructed F-A database
$0 \leq a_1/t \leq 0.95$! domain of the reconstructed F-A database
$0 \leq a_2/t \leq 0.95$! domain of the reconstructed F-A database
$(D+c_1)/(2B-c_1) \leq 0.7$! required by the AFGROW hole offset correction equation
$(D+c_2)/[2(W-B)-c_2] \leq 0.7$! required by the AFGROW hole offset correction equation

References: [C64], [C65]

CC19 – Corner crack at hole in lug – univariant WF

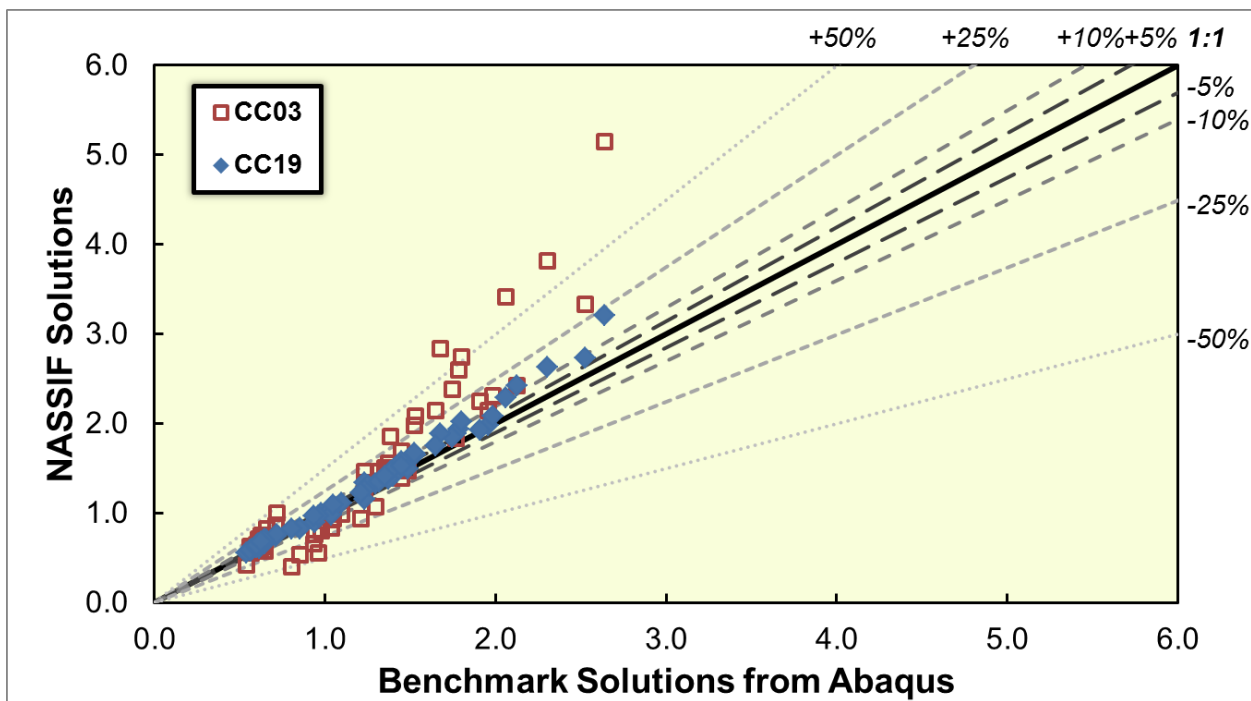
Crack case CC19 represents an elliptical corner-crack crack initiated at the hole of a straight lug under pin-loading. Nominally, CC19 has the same geometry and loading as CC03. However, CC19 employs the weight function solution CC08 and the nonlinear stress variation for an uncracked lug. Consequently, CC19 represents a more powerful analysis tool, e.g., it can handle residual stresses. CC19 has a larger range of geometric parameters, e.g., $W/D \geq 1.25$ for CC19 but $W/D \geq 2$ for CC03. Finally, comparisons between CC03/CC19 and benchmark results (obtained from finite element analyses) demonstrate that CC19 is more accurate than CC03. Crack case CC19 provides stress intensity factor solutions input as values of the pin-loading ($S_3 = P/Dt$). Individual magnitudes of the pin-loading are specified through the GUI for load block definitions. The fracture mechanics module internally estimates the local stress variations on the crack plane (in the corresponding uncracked body) along the net section and then invokes CC08.

Nonlinear stress variations along the crack plane were computed using the same assumptions as used in TC27. Please refer to TC27 for additional information on the nonlinear stress variations that drive these solutions.

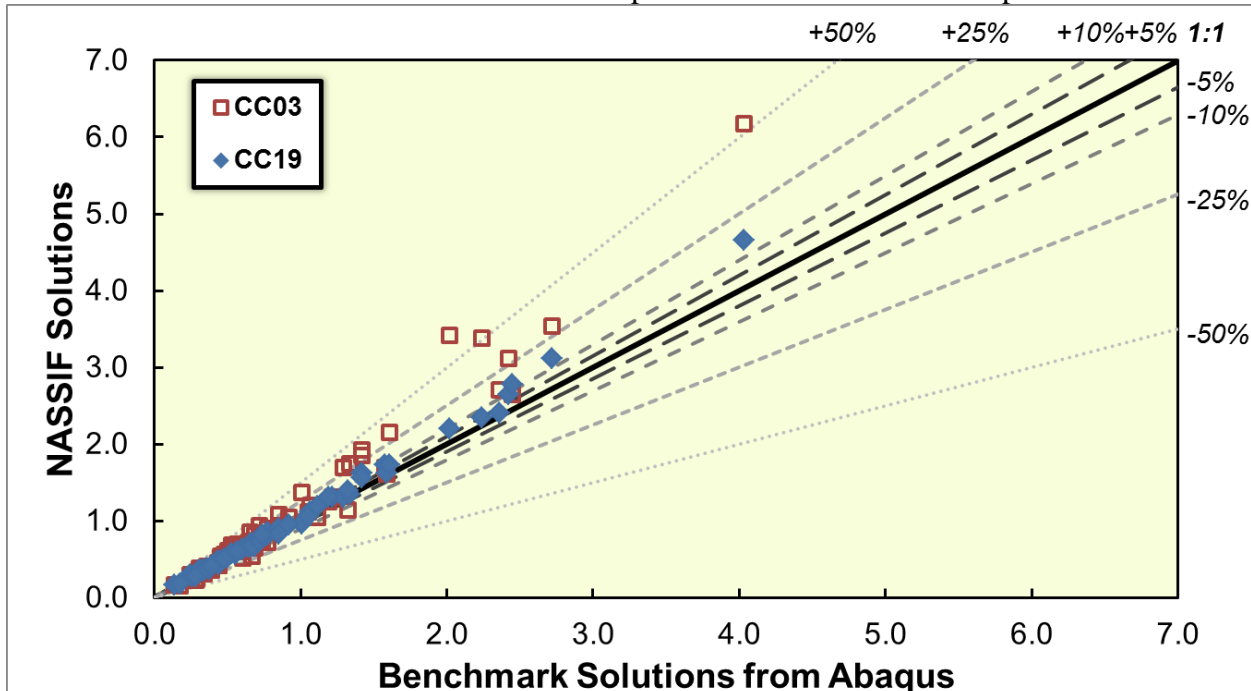
CC19 has the same geometric validity ranges as CC08, except for the additional constraint that $W/D \geq 1.25$. This ratio represents a lower limit for most straight lug geometries. The overall range of validity of this crack case is:

$$\begin{aligned} 0.1 &\leq \frac{D}{2t} \leq 10.0; \\ 0 &\leq \frac{c}{W-D} \leq 0.45; \\ 0.1 &\leq \frac{a}{c}; \\ 0 &\leq \frac{a}{t} \leq 0.95; \\ 1.25 &\leq \frac{W}{D} \leq 10 \end{aligned}$$

Please refer to CC08 for additional information on integration of the weight functions.



Verification of CC19 and comparison with CC03 at the a-tip



Verification of CC19 and comparison with CC03 at the c-tip

The previous figures show verification studies of CC19 at the a-tip and c-tip. Values of stress intensity factors from detailed finite element analyses (using Abaqus 6.12-1) provide the benchmark data. Almost all stress intensity factors computed with CC19 have less than 10% error in comparison with the benchmark data. Error with CC03 may exceed 50%. For both crack cases, the error tends to be conservative (i.e., driving increased crack advance). This figure also highlights the increased range of geometries in CC19 vs. CC03; several computed values of

CC19 do not have corresponding values of CC03 since the input geometry lies outside of the range of CC03 solutions.

Calculation of stress intensity factors for two symmetric corner cracks

For two symmetric corner cracks, stress intensity factors may be computed based on a correction of the stress intensity factor of a single, non-symmetric crack. Verification studies of the two crack solution using finite element simulations lead to the following relationship:

$$K_{2crks}^{a-tip} = \frac{1}{F_{Shah}} \times K_{1crk}^{a-tip}$$

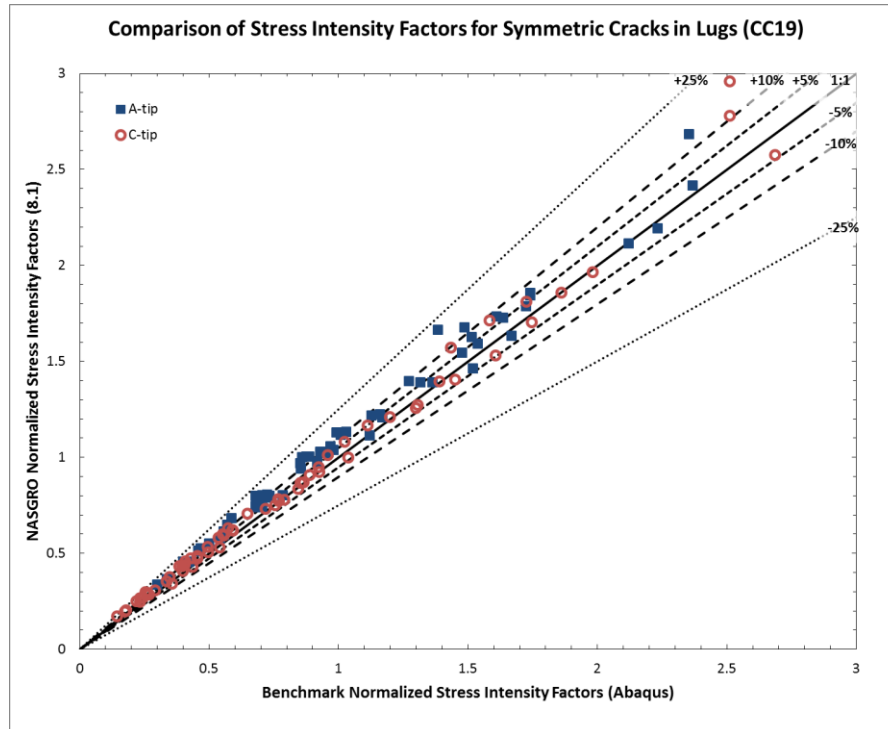
$$K_{2crks}^{c-tip} = \max \left(1, \frac{1}{F_{Shah} \times F_{FW}} \right) \times K_{1crk}^{c-tip}$$

$$F_{Shah} = \sqrt{\frac{D + \pi ac/4t}{D + \pi ac/2t}}$$

$$F_{FW} = \sqrt{\frac{D + 0.05 \times (W - D)}{D + c}}$$

Here, F_{Shah} represents the Shah correction factor for a corner crack. It is an appropriate correction for the stress intensity factor at the a-tip. The F_{FW} factor prevents non-conservative stress intensity factor solutions at the c-tip for short, straight lugs when the crack is large relative to the hole diameter.

The figure below highlights key results from the verification studies. It compares stress intensity factors (normalized by $S_3 \times \sqrt{\pi a}$) for two symmetric cracks computed using benchmark Abaqus solutions to results from NASGRO. For most cases, stress intensity factors are within 10% of the benchmark solution.



CC20 – Corner crack in plate – displacement control

CC20 is similar to TC14 and TC24 in being one of the few NASGRO fracture mechanics crack models subjected to displacement-controlled load conditions. The crack model represents a quarter-elliptical corner crack at the mid-section of a rectangular bar with remote ends subjected to displacement-controlled load conditions. Besides the load type, the formulation also accounts for the constraint condition. In the following, the applicable displacement constraint conditions are highlighted.

Remote displacement type

- Displacement field derived from remote tension, in-plane bending, and out-of-plane bending
- User-specified remote displacement

Displacement constraint type

- Type I: no constraint for displacements in the both x - and y - directions; displacement in z -direction is user-defined
- Type II: fixed constraint for displacements in both x - and y -directions; displacement in z -direction is user-defined

Note that the loading direction is the z -direction, coinciding with the longitudinal direction of the rectangular bar, and the displacement variation at the remote ends is bivariant or in terms of two coordinate directions: x and y , with the rectangular cross section. The definition of the displacement variations is required to be specified by the external usage of displacement files. The format of the bivariant displacement files is the same as the historical NASGRO bivariant format (the alternative bivariant format is not available for CC20) for tabular input from file utilized by CC09.

The SIF formulation of CC20 FM module is based on interpolation among reference SIF solutions determined at the two surface tips of the corner crack. The reference solutions [C69] were generated using the finite element software ABAQUS by the National Aerospace Laboratory of the Netherlands (NLR). The supplemental solutions for geometrically small cracks were provided by SwRI based on the CC09 crack model with crack plane stress derived from the constrained boundary. The solution matrix was in terms of a limited number of combinations of geometric ratios, reference displacement variations and two displacement end constraints. The discrete geometric ratios are in terms of a/c , a/t , c/W and L/W , where a and c are the depth and the width of the corner crack, t is the thickness of the plate, W the width and L is the height of the plate (as depicted in GUI bitmap). The reference displacement variations are the nine components of second order bivariant functions, respectively, given by

- 1
- $1 - x/W$
- $1 - y/t$
- $(1 - x/W)^2$
- $(1 - x/W)(1 - y/t)$
- $(1 - y/t)^2$
- $(1 - x/W)^2(1 - y/t)$
- $(1 - x/W)(1 - y/t)^2$

- $(1 - x/W)^2(1 - y/t)^2$

The validity limits of the solution are given by

$$\begin{aligned}0.1 &\leq a/c \leq 10 \\0 &\leq a/t \leq 0.9 \\0 &\leq c/W \leq 0.9 \\0.2 &\leq L/W \leq 10\end{aligned}$$

To compute SIFs, the user-specified displacement variations in discrete format are first converted into bivariate polynomial form. The conversion is through a least square method for two variables and thus determines the polynomial coefficients with the nine function components. For reference, the polynomial denoting the user-specified displacement variation D_i is given by

$$\begin{aligned}D_i(x, y) &= a_i^{0,0} + a_i^{1,0} \left(1 - \frac{x}{W}\right) + a_i^{0,1} \left(1 - \frac{y}{t}\right) + a_i^{2,0} \left(1 - \frac{x}{W}\right)^2 + a_i^{1,1} \left(1 - \frac{x}{W}\right) \left(1 - \frac{y}{t}\right) \\&\quad + a_i^{0,2} \left(1 - \frac{y}{t}\right)^2 + a_i^{2,1} \left(1 - \frac{x}{W}\right)^2 \left(1 - \frac{y}{t}\right) + a_i^{1,2} \left(1 - \frac{x}{W}\right) \left(1 - \frac{y}{t}\right)^2 \\&\quad + a_i^{2,2} \left(1 - \frac{x}{W}\right)^2 \left(1 - \frac{y}{t}\right)^2 = \sum_k \sum_l a_i^{k,l} \left(1 - \frac{x}{W}\right)^k \left(1 - \frac{y}{t}\right)^l\end{aligned}$$

where the subscript i ranges from 1 to 4 designating the displacement variations, and the superscripts k and l denote the dual-indexed coefficient $a_i^{k,l}$ and the exponents of the normalized functions $(1 - x/W)$ and $(1 - y/t)$.

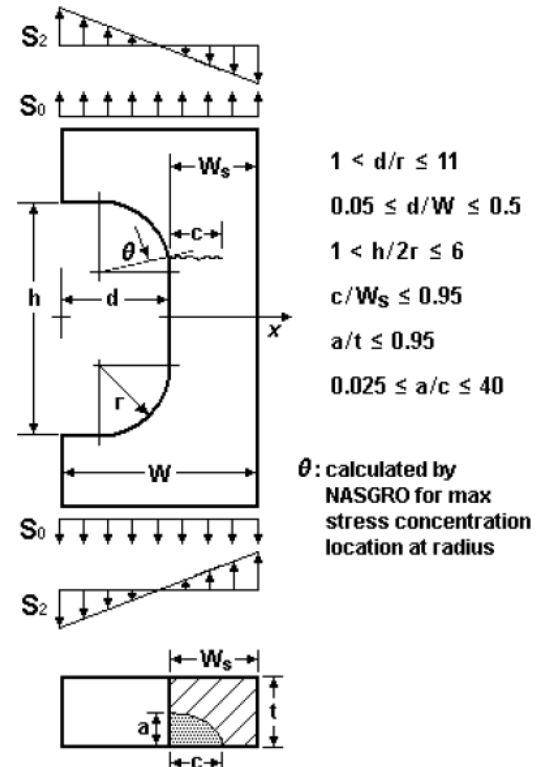
CC21 – Corner Crack at Edge Rectangular Cutout with Rounded Corners

The crack configuration for CC21 is very similar to TC25. Both are for cracks at the rounded corner of the rectangular cutout of a plate. CC21 utilizes the crack opening stress extracted along the crack plane and computes the stress intensity factors at both surface tips using weight function formulation. The following figure shows the crack model. The initiation site of the corner crack, designated by the θ angle, is numerically determined in accordance with the approach deployed for TC25. For details, please refer to the description in the section for TC25.

The crack plane is assumed perpendicular to the load direction. Due to the θ angle, the sectional width W_s , defined by $[W - d + r(1 - \cos \theta)]$, could be slightly larger than the net section ($W - d$). The variation of crack opening stress across the crack plane is the same as the one for TC25, which is interpolated among reference solutions determined using finite element method at discrete geometric ratios with reference stresses. NASGRO computes the θ angle based on the load ratio and determines the univariant stress gradient along the crack plane direction.

The crack model can be subjected to remote stress variations consisting of two load types: remote tension S_0 and in-plane bending stress S_2 . The weight function approach is the same as the one deployed in CC11 for two surface tips and univariant stress gradient along the net section direction. Validity limits are in terms of geometric ratios and given as follows with d denoting the nominal depth of the cutout, h the height of the cutout, r the radius of the rounded corner, W the plate width and t the thickness.

These limits are as follows:



$$\begin{aligned}
 1 &< \frac{d}{r} \leq 11 \\
 0.05 &\leq \frac{d}{W} \leq 0.5 \\
 1 &< \frac{h}{2r} \leq 6 \\
 \frac{c}{W_s} &\leq 0.95 \\
 \frac{a}{t} &\leq 0.95 \\
 0.025 &\leq \frac{a}{c} \leq 40
 \end{aligned}$$

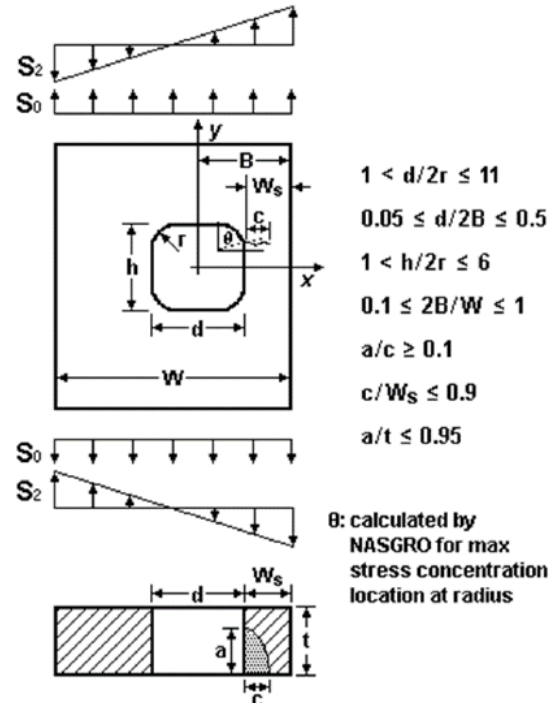
CC22 – Corner Crack at Offset Internal Rectangular Cutout with Rounded Corners

The cracked configuration of CC22 is very similar to TC26. Both crack locations are at the rounded corner of the internal cutout (in reference to the figure below). This corner crack model utilizes the crack opening stress extracted along the crack plane and computes the stress intensity factors at both surface tips using weight function formulation. The schematic provided in the following is identical to the bitmap in the GUI. The geometric parameters involved in defining this crack model are the plate width ($W=2b$), the cutout height (h), the cutout width (d), the radius (r), and the offset of the cutout (B) from the right side of the plate. The loading specification allows for a combination of remote tension (S_0) and in-plane bending (S_2) with their individual stress scaling factors. The θ angle designating the crack initiation site is determined in accordance with the approach deployed in TC26 crack model. NASGRO will determine the univariant stress gradient along the crack plane direction through interpolation among reference stress solutions.

The weight function formulation adapts a hybrid approach pending on the slenderness of the internal rectangular cutout described by the h/d ratio. If the aspect ratio in terms of the ratio of h over d is less than or equal to 1.0, the weight function result from CC08 is used. If h/d is larger than 1, an interpolative approach between the results from CC08 and CC11 is used. The approach is to account for the loss of material in the longitudinal direction in view of the assumption of a circular hole configuration with CC08 crack model

The validity limits are expressed in terms of geometric ratios and result from reference stress limits imposed on TC26 as well as the limits on weight function solutions. The specification is given in the GUI bitmap (see also in the above figure). The limits are as follows:

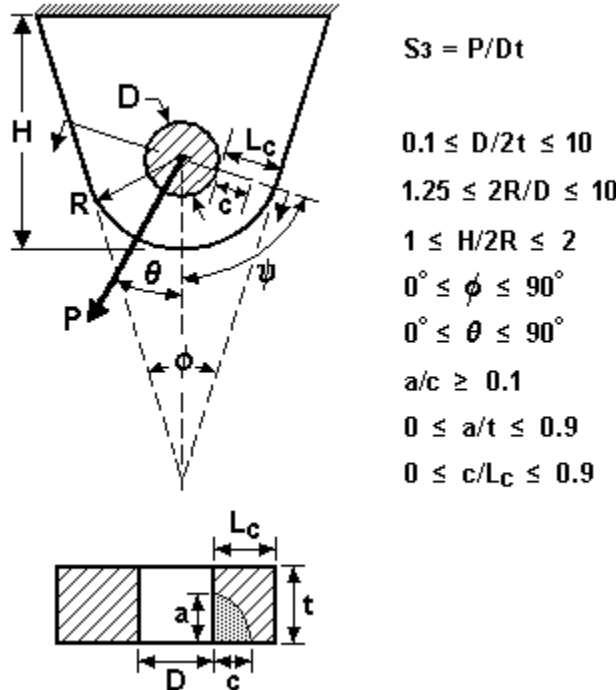
$$\begin{aligned} 1 < \frac{d}{2r} &\leq 11 \\ 0.05 \leq \frac{d}{2B} &\leq 0.5 \\ 1 < \frac{h}{2r} &\leq 6 \\ 0.1 \leq \frac{2B}{W} &\leq 1 \\ \frac{a}{c} &> 0.1 \end{aligned}$$



$$\frac{c}{W_s} \leq 0.9$$

$$\frac{a}{t} \leq 0.95$$

CC23 – Corner crack at hole in obliquely loaded and tapered lug – univariant WF



Configuration of crack case CC23

Crack case CC23 represents a semi-elliptical corner crack initiated at the hole of a symmetric tapered lug under oblique pin-loading. It is a new solution that is distinct and separate from earlier lug solutions that assumed straight, short lugs under vertical loading. Straight means that the lug geometry has no taper. Short implies that these lugs have height equal to their width. Vertical loading restricts loads to a constant angle. CC30 supports a much larger range of geometries and loadings for pin-loaded holes in lugs as indicated by the previous figure:

$$0.1 \leq \frac{D}{2t} \leq 10$$

$$1.25 \leq \frac{2R}{D} \leq 10$$

$$1 \leq \frac{H}{2R} \leq 2$$

$$0^\circ \leq \phi \leq 90^\circ$$

$$0^\circ \leq \theta \leq 90^\circ$$

$$\frac{a}{c} \geq 0.1$$

$$0 \leq \frac{a}{t} \leq 0.9$$

$$0 \leq \frac{c}{L_c} \leq 0.9$$

Here, the ratio $D/2t$ establishes the hole diameter relative to the lug thickness. The ratio $2R/D$ provides the ratio of the lug's outer radius (R) to its pin-hole diameter (D). The limits range from a very large hole ($2R/D = 1.25$) to a very small hole ($2R/D = 10$) and can cover earlier solutions for straight, short lugs under normal loading (CC19). The lug's heel-to-toe height (H) is variable in CC23 with limits for a short lug ($H = 2R$) to a much longer lug ($H = 4R$). CC23 supports symmetrically tapered lugs with symmetric taper angle (ϕ) that supports straight lugs ($\phi = 0^\circ$) to right-angled tapers ($\phi = 90^\circ$). The oblique loading angle (θ) varies from perpendicular to the base ($\theta = 0^\circ$) to parallel to the base ($\theta = 90^\circ$). CC23 has a large range of crack shapes controlled by the elliptical size ratio (a/c). Limits for the crack size (a/t and c/L_c) support most applicable geometries. Corner cracks (CC23) transition to through-thickness cracks (TC30) as a/t reaches the upper limit.

Please refer to crack case TC30 for more information on the crack angle (ψ), the crack path (L_c), crack kinking, internal stress processing, and generation of benchmark finite element analyses. Please refer to crack case CC08 for more information on integration of the underlying weight function used by CC23.

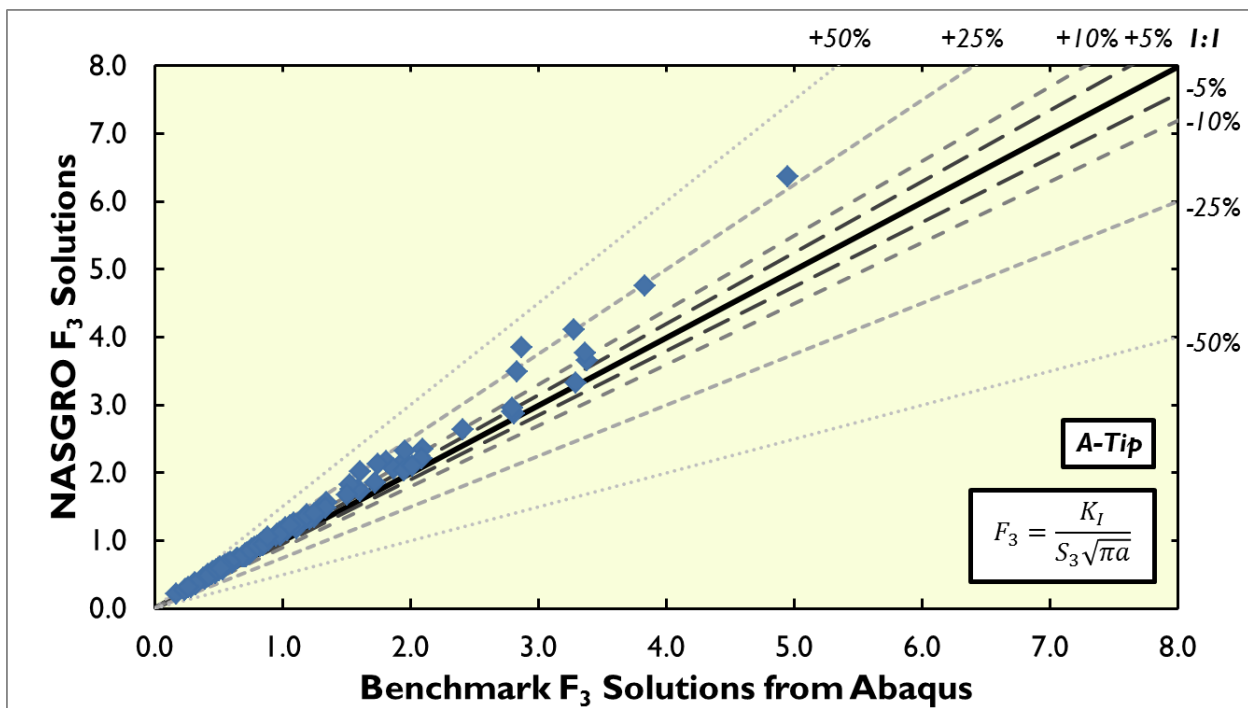
Crack case CC23 provides SIF solutions input as values of the pin-loading ($S_3=P/Dt$). Individual magnitudes of the pin-loading are specified through the GUI for load block definitions. The fracture mechanics module internally estimates the local stress variations on the crack plane (in the corresponding uncracked body) along the net section and then integrates these stresses with the weight function TC13 over the crack face.

CC23 has the same geometric validity ranges as CC08, except for the additional constraint that $2R/D \geq 1.25$. This ratio represents a lower limit for most lug geometries. This ratio matches the lower limit for lug geometries in CC19.

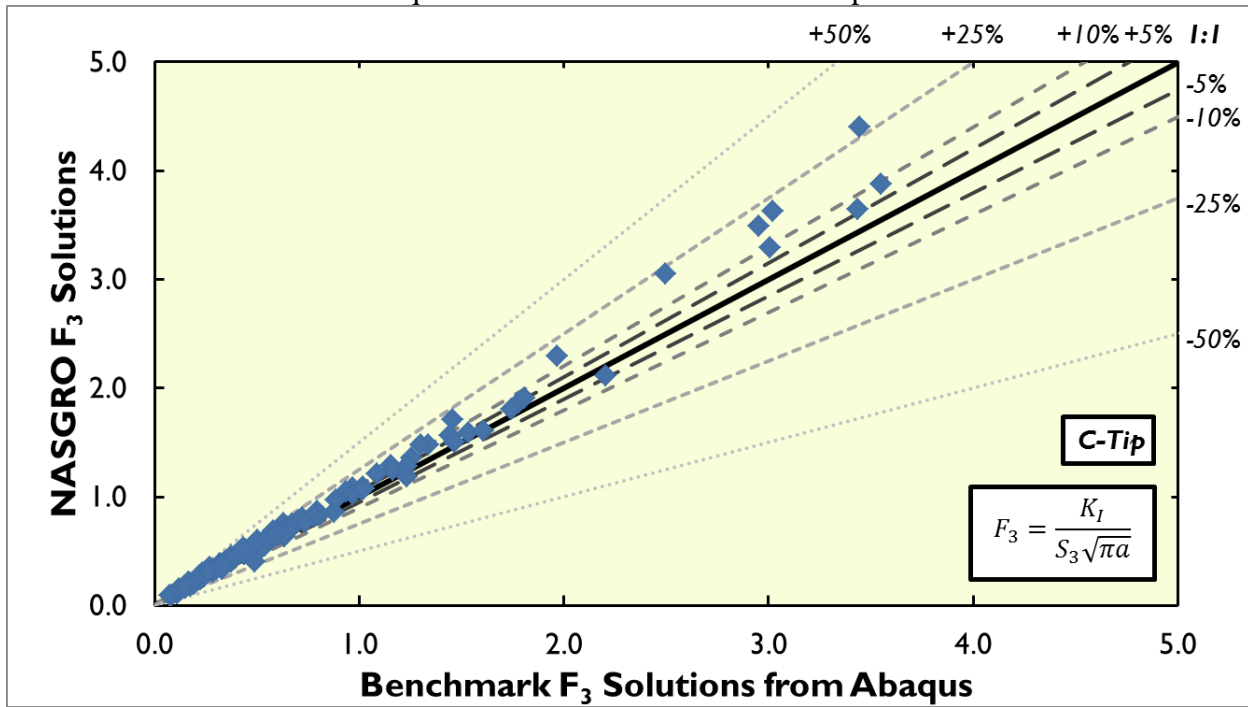
CC23 supports residual stresses along the crack path – that is, from $0 \leq X/L_c \leq 1$ at the angle ψ . Residual stresses will not alter the crack path. Consequently, a user may execute a NASFLA analysis to obtain ψ and then pick out the residual stress along the crack path.

CC23 supports negative pin-loading options: compression clipping or full range. Please refer to the appropriate documentation for more information.

The following figure summarizes verification studies of CC23. Values of SIFs from detailed finite element analyses (using Abaqus 6.12-1) provide the benchmark SIFs from crack geometries. Most SIFs computed with CC23 have less than 10% error in comparison with the benchmark data. Excessive error tends to be conservative (i.e., driving increased crack advance), though there are a few outliers where the error is non-conservative. These outliers represent geometries that have crack tips intersecting the straight taper edge at an angle.



Verification of CC23 with Abaqus benchmark solutions at the a-tip.



Verification of CC23 with Abaqus benchmark solutions at the c-tip.

CC23 represents a more powerful analysis tool than CC19, which is limited to straight, short lugs under normal loading. Both analyses are based on the same weight function solution, CC08. The main differences between CC19 and CC23 are the crack angle and stress gradient set. CC19 sets a constant crack angle that is perpendicular to the loading, whereas CC23 sets the crack angle

based on the geometry and loading. CC19 also uses a different set of stress gradient solutions. While CC23 may be set to the same geometry as CC19 ($W = 2R$; $H = 2R$; $\phi = 0^\circ$; $\theta = 0^\circ$), CC23 is intended to span the range of tapered and obliquely-loaded lug geometries that exist on aerospace platforms. CC19 is intended as a replacement for CC03. The differing assumptions of CC19 and CC23 lead to different SIFs over the solution space. Direct comparisons between CC19 and CC23 reveal that SIF solutions from CC23 are mostly within 3% of CC19 for holes with $2R/D \geq 2$. The impact on fatigue crack growth lives is complicated. SIFs from CC23 may be above SIFs from CC19 for smaller cracks and below SIFs from CC19 for larger cracks. Furthermore, CC19 sets a minimum crack ligament, whereas CC23 may have a longer crack path than the minimum possible ligament.

Section C3: Embedded Cracks

EC01 – Embedded Crack in a Plate

$$F_0 = M_0 g f_\phi f_w f_x$$

$$M_1 = 1 \quad \text{for } x \leq 1$$

$$= 1/\sqrt{x} \text{ for } x > 1$$

$$M_2 = 0.05 / (0.11 + x^{3/2})$$

$$M_3 = 0.29 / (0.23 + x^{3/2})$$

$$M_0 = M_1 + M_2 h^2 + M_3 h^4$$

$$g = 1 - [h^4 (2.6 - 2h)^{1/2} / (1 + 4x)] \cos \phi$$

$$f_w = \{\sec[(\pi c/W)\sqrt{h}]\}^{1/2}$$

$$h = 2v = 2a/t$$

$$\phi = 0^\circ \text{ for } dc/dN$$

$$= 90^\circ \text{ for } da/dN$$

Reference: [C13]

EC02 – Offset Embedded Crack in a Plate

This case is a more general version of EC01. The center of the crack can have offset in both the width and thickness direction. Computation of stress intensity factors is possible for simple tension, bend loads, a nonlinear stress specified by polynomial coefficients or nonlinear stress specified by a table. The stress variation is possible only along the thickness direction. Because of the offset, in general, the four crack tips can have different values of the stress intensity factors. The crack growth algorithm allows the four crack tips to grow independently based on the computed SIF values. As a result, an initially elliptical shaped can grow into a non elliptical crack. However, only elliptical shape is allowed by the routines supplied by SWRI. Hence, an approximate elliptical shape is assumed for the purpose of computing the stress intensity factors after every crack growth increment by using average values of the two opposing crack tips. Let the crack tips be denoted by a, c, a_1, c_1 . The values of a, c used in the SIF computation after every crack growth increment and the new position of the center of the crack are as follows:

$$a^* = (a + a_1)/2$$

$$c^* = (c + c_1)/2$$

Reference: [C13].

EC04 – Elliptical Embedded Crack (Offset) in a Plate – Bivariant Stressing

Crack case EC04 is a bivariant weight function solution for an embedded crack in a plate with rectangular cross-section subjected to remote stressing. The differences from EC02 are as follows: (1) EC04 is for a plate subjected to bivariant stressing while EC02 is for univariant stressing, (2) EC04 has wider solution limits, and (3) EC04 is based on a new set of highly accurate reference solutions generated by the advanced hybrid finite/boundary element computer program FADD3D for determining SIF variation along the crack perimeter. EC04 will give results in agreement with EC05 when the prescribed stress field is univariant in nature.

The bivariant stresses are input via a file that contains the normalized coordinates and stress values. The input format is the same as those for the CC09 solution. The solution limits in terms of dimensionless geometric parameters are given by

$$\begin{aligned} 0 \leq \text{Min}\left(\frac{a}{B_t}, \frac{a}{t - B_t}\right) &\leq 0.99 \\ 0 \leq \text{Min}\left(\frac{c}{B_w}, \frac{c}{W - B_w}\right) &\leq 0.99 \\ 0.1 \leq \frac{a}{c} &\leq 10 \end{aligned}$$

The EC04 solution is based on a new weight function formulation similar to the formulation used in CC09 and SC19 and has its own independent set of reference solutions. Its basic weight function (see the figure below) is identical to the point weight function proposed by Orynyak and the basic weight functions used in CC09 and SC19. To account for the effects of free surfaces, three correction terms were used and the approximate weight function for the formulation is given by

$$\begin{aligned} W &= W_{\text{basic}} + W_{\text{correction}} \\ &= \frac{\sqrt{R^2 - r^2}}{\pi \sqrt{\pi R} \ell_{QQ'}^2} \left\{ 1 + \Pi_1 \sqrt{1 - \frac{r}{R}} + \Pi_2 \left[1 - \frac{y}{\text{SIGN}(Q', y)y'} \right] + \Pi_3 \left[1 - \frac{x}{\text{SIGN}(Q', x)x'} \right] \right\} \end{aligned}$$

where $W_{\text{correction}}$ represents the correction terms with coefficients Π_1 , Π_2 , and Π_3 , and $Q(x,y)$ denotes the location where the point load is applied. The chordal lengths x' and y' can be determined by

$$x' = c \sqrt{1 - \frac{y^2}{a^2}}, \quad y' = a \sqrt{1 - \frac{x^2}{c^2}}$$

$\text{SIGN}(Q',y)$ denotes the sign of x -coordinate of Q' and $\text{SIGN}(Q',x)$ the sign of y -coordinate of Q' . The stress intensity factor for any location Q' along the crack perimeter can thus be written as

$$K^Q = \int_A W\sigma(x, y)dA$$

where the integration is carried out over the whole embedded crack surface.

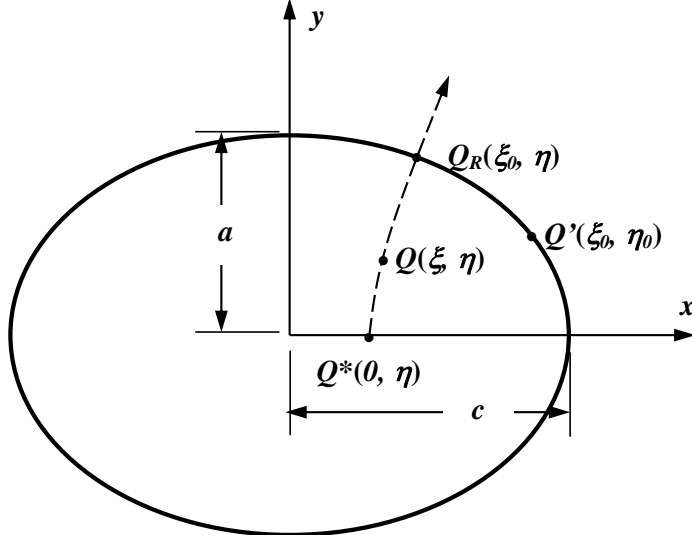


Figure: Embedded crack in an infinite domain.

The surface integral can be transformed to be in reference to an elliptical coordinate system with its origin at the crack center to facilitate further mathematical manipulations. In that case, Q^* , Q and Q_R are defined to share the same elliptical angle η , and Q' and Q_R have the same elliptical “radius” ξ_0 . The value of ξ_0 depends on the crack aspect ratio $\alpha=a/c$. For $a/c<1$ and $b=\sqrt{c^2-a^2}$

$$x = b \cdot \cosh \xi \cdot \cos \eta, \quad y = b \cdot \sinh \xi \cdot \sin \eta$$

$$\xi_0 = \ln \left(\frac{1+\alpha}{1-\alpha} \right)$$

$$R = b \sqrt{(\cosh \xi_0 \cdot \cos \eta - \cos \eta)^2 + \sinh^2 \xi_0 \cdot \sin^2 \eta}$$

$$r = b \sqrt{(\cosh \xi \cdot \cos \eta - \cos \eta)^2 + \sinh^2 \xi \cdot \sin^2 \eta}$$

$$\ell_{QQ'} = b \sqrt{(\cosh \xi \cdot \cos \eta - \cosh \xi_0 \cdot \cos \eta_0)^2 + (\sinh \xi \cdot \sin \eta - \sinh \xi_0 \cdot \sin \eta_0)^2}$$

$$\frac{y}{y'} = \frac{\sinh \xi \cdot \sin \eta}{\alpha \sqrt{\cosh^2 \xi_0 - \cosh^2 \xi \cdot \cos^2 \eta}}, \quad \frac{x}{x'} = \frac{\alpha \cdot \cosh \xi \cdot \cos \eta}{\sqrt{\sinh^2 \xi_0 - \sinh^2 \xi \cdot \sin^2 \eta}}$$

$$dA = b^2 (\sin^2 \eta + \sinh^2 \xi) \cdot d\xi d\eta$$

and the integral becomes

$$K^Q = \int_0^{\xi_0} \int_0^{2\pi} (W_{basic} + W_{correction}) \cdot \sigma(\xi, \eta) \cdot c^2 (\sin^2 \eta + \sinh^2 \xi) \cdot d\eta d\xi$$

The coefficients Π_1 , Π_2 , and Π_3 are determined by three sets of reference solutions at the preferred crack tip locations. The surface integral can be determined by the Gauss-Chebyshev numerical integration scheme.

EC05 – Elliptical Embedded Crack (Offset) in a Plate – Univariant Stressing

Crack case EC05 is a univariant weight function solution for an embedded crack in a plate with rectangular cross-section subjected to remote stressing. Both EC02 and EC05 are for a plate subjected to univariant stressing. The differences are as follows: (1) EC05 makes use of a subset of the more accurate reference solutions generated for the EC04 crack case, (2) EC05 has wider solution limits, and (3) EC05 makes use of the point weight function similar to Glinka's derivation for surface cracks.

The solution limits in terms of dimensionless geometric parameters are identical to those for EC04 and are given by

$$0 \leq \text{Min}\left(\frac{a}{B_t}, \frac{a}{t - B_t}\right) \leq 0.99$$

$$0 \leq \text{Min}\left(\frac{c}{B_w}, \frac{c}{W - B_w}\right) \leq 0.99$$

$$0.1 \leq \frac{a}{c} \leq 10$$

Assume the stress variation is univariant and varying along the local y -axis. The 1D basic weight function varying along y -axis for a -, c -, a_1 - and c_1 -tips can be determined by integrating the point weight function for a penny-shape embedded crack in an infinite domain with a unit load along the chordal length intersected by a fixed y -value. By preserving the singular terms in the basic weight functions and on account of two sets of reference solution, the approximate 1D weight functions for an embedded crack with elliptical crack perimeter can thus be postulated as

$$W^a(y) = \frac{2}{\sqrt{2\pi(a-y)}} \left[1 + M_1^a \sqrt{1 - \frac{y}{a}} + M_2^a \left(1 - \frac{y}{a} \right) + M_3^a \left(1 - \frac{y}{a} \right)^{3/2} \right]$$

$$W^{a_1}(y) = \frac{2}{\sqrt{2\pi(a+y)}} \left[1 + M_1^{a_1} \sqrt{1 + \frac{y}{a}} + M_2^{a_1} \left(1 + \frac{y}{a} \right) + M_3^{a_1} \left(1 + \frac{y}{a} \right)^{3/2} \right]$$

$$W^c(y) = W^{c_1}(y) = \begin{cases} \frac{1}{\sqrt{\pi y}} \left[1 + M_1^c \sqrt{\frac{y}{a}} + M_2^c \frac{y}{a} \right] & \text{if } y \geq 0 \\ \frac{1}{\sqrt{\pi(-y)}} \left[1 + M_1^c \sqrt{\frac{-y}{a}} + M_2^c \frac{y}{a} \right] & \text{if } y < 0 \end{cases}$$

The coefficient M 's in the above equations are for correction terms, and the weight function solutions for a -, a_1 - and c -tips (or c_1 -tip) are given by

$$\begin{aligned} K^a &= \int_{-a}^a \frac{2\sigma(y)}{\sqrt{2\pi(a-y)}} \left[1 + M_1^a \sqrt{1 - \frac{y}{a}} + M_2^a \left(1 - \frac{y}{a} \right) + M_3^a \left(1 - \frac{y}{a} \right)^{3/2} \right] dy \\ K^{a_1} &= \int_{-a}^a \frac{2\sigma(y)}{\sqrt{2\pi(a+y)}} \left[1 + M_1^{a_1} \sqrt{1 + \frac{y}{a}} + M_2^{a_1} \left(1 + \frac{y}{a} \right) + M_3^{a_1} \left(1 + \frac{y}{a} \right)^{3/2} \right] dy \\ &= \int_{-a}^a \frac{2\sigma(-y)}{\sqrt{2\pi(a-y)}} \left[1 + M_1^{a_1} \sqrt{1 - \frac{y}{a}} + M_2^{a_1} \left(1 - \frac{y}{a} \right) + M_3^{a_1} \left(1 - \frac{y}{a} \right)^{3/2} \right] dy \\ K^c = K^{c_1} &= \int_0^a \frac{[\sigma(y) + \sigma(-y)]}{\sqrt{\pi y}} \left[1 + M_1^c \sqrt{\frac{y}{a}} + M_2^c \frac{y}{a} \right] dy \end{aligned}$$

These coefficients can be determined by boundary conditions and reference solutions. Details are described in the following

(1) At $y=-a$, $W^a(-a)=0$ which leads to

$$1 + \sqrt{2}M_1^a + 2M_2^a + 2^{\frac{3}{2}}M_3^a = 0$$

(2) Using the reference solutions at a -tip for reference stress $\sigma(y)=1$, κ_u^a gives

$$K_u^a = \int_{-a}^a \frac{2}{\sqrt{2\pi(a-y)}} \left[1 + M_1^a \sqrt{1 - \frac{y}{a}} + M_2^a \left(1 - \frac{y}{a} \right) + M_3^a \left(1 - \frac{y}{a} \right)^{3/2} \right] dy$$

(3) Using the other reference solutions at a -tip for reference stress $\sigma(y)=y/a$, κ_b^a gives

$$K_b^a = \int_{-a}^a \frac{2\left(\frac{y}{a}\right)}{\sqrt{2\pi(a-y)}} \left[1 + M_1^a \sqrt{1 - \frac{y}{a}} + M_2^a \left(1 - \frac{y}{a} \right) + M_3^a \left(1 - \frac{y}{a} \right)^{3/2} \right] dy$$

The above three conditions uniquely determine the coefficients for a -tip: M_1^a , M_2^a , and M_3^a . Respectively, they are given by

$$\begin{aligned} M_1^a &= -4\sqrt{2} - \frac{3}{2} \frac{\pi}{\sqrt{2Q}} \tilde{K}_u^a + \frac{15}{2} \frac{\pi}{\sqrt{2Q}} \tilde{K}_b^a \\ M_2^a &= \frac{15}{2} + \frac{15}{4} \frac{\pi}{\sqrt{Q}} \tilde{K}_u^a - \frac{45}{4} \frac{\pi}{\sqrt{Q}} \tilde{K}_b^a \\ M_3^a &= -2\sqrt{2} - 3 \frac{\pi}{\sqrt{2Q}} \tilde{K}_u^a + \frac{15}{2} \frac{\pi}{\sqrt{2Q}} \tilde{K}_b^a \end{aligned}$$

where \tilde{K}_u^a and \tilde{K}_b^a are the normalized reference solutions of K_u^a and K_b^a by $\sqrt{\pi a/Q}$ and Q is the shape factor for an ellipse. Using a similar approach, the other coefficients can be determined and listed as follows.

$$\begin{aligned} M_1^{a_1} &= -4\sqrt{2} - \frac{3}{2} \frac{\pi}{\sqrt{2Q}} \tilde{K}_u^{a_1} - \frac{15}{2} \frac{\pi}{\sqrt{2Q}} \tilde{K}_b^{a_1} \\ M_2^{a_1} &= \frac{15}{2} + \frac{15}{4} \frac{\pi}{\sqrt{Q}} \tilde{K}_u^{a_1} + \frac{45}{4} \frac{\pi}{\sqrt{Q}} \tilde{K}_b^{a_1} \\ M_3^{a_1} &= -2\sqrt{2} - 3 \frac{\pi}{\sqrt{2Q}} \tilde{K}_u^{a_1} - \frac{15}{2} \frac{\pi}{\sqrt{2Q}} \tilde{K}_b^{a_1} \\ M_1^c &= -4 + \frac{3}{2} \frac{\pi}{\sqrt{Q}} \tilde{K}_u^c \\ M_2^c &= 3 - \frac{3}{2} \frac{\pi}{\sqrt{Q}} \tilde{K}_u^c \end{aligned}$$

The normalized reference solutions are based on the same two reference stresses: unit tension and unit bending along the local x -axis.

Section C4: Surface Cracks

SC01 – Surface Crack in Finite Width Plate – Tension and Bending

The solution in the previous version was based on empirical equations of Newman and Raju [C13]. It is now replaced in the current version by using direct tabular interpolation of the finite element solution given in tables C16 and C17. More results may be found in ref. [C29] for certain types of nonuniform loads. This crack case allows only tension and bending loads as in the previous version. The values listed in tables C16 and C17 are factors $F_p = K_I / f_x \sigma_0 \sqrt{\pi a}$, where σ_0 is the peak stress applied. Some of the following part-through cracks (indicated where used) use this definition of F_p .

References: [C13], [C29]

SC02 – Surface Crack in a Finite Width Plate – Nonlinear Stress

This is a more general version of the case SC01. The loading for this case may include nonlinear stresses. The stress variation across the thickness of a plate is input in a numerical form as pairs of $((x/t)_i, S_i)$. A plot of the data and a smooth curve through them may be obtained. A weight function method is used to obtain the stress intensity factor for nonlinear stresses as explained in ref. [C14]. Up to four such nonlinear stress distributions may be input, and the resultant stress intensity factor may be computed. The results shown in ref. [C29] for quadratic and cubic loading were used to verify the weight function method. The numerical results for tension and bending given in tables C16 and C17 were used as reference solutions in the weight function method.

References: [C14], [C29]

Table C16: Stress Intensity Correction Factors, F_p

At the c-tip: Tensile Loading

2c/W	a / c	$a / t \rightarrow 0.0$	0.20	0.50	0.80	1.0
0.0	0.20	0.5622	0.6110	0.7802	1.1155	1.4436
0.0	0.40	0.6856	0.7817	0.9402	1.1583	1.3383
0.0	1.00	1.1365	1.1595	1.2328	1.3772	1.5145
0.1	0.20	0.5685	0.6133	0.7900	1.1477	1.5014
0.1	0.40	0.6974	0.7824	0.9456	1.2008	1.4256
0.1	1.00	1.1291	1.1544	1.2389	1.3892	1.5273
0.4	0.20	0.5849	0.6265	0.8438	1.3154	1.7999
0.4	0.40	0.7278	0.8029	1.0127	1.4012	1.7739
0.4	1.00	1.1366	1.1969	1.3475	1.5539	1.7238
0.6	0.20	0.5939	0.6415	0.9045	1.5056	2.1422
0.6	0.40	0.7385	0.8351	1.1106	1.6159	2.1036
0.6	1.00	1.1720	1.2855	1.5215	1.8229	2.0621
0.8	0.20	0.6155	0.6739	1.0240	1.8964	2.8650
0.8	0.40	0.7778	0.9036	1.3151	2.1102	2.9068
0.8	1.00	1.2630	1.4957	1.9284	2.4905	2.9440
1.0	0.20	0.6565	0.7237	1.2056	2.6060	4.2705
1.0	0.40	0.8375	1.0093	1.6395	2.9652	4.3596
1.0	1.00	1.3956	1.8446	2.6292	3.6964	4.5865

At the a-tip: Tensile Loading

0.0	0.20	1.1120	1.1445	1.4504	1.7620	1.9729
0.0	0.40	1.0900	1.0945	1.2409	1.3672	1.4404
0.0	1.00	1.0400	1.0400	1.0672	1.0883	1.0800
0.1	0.20	1.1120	1.1452	1.4595	1.7744	1.9847
0.1	0.40	1.0900	1.0950	1.2442	1.3699	1.4409
0.1	1.00	1.0400	1.0260	1.0579	1.0846	1.0820
0.4	0.20	1.1120	1.1577	1.5126	1.8662	2.1012
0.4	0.40	1.0900	1.1140	1.2915	1.4254	1.4912
0.4	1.00	1.0400	1.0525	1.1046	1.1093	1.0863
0.6	0.20	1.1120	1.1764	1.5742	1.9849	2.2659
0.6	0.40	1.0900	1.1442	1.3617	1.5117	1.5761
0.6	1.00	1.0400	1.1023	1.1816	1.1623	1.0955
0.8	0.20	1.1120	1.2047	1.6720	2.2010	2.5895
0.8	0.40	1.0900	1.1885	1.4825	1.6849	1.7727
0.8	1.00	1.0400	1.1685	1.3089	1.2767	1.1638
1.0	0.20	1.1120	1.2426	1.8071	2.5259	3.0993
1.0	0.40	1.0900	1.2500	1.6564	1.9534	2.0947
1.0	1.00	1.0400	1.2613	1.4890	1.4558	1.3010

Table C17: Stress Intensity Correction Factors, F_p

At the c-tip: Bending Loading

2c/W	a / c	$a / t \rightarrow 0.0$	0.20	0.50	0.80	1.0
0.0	0.20	0.5622	0.5772	0.6464	0.7431	0.8230
0.0	0.40	0.6856	0.7301	0.7694	0.7358	0.6729
0.0	1.00	1.1365	1.0778	1.0184	0.9716	0.9474
0.1	0.20	0.5685	0.5809	0.6524	0.7646	0.8624
0.1	0.40	0.6974	0.7315	0.7856	0.8008	0.7895
0.1	1.00	1.1291	1.0740	1.0114	0.9652	0.9435
0.4	0.20	0.5849	0.5981	0.6934	0.8654	1.0249
0.4	0.40	0.7278	0.7519	0.8327	0.9312	1.0068
0.4	1.00	1.1366	1.1079	1.0634	1.0358	1.0268
0.6	0.20	0.5939	0.6158	0.7438	0.9704	1.1802
0.6	0.40	0.7385	0.7816	0.8906	1.0215	1.1211
0.6	1.00	1.1720	1.1769	1.1759	1.1820	1.1900
0.8	0.20	0.6155	0.6446	0.8320	1.1794	1.5113
0.8	0.40	0.7778	0.8386	1.0150	1.2791	1.5073
0.8	1.00	1.2630	1.3633	1.4785	1.5360	1.5431
1.0	0.20	0.6565	0.6848	0.9593	1.5053	2.0518
1.0	0.40	0.8375	0.9232	1.2285	1.7607	2.2637
1.0	1.00	1.3956	1.6821	2.0140	2.1482	2.1446

At the a-tip: Bending Loading

0.0	0.20	1.1120	0.8825	0.6793	0.3063	-.0497
0.0	0.40	1.0900	0.8292	0.5291	0.1070	-.2489
0.0	1.00	1.0400	0.7411	0.3348	-.1149	-.4396
0.1	0.20	1.1120	0.8727	0.6697	0.3071	-.0348
0.1	0.40	1.0900	0.8243	0.5170	0.1047	-.2336
0.1	1.00	1.0400	0.7398	0.3322	-.1172	-.4408
0.4	0.20	1.1120	0.8683	0.6794	0.3439	0.0291
0.4	0.40	1.0900	0.8330	0.5270	0.1257	-.1989
0.4	1.00	1.0400	0.7602	0.3572	-.1080	-.4543
0.6	0.20	1.1120	0.8904	0.7248	0.4033	0.0915
0.6	0.40	1.0900	0.8625	0.5803	0.1678	-.1874
0.6	1.00	1.0400	0.7982	0.4072	-.0856	-.4750
0.8	0.20	1.1120	0.9191	0.7925	0.5102	0.2254
0.8	0.40	1.0900	0.8987	0.6619	0.2524	-.1300
0.8	1.00	1.0400	0.8556	0.4981	-.0329	-.4960
1.0	0.20	1.1120	0.9545	0.8827	0.6666	0.4351
1.0	0.40	1.0900	0.9417	0.7723	0.3810	-.0250
1.0	1.00	1.0400	0.9323	0.6312	0.0505	-.5249

SC03 – Surface Crack in a Sphere

The solution for this crack case is made up of a combination of the flat plate solution (SC01) assuming a wide plate and applying the corrections due to the curvature from crack cases SC04 and SC05 for cylinders. This procedure was applied only for tensile loading. The solution for bending loading is assumed to be the same as that of a flat plate.

$$F_0 = F_{01} \left(F_{04} F_{05} / F_{01}^2 \right)$$

$$F_1 = F_{11}$$

F_{01}, F_{11} are obtained from tables C16 and C17 for wide plates using $2c/W = 0.05$ for tension and bending, respectively. The factors F_{04}, F_{14} are obtained from crack case SC04 for tension and bending. Similarly, F_{05} and F_{15} are obtained from crack case SC05 for tension and bending.

SC04 – Surface Crack in a Hollow Cylinder, Longitudinal Crack – Nonlinear Stress

The empirical solution for tension and bending loads in the previous version [C16] is now replaced by direct tabular interpolation from the finite element results given in tables C18 and C19. The values listed are factors $F_p = F_0 / f_x$. As in the case of SC02, the tension and bending results are used as reference solution in the weight function method and the solution for nonlinear stresses is obtained by numerical integration as documented in ref. [C28]. Ref. [C29] gives all the available results for this crack case for certain other types of nonlinear stresses.

Provision is made in the program to allow the user to specify internal pressure in the cylinder, for which hoop stresses are calculated by the program. In the case of an internal crack, the operative stresses (in the weight function calculation of stress intensity) are the sum of the hoop stresses and the crack-face pressure, while for an external crack, hoop stresses alone are present.

Reference: [C16], [C28] and [C29]

Table C18: SIF Correction Factors for Internal Cracks
 Cylinder – Longitudinal Crack, F_p

$a/t \rightarrow$	$a/c = 0.2$						$a/c = 0.4$						$a/c = 1.0$					
	0	.2	.5	.8	1.0	0	.2	.5	.8	1.0	0	.2	.5	.8	1.0			
R/t																		
<i>c</i> -tip, Uniform Loading ($n = 0$)																		
1.0	0.608	0.615	0.871	1.554	2.277	0.740	0.745	0.916	1.334	1.752	1.044	1.080	1.116	1.217	1.315			
2.0	0.600	0.614	0.817	1.300	1.783	0.730	0.760	0.919	1.231	1.519	1.132	1.113	1.155	1.286	1.416			
4.0	0.577	0.606	0.797	1.201	1.586	0.737	0.770	0.924	1.219	1.487	1.119	1.128	1.191	1.316	1.428			
10.0	0.579	0.607	0.791	1.179	1.548	0.733	0.777	0.936	1.219	1.469	1.114	1.140	1.219	1.348	1.456			
50.0	0.582	0.613	0.790	1.148	1.482	0.721	0.782	0.946	1.201	1.413	1.133	1.154	1.239	1.389	1.520			
<i>c</i> -tip, Linear Loading ($n = 1.0$)																		
1.0	0.083	0.085	0.171	0.363	0.544	0.112	0.119	0.181	0.307	0.421	0.169	0.182	0.200	0.218	0.229			
2.0	0.078	0.083	0.150	0.291	0.421	0.072	0.122	0.197	0.271	0.317	0.192	0.190	0.207	0.247	0.285			
4.0	0.070	0.079	0.141	0.262	0.370	0.110	0.123	0.174	0.263	0.339	0.188	0.194	0.214	0.248	0.277			
10.0	0.070	0.079	0.138	0.253	0.356	0.109	0.125	0.176	0.259	0.328	0.187	0.197	0.221	0.255	0.282			
50.0	0.068	0.081	0.138	0.239	0.328	0.103	0.127	0.180	0.253	0.310	0.189	0.201	0.227	0.265	0.294			
<i>a</i> -tip, Uniform Loading ($n = 0$)																		
1.0	1.076	1.056	1.395	2.530	3.846	1.051	1.011	1.149	1.600	2.087	0.992	0.987	1.010	1.155	1.314			
2.0	1.049	1.091	1.384	2.059	2.739	1.075	1.045	1.160	1.510	1.876	1.037	1.003	1.023	1.129	1.242			
4.0	1.003	1.097	1.405	1.959	2.461	1.024	1.057	1.193	1.443	1.665	1.005	1.009	1.041	1.105	1.162			
10.0	0.973	1.115	1.427	1.872	2.230	0.992	1.072	1.217	1.393	1.521	0.994	1.015	1.050	1.090	1.118			
50.0	0.936	1.145	1.459	1.774	1.974	0.982	1.095	1.244	1.370	1.438	1.002	1.026	1.058	1.085	1.099			
<i>a</i> -tip, Linear Loading ($n = 1.0$)																		
1.0	0.693	0.647	0.767	1.174	1.615	0.689	0.646	0.694	0.889	1.093	0.704	0.701	0.709	0.730	0.750			
2.0	0.673	0.661	0.764	1.033	1.301	0.674	0.659	0.710	0.854	0.995	0.732	0.707	0.714	0.774	0.840			
4.0	0.649	0.666	0.776	0.996	1.197	0.668	0.666	0.715	0.828	0.934	0.720	0.713	0.726	0.768	0.810			
10.0	0.635	0.673	0.783	0.960	1.108	0.656	0.672	0.723	0.806	0.875	0.715	0.715	0.729	0.760	0.788			
50.0	0.620	0.681	0.790	0.917	1.008	0.651	0.677	0.727	0.791	0.838	0.716	0.715	0.726	0.751	0.775			

Note: R is the inner radius of the cylinder

Table C19: SIF Correction Factors for External Cracks
 Cylinder – Longitudinal Crack, F_p

$a/t \rightarrow$	$a/c = 0.2$						$a/c = 0.4$						$a/c = 1.0$					
	0	.2	.5	.8	1.0	0	.2	.5	.8	1.0	0	.2	.5	.8	1.0			
R/t																		
<i>c</i> -tip, Uniform Loading ($n = 0$)																		
1.0	0.755	0.594	0.648	1.293	2.129	0.889	0.809	0.934	1.492	2.143	1.148	1.202	1.354	1.594	1.796			
2.0	0.720	0.611	0.693	1.207	1.826	0.817	0.796	0.959	1.425	1.915	1.152	1.185	1.318	1.560	1.775			
4.0	0.589	0.612	0.786	1.160	1.517	0.754	0.793	0.994	1.400	1.781	1.127	1.163	1.286	1.498	1.681			
10.0	0.598	0.612	0.806	1.262	1.715	0.750	0.788	0.984	1.378	1.747	1.123	1.156	1.266	1.453	1.613			
50.0	0.582	0.613	0.790	1.148	1.482	0.721	0.782	0.946	1.201	1.413	1.133	1.154	1.239	1.389	1.520			
<i>c</i> -tip, Linear Loading ($n = 1.0$)																		
1.0	0.153	0.076	0.089	0.271	0.481	0.170	0.132	0.170	0.329	0.497	0.202	0.214	0.256	0.327	0.387			
2.0	0.121	0.079	0.105	0.245	0.395	0.140	0.130	0.182	0.315	0.443	0.196	0.209	0.250	0.315	0.370			
4.0	0.073	0.080	0.134	0.242	0.339	0.118	0.130	0.195	0.318	0.427	0.189	0.204	0.243	0.302	0.350			
10.0	0.078	0.080	0.142	0.277	0.402	0.114	0.128	0.192	0.309	0.411	0.188	0.202	0.236	0.286	0.326			
50.0	0.068	0.081	0.138	0.239	0.328	0.103	0.127	0.180	0.253	0.310	0.189	0.201	0.227	0.265	0.294			
<i>a</i> -tip, Uniform Loading ($n = 0$)																		
1.0	1.244	1.237	1.641	2.965	4.498	1.146	1.175	1.452	2.119	2.800	1.030	1.054	1.146	1.305	1.442			
2.0	1.111	1.193	1.655	2.732	3.842	1.077	1.136	1.403	1.942	2.454	1.020	1.044	1.117	1.236	1.335			
4.0	1.009	1.162	1.640	2.510	3.313	1.000	1.109	1.360	1.727	2.025	0.986	1.030	1.094	1.156	1.194			
10.0	0.981	1.147	1.584	2.298	2.921	0.975	1.096	1.310	1.565	1.749	0.982	1.025	1.078	1.118	1.137			
50.0	0.936	1.145	1.459	1.774	1.974	0.982	1.095	1.244	1.370	1.438	1.002	1.026	1.058	1.085	1.099			
<i>a</i> -tip, Linear Loading ($n = 1.0$)																		
1.0	0.754	0.719	0.867	1.336	1.839	0.716	0.709	0.806	1.046	1.279	0.715	0.725	0.760	0.817	0.866			
2.0	0.688	0.700	0.868	1.255	1.634	0.685	0.692	0.785	0.984	1.168	0.720	0.722	0.746	0.797	0.844			
4.0	0.650	0.691	0.861	1.178	1.464	0.655	0.685	0.773	0.914	1.032	0.711	0.720	0.743	0.777	0.804			
10.0	0.636	0.685	0.839	1.099	1.323	0.645	0.680	0.755	0.858	0.938	0.709	0.718	0.738	0.765	0.786			
50.0	0.620	0.681	0.790	0.917	1.008	0.651	0.677	0.727	0.791	0.838	0.716	0.715	0.726	0.751	0.775			

Note: R is the inner radius of the cylinder

SC05 – Circumferential (thumbnail) Crack in Hollow Cylinder

The solution is based on direct tabular interpolation of the finite element results given in tables C20 and C21. The values listed are factors F_0 for tension and F_l for bending. Extrapolated values are used for cases where, as the crack grows, the a/c value may become greater than 1.0, up to 1.2. At the lower end, a/c values down to 0.1 are now allowed, the values below 0.2 representing an extrapolation of finite element results. Only tension and bending loading is possible for this case.

Reference: [C29]

Table C20: SIF Correction Factors F_0 for Internal Cracks

$a/t \rightarrow R/t$	$a/c = 0.2$				$a/c = 0.4$				$a/c = 0.6$				$a/c = 0.8$				$a/c = 1.0$								
	0	.2	.5	.8	1.0	0	.2	.5	.8	1.0	0	.2	.5	.8	1.0	0	.2	.5	.8	1.0	0	.2	.5	.8	1.0
<i>c</i> -tip, Uniform Loading																									
1.0	0.580	0.593	0.610	0.846	1.117	0.630	0.650	0.665	0.841	1.041	0.670	0.688	0.702	0.831	0.976	0.695	0.709	0.722	0.817	0.919	0.700	0.713	0.726	0.796	0.872
2.0	0.600	0.617	0.671	0.824	0.975	0.660	0.669	0.714	0.837	0.956	0.695	0.703	0.741	0.838	0.930	0.715	0.721	0.752	0.828	0.898	0.710	0.722	0.747	0.806	0.860
4.0	0.613	0.633	0.726	0.898	1.049	0.664	0.681	0.756	0.894	1.014	0.698	0.712	0.772	0.880	0.974	0.716	0.727	0.774	0.858	0.930	0.718	0.727	0.762	0.827	0.883
10.0	0.591	0.644	0.785	1.000	1.178	0.651	0.689	0.797	0.967	1.108	0.692	0.718	0.799	0.930	1.041	0.714	0.732	0.791	0.891	0.975	0.717	0.730	0.774	0.849	0.913
300.0	0.538	0.583	0.747	1.075	1.398	0.601	0.679	0.818	1.023	1.199	0.668	0.722	0.829	0.969	1.074	0.700	0.739	0.817	0.919	0.996	0.726	0.736	0.785	0.878	0.960
<i>c</i> -tip, Bending Loading																									
1.0	0.337	0.265	0.111	0.080	0.050	0.358	0.308	0.216	0.150	0.120	0.370	0.338	0.293	0.253	0.230	0.375	0.355	0.340	0.343	0.354	0.371	0.360	0.359	0.378	0.400
2.0	0.400	0.403	0.410	0.420	0.430	0.443	0.450	0.465	0.493	0.460	0.470	0.482	0.520	0.559	0.480	0.485	0.503	0.548	0.590	0.482	0.486	0.505	0.547	0.587	
4.0	0.498	0.510	0.569	0.678	0.775	0.539	0.550	0.602	0.698	0.782	0.567	0.577	0.622	0.704	0.775	0.581	0.590	0.628	0.696	0.756	0.583	0.590	0.620	0.675	0.723
10.0	0.544	0.595	0.722	0.915	1.072	0.605	0.637	0.732	0.888	1.019	0.646	0.664	0.734	0.858	0.965	0.668	0.677	0.728	0.824	0.909	0.670	0.675	0.713	0.786	0.851
300.0	0.538	0.583	0.747	1.075	1.398	0.601	0.679	0.818	1.023	1.199	0.668	0.722	0.829	0.969	1.074	0.700	0.739	0.817	0.919	0.996	0.726	0.736	0.785	0.878	0.960
<i>a</i> -tip, Uniform Loading																									
1.0	0.960	0.987	1.064	1.665	2.406	0.875	0.888	0.944	1.360	1.857	0.795	0.799	0.841	1.119	1.437	0.720	0.721	0.754	0.941	1.146	0.650	0.653	0.684	0.823	0.969
2.0	0.990	1.022	1.093	1.380	1.685	0.900	0.911	0.961	1.163	1.377	0.800	0.813	0.847	0.985	1.130	0.710	0.726	0.751	0.846	0.943	0.620	0.652	0.674	0.745	0.815
4.0	1.031	1.045	1.141	1.332	1.504	0.920	0.926	0.991	1.123	1.243	0.819	0.821	0.862	0.951	1.031	0.729	0.729	0.756	0.814	0.868	0.650	0.652	0.672	0.713	0.751
10.0	0.983	1.059	1.189	1.337	1.440	0.888	0.936	1.020	1.120	1.192	0.800	0.827	0.878	0.941	0.989	0.718	0.732	0.761	0.801	0.831	0.642	0.651	0.671	0.697	0.717
300.0	1.059	1.090	1.384	1.682	1.881	0.948	0.951	1.079	1.188	1.251	0.792	0.832	0.888	0.940	0.971	0.720	0.733	0.754	0.777	0.792	0.642	0.656	0.675	0.691	0.700
<i>a</i> -tip, Bending Loading																									
1.0	0.520	0.545	0.659	1.074	1.523	0.470	0.493	0.597	0.919	1.254	0.430	0.446	0.542	0.792	1.039	0.385	0.405	0.494	0.693	0.879	0.350	0.368	0.454	0.621	0.771
2.0	0.700	0.719	0.821	1.088	1.352	0.630	0.643	0.728	0.935	1.135	0.560	0.575	0.648	0.808	0.957	0.503	0.515	0.579	0.706	0.819	0.448	0.463	0.523	0.629	0.720
4.0	0.839	0.865	0.974	1.173	1.347	0.748	0.767	0.849	0.997	1.126	0.666	0.681	0.743	0.852	0.946	0.592	0.606	0.654	0.735	0.805	0.528	0.542	0.583	0.648	0.702
10.0	0.902	0.985	1.120	1.267	1.366	0.822	0.871	0.959	1.064	1.141	0.744	0.770	0.824	0.897	0.954	0.669	0.682	0.715	0.765	0.806	0.597	0.607	0.631	0.667	0.695
300.0	1.059	1.090	1.384	1.682	1.881	0.948	0.951	1.079	1.188	1.251	0.792	0.832	0.888	0.940	0.971	0.720	0.733	0.754	0.777	0.792	0.642	0.656	0.675	0.691	0.700

Note: R is the inner radius of the cylinder

Table C21: SIF Correction Factors F_0 for External Cracks

$a/t \rightarrow R/t$	$a/c = 0.2$					$a/c = 0.4$					$a/c = 0.6$					$a/c = 0.8$					$a/c = 1.0$					
	0	.2	.5	.8	1.0	0	.2	.5	.8	1.0	0	.2	.5	.8	1.0	0	.2	.5	.8	1.0	0	.2	.5	.8	1.0	
<i>c</i> -tip, Uniform Loading																										
1.0	0.590	0.672	0.893	1.249	1.552	0.664	0.713	0.871	1.138	1.368	0.712	0.739	0.846	1.039	1.209	0.734	0.747	0.818	0.954	1.075	0.731	0.739	0.788	0.882	0.966	
2.0	0.560	0.660	0.876	1.177	1.416	0.643	0.706	0.859	1.086	1.271	0.699	0.734	0.838	1.006	1.148	0.727	0.744	0.814	0.938	1.046	0.728	0.737	0.787	0.881	0.964	
4.0	0.540	0.653	0.873	1.162	1.383	0.630	0.701	0.858	1.081	1.257	0.691	0.731	0.839	1.006	1.145	0.722	0.742	0.815	0.940	1.046	0.725	0.735	0.786	0.880	0.962	
10.0	0.542	0.646	0.867	1.172	1.414	0.630	0.697	0.855	1.087	1.275	0.689	0.728	0.838	1.010	1.153	0.720	0.741	0.815	0.941	1.049	0.722	0.734	0.785	0.879	0.961	
300.0	0.538	0.583	0.747	1.075	1.398	0.601	0.679	0.818	1.023	1.199	0.668	0.722	0.829	0.969	1.074	0.700	0.739	0.817	0.919	0.996	0.726	0.736	0.785	0.878	0.960	
<i>c</i> -tip, Bending Loading																										
1.0	0.592	0.643	0.742	0.870	0.967	0.659	0.690	0.761	0.861	0.940	0.704	0.720	0.768	0.844	0.908	0.727	0.731	0.760	0.819	0.871	0.729	0.724	0.740	0.785	0.829	
2.0	0.552	0.645	0.798	0.972	1.092	0.632	0.691	0.801	0.939	1.040	0.687	0.720	0.795	0.902	0.987	0.716	0.731	0.780	0.863	0.932	0.720	0.724	0.757	0.820	0.876	
4.0	0.545	0.645	0.835	1.075	1.254	0.624	0.690	0.827	1.014	1.158	0.678	0.717	0.814	0.956	1.069	0.706	0.728	0.794	0.899	0.987	0.710	0.722	0.767	0.845	0.912	
10.0	0.524	0.633	0.850	1.136	1.357	0.612	0.684	0.840	1.057	1.229	0.672	0.715	0.823	0.984	1.115	0.703	0.727	0.801	0.918	1.016	0.705	0.721	0.772	0.859	0.932	
300.0	0.538	0.583	0.747	1.075	1.398	0.601	0.679	0.818	1.023	1.199	0.668	0.722	0.829	0.969	1.074	0.700	0.739	0.817	0.919	0.996	0.726	0.736	0.785	0.878	0.960	
<i>a</i> -tip, Uniform Loading																										
1.0	1.140	1.189	1.469	2.179	2.898	1.000	1.019	1.188	1.583	1.969	0.860	0.872	0.960	1.140	1.303	0.737	0.748	0.785	0.847	0.899	0.644	0.647	0.660	0.685	0.708	
2.0	1.126	1.167	1.370	1.759	2.112	0.975	1.005	1.132	1.362	1.564	0.844	0.865	0.935	1.051	1.149	0.733	0.746	0.780	0.827	0.866	0.640	0.648	0.663	0.683	0.698	
4.0	1.099	1.157	1.320	1.576	1.790	0.959	0.999	1.103	1.260	1.388	0.835	0.862	0.923	1.006	1.072	0.728	0.746	0.777	0.815	0.843	0.637	0.649	0.666	0.683	0.693	
10.0	1.079	1.146	1.284	1.470	1.615	0.945	0.993	1.083	1.198	1.284	0.827	0.859	0.914	0.977	1.020	0.724	0.745	0.776	0.806	0.825	0.636	0.650	0.668	0.684	0.693	
300.0	1.059	1.090	1.384	1.682	1.881	0.948	0.951	1.079	1.188	1.251	0.792	0.832	0.888	0.940	0.971	0.720	0.733	0.754	0.777	0.792	0.642	0.656	0.675	0.691	0.700	
<i>a</i> -tip, Bending Loading																										
1.0	1.110	1.124	1.252	1.676	2.120	0.945	0.958	1.008	1.207	1.419	0.850	0.816	0.810	0.857	0.914	0.729	0.697	0.656	0.624	0.608	0.641	0.601	0.545	0.495	0.466	
2.0	1.115	1.121	1.236	1.487	1.721	0.966	0.964	1.018	1.144	1.263	0.836	0.827	0.837	0.876	0.915	0.726	0.711	0.694	0.681	0.675	0.635	0.615	0.585	0.554	0.534	
4.0	1.097	1.124	1.242	1.429	1.586	0.949	0.969	1.035	1.138	1.223	0.822	0.834	0.863	0.905	0.937	0.716	0.720	0.725	0.728	0.730	0.630	0.625	0.619	0.605	0.593	
10.0	1.042	1.117	1.248	1.403	1.514	0.918	0.969	1.051	1.142	1.205	0.808	0.839	0.885	0.930	0.959	0.709	0.727	0.750	0.767	0.775	0.623	0.634	0.645	0.649	0.649	
300.0	1.059	1.090	1.384	1.682	1.881	0.948	0.951	1.079	1.188	1.251	0.792	0.832	0.888	0.940	0.971	0.720	0.733	0.754	0.777	0.792	0.642	0.656	0.675	0.691	0.700	

Note: R is the inner radius of the cylinder

SC06 – Circumferential Crack in Pipe – Nonlinear Stress

The valid range of geometric parameters for this case is extended to cover the full range of R_i / R_0 , the ratio of internal to external radius. In addition to the existing tension loading, the current solution is extended to nonlinear stress by using the weight function method. Tables C22 and C23 give the solution for tensile loading obtained using p-version finite element method. Ref. [C26] documents this case including estimates of errors in the weight function method. The stress intensity factor is defined as usual by

$$K_I = \sigma_0 F_o \sqrt{\pi a}$$

where σ_0 is the applied uniform tensile stress. The correction factors listed in table C22 for internal crack are defined as

$$F_{int} = F_o \sqrt{1 - a/t}$$

Table C23 lists similar results for the external crack. Here, the stress intensity correction factors are defined as

$$F_{ext} = F_o \sqrt{1 - a/t} / (1 + R_0 / R_i)$$

Reference: [C26]

Table C22: Stress Intensity Correction Factors Internal Crack, F_{int}

Crack Length a/t	Values of R_i/R_o											
	.1	.2	.3	.4	.5	.6	.7	.8	.9	.95	.99	.995
0.02	0.997	1.050	1.071	1.082	1.089	1.094	1.098	1.101	1.103	1.105	1.106	1.106
0.05	0.891	0.976	1.017	1.042	1.058	1.070	1.080	1.088	1.095	1.099	1.103	1.104
0.10	0.792	0.887	0.944	0.983	1.013	1.037	1.057	1.076	1.094	1.105	1.117	1.120
0.15	0.733	0.823	0.887	0.935	0.975	1.009	1.040	1.071	1.103	1.124	1.148	1.153
0.20	0.688	0.773	0.839	0.893	0.941	0.984	1.026	1.069	1.119	1.151	1.191	1.202
0.25	0.654	0.732	0.799	0.857	0.911	0.962	1.014	1.070	1.139	1.185	1.246	1.265
0.30	0.625	0.698	0.764	0.825	0.883	0.942	1.004	1.073	1.162	1.225	1.313	1.340
0.35	0.601	0.670	0.734	0.797	0.859	0.923	0.993	1.076	1.185	1.269	1.390	1.429
0.40	0.580	0.645	0.708	0.771	0.836	0.905	0.983	1.078	1.210	1.315	1.477	1.533
0.45	0.560	0.622	0.684	0.748	0.815	0.888	0.973	1.078	1.233	1.362	1.575	1.651
0.50	0.543	0.603	0.664	0.727	0.795	0.871	0.961	1.076	1.253	1.407	1.677	1.786
0.55	0.528	0.585	0.645	0.708	0.777	0.855	0.948	1.071	1.267	1.447	1.793	1.936
0.60	0.514	0.569	0.628	0.690	0.759	0.838	0.933	1.062	1.274	1.479	1.908	2.102
0.65	0.502	0.555	0.612	0.674	0.742	0.820	0.916	1.047	1.271	1.498	2.019	2.279
0.70	0.491	0.543	0.599	0.659	0.725	0.802	0.897	1.027	1.255	1.499	2.114	2.456
0.75	0.481	0.532	0.586	0.644	0.709	0.783	0.875	1.001	1.225	1.474	2.171	2.611
0.80	0.473	0.523	0.575	0.631	0.692	0.763	0.849	0.966	1.176	1.417	2.161	2.701
0.85	0.467	0.514	0.565	0.618	0.676	0.741	0.819	0.924	1.108	1.324	2.047	2.649
0.90	0.462	0.508	0.555	0.605	0.658	0.717	0.785	0.872	1.019	1.187	1.789	2.354
0.95	0.458	0.502	0.546	0.592	0.640	0.690	0.745	0.811	0.910	1.012	1.371	1.733
0.985	0.456	0.498	0.540	0.583	0.626	0.670	0.715	0.764	0.823	0.869	0.996	1.118

Table C23: Stress Intensity Correction Factors External Crack, F_{ext}

Crack Length a/t	Values of R_i/R_o											
	.1	.2	.3	.4	.5	.6	.7	.8	.9	.95	.99	.995
0.02	0.102	0.186	0.258	0.319	0.371	0.418	0.458	0.494	0.526	0.541	0.552	0.554
0.05	0.101	0.186	0.257	0.318	0.370	0.416	0.456	0.492	0.524	0.539	0.551	0.553
0.10	0.101	0.185	0.256	0.316	0.369	0.415	0.455	0.492	0.526	0.542	0.557	0.560
0.15	0.101	0.184	0.255	0.315	0.368	0.414	0.456	0.495	0.533	0.553	0.572	0.576
0.20	0.101	0.184	0.254	0.314	0.367	0.415	0.458	0.500	0.543	0.567	0.594	0.600
0.25	0.102	0.184	0.254	0.314	0.367	0.416	0.461	0.507	0.556	0.586	0.622	0.632
0.30	0.103	0.185	0.254	0.314	0.367	0.417	0.465	0.514	0.570	0.607	0.655	0.670
0.35	0.104	0.187	0.256	0.315	0.368	0.418	0.467	0.521	0.585	0.631	0.694	0.714
0.40	0.107	0.190	0.257	0.316	0.369	0.419	0.470	0.527	0.600	0.655	0.738	0.766
0.45	0.110	0.193	0.260	0.317	0.370	0.420	0.472	0.532	0.615	0.680	0.787	0.826
0.50	0.114	0.197	0.264	0.320	0.371	0.421	0.473	0.536	0.627	0.705	0.841	0.893
0.55	0.119	0.203	0.268	0.323	0.373	0.421	0.474	0.539	0.637	0.726	0.897	0.969
0.60	0.125	0.210	0.274	0.327	0.375	0.422	0.473	0.539	0.643	0.744	0.956	1.052
0.65	0.133	0.218	0.281	0.332	0.377	0.422	0.472	0.536	0.644	0.755	1.012	1.141
0.70	0.143	0.229	0.289	0.337	0.379	0.421	0.468	0.530	0.638	0.756	1.059	1.230
0.75	0.156	0.242	0.299	0.344	0.383	0.421	0.463	0.521	0.625	0.745	1.088	1.307
0.80	0.173	0.258	0.312	0.352	0.386	0.419	0.457	0.508	0.602	0.717	1.083	1.352
0.85	0.197	0.279	0.327	0.361	0.390	0.418	0.448	0.490	0.570	0.670	1.026	1.326
0.90	0.232	0.306	0.346	0.373	0.395	0.415	0.438	0.468	0.527	0.603	0.897	1.178
0.95	0.288	0.345	0.372	0.389	0.401	0.413	0.425	0.442	0.474	0.516	0.688	0.868
0.985	0.358	0.386	0.397	0.403	0.408	0.412	0.416	0.421	0.432	0.445	0.500	0.560

SC07 – Thumbnail Crack in Solid Cylinder

$$F_0 = G[0.752 + 1.286\beta + 0.37Y^3]$$

$$F_1 = G[0.923 + 0.199Y^4]$$

$$G = 0.92(2 / \pi) \sec \beta [(\tan \beta) / \beta]^{1/2}$$

$$Y = 1 - \sin \beta$$

$$\beta = (\pi / 2)a / D$$

Note: Crack front for this case is circular and intersects the cylinder's surface orthogonally. The crack depth a and length c are each connected to the other by the following expressions, the second being the inverse of the first and valid if $a < D/2$:

$$a = \frac{D}{2} \left(1 + \tan \left(\frac{2c}{D} \right) - \sec \left(\frac{2c}{D} \right) \right)$$

$$c = \frac{D}{2} \arctan \left(\frac{a(D-a)}{D \left(\frac{D}{2} - a \right)} \right)$$

Reference: [C15]

SC08 – Surface Crack in Bolt Thread (Thumbnail Crack)

This crack case applies to aerospace-quality fasteners and to rolled threads only. For machined threads, stress concentration must be accounted for via SIF compounding. Table C24 lists values of F_0 and F_1 . Note that only $a/c=1$ is used.

Reference: [C27]

SC09 – Circumferential Crack in Bolt Thread

$$F_0 = G_0 / k^{3/2}$$

$$G_0 = 0.5 + 0.25k + 0.1875k^2 - 0.1815k^3 + 0.3655k^4$$

$$k = 1 - 2a / D$$

$$F_1 = G_1 \sqrt{r} / r^3$$

$$G_1 = 0.375(1 + 0.5r + 0.375r^2 + 0.3125r^3 + 0.2734r^4 + 0.531r^5)$$

$$r = (D - 2a) / D$$

Reference: [C3], [C30]

SC10 – Circumferential Crack in a Threaded Pipe

This crack case uses the same basic solution as the case SC06. Tables C20 and C21 are used as reference solutions for the weight function method.

Reference: [C26]

SC11 - Surface Cracks (one or two) from Hole in a Plate

$$\begin{aligned}
 F_o &= M_o g_1 g_2 g_3 f_\phi f_w f_x f_{shah}, \quad F_3 = M_o g_1 g_{2p} g_3 f_\phi f_w f_x f_{shah} \\
 M_2 &= \frac{0.05}{0.11 + x^{3/2}} \\
 M_3 &= \frac{0.29}{0.23 + x^{3/2}} \\
 g_1 &= 1 - \frac{\nu^4 (2.6 - 2\nu)^{1/2}}{1 + 4x} \cos \phi \\
 g_2 &= \frac{1 + 0.358\lambda + 1.425\lambda^2 - 1.578\lambda^3 + 2.156\lambda^4}{1 + 0.08\lambda^2} \\
 g_{2p} &= .00982278 + 0.0502815\lambda + 1.83559\lambda^2 - 3.27483\lambda^3 + 2.49104\lambda^4 \\
 g_3 &= 1 + 0.1(1 - \cos \phi)^2 (1 - \nu)^{10} \\
 \lambda &= \frac{1}{1 + \frac{2c}{D} \cos(0.9\phi)} \\
 f_w &= \left\{ \sec \frac{\pi D}{2W} \sec \left[\frac{\pi}{2} \frac{(D + Nc)}{(W - 2c + Nc)} \sqrt{\nu} \right] \right\}^{1/2} \\
 f_{shah} &= 1 \quad \text{for } N = 2 \\
 f_{shah} &= \left[\frac{2/\pi + ac/tD}{2/\pi + 2ac/tD} \right]^{1/2} \quad \text{for } N = 1
 \end{aligned}$$

For $a/c < 1$

$$M_1 = 1$$

$$f_\phi = [x^2 \cos^2 \phi + \sin^2 \phi]^{1/4}$$

For $a/c > 1$

$$M_1 = \sqrt{c/a}$$

$$f_\phi = [x^{-2} \sin^2 \phi + \cos^2 \phi]^{1/4}$$

Reference: [C13]

SC12 - Surface Cracks (one or two) from Hole in a Lug

$$F_3 = M_o g_1 g_{2p} g_3 f_\phi f_w f_x f_{shah}$$

$$M_2 = \frac{0.05}{0.11 + x^{3/2}}$$

$$M_3 = \frac{0.29}{0.23 + x^{3/2}}$$

$$g_1 = 1 - \frac{v^4(2.6 - 2v)^{1/2}}{1 + 4x} \cos \phi$$

$$g_{2p} = 0.00982278 + 0.0502815\lambda + 1.83559\lambda^2 - 3.27483\lambda^3 + 2.49104\lambda^4$$

$$g_3 = 1 + 0.1(1 - \cos \phi)^2 (1 - v)^{10}$$

$$\lambda = \frac{1}{1 + \frac{2c}{D} \cos(.9\phi)}$$

$$f_w = \left\{ \sec\left(\frac{\pi D}{2W}\right) \sec\left[\frac{\pi}{2} \frac{(D + Nc)}{(W - 2c + Nc)} \sqrt{v} \right] \right\}^{1/2}$$

$$f_{shah} = 1 \quad \text{for } N = 2$$

$$f_{shah} = \left[\frac{2/\pi + ac/tD}{2/\pi + 2ac/tD} \right]^{1/2} \quad \text{for } N = 1$$

For a/c<1:

$$M_1 = 1$$

$$f_\phi = [x^2 \cos^2 \phi + \sin^2 \phi]^{1/4}$$

For a/c>1:

$$M_1 = \sqrt{c/a}$$

$$f_\phi = [x^{-2} \sin^2 \phi + \cos^2 \phi]^{1/4}$$

Reference: [C13]

SC13 - Surface crack from cut fillet under a shear bolt head

This crack case applies to a cut (machined) fillet under a shear bolt head. Table C24 lists values of F_0 and F_1 . Only the values for a/c=0.645 are used.

The stress concentration factor for a given fillet radius ratio, r/D is obtained from table C25 which is based on finite element analysis.

Reference: [C27]

Table C24: Stress Intensity Factors for a bolt in tension and bending

a/D	F_0		F_1	
	a/c = 0.645	a/c = 1.0	a/c = 0.645	a/c = 1.0
0.0	$K_t f_x$	1.00	$K_t f_x$	0.60
0.05	-	0.84	-	0.54
0.1	0.95	0.76	0.61	0.48
0.2	0.90	0.65	0.54	0.37
0.3	0.98	0.59	0.55	0.31
0.4	1.29	0.62	0.64	0.30
0.5	2.05	1.0	0.84	0.50

Table C25: Stress Concentration Factors for a bolt in tension and bending

r/D	.005	.01	.015	.02	.025	.03	.035	.04	.045	.05.
K_t	10.8	7.89	6.55	5.73	5.17	4.77	4.48	4.19	3.97	3.79
r/D	.055	.06	.065	.07	.075	.08	.085	.09	.095	.10
K_t	3.63	3.49	3.37	3.26	3.16	3.07	2.97	2.91	2.84	2.78

SC14 - Surface crack from rolled fillet under a tension bolt head

This crack case applies to a rolled fillet under a tension bolt head. Table C24 lists values of F_0 and F_1 . Only the values for a/c=1 are used.

Since r/D is set to 0.1, the stress concentration factor 2.78 is used for a/d =0 and then smooth interpolation is done to determine the values of F_0 and F_1 for a/D =0.05.

Reference: [C27]

SC15 – Surface Crack in a Plate – 2D Nonlinear Stress

The geometry is similar to SC01 but loading can be bi-variant as in the case of CC05, i.e., stress variation in both the width(x-axis) and thickness(y-axis) directions is allowed. The stresses are to be input via a file containing the coordinates and stress values. A sample file has been shown for case CC05. The distribution is assumed to be symmetric about the center line of the plate, so that both the surface crack tips grow at the same pace. The stress intensity correction factors for this case are also computed using the 3D weight function method developed by Fujimoto [C34.]. The method requires a reference solution for the geometry under consideration. The current NASGRO solution, for a surface crack in a plate subjected to uniform tension is used as the reference solution.

References: [C36] and [C37]

SC17 – Off-Center Surface Crack in a Finite Width Plate – Nonlinear Stress

Crack case SC17 is a new weight function solution for the surface crack in a finite width plate with a general nonlinear stress distribution. It is nominally the same crack case as SC02. The SC17 solution is based on a completely new set of reference solutions obtained using the boundary element computer program FADD-3D [C39, C40]. The new solution provides a wider validity range for a/c (up to 4.0), some improvements in solution accuracy, and also permits cracks that are off-center in the plate (but does not require the crack to be off-center in the plate). The new SC17 solution does not yet perform automatic transitioning to corner or through cracks. The previous SC02 solution has been left unchanged for legacy purposes.

Crack case SC17 currently permits direct input of the principal normal stresses on the crack plane as pairs of $[(x/t)_i, S_i]$, where the x -axis originates from the plate surface and crosses the thickness of the plate. Note that these input stresses are the stresses on the crack plane in the corresponding uncracked body.

The geometry validity range for all SC17 solutions is as follows:

$$\begin{aligned} 0 &\leq a/c \leq 8.0 \\ 0 &\leq a/t \leq 0.9 \\ 0 &\leq c/B \leq 0.9 \\ 0 &\leq 1-(2B/W) \leq 0.8 \end{aligned}$$

The reference solutions along the crack perimeter near the plate surface generally exhibited increasing values approaching the surface and then decreased sharply immediately at the surface. The reference solutions assigned to the surface value (the c-tip) were selected at the maximum value of K near the surface, which typically occurred about three degrees inside the surface. Fatigue crack growth calculations in NASGRO multiply this near-surface ΔK value by the crack closure factor, β_R .

The SC17 solution uses the approximate weight function proposed by Glinka [C41, C43]. The weight function at the a -tip (the maximum depth position for the surface crack) is

$$W_a = \frac{2}{\sqrt{2\pi(a-x)}} \left[1 + M_{1a} \sqrt{\frac{a-x}{a}} + M_{2a} \frac{a-x}{a} + M_{3a} \left(\frac{a-x}{a} \right)^{\frac{3}{2}} \right] \quad (1)$$

The weight function at the c -tip (the crack tip at the specimen surface) is

$$W_c = \frac{2}{\sqrt{\pi x}} \left[1 + M_{1c} \sqrt{\frac{x}{a}} + M_{2c} \cdot \frac{x}{a} + M_{3c} \left(\frac{x}{a} \right)^{\frac{3}{2}} \right] \quad (2)$$

When the surface crack is off-center in the plate, then independent solutions are derived for the two different c -tips. For simplicity, the descriptions given here correspond to a symmetric solution with the crack in the center of the plate width.

The variable x is the distance normal to the plate surface measured from the location where the crack emanates. The parameters M_{1c} , M_{2c} , ..., etc. depend on the geometrical parameters and are defined by reference solutions.

At the a -tip, M_{1a} , M_{2a} , and M_{3a} are defined by [4]

$$\begin{aligned} M_{1a} &= \frac{\pi}{\sqrt{2Q}} (4Y_0 - 6Y_1) - \frac{24}{5} \\ M_{2a} &= 3 \\ M_{3a} &= 2 \left(\frac{\pi}{\sqrt{2Q}} Y_0 - M_{1a} - 4 \right) \end{aligned} \quad (3)$$

and at the c -tip, M_{1c} , M_{2c} , and M_{3c} are given by

$$\begin{aligned} M_{1c} &= \frac{\pi}{\sqrt{4Q}} (30F_1 - 18F_0) - 8 \\ M_{2c} &= \frac{\pi}{\sqrt{4Q}} (60F_0 - 90F_1) + 15 \\ M_{3c} &= -(1 + M_{1c} + M_{2c}) \end{aligned} \quad (4)$$

Q is the shape factor for an elliptical crack approximated by

$$Q = \begin{cases} 1 + 1.464(a/c)^{1.65}, & a/c \leq 1 \\ 1 + 1.464(a/c)^{-1.65}, & a/c > 1 \end{cases} \quad (5)$$

and F_0 , F_1 , Y_0 and Y_1 are normalized SIFs or the reference solutions. F_0 , F_1 are obtained at the c -tip, and Y_0 and Y_1 are at the a -tip. The subscripts identify the two associated reference stress variations applied on the crack surfaces: 0 denotes uniform tension $\sigma_{ref}(x)=1$, and 1 denotes a linearly increasing bending stress $\sigma_{ref}(x)=x/a$.

The stress intensity factors at the a - and c -tips, $K_{a,c}$, can thus be determined by direct integration as

$$K_{a,c} = \int_0^c W_{a,c} \sigma(x) dx \quad (6)$$

where $\sigma(x)$ is the univariant stress applied on the crack surface, and the integration is carried out from $x=0$ to $x=a$.

However, with the introduction of SC30, it should be noted that it is a newer crack case than SC17. Both are based on the same univariant weight function formation and provide the same analysis options. However, SC30 has improved accuracy for small crack aspect ratio $a/c < 1$ with this crack geometry and bivariant stress gradient type. The solutions of SC17 and SC30 are identical for $a/c \geq 1$. The use of SC30 is preferred over SC17 except when there is a need to perform a direct comparison with a legacy analysis using SC17.

References: [C39], [C40], [C41], [C43]

SC18 – Surface Crack (or Twin Cracks) at a Hole in a Plate – Nonlinear Stress

Crack case SC18 is a weight function solution for an offset surface crack at an off-center hole in a finite width plate with a general univariant stress distribution. SC18 [from NASGRO 6.0 onwards] includes a symmetric geometry (with twin cracks) loaded symmetrically. The derivation of the weight function methodology used for this crack case is outlined in the discussion of CC08. The stress input format for SC18 is consistent with other univariant weight function crack cases and is detailed in discussion of CC08.

The current geometry validity range for SC18 is as follows:

$$0 \leq \text{Max}\left(\frac{a_1}{T}, \frac{a}{t-T}\right) \leq 0.8$$

$$0 \leq \frac{c}{B - \frac{D}{2}} \leq 0.8$$

$$0.5 \leq \frac{a}{c} \leq 10$$

$$0.25 \leq \frac{D}{t} \leq 2$$

$$0.1 \leq \frac{B}{W} \leq 0.5$$

$$0.1 \leq \frac{T}{t} \leq 0.9$$

SC19 – Surface crack in a plate, bivariant weight function solution

Highlights:

- Bivariant stress gradient, three input methods:
 - Remote tension, in-plane bending, and out-of-plane bending
 - Polynomial
 - User-specified stress gradient entry (from file)
- Crack can be offset from plane center

SC19 is a second-generation weight function solution for a surface crack in a plate subjected to a bivariant stress field. The improved formulation used in SC19 is recommended over the first-generation solution (SC15). The benefits of the improved formulation for SC19 are improved accuracy and speed, as well as the ability to input a non-symmetric bivariant stress field (not available for SC15). Three input methods are available for entering a bivariant stress field: remote tension/bends, polynomial, or user-specified. If remote tension/bends are selected, the first three stress distributions are populated with unit tension (S_0), unit in-plane bending (S_1), and unit out-of-plane bending (S_2). In equation form the remote distributions are defined as

$$\begin{aligned} S_0(X,Y) &= 1 \\ S_1(X,Y) &= 1 - 2Y/t \\ S_2(X,Y) &= -2X/W \end{aligned}$$

If polynomial is selected, the constants for a 2D polynomial function are required to be entered by the user on the GUI screen. The 2D polynomial function is referenced to the global coordinate system (see Figure in the GUI). The polynomial may be specified as symmetric (about the x-axis) or non-symmetric. The mathematical form for the symmetric case is given as

$$\begin{aligned}
{}^{SYM}S_i^{POLY} &= \sum d_i^{m,n} \left(\frac{2|X|}{W} \right)^m \left(\frac{Y}{t} \right)^n \\
&= d_i^{0,0} + d_i^{1,0} \frac{2|X|}{W} + d_i^{0,1} \frac{Y}{t} + d_i^{2,0} \left(\frac{2|X|}{W} \right)^2 + d_i^{1,1} \frac{2|X|}{W} \frac{Y}{t} + d_i^{0,2} \left(\frac{Y}{t} \right)^2 + \\
&\quad d_i^{3,0} \left(\frac{2|X|}{W} \right)^3 + d_i^{2,1} \left(\frac{2|X|}{W} \right)^2 \frac{Y}{t} + d_i^{1,2} \frac{2|X|}{W} \left(\frac{Y}{t} \right)^2 + d_i^{0,3} \left(\frac{Y}{t} \right)^3 + \\
&\quad d_i^{3,1} \left(\frac{2|X|}{W} \right)^3 \frac{Y}{t} + d_i^{2,2} \left(\frac{2|X|}{W} \right)^2 \left(\frac{Y}{t} \right)^2 + d_i^{1,3} \frac{2|X|}{W} \left(\frac{Y}{t} \right)^3 + \\
&\quad d_i^{3,2} \left(\frac{2|X|}{W} \right)^3 \left(\frac{Y}{t} \right)^2 + d_i^{2,3} \left(\frac{2|X|}{W} \right)^2 \left(\frac{Y}{t} \right)^3 + d_i^{3,3} \left(\frac{2|X|}{W} \right)^3 \left(\frac{Y}{t} \right)^3
\end{aligned}$$

The mathematical form for the non-symmetric case is given as

$$\begin{aligned}
{}^{NONSYM}S_i^{POLY} &= \sum c_i^{m,n} \left(\frac{2X}{W} \right)^m \left(\frac{Y}{t} \right)^n \\
&= c_i^{0,0} + c_i^{1,0} \frac{2X}{W} + c_i^{0,1} \frac{Y}{t} + c_i^{2,0} \left(\frac{2X}{W} \right)^2 + c_i^{1,1} \frac{2X}{W} \frac{Y}{t} + c_i^{0,2} \left(\frac{Y}{t} \right)^2 + \\
&\quad c_i^{3,0} \left(\frac{2X}{W} \right)^3 + c_i^{2,1} \left(\frac{2X}{W} \right)^2 \frac{Y}{t} + c_i^{1,2} \frac{2X}{W} \left(\frac{Y}{t} \right)^2 + c_i^{0,3} \left(\frac{Y}{t} \right)^3 + \\
&\quad c_i^{3,1} \left(\frac{2X}{W} \right)^3 \frac{Y}{t} + c_i^{2,2} \left(\frac{2X}{W} \right)^2 \left(\frac{Y}{t} \right)^2 + c_i^{1,3} \frac{2X}{W} \left(\frac{Y}{t} \right)^3 + \\
&\quad c_i^{3,2} \left(\frac{2X}{W} \right)^3 \left(\frac{Y}{t} \right)^2 + c_i^{2,3} \left(\frac{2X}{W} \right)^2 \left(\frac{Y}{t} \right)^3 + c_i^{3,3} \left(\frac{2X}{W} \right)^3 \left(\frac{Y}{t} \right)^3
\end{aligned}$$

For both the symmetric and non-symmetric case, 16 polynomial coefficients are required for each stress distribution, up to 4 total stress distributions. It is important to note, the option for symmetric stress input is only available when the surface crack is located at the center of the plate width and remains at the plate center during crack propagation.

If user-specified is selected, the bivariant stress distribution is read from a text file, tabular entry is not available. The stress distribution file uses the same format as described for CC05. For completeness, the file format is given in Table SC19-1.

Table 1. Data format for specifying two-dimensional stress distribution used for SC19 bivariant WF solutions

Data	Data type	Description
nx, ny	Integer	nx: number of data points along the X-axis ny: number of data points along the Y-axis
X(1)	Real	Normalized X-Coordinate of the 1 st data point along the X-axis.
...	Real	[Repeat the input for nx times]
X(nx)	Real	Normalized X-coordinate of the nx-th data point along the X-axis
Y(1), S(1,1)	Real	Normalized Y-coordinate of the 1 st data point along the Y-axis and the stress at (X(1), Y(1))
...		[Repeat the input for ny times]
Y(ny), S(1,ny)	Real	Normalized Y-coordinate of the ny-th data point along the Y-axis and the stress at (X(1), Y(ny))
Y(1), S(2,1)	Real	Normalized Y-coordinate of the 1 st data point along the Y-axis and the stress at (X(2), Y(1))
...		[Repeat the input for ny times]
Y(ny), S(2,ny)	Real	Normalized Y-coordinate of the ny-th data point along the Y-axis and the stress at (X(2), Y(ny))
...		
Y(1), S(nx,1)	Real	Normalized Y-coordinate of the 1 st data point along the Y-axis and the stress at (X(nx), Y(1))
...		[Repeat the input for ny times]
Y(ny), S(nx,ny)	Real	Normalized Y-coordinate of the ny-th data point along the Y-axis and the stress at (X(nx), Y(ny))

However, with the introduction of SC31, it should be noted that it is a newer crack case than SC19. Both are based on the same bivariant weight function formation and provide the same analysis options. However, SC31 has improved accuracy for small crack aspect ratio $a/c < 1$ with this crack geometry and bivariant stress gradient type. The solutions of SC19 and SC31 are identical for $a/c \geq 1$. The use of SC31 is preferred over SC19 except when there is a need to perform a direct comparison with a legacy analysis using SC19.

SC26 – Surface Crack at Edge Notch in a Plate

The SIF solution of this crack model is based on the same weight function formulation for univariant stresses as that used by SC17 (in v7.0f) and SC30 (in v7.1a). The univariant distribution of crack opening stress along the crack growth direction is required along with the weight functions to determine the stress intensity factors at three tips: two at surface along the notch root and one at the deepest of the crack front.

There are three options to specify stress definition. The simplest one is applying tension and bending stresses remotely. For this stress definition, the SC26 fracture

mechanics module internally computes the crack opening stress variation resulting from remote stressing. The interpolation scheme for net sectional stress variations is identical to the one used by CC13 and based on an array of net section stress variations extracted from finite element results at discrete geometric aspect ratios.

The other two stress definitions require users to specify the crack opening stress variations along the crack growth plane. Respectively, they can be defined by polynomial functions or by stress pairs (see the similar stress definition description for CC13). The width of the “effective” net section in reference is W_{net} and is given by $W - (d + r)$ for angular notch or $W - (e_1 - B)$ for elliptical notch.

Similar to the notch definition for CC13 crack model, there are two notch types with this crack model; one is of angular notch type and the other of elliptical notch type. The angular notch is characterized by two straight edges and an enclosed angle θ resulting in a nominal notch depth d and a local root radius r at the notch tip. In contrast, the elliptical notch is fully described by an ellipse of e_1 as the long axis and e_2 as the short axis with an additional offset B . The validity limits of the SIF solutions thus depends on the user-selected notch shape and are listed as follows. Note the crack is described by the semi-elliptical crack front of full surface length $2a$ along the root of the notch and depth c along the plate width direction that corresponds to the deepest point of the semi-elliptical crack front. The offset of the crack center along the thickness is denoted by T .

- Angular notch:

$$\begin{aligned} 0^\circ &\leq \theta \leq 75^\circ \\ 0 < \frac{d+r}{W} &\leq 0.75 \\ 0 \leq \frac{d}{r} &\leq 24 \\ \frac{c}{W-d-r} &\leq 0.95 \\ 0.1 \leq \frac{T}{t} &\leq 0.9 \\ \text{Max} \left(\frac{a}{T}, \frac{a}{t-T} \right) &\leq 0.95 \\ 0 < \frac{c}{a} &\leq 8 \end{aligned}$$

The normalized coordinate is defined by $x/(W - d - r)$. The coordinate x is measured from the notch tip along the crack growth path.

- Elliptical notch:

$$\begin{aligned} 0.2 \leq \frac{e_1}{e_2} &\leq 5 \\ 0 < \frac{e_1 - B}{W} &\leq 0.75 \\ \frac{c}{W + B - e_1} &\leq 0.95 \end{aligned}$$

$$\begin{aligned}
0 &\leq B < e_1 \\
0.1 &\leq \frac{T}{t} \leq 0.9 \\
\text{Max} \left(\frac{a}{T}, \frac{a}{t - T} \right) &\leq 0.95 \\
0 &< \frac{c}{a} \leq 8
\end{aligned}$$

The normalized coordinate is defined by $x/(W + B - e_1)$. The coordinate x is measured from the notch tip along the crack growth path.

SC27 – Surface Crack at Offset Embedded Slot or Elliptical Hole in a Plate

The SIF solution of this crack model is mostly based on the same weight function formulation as that for surface cracks at a hole subjected to univariant stressing; i.e., the one used by SC18. The only exception is for elliptical holes with $e_2/e_1 > 1$ where additional adjustments through interpolation are needed. The weight function formulation is in terms of the univariant distribution of crack opening stress along the crack growth direction to determine the stress intensity factors at three tips; two surface tips and one deepest tip along the semi-elliptical crack front.

Similar to CC14, two types of stress definition are provided. The simplest one is to apply tension and bending stresses at remote ends. Subjected to this stressing, the crack opening stress variation is determined internally by the SC27 fracture mechanics module through interpolation among an array of net section stress variations extracted from finite element results.

The second type of stress definition describes the stress variation in terms of stress pairs (see the similar stress definition description for CC14). One normalized coordinate and one stress value form a stress pair. The normalized coordinate is with respect to the smaller net section identifiable by the offset of the slot B . The coordinate x is measured from the notch tip across the net section along which the crack growth path is assumed. By this definition, the variation of normalized coordinate is from 0 to 1.

Most of the SC27 SIF solutions are based on the same weight function approach as for SC18 where the radius of the hole characterizing SC18 crack model is replaced by the “effective” notch depth in SC27 crack model. The definition of this “effective” notch depth depends of the type of the slot. For elliptical holes, it is the long axis e_1 while for straight-edge slots, it is the straight edge plus the root radius, $d + r$. For elliptical holes with $e_2/e_1 > 1$, the following interpolation between the SIF results computed from SC18 and SC17 (in v7.0f)/SC30 (in v7.1a) weight function solutions is used.

$$K^{SC27} = (K^{SC18} - K^{SC17/SC30}) \left(\frac{e_1^2}{e_2^2} \right)^{0.2} + K^{SC17/SC30}$$

The interpolative relationship is empirically determined based on finite element results and is used to ensure that when the ratio of short axis to long axis e_2/e_1 equals to 1.0, the SIF solution for SC27 crack model is solely based on the weight function approach for SC18 crack model; *i.e.*, $K^{SC27} = K^{SC18}$, while when $e_2/e_1 \rightarrow \infty$ or $e_1/e_2 \rightarrow 0$, the SIF solution retreats to the one for SC17 (in v7.0f)/SC30 (in v7.1a) crack model.

There are two types of slot with this crack model; one is straight-edge slots and the other elliptical holes. The straight-edge slot is characterized two parallel straight edges and two semi-circular notch ends. The straight edge defines the nominal notch depth d and the semi-circular notch tip defines the local root radius r with the notch tip. In contrast, the elliptical hole is described by an ellipse of e_1 as the long axis and e_2 as the short axis. The offset of the slot or hole from the right side of the plate defines the offset B . the crack is described by the semi-elliptical crack front of full surface length $2a$ along the bore and depth c along the plate width direction. The offset of the crack center along the thickness is denoted by T . The validity limits of the SIF solutions depend on the user-selected notch shape and are listed as follows.

- Straight-edge slot:

$$0 \leq \frac{d+r}{B} \leq 0.75$$

$$0.25 \leq \frac{d+r}{t} \leq 2$$

$$0 \leq \frac{d}{r} \leq 24$$

$$0.2 \leq \frac{2B}{W} \leq 1$$

$$0 \leq \frac{c}{B-d-r} \leq 0.8$$

$$0.5 \leq \frac{a}{c} \leq 10$$

$$0.1 \leq \frac{T}{t} \leq 0.9$$

$$\text{Max} \left(\frac{a}{T}, \frac{a}{t-T} \right) \leq 0.9$$

The normalized coordinate is defined by $x/(B - d - r)$. The coordinate x is measured from the notch tip along the smaller net section.

- Elliptical notch:

$$0 \leq \frac{e_1}{B} \leq 0.75$$

$$0.25 \leq \frac{e_1}{t} \leq 2$$

$$0.2 \leq \frac{e_1}{e_2} \leq 5$$

$$0.2 \leq \frac{2B}{W} \leq 1$$

$$0 \leq \frac{c}{B - e_1} \leq 0.8$$

$$0.5 \leq \frac{a}{c} \leq 10$$

$$0.1 \leq \frac{T}{t} \leq 0.9$$

$$\text{Max} \left(\frac{a}{T}, \frac{a}{t-T} \right) \leq 0.9$$

The normalized coordinate is defined by $x/(B - e_1)$. The coordinate x is measured from the tip of the elliptical notch along the smaller net section.

SC28 – Surface crack at Offset Hole in a Plate with Broken Ligament

The weight function approach for SC28 crack model is identical to the one used by SC17 (in v7.0f) or SC30 (in v7.1a). It is based on the univariant distribution of crack opening stress along the net section. The fracture mechanics module provides the stress intensity factors at three crack tips: two surface tips along the bore and one deepest tip along the semi-elliptical crack tip perimeter.

Three options for defining stress definition similar to those for CC15 are provided. Respectively, they are (1) remote tension/bend, (2) polynomial stressing, and (3) tabulated stress variations. The first stress definition option, which is in terms of remote tension and bend, implicitly invokes stress interpolation to determine the crack opening stresses defined along the net section, following an identical procedure as described above for CC15. The interpolation is among an array of net sections stress variations from finite element results at discrete geometric aspect ratios.

The last two options are for describing the crack opening stress distributions along the crack growth surface that can be described by either (1) polynomial functions or (2) arrays of stress pairs. To specify in terms of polynomial functions, the user only needs to provide the coefficients a_i 's as defined in the following polynomial stress functions.

$$\sigma(x) = \sum_{i=0}^6 a_i \left(\frac{x}{W_{net}} \right)^i$$

where the “effective” sectional width W_{net} is given by $W - (B + D/2)$. The length parameters: W , D , and B , are the width of the plate, the diameter of the hole, and the offset of the hole. The coordinate x is measured from the root of the hole and along the crack growth plane or the net section.

To specify the crack opening stress distributions in terms of stress pairs, the NASGRO convention for stress definition is used. Stress pairs consist of one

normalized coordinate and one stress value and the arrays of these pairs are arranged according to ascending normalized coordinates. The fracture mechanics module will interpolate the intermediate stress value when evaluating the integration for weight function solutions.

To make use of the weight function formulation for SC17 (in v7.0f) or SC30 (in v7.1a) crack model, the following transformations are used:

- a. The “effective” sectional width W_{net} of this crack model replaces the “thickness” used by SC17/SC30
- b. The surface crack length c along the plate width direction of this crack model replaces the “crack depth” a used by SC17/SC30.
- c. The surface crack length a along the bore of this crack model replaces the “surface crack length” c used by SC17/SC30.
- d. The offset T along the bore of this crack replaces the “offset” of the surface crack center B used by SC17/SC30.

The validity limits are listed as follows:

$$\begin{aligned} 0 &\leq \frac{2B}{D} \leq 24 \\ 0 &\leq \frac{B + \frac{D}{2}}{W} \leq 0.75 \\ \frac{\frac{B}{c}}{W - B - \frac{D}{2}} &\leq 0.9 \\ 0.1 &\leq \frac{T}{t} \leq 0.9 \\ \frac{a}{t} &\leq 0.95 \\ \frac{c}{a} &\leq 8 \end{aligned}$$

The normalized coordinate is defined by $x/[W - (B + D/2)]$. The coordinate x is measured from the root of the hole along the crack growth path.

SC30 – Off-Center Surface Crack in a Finite Width Plate – Nonlinear Stress

Crack case SC30 is a new weight function solution for the surface crack in a finite width plate with a general nonlinear stress distribution. It is nominally the same crack case as SC02 and SC17. Compared to SC02, both SC30 and SC17 solutions are based on a completely different set of reference solutions with much higher resolutions. As a result, the new solution provides a wider validity range for a/c (up to 8.0), some improvements in solution accuracy, and also permits cracks that are off-center in the plate (but does not require the crack to be off-center in the plate). Compared to SC17 whose reference solutions were determined using the boundary element computer program FADD-3D [C39, C40], the SC30 employs updated FEA-based reference solutions for small crack aspect ratio $a/c < 1$. Its FEA mesh was generated using FEACrack, and the reference solutions were extracted from the contour integrals

computed by Abaqus. The previous SC02 and SC17 solutions have been left unchanged for legacy purposes.

Crack case SC30 currently permits direct input of the principal normal stresses on the crack plane as pairs of $[(x/t)_i, S_i]$, where the x -axis originates from the plate surface and crosses the thickness of the plate. Note that these input stresses are the stresses on the crack plane in the corresponding uncracked body.

The geometry validity range for all SC30 solutions is as follows:

$$\begin{aligned} 0.1 &\leq a/c \leq 8.0 \\ 0 &\leq a/t \leq 0.95 \\ 0 &\leq c/\min(B, W - B) \leq 1 \\ |W - 2B|/W &\leq 0.9 \end{aligned}$$

The reference solutions along the crack perimeter near the plate surface generally exhibited increasing values approaching the surface and then decreased sharply immediately at the surface. The reference solutions assigned to the surface value (the c -tip) were selected at the maximum value of K near the surface, which typically occurred about three degrees inside the surface. Fatigue crack growth calculations in NASGRO multiply this near-surface ΔK value by the crack closure factor, β_R .

The SC30 solution uses the approximate weight function proposed by Glinka [C41, C43]. The weight function at the a -tip (the maximum depth position for the surface crack) is

$$W_a = \frac{2}{\sqrt{2\pi(a-x)}} \left[1 + M_{1a} \sqrt{\frac{a-x}{a}} + M_{2a} \frac{a-x}{a} + M_{3a} \left(\frac{a-x}{a} \right)^{\frac{3}{2}} \right] \quad (1)$$

The weight function at the c -tip (the crack tip at the specimen surface) is

$$W_c = \frac{2}{\sqrt{\pi x}} \left[1 + M_{1c} \sqrt{\frac{x}{a}} + M_{2c} \cdot \frac{x}{a} + M_{3c} \left(\frac{x}{a} \right)^{\frac{3}{2}} \right] \quad (2)$$

When the surface crack is off-center in the plate, then independent solutions are derived for the two different c -tips. For simplicity, the descriptions given here correspond to a symmetric solution with the crack in the center of the plate width.

The variable x is the distance normal to the plate surface measured from the location where the crack emanates. The parameters M_{1c}, M_{2c}, \dots , etc. depend on the geometrical parameters and are defined by reference solutions.

At the a -tip, M_{1a} , M_{2a} , and M_{3a} are defined by [4]

$$\begin{aligned} M_{1a} &= \frac{\pi}{\sqrt{2Q}} (4Y_0 - 6Y_1) - \frac{24}{5} \\ M_{2a} &= 3 \\ M_{3a} &= 2 \left(\frac{\pi}{\sqrt{2Q}} Y_0 - M_{1a} - 4 \right) \end{aligned} \quad (3)$$

and at the c -tip, M_{1c} , M_{2c} , and M_{3c} are given by

$$\begin{aligned} M_{1c} &= \frac{\pi}{\sqrt{4Q}} (30F_1 - 18F_0) - 8 \\ M_{2c} &= \frac{\pi}{\sqrt{4Q}} (60F_0 - 90F_1) + 15 \\ M_{3c} &= -(1 + M_{1c} + M_{2c}) \end{aligned} \quad (4)$$

Q is the shape factor for an elliptical crack approximated by

$$Q = \begin{cases} 1 + 1.464(a/c)^{1.65}, & a/c \leq 1 \\ 1 + 1.464(a/c)^{-1.65}, & a/c > 1 \end{cases} \quad (5)$$

and F_0 , F_1 , Y_0 and Y_1 are normalized SIFs or the reference solutions. F_0 , F_1 are obtained at the c -tip, and Y_0 and Y_1 are at the a -tip. The subscripts identify the two associated reference stress variations applied on the crack surfaces: 0 denotes uniform tension $\sigma_{ref}(x)=1$, and 1 denotes a linearly increasing bending stress $\sigma_{ref}(x)=x/a$.

The stress intensity factors at the a - and c -tips, $K_{a,c}$, can thus be determined by direct integration as

$$K_{a,c} = \int_0^c W_{a,c} \sigma(x) dx \quad (6)$$

where $\sigma(x)$ is the univariant stress applied on the crack surface, and the integration is carried out from $x=0$ to $x=a$.

References: [C39], [C40], [C41], [C43]

SC31 – Surface crack in a plate, bivariant weight function solution

Highlights:

- Bivariant stress gradient, three input methods:
 - Remote tension, out-of-plane bending, and in-plane bending
 - Polynomial
 - User-specified stress gradient entry (from file)
- Crack can be offset from plane center

Similar to the legacy SC19 solution, SC31 [C68] is a second-generation weight function solution for a surface crack in a plate subjected to a bivariant stress field. The improved formation used by both SC19 and SC31 is recommended over the first-generation solution SC15. Compared to SC19 whose reference solutions were derived from BEM using FADD-3D [C39, C40], the SC31 solution makes use of updated FEA-based reference solutions for small crack aspect ratio $a/c < 1$. The similar FEA computation procedure to the one for SC30 was deployed. However, as a result of extra reference stress, the new FEA mesh set is slightly larger than the one used by SC30. Both SC15 and SC19 solutions have remained unchanged for legacy purpose.

The geometry validity range for all SC31 solutions is as follows:

$$\begin{aligned}0.1 \leq a/c \leq 8.0 \\ 0 \leq a/t \leq 0.95 \\ 0 \leq c/\min(B, W - B) \leq 0.9 \\ |W - 2B|/W \leq 0.9\end{aligned}$$

The SIF solution makes use of a point weight function (PWF) to describe the effect of the point load applied at Q to the crack tip location at Q' . In reference to Figure 1 below, the point weight function is given by

$$W_{QQ'} = \frac{\sqrt{\ell_{QQ^*}^2 - \ell_{Q'Q^*}^2}}{\pi \ell_{QQ'}^2 \sqrt{\pi \ell_{QQ^*}}} \left(1 + \frac{\ell_{QQ'}^2}{\ell_{Q'Q^*}^2} \right) \left\{ 1 + \Pi_1 \sqrt{1 - \left(\frac{\ell_{QQ^*}}{\ell_{Q'Q^*}} \right)^2} + \Pi_2 \left(1 - \frac{y'}{y} \right)^2 \right. \\ \left. + \Pi_3 \left[1 - \frac{x}{\text{sign}(Q')x'} \right]^{1.5} \sqrt{1 - \frac{y}{a}} \right\}$$

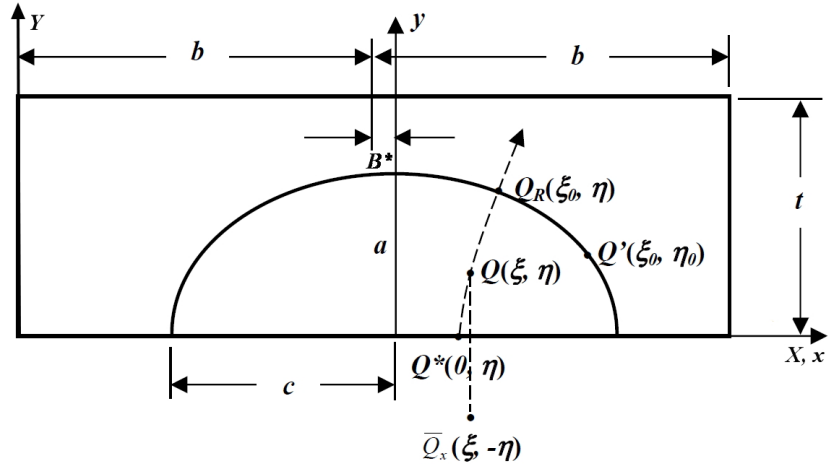


Figure 1. Geometry configuration and nomenclature for SC31: point locations, crack length designation and coordinate system referenced in PWF

The definition of the point locations referred in the above equation can be found in Table 1 below. The coordinates are in elliptical coordinate system: *i.e.*, represented by elliptical radius ξ and angle η , for conciseness. The elliptical radius corresponding to the crack tip perimeter is denoted by ξ_0 . The script ℓ denotes the distance between the two points indicated in its subscript; for example, $\ell_{QQ'}$ is the distance between two points Q and Q' . The interceptions of the axes of the local xy -coordinate system with the crack tip perimeter defines two crack lengths a and c . The chord lengths x' and y' are derived by fixing y and x values with any interior point Q . The remaining unknowns in the above PWF: Π_1 , Π_2 , and Π_3 , will be determined by the reference solutions.

Table 1. Definition of point locations indicated in PWF

Point designation	Location coordinate in elliptical system
Q	(ξ, η)
Q_R	(ξ_0, η)
Q'	(ξ_0, η_0)
Q^*	$(0, \eta)$
Q_x	$(\xi, -\eta)$

The SIF solutions are determined by evaluating the following surface integration across the semi-elliptical crack area. For a given stress variation $\sigma(x, y)$ applied on the crack plane obtained from an un-cracked body the stress intensity factor is given by

$$K = \int_0^a \int_{-\sqrt{1-(\frac{y}{a})^2}}^{\sqrt{1-(\frac{y}{a})^2}} W_{QQ'} \cdot \sigma(x, y) dx dy$$

For SC31, the SIFs with three crack tips of concern are computed. Respectively, they are corresponding to two surface tips: the c- and c1-tips, and one deepest tip or the a-tip. For the crack tip designation, please refer to the SC31 GUI bitmap.

Note the local coordinate in *xy*-coordinate system in Figure 1 above is in reference to the center of the surface crack, which is different from the one shown in GUI bitmap. The global normalized XY-coordinate system in Figure 1 is consistent with the designation depicted in the SC31 GUI bitmap, where the bottom left corner of the rectangular section is always the origin.

Three input methods are available for users to specify bivariant stress fields. Respectively, the stress fields can be represented by (1) remote tension/bends, (2) bivariant polynomial functions, or (3) user-specified gradients in tabular format. In all cases, the normalized coordinates X and Y are used and the crack definition is If the simple load type in terms of remote tension and bends is selected, the first three stress quantities are internally generated assuming the stress variations are in terms of unit tension (S_0), unit out-of-plane bending (S_1), and unit in-plane bending (S_2). In equation form, their variations are given by

- Unit tension: $S_0(X, Y) = 1$
- Unit out-of-plane bending: $S_1(X, Y) = 1 - 2Y$
- Unit in-plane bending: $S_2(X, Y) = 1 - 2X$

The normalized coordinates (X, Y) are in reference to the thickness t and the width $W=2b$ of the plate and defined by $X=x/W$ and $Y=y/t$ where the *xy*-coordinate system is the same as the one described in the GUI bitmap (not the one shown in Figure 1 above).

If to use bivariant polynomial functions is selected, the coefficients for 2D polynomial functions are required to be provided by the user on the GUI screen. The bivariant polynomial function is represented in terms of normalized coordinate X and Y and is given by

$$S_i^{poly} = \sum C_i^{m,n} X^m Y^n = C_i^{0,0} + C_i^{1,0}X + C_i^{0,1}Y + C_i^{2,0}X^2 + C_i^{1,1}XY + C_i^{0,2}Y^2 + C_i^{3,0}X^3 + C_i^{2,1}X^2Y + C_i^{1,2}XY^2 + C_i^{0,3}Y^3 + C_i^{3,1}X^3Y + C_i^{2,2}X^2Y^2 + C_i^{1,3}XY^3 + C_i^{3,2}X^3Y^2 + C_i^{2,3}X^2Y^3 + C_i^{3,3}X^3Y^3$$

where the subscript i of the polynomial coefficients $C_i^{m,n}$ denotes the index of applied stress quantity, and the superscripts m and n designates the exponents of normalized dimensions X and Y, respectively.

If other stress specifications that can not be described by either remote tension and bends or bivariant polynomial functions are to be used, the stress variations are required to be organized in tabular form and stored in text file format. GUI is then used to specify the file locations and names for analysis. The bivariant stress file

format is of generic NASGRO format for bivariant stress used by bivariant SIF solution modules. For more details, please refer to Section C10.1 – Stress Gradient Input Formats in the latter part of this appendix.

SC32 – Surface crack at hole in lug – univariant WF

Crack case SC32 represents an elliptical surface-crack crack initiated at the hole of a straight lug under pin-loading. Nominally, SC32 has the same geometry and loading as SC12. However, SC32 employs the weight function solution SC18 and the nonlinear stress variation for an uncracked lug. Consequently, SC32 represents a more powerful analysis tool, e.g., it can handle residual stresses. SC32 has a larger range of geometric parameters, e.g., $W/D \geq 1.25$ for SC32 but $W/D \geq 2$ for SC12. Finally, comparisons between SC12/SC32 and benchmark results (obtained from finite element analyses) demonstrate that SC32 is more accurate than SC12.

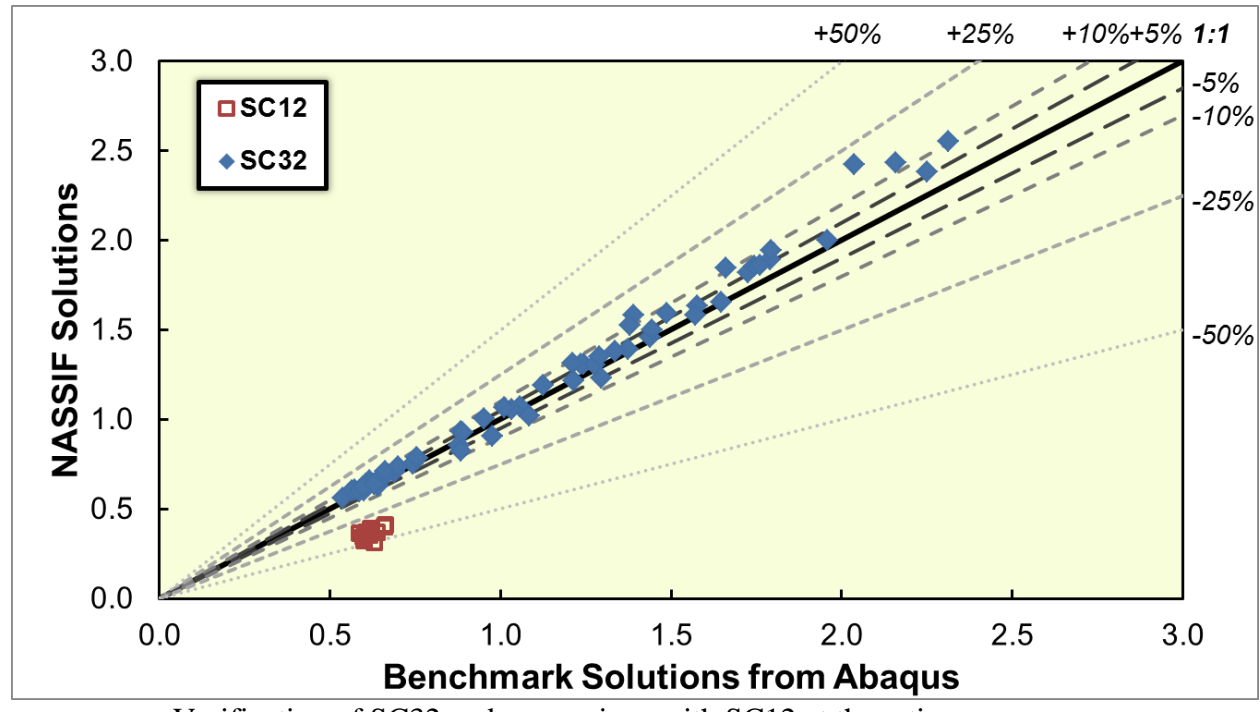
Crack case SC32 provides stress intensity factor solutions input as values of the pin-loading ($S_3 = P/Dt$). Individual magnitudes of the pin-loading are specified through the GUI for load block definitions. The fracture mechanics module internally estimates the local stress variations on the crack plane (in the corresponding uncracked body) along the net section and then invokes SC18.

Nonlinear stress variations along the crack plane were computed using the same assumptions as used in TC27. Please refer to TC27 for additional information on the nonlinear stress variations that drive these solutions.

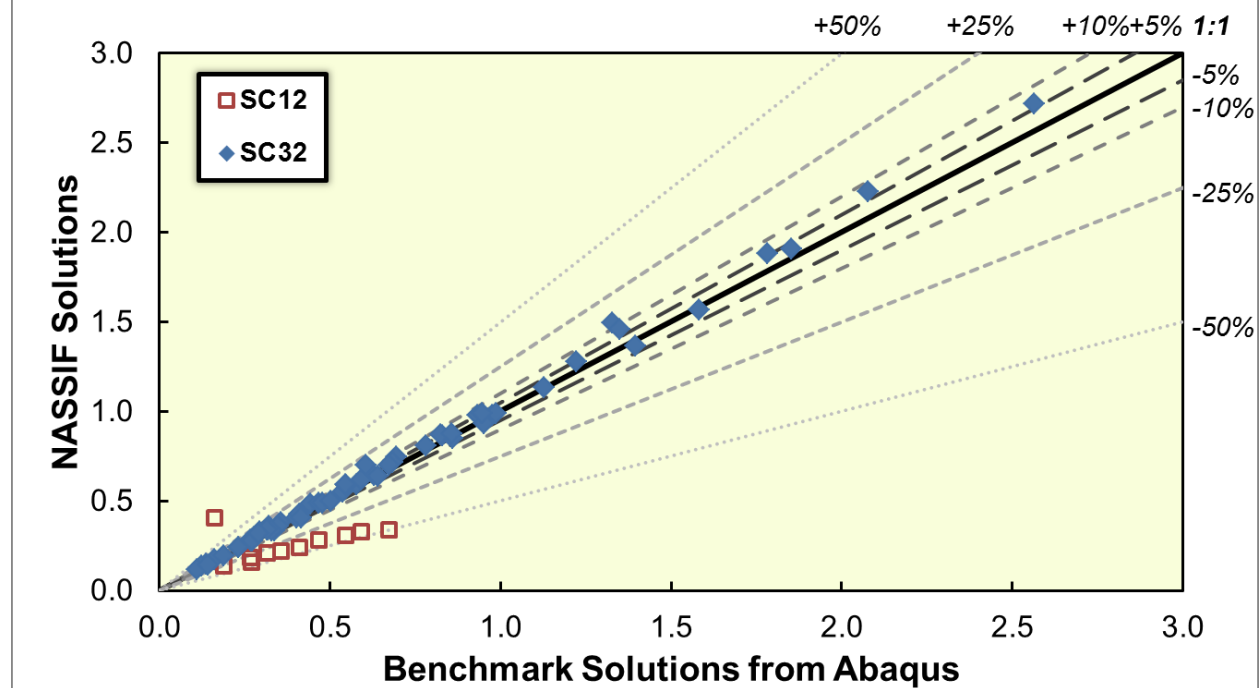
SC32 has the same geometric validity ranges as SC18, except for the additional constraint that $W/D \geq 1.25$. This ratio represents a lower limit for most straight lug geometries. The overall range of validity of this crack case is:

$$\begin{aligned} 0.25 &\leq \frac{D}{t} \leq 2; \\ 0 &\leq \frac{c}{W-D} \leq 0.4; \\ 0.5 &\leq \frac{a}{c} \leq 10; \\ 0.1 &\leq \text{Max}\left(\frac{a}{t}, \frac{a}{T-t}\right) \leq 0.9; \\ 0.1 &\leq \frac{T}{t} \leq 0.9; \\ 1.25 &\leq \frac{W}{D} \leq 10 \end{aligned}$$

Please refer to SC18 for additional information on integration of the weight functions.



Verification of SC32 and comparison with SC12 at the a-tip



Verification of SC32 and comparison with SC12 at the c-tip

The previous figures show verification studies of SC32 at the a-tip and c-tip. Values of stress intensity factors from detailed finite element analyses (using Abaqus 6.12-1) provide the benchmark data. Almost all stress intensity factors computed with SC32 have less than 10% error in comparison with the benchmark data. Error with SC12 may exceed 50%. For both crack cases, the error tends to be conservative (i.e., driving increased crack advance). This figure also highlights the increased range of

geometries in SC32 vs. SC12; several computed values of SC32 do not have corresponding values of SC12 since the input geometry lies outside of the range of SC12 solutions.

Section C5: Standard Specimens

SS01 – Standard Center Cracked Tension Specimen

$$F_o = (\sec \pi w)^{1/2}$$

Reference: [C1]

SS02 – Standard Compact Specimen

$$F_3 = D(\pi c W)^{-1/2} [(2+w)(1-w)^{-3/2}] G$$
$$G = 0.886 + 4.64w - 13.32w^2 + 14.72w^3 - 5.6w^4$$

Reference: [C18]

SS03 – Standard Round Compact Specimen

$$F_3 = D(\pi c W)^{-1/2} [(2+w)(1-w)^{-3/2}] G$$
$$G = 0.76 + 4.8w - 11.58w^2 + 11.43w^3 - 4.08w^4$$

Reference: [C18]

SS04 – Standard Arc-Shaped Specimen

$$F_3 = D(\pi c W)^{-1/2} [3X/W + 1.9 + 1.1w] G Y$$
$$G = 1 + 0.25(1-w)^2 [1 - R/(R+W)]$$
$$Y = \sqrt{w}(1-w)^{-3/2} [3.74 - 6.3w + 6.32w^2 - 2.43w^3]$$

Reference: [C18]

SS05 – Standard Bend Specimen

$$F_2 = [1.99 - w(1-w)(2.15 - 3.93w + 2.7w^2)] / G$$
$$G = \sqrt{\pi}(1+2w)(1-w)^{3/2}$$

Reference: [C18]

SS06 – Standard Edge-Cracked Specimen (Constrained Rotation)

F_0 is given in Table C26 below.

Table C26: Stress Intensity Correction Factors F_0

$h/W \rightarrow$ a/W	0.5	0.75	1.00	2.00	3.00	5.00	8.00	12.00
0.01	1.1273	1.1273	1.1273	1.1273	1.1273	1.1284	1.1284	1.1284
0.05	1.1160	1.1263	1.1311	1.1389	1.1422	1.1435	1.1444	1.1437
0.10	1.0769	1.1133	1.1302	1.1581	1.1702	1.1745	1.1731	1.1773
0.15	1.0404	1.1119	1.1480	1.1986	1.2369	1.2481	1.2580	1.2644
0.20	0.9849	1.0836	1.1370	1.2291	1.2744	1.2935	1.3103	1.3234
0.25	0.9607	1.0937	1.1724	1.3196	1.3967	1.4303	1.4615	1.4838
0.30	0.9273	1.0763	1.1717	1.3604	1.4655	1.5129	1.5583	1.5801
0.40	0.9180	1.0905	1.2201	1.5178	1.7133	1.8104	1.9058	1.9670
0.50	0.9625	1.1441	1.2966	1.7029	2.0218	2.1989	2.3903	2.5189
0.60	1.0697	1.2554	1.4194	1.9192	2.3929	2.6933	3.0553	3.3221
0.70	1.2700	1.4537	1.6177	2.1801	2.8153	3.2868	3.9387	4.4944
0.80	1.6474	1.8147	1.9648	2.5322	3.2758	3.9151	4.9617	6.0120
0.85	1.9114	2.0634	2.2025	2.7412	3.4866	4.1606	5.3394	6.6641
0.90	2.4410	2.5691	2.6880	3.1637	3.8605	4.5313	5.7420	7.2435
0.95	3.5966	3.6891	3.7756	4.1370	4.6812	5.2354	6.2295	7.5713
0.98	5.7072	5.7693	5.8251	6.0668	6.4520	6.8248	7.4824	8.4234

Reference: [C19]

SS07 – Circumferential Crack in Round Bar

$$F_0 = G_0 / k^{3/2}$$

$$G_0 = 0.5 + 0.25k + 0.1875k^2 - 0.1815k^3 + 0.3655k^4$$

$$k = 1 - 2c/D$$

Reference: [C3]

SS08 – Notched Plate with a Surface Crack

$$F_0 = F_m g_1 g_2 g_3 g_4 g_5 f_\phi f_w$$

where

$$F_m = \left[M_1 + M_2 \left(\frac{a}{t} \right)^2 + M_3 \left(\frac{a}{t} \right)^4 \right] f_x$$

For $a/c \leq 1$,

$$M_1 = 1$$

$$M_2 = \frac{.05}{0.11 + (a/c)^{3/2}}$$

$$M_3 = \frac{0.29}{0.23 + (a/c)^{3/2}}$$

$$g_1 = 1 - \frac{(a/t)^4 (2.6 - 2a/t)^{1/2}}{(1+4a/c)} \cos \phi$$

$$g_2 = \frac{1 + 0.358\lambda + 1.425\lambda^2 - 1.578\lambda^3 + 2.156\lambda^4}{1 + 0.08\lambda^2}$$

$$\lambda = \frac{1}{1 + (c/R) \cos(0.9\phi)}$$

$$g_3 = 1 + 0.1(1 - \cos \phi)^2 (1 - a/t)^{10}$$

$$g_4 = K_t \left[0.36 - \frac{0.032}{(1+c/R)^{1/2}} \right]$$

$$K_t = 3.17$$

$$g_5 = 1 + (a/c)^{1/2} [0.003(R/t)^2 + 0.035(R/t)(1 - \cos \phi)^3] - 0.35(a/t)^2 (1 - a/2c)^3 \cos \phi$$

$$f_w = 1 - 0.2\gamma + 9.4\gamma^2 - 19.4\gamma^3 + 27.1\gamma^4 \text{ where } \gamma = (a/t)^{1/2} \frac{c+R}{W} < 0.6$$

$$f_\phi = [(a/c)^2 \cos^2 \phi + \sin^2 \phi]^{1/4}$$

For $a/c > 1$

$$M_1 = (c/a)^{1/2} (1.04 - 0.04c/a)$$

$$f_\phi = [(c/a)^2 \sin^2 \phi + \cos^2 \phi]^{1/4}$$

Reference: [C35]

SS09 – Notched Plate with a Corner Crack

$$F_0 = F_m g_1 g_2 g_3 g_4 g_5 f_\phi f_w$$

where

$$F_m = \left[M_1 + M_2 \left(\frac{a}{t} \right)^2 + M_3 \left(\frac{a}{t} \right)^4 \right] f_x$$

For $a/c \leq 1$,

$$M_1 = 1.13 - .09a/c$$

$$M_2 = -0.54 + \frac{0.89}{0.2 + (a/c)}$$

$$M_3 = 0.5 - \frac{1}{0.65 + (a/c)}$$

$$g_1 = 1 + [0.1 + 0.2(a/t)^2](1 - \sin \phi)^2 - 0.16(a/t)\sin \phi \cos \phi$$

$$g_2 = \frac{1 + 0.358\lambda + 1.425\lambda^2 - 1.578\lambda^3 + 2.156\lambda^4}{1 + 0.13\lambda^2}$$

$$\lambda = \frac{1}{1 + (c/R)\cos(0.8\phi)}$$

$$g_3 = (1 + 0.04a/c)[1 + 0.1(1 - \cos \phi)^2][0.97 + 0.03(a/t)^{1/4}]$$

$$g_4 = K_t \left[0.36 - \frac{0.032}{(1 + c/R)^{1/2}} \right]$$

$$K_t = 3.17$$

$$g_5 = 1 + (a/c)^{1/2} [0.003(R/t)^2 + 0.035(R/t)(1 - \cos \phi)^3] - 0.35(a/t)^2(1 - a/2c)^3 \cos \phi$$

$$f_w = 1 - 0.2\gamma + 9.4\gamma^2 - 19.4\gamma^3 + 27.1\gamma^4 \text{ where } \gamma = (a/t)^{1/2} \frac{c+R}{W} < 0.6$$

$$f_\phi = [(a/c)^2 \cos^2 \phi + \sin^2 \phi]^{1/4}$$

For $a/c > 1$

$$M_1 = (c/a)^{1/2}(1.0 + 0.04c/a)$$

$$M_2 = 0.2(c/a)^4$$

$$M_3 = -0.11(c/a)^4$$

$$g_1 = 1 + \frac{c}{a}[0.1 + 0.2(a/t)^2](1 - \sin \phi)^2 - 0.16(a/t)(c/a)\sin \phi \cos \phi + 0.07(1 - a/c)(1 - a/t)\cos^2 \phi$$

$$g_3 = (1.13 - 0.09c/a)[1 + 0.1(1 - \cos \phi)^2][0.97 + 0.03(a/t)^{1/4}]$$

$$f_\phi = [(c/a)^2 \sin^2 \phi + \cos^2 \phi]^{1/4}$$

Reference: [C35]

SS10: Notched Plate with a through crack

$$F_0 = f_1 g_4 f_w$$

where

$$f_1 = 1 + 0.358\lambda + 1.425\lambda^2 - 1.578\lambda^3 + 2.156\lambda^4$$

where $\lambda = 1/[1 + (c/R)]$

$$g_4 = K_t \left[0.36 - \frac{0.032}{(1 + c/R)^{1/2}} \right]$$

$$f_w = 1 - 0.2\gamma + 9.4\gamma^2 - 19.4\gamma^3 + 27.1\gamma^4$$

where $\gamma = (c+R)/W$

the above equations are valid for $\gamma < 0.6$.

Reference: [C35]

SS11: Plate with a corner crack from hole

The solution for this case is derived by specializing the solution for case CC02. Note that the hole is symmetric and only tensile loading is applied.

All the expressions for CC02 apply to this case except for f_{w0}

The correction factor for finite width is defined as follows:

$$f_{w0} = 1, \quad D/W < 0.1$$

$$f_{w0} = 1.01, \quad 0.1 \leq D/W < 0.2$$

$$f_{w0} = 1.024 + 3.42(a/t) - 17.91(a/t)^2 + 33.79(a/t)^3, \quad 0.2 \leq D/W < 0.334$$

$$f_{w0} = 1.063 - 0.041(a/t) + 0.496(a/t)^2 - 0.37(a/t)^3, \quad 0.334 \leq D/W < 0.5$$

SS12 – Standard Eccentrically-Loaded Single Edge Crack Tension Specimen ESE(T)

$$F_3 = D(\pi c W)^{-1/2} (1.4 + w)(1 - w)^{-3/2} G$$

$$G = 3.97 - 10.88w + 26.25w^2 - 38.9w^3 + 30.15w^4 - 9.27w^5$$

Reference: [C49]

SS13 – Surface Crack in Finite Width Plate Specimen (SC01)

This crack case uses the same solution as SC01. It is specialized for use in the NASMAT module, with remote uniform tension being the only loading considered.

References: [C13], [C29]

SS14 – Surface Crack in Finite Width Plate Specimen (SC17)

This crack case uses the same solution as SC17. It is specialized for use in the NASMAT module, with remote uniform tension being the only loading considered.

References: [C39], [C40], [C41], [C43]

Section C6: Polynomial Series

$$F_0 = C_0 + C_1 u + C_2 u^2 + \cdots + C_n u^n$$

where $u = (a / D)^m$

D is a user defined dimension

m is a user defined exponent (real number)

$n \leq 5$

Section C7: Crack Cases of Tabular Data

DT01, DT02, and DT03

Three crack cases (DT01, DT02, and DT03) are provided for the user to enter stress intensity geometry factors (the SIF geometry factors) as a function of crack sizes in tabular forms for fatigue life analysis.

DT01: one-dimensional data table for a through crack (one tip)

a/D	F_i ($i=1, 2, 3$, or 4)

The SIF geometry factors (F_i) corresponding to the stress quantity S_i at the crack tip are entered as a function of the normalized crack size a/D , where D is user-defined dimension.

DT02: two-dimensional data table for a through crack (one tip)

a/D_1	a/D_2			
		F_i ($i=1, 2, 3$, or 4)		

The SIF geometry factors (F_i) corresponding to the stress quantity S_i at the crack tip are entered as a function of the normalized crack sizes a/D_1 and a/D_2 , where D_1 and D_2 are user-defined dimensions.

DT03: two-dimensional data table for a part-through crack (two tips)

a/D	a/c			
		F_i ($i=1, 2, 3$, or 4)		

The SIF geometry factors (F_i) corresponding to the stress quantity S_i at a specific crack tip (a -tip or c -tip) are entered as a function of the normalized crack size a/D and crack aspect ratio a/c , where D is user-defined dimension.

In each of the SIF geometry factor tables, the user can enter up to 50 data pairs.

During crack propagation, the stress intensity factor for a given crack size is obtained by interpolating off the user-entered SIF geometry tables, and the stress intensity factor is calculated accordingly.

KT01, KT02, and KT03

Three crack cases (KT01, KT02, and KT03) are introduced in v8.0 for the user to enter stress intensity factors directly as a function of crack sizes in tabular forms for fatigue life analysis. The KT crack cases are very similar to their counterparts, the DT cases. For running the KT crack cases, the user provides stress intensity factors as a function of crack sizes in tabular forms. During crack propagation, the stress intensity factor for a given crack size is obtained by interpolating off the user-entered tables.

For the KT crack cases, a new feature is introduced for the user to enter different stress intensity factor values at t_1 and t_2 of fatigue loading. During crack propagation, the stress intensity factors for a given crack size at t_1 and t_2 are calculated by interpolating the stress intensity factor tables for t_1 and t_2 , respectively, and then the maximum stress intensity factor and the range of stress intensity factor for crack growth calculation are obtained accordingly.

Section C8: Boundary Element Solutions

BE02 – Two Through Cracks from Hole in a Plate

This is a special crack case that may be used to model multi-site damage in aircraft panels. Two through cracks are assumed to be simultaneously present and growing independently under the influence of remote load. The stress intensity solutions for the two crack tips (one for each of the through cracks) are derived from boundary element solution of the problem. The solution is stored in a file for various geometric parameters such as crack depth and crack size ratio. Interpolation is performed for the specific geometry being analyzed.

BE03 – Corner Crack, Through Crack from Hole in a Plate

This is also a special crack case that may be used to model multi-site damage in aircraft panels. A corner crack and a through crack are assumed to be simultaneously present and growing independently under the influence of remote load. The stress intensity solutions for the three crack tips (two for the corner crack and one for the through crack) are derived from boundary element solution of the problem with two through cracks and certain analogies (defined below) are used to develop the solution for the part through crack. The BE02 solution is stored in a file for various geometric parameters such as crack depth and crack aspect ratio. Interpolation is performed for the specific geometry being analyzed. The correction factors F_0 are defined in terms of the factors for three cases as follows:

$$F_0 = F_{0CC02} \frac{F_{0BE02}}{F_{0TC03}}$$

where

F_{0CC02} is the solution for case CC02 ,

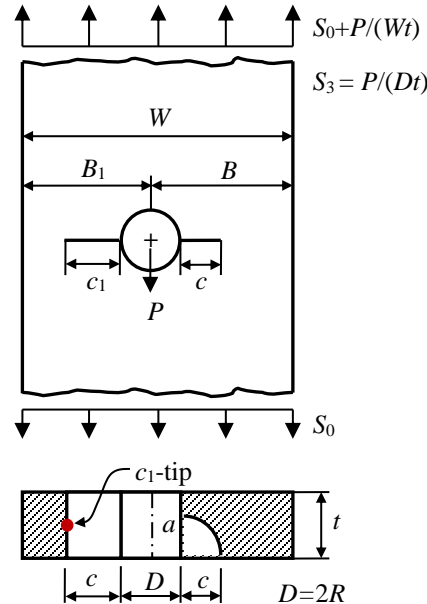
F_{0BE02} is the solution for case BE02 ,

F_{0TC03} is the solution for case TC03.

Section C9: Hybrid Cracks

HC01 – Corner Crack and Through Crack at an Offset Hole

HC01 is a crack model with combined corner crack and through crack at an offset hole in a finite plate subjected to remote tension (S_0) and pin load (S_3), as shown below.



Configuration of HC01

The stress intensity factors are calculated by the compounding method developed by Guo [66]:

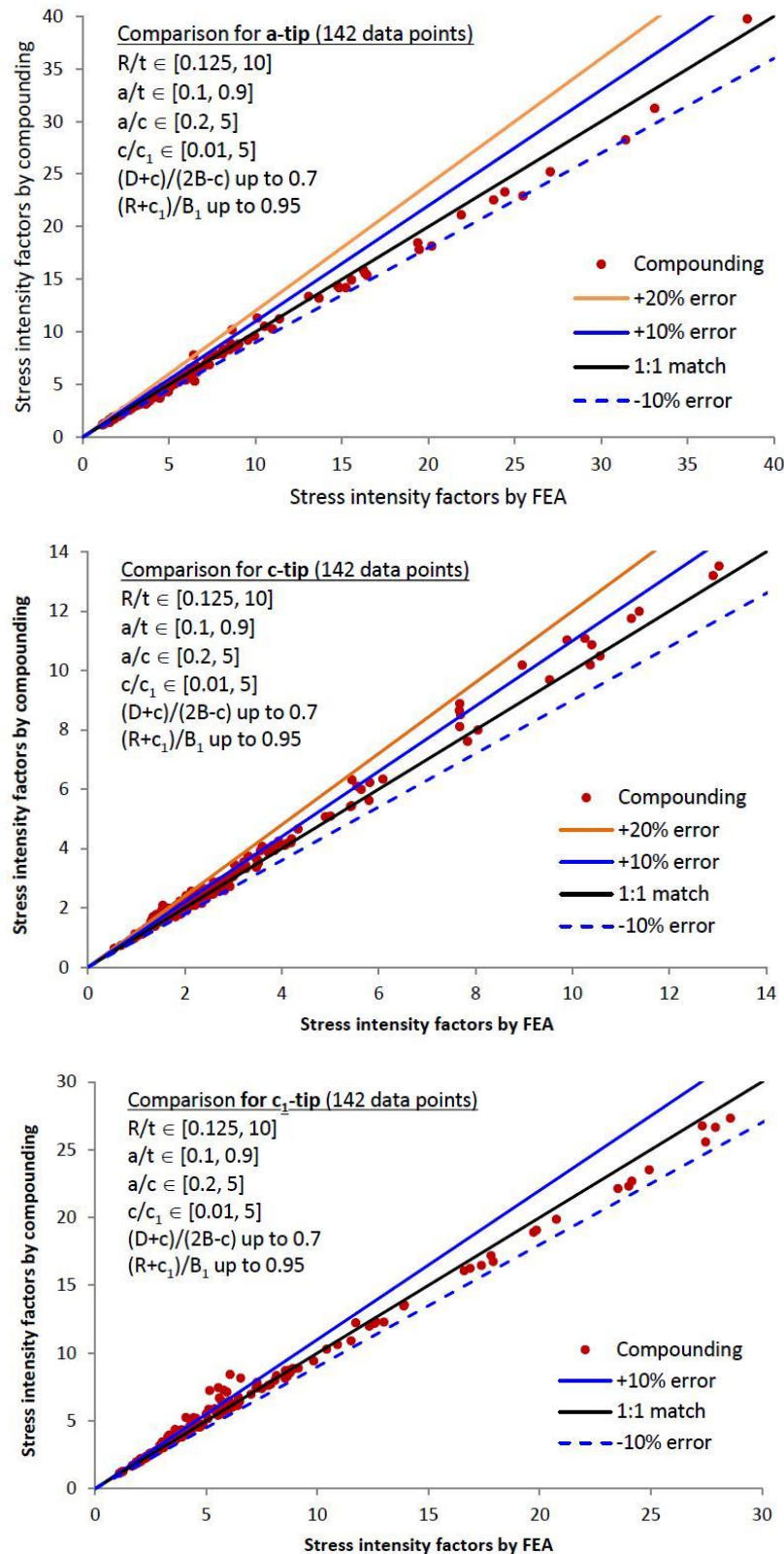
$$K_{HC01,a} = K_{CC16,a} \cdot C_{F,a} \quad \text{at } a\text{-tip}$$

$$K_{HC01,c} = K_{CC16,c} \cdot C_{F,c} \quad \text{at } c\text{-tip}$$

$$K_{HC01,c_1} = 1.05 \cdot K_{TC23,c_1} \quad \text{at } c_1\text{-tip}$$

Where $K_{CC16,a}$ and $K_{CC16,c}$ are the stress intensity factors at a - and c -tip of the corner crack alone, calculated by CC16. $C_{F,a}$ and $C_{F,c}$ are the compounding factors at a -tip and c -tip of HC01, respectively, which account for the effects of the through crack on the stress intensity factors of the corner crack. They are determined by the stress intensity factor solution of crack case TC23. K_{TC23,c_1} is the stress intensity factor at c_1 -tip of the two through cracks with lengths c_1 and \bar{c} , calculated by TC23. \bar{c} is the equivalent crack length of the corner crack, $\bar{c} = \frac{\pi ac}{4t} \sqrt{\frac{a}{t}}$. The factor 1.05 is used to better calibrate the solution with the FEA results. Note that the c_1 -tip of HC01 is at the mid-point of the through crack front.

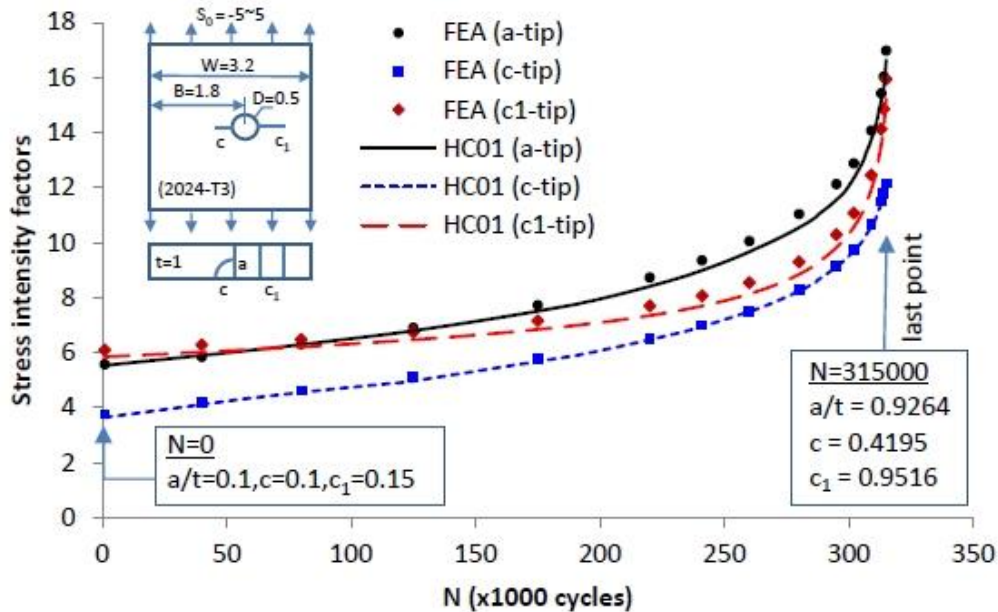
The compounding method is verified extensively under remote tension by the FEA [C66] in the following range of geometry dimensions and crack sizes: $B/D \geq 1$, $0.25 \leq D/t \leq 20$, $0.1 \leq a/t \leq 0.9$, $0.2 \leq a/c \leq 5$, $0.01 \leq c/c_1 \leq 5$, $(D+c)/(2B-c) \leq 0.7$, $(D/2+c_1)/(W-B) \leq 0.95$, as shown in the three figures below.



Verification of the compounding method for obtaining the stress intensity factors at a -, c -, and c_1 -tip of HC01 under remote tension

The three figures show that the compounding method works quite well. Among the $142 \times 3 = 426$ data of the stress intensity factors for the 142 cases, more than 70% of the data have errors less than 5%, and 97% of the data have errors less than 10%. A few data have errors larger than 15%. The bigger errors ($>15\%$) are all from the crack configurations with a small a/c ratio and a very small hole ($R/t = 0.125$), or from the configurations with a very large through crack ($(R+c_1)/B_1 = 0.95$). The bigger errors may come from the compounding procedures, the solutions of CC16 and TC23 themselves, or both. The compounding method based on CC16 and TC23 may be not very accurate for the geometries with a small a/c ratio and a very small hole, but overall it is a solid approach in terms of the complexity of the crack model. It covers wide range of geometry dimensions and crack sizes too.

Additional verification is performed by comparing the stress intensity factors calculated by HC01 and the FEA during crack propagation under constant amplitude tensile loading, as shown in the figure below, where the curves are the results calculated by HC01 under the peak stress. The discrete data points are the results obtained from the FEA software StressCheck. The two sets of results given by HC01 and the FEA are in excellent agreement with errors all less than 5% at all three crack tips during the entire crack propagation.



Comparison of the stress intensity factors given by HC01 and the FEA during crack propagation under constant amplitude tensile loading

In order to deal with small cracks and very large cracks of HC01, the lower limit of a/t is extended down to zero, and the upper limit of a/t is extended up to 0.95. The extension makes sense because the K -solution of HC01 is obtained from compounding CC16 and TC23, and the K -solution of CC16 is valid for $0 \leq a/t \leq 0.95$. The upper limit of $(D/2+c_1)/(W-B)$ is also extended to 1.0. The geometry limits of HC01 thus become: $B/D \geq$

$$1, \quad 0.25 \leq D/t \leq 20, \quad 0 \leq a/t \leq 0.95, \quad 0.2 \leq a/c \leq 5, \quad 0.01 \leq c/c_1 \leq 5, \quad (D+c)/(2B-c) \leq 0.7, \\ (D/2+c_1)/(W-B) \leq 1.0.$$

The beta correction is applied to the crack tips of the corner crack (i.e. a - and c -tip) for ΔK calculation in NASFLA. Suppose the applied maximum and minimum stress intensity factors are K_{max} and K_{min} , respectively. The range of stress intensity factors with the beta correction is,

$$\Delta K = \beta_R \cdot (K_{max} - K_{min})$$

where

$$\beta_R = \begin{cases} 0.9 + 0.2R^2 - 0.1R^4 & \text{if } R \geq 0 \\ 0.9 & \text{if } R < 0 \end{cases}$$

Note that the original K_{max} , K_{min} , and R remain unchanged; only ΔK is changed. The beta correction is not applied to the through crack (c_1 -tip).

The SIF geometry factors of HC01 in NASSIF are defined as:

$$F_i = \frac{K}{S_i \sqrt{\pi a}} \quad \text{at } a\text{-tip and } c\text{-tip}$$

$$F_i = \frac{K}{S_i \sqrt{\pi c_1}} \quad \text{at } c_1\text{-tip}$$

Where $i = 0$ for remote tension, and 3 for pin-load.

References: [C66]

Section C10: Weight Function Solution Options

Weight function stress intensity factor (SIF) solutions are calculated based on the stresses acting normal to the crack plane along the crack surface in the corresponding uncracked body. Some weight function solutions also permit the specification of a remote stress field (often uniform tension), but these solutions actually use a crack plane stress distribution that is either assumed to be identical to the remote stress (for example, a crack in a uniform rectangular plate, such as SC17) or a crack plane stress distribution that is calculated from the remote stress (for example, the concentrated stress distribution near a circular hole under uniform remote tension, such as TC13).

Several options are generally available for user input of the crack plane stresses, although not all options are available for all weight function solutions. These options include direct input in the GUI vs. file input, and input of tabulated stresses vs. input of polynomial series coefficients. In some cases, users can also provide more than one stress gradient for the same geometry, and allow the code to sum their effects when calculating the stress intensity factor.

Most weight function solutions include an “optimum point spacing” (OPS) option described further below. Invoking the OPS option generally relaxes some restrictions on tabular input of the stress fields.

Most weight function solutions also provide the option of superimposing a static residual stress field, also described further below. This residual stress field does not change the calculated range of the stress intensity factor, but it may change the local stress ratio, and hence can change the calculated range of the effective stress intensity factor.

C10.1 Stress Gradient Input Formats

Univariant Stresses

Univariant stresses are input in terms of a normalized dimensional variable X_i which generally ranges from 0.0 to 1.0. In a few cases, X_i ranges from -1.0 to +1.0. This variable is generally equal to x/D , where D denotes the appropriate normalizing dimension (e.g., width or thickness).

Polynomial Input

Crack plane stresses for some univariant weight function SIF solutions can be entered in the GUI directly from the keyboard as coefficients in a polynomial series expression for the stress field. The user is responsible for determining the most appropriate values of the coefficients that describe the intended stress field. In general, the polynomial series is given by

$$\sigma(X) = C_0 + C_1X + C_2X^2 + C_3X^3 + C_4X^4 + C_5X^5 + C_6X^6$$

Any of the coefficients C_i may be set equal to zero.

Tabular Input - General

Crack plane stresses for all univariant weight function SIF solutions can be entered as paired values of normalized position vs. stress normal to the crack plane. These values must be entered in ascending order of the normalized position variable. This input can be entered directly from the keyboard into a grid in the GUI, or it can be entered via file.

If the optimum point spacing (OPS) option is NOT selected (see below), then a maximum of 50 points are permitted. If the OPS option IS selected, then up to 500 points can be specified. Unlike some earlier versions of NASGRO, these points do NOT have to be equally spaced. In either OPS or non-OPS mode, at least two points must be supplied.

Tabular Input from File – Standard Format

Crack plane stresses for all univariant weight function SIF solutions can be entered from an ASCII file. The GUI will prompt the user to supply the appropriate path and filename. This file has the following format:

Line 1: N (number of position-stress pairs)
Line 2: X₁, S(X₁)
Line 3: X₂, S(X₂)
Line 4: X₃, S(X₃)
...
Line (N+1): X_N, S(X_N)

Multiple values on the same line may be separated by a comma, a space, or a tab.

Tabular Input from File – Full Stress Tensor

Instead of providing the value of the stress normal to the crack plane, the user is also allowed to provide the full stress tensor at each location along the crack line. This option is only available through file input (not keyboard input), and it is only available when the shakedown option is selected. The values in the stress tensor other than the stress normal to the crack plane have no direct effect on the calculated stress intensity factor, so the additional stress values will only have an effect on the calculated stress intensity factor when local yielding occurs.

This file format is defined as

Line 1: N (number of positions)
Line 2: X₁, S_{xx}(X₁), S_{yy}(X₁), S_{zz}(X₁), S_{xy}(X₁), S_{xz}(X₁), S_{yz}(X₁)
...
Line (N+1): X_N, S_{xx}(X_N), S_{yy}(X_N), S_{zz}(X_N), S_{xy}(X_N), S_{xz}(X_N), S_{yz}(X_N)

Note that in general, the coordinate system defined by the univariant weight function crack geometry bitmaps in NASGRO is

x – in the crack plane in the width direction

y – in the crack plane in the thickness direction
 z – normal to the crack plane

The exceptions to this coordinate system are CC11 and SC17, where x denotes the thickness direction in the crack plane, and y denotes the width direction in the crack plane.

Bivariant Stresses

Polynomial Input

Some bivariant SIF solutions permit the stress distribution to be input directly into the GUI as coefficients for a two-dimensional polynomial series. The specific format of this polynomial series can vary from solution to solution. The documentation for each specific solution should be consulted for further details.

Tabular Input from File – General

For crack geometries with bivariant stress distributions, tabulated stresses on the crack plane must be entered via a file. Two file format options are available for data entry.

For both bivariant options, if optimum point spacing is selected, then the x-coordinates and y-coordinates do NOT have to be equally spaced, and there is no limit on the number of points that can be entered. If optimum point spacing is NOT selected, then the x-coordinates and y-coordinates DO have to be equally spaced (but, as noted earlier, the x-spacing does not have to be the same as the y-spacing). In this case, the maximum number of points in both the x-direction and y-direction is 20.

Tabular Input from File – Historical NASGRO Bivariant Format

The historical NASGRO format for bivariant stress fields is illustrated in the following figure. The first line identifies the number of points in the x and y directions, N_x and N_y , respectively. These two values do not have to be identical. The next N_x lines give the normalized x -direction coordinates (X_i), ranging from 0.0 to 1.0. The following N_y lines give the normalized y -direction coordinates (Y_i) and the corresponding stress values for the first normalized x -direction coordinate; the y -direction coordinates are normalized from 0.0 to 1.0. Succeeding sets of N_y lines give the normalized y -direction coordinates and stresses at the subsequent normalized x -direction coordinates. Multiple values on the same line can be delimited by a comma and/or a space, but not a tab.

This takes the general form

Line 1:	N_x, N_y
Line 2:	$X_1 (= 0.0)$
Line 3:	X_2
Line 4:	X_3
...	

Normalized x-coordinates

Line (Nx+1)	X _{Nx} (= 1.0)	
Line (Nx+2)	Y ₁ , S(X ₁ , Y ₁)	
Line (Nx+3)	Y ₂ , S(X ₁ , Y ₂)	Normalized y-coordinates, and stress values at corresponding first normalized x-coordinate
...		
Line (Nx+Ny+1)	Y _{Ny} , S(X ₁ , Y _{Ny})	
Line (Nx+Ny+2)	Y ₁ , S(X ₂ , Y ₁)	Normalized y-coordinates, and stress values at corresponding second normalized x-coordinate
Line (Nx+Ny+3)	Y ₂ , S(X ₂ , Y ₂)	
...		
Line (Nx+2Ny+1)	Y _{Ny} , S(X ₂ , Y _{Ny})	
...		
Line (Nx+NxNy+1)	Y _{Ny} , S(X _{Nx} , Y _{Ny})	

Tabular Input from File – Alternative Bivariant Format

An alternative format now available for bivariant stress input (beginning in Version 6.0) is patterned from the standard stress report formats commonly employed in finite element software. The stress input file has the following format (multiple values on the same line can be delimited by space, comma, or tab):

```

Line 1:      x1, y1, z, Sxx, Syy, Szz, Sxy, Syz, Sxz
Line 2:      x1, y2, z, Sxx, Syy, Szz, Sxy, Syz, Sxz
.....
Line (Ny):    x1, yNy, z, Sxx, Syy, Szz, Sxy, Syz, Sxz
Line (Ny+1):  x2, y1, z, Sxx, Syy, Szz, Sxy, Syz, Sxz
Line (Ny+2):  x2, y2, z, Sxx, Syy, Szz, Sxy, Syz, Sxz
.....
Line (2Ny):   x2, yNy, z, Sxx, Syy, Szz, Sxy, Syz, Sxz
.....
Line (Nx Ny): xNx, yNy, z, Sxx, Syy, Szz, Sxy, Syz, Sxz

```

Here the x_i and y_i are the x -coordinates and y -coordinates in non-normalized form. The stress conversion routine in NASGRO determines the x and y limits from the data and performs the coordinate normalization required for the standard NASGRO input. This input method assumes that all of the x_i and y_i values occur on a plane with constant z -value. This z -value can be set equal to 0.0 for convenience.

If optimum point spacing is selected, then the x -coordinates and y -coordinates do NOT have to be equally spaced. If optimum point spacing is NOT selected, then the x -coordinates and y -coordinates DO have to be equally spaced (but, as noted earlier, the x -spacing does not have to be the same as the y -spacing).

Currently, NASGRO uses only the x_i , y_i , and S_{zz} values from this input format. A bivariant shakedown module is planned for future development, and once this is developed, the remaining S_{ij} terms will be incorporated into the shakedown calculation. Until then, the remaining stress terms can be set equal to zero without any effect on the results.

File Input – Bivariant Examples

Simple examples showing both input formats for the same data set are given in the following.

Here $W = 8$ units, and the x -coordinates are equally spaced at intervals of 2 units, so there are a total of 5 x -coordinate values. The thickness $t = 10$ units, and the y -coordinates are equally spaced at intervals of 5 units, so there are a total of 3 y -coordinate values.

Historical Format:

```
5, 3  
0.0  
0.25  
0.50  
0.75  
1.0  
0.0, 10.3  
0.5, 9.2  
1.0, 8.1  
0.0, 8.6  
0.5, 7.9  
1.0, 7.2  
0.0, 6.2  
0.5, 5.8  
1.0, 5.3  
0.0, 4.1  
0.5, 3.6  
1.0, 3.2  
0.0, 3.4  
0.5, 2.3  
1.0, 1.2
```

Alternative Format:

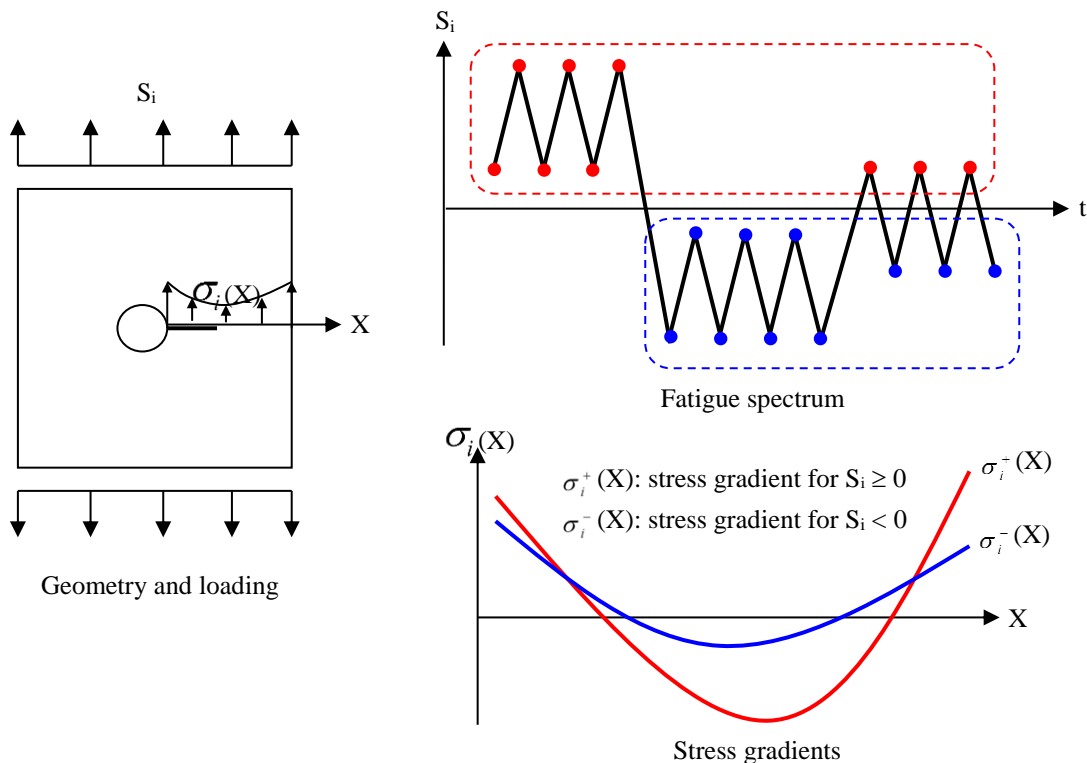
(Here all unused stress and geometry terms are shown as 0. for clarity)

```
0., 0., 0., 0., 0., 10.3, 0., 0., 0.  
0., 5., 0., 0., 0., 9.2, 0., 0., 0.  
0., 10., 0., 0., 0., 8.1, 0., 0., 0.  
2., 0., 0., 0., 0., 8.6, 0., 0., 0.  
2., 5., 0., 0., 0., 7.9, 0., 0., 0.  
2., 10., 0., 0., 0., 7.2, 0., 0., 0.  
4., 0., 0., 0., 0., 6.2, 0., 0., 0.  
4., 5., 0., 0., 0., 5.8, 0., 0., 0.  
4., 10.0., 0., 0., 5.3, 0., 0., 0.  
6., 0., 0., 0., 0., 4.1, 0., 0., 0.
```

6., 5., 0., 0., 0., 3.6, 0., 0., 0.
 6., 10., 0., 0., 0., 3.2, 0., 0., 0.
 8., 0., 0., 0., 0., 3.4, 0., 0., 0.
 8., 5., 0., 0., 0., 2.3, 0., 0., 0.
 8., 10., 0., 0., 0., 1.2, 0., 0., 0.

C10.1B Tension and Compression Stress Gradients

Due to complex structural interactions on airframe components, situations arise in which the stress gradient on a component under a tensile remote load is different from the one under a compressive remote load, as shown in the figure below, where σ_i^+ and σ_i^- denote the stress gradients associated with tensile and compressive remote loading, respectively. The purpose of tension/compression capabilities is to perform crack propagation analysis under this kind of situation.



Schematic diagram illustrating tension/compression stress gradients

Tension/compression is a NASFLA feature. It is implemented for the following weight function cases where stress gradients are specified discretely either by tables or by files:

- Uni-variant weight function cases: TC11, TC12, TC13, TC17, TC18, TC19, CC08, CC11, SC17, SC18, EC02, and EC05.
- Bi-variant weight function cases: CC09, CC10, CC12, SC19, and EC04.

Implementation of tension/compression stress gradients involves almost every major phase of computation, including the OPS, shakedown, stress intensity calculation, NSY analysis, and transition analysis, and so on.

- Input of stress gradients and data preprocessing
 - Read in stress gradients for both tension and compression.
 - Conduct the OPS calculation for both tension and compression stress gradients.
 - Calculate force and bending moments for both tension and compression stress gradients.
- Shakedown

The first task in shakedown analysis is to determine the type of shakedown, i.e. monotonic or cyclic shakedown based on the applied cyclic stresses. If monotonic shakedown is assumed, the real static residual stresses will be determined and stored during the stage of load schedule input. The stress intensity factors are then obtained by superposing the contribution of the static residual stress to the stress intensity factors caused by fatigue loading. If cyclic shakedown is identified, the total real stresses at instants t_1 and t_2 will be calculated based on elasto-plastic analysis. The stress intensity factors will be determined by the derived elasto-plastic stresses solely. The above mechanism is extended to consider two different stress gradients for tension and compression remote loading.

- Stress intensity factor calculation

For a specific fatigue step, the maximum stress intensity factor and stress intensity range can be expressed by

$$K_{\max} = \max\{K(t_1), K(t_2)\}$$

$$\Delta K = |K(t_1) - K(t_2)|$$

where $K(t_1)$ and $K(t_2)$ are the stress intensity factors at instant t_1 or t_2 . They are calculated by the following formula:

$$K = \sum_i F_i \cdot S_i \cdot \sqrt{\pi a}$$

where i is stress quantity index. F_i denotes the SIF-correction factor corresponding to the i th stress (S_i). $F_i = F_i^+$ if $S_i \geq 0$. $F_i = F_i^-$ if $S_i < 0$. F_i^+ and F_i^- are the SIF-correction factors caused by tension stress gradients (σ_i^+) and compression stress gradients (σ_i^-), respectively.

- NSY analysis

For tension/compression stress gradients, net section stresses at instants t_1 and t_2 are calculated by using the corresponding force and bending moments depending on the sign of the remote loading. The force and bending moments caused by both tension and compression stress gradients are pre-calculated before crack propagation analysis.

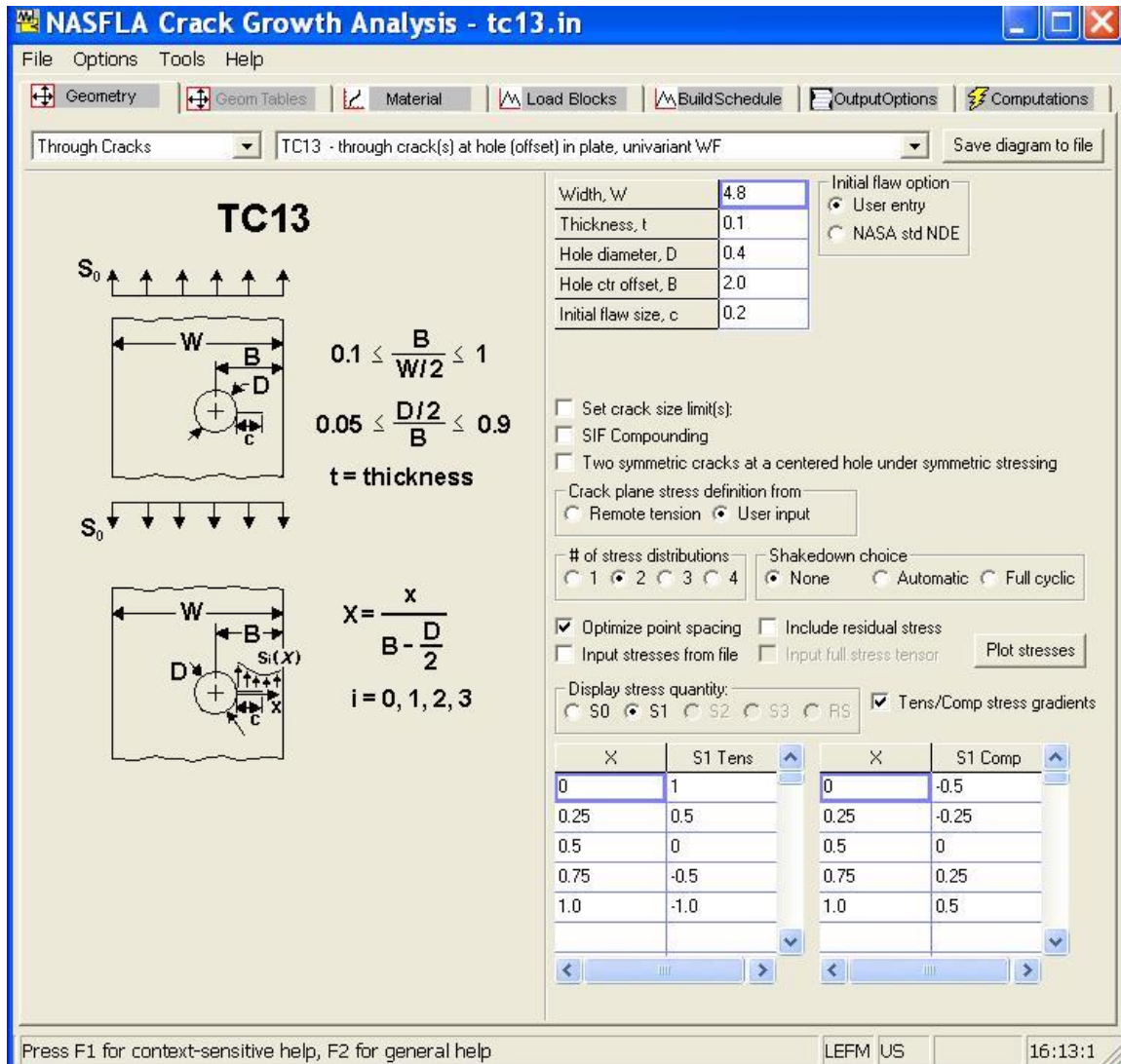
- Transition

After transition, both tension and compression stress gradients are converted if needed, the converted stress gradients are then applied to the post-transition geometry.

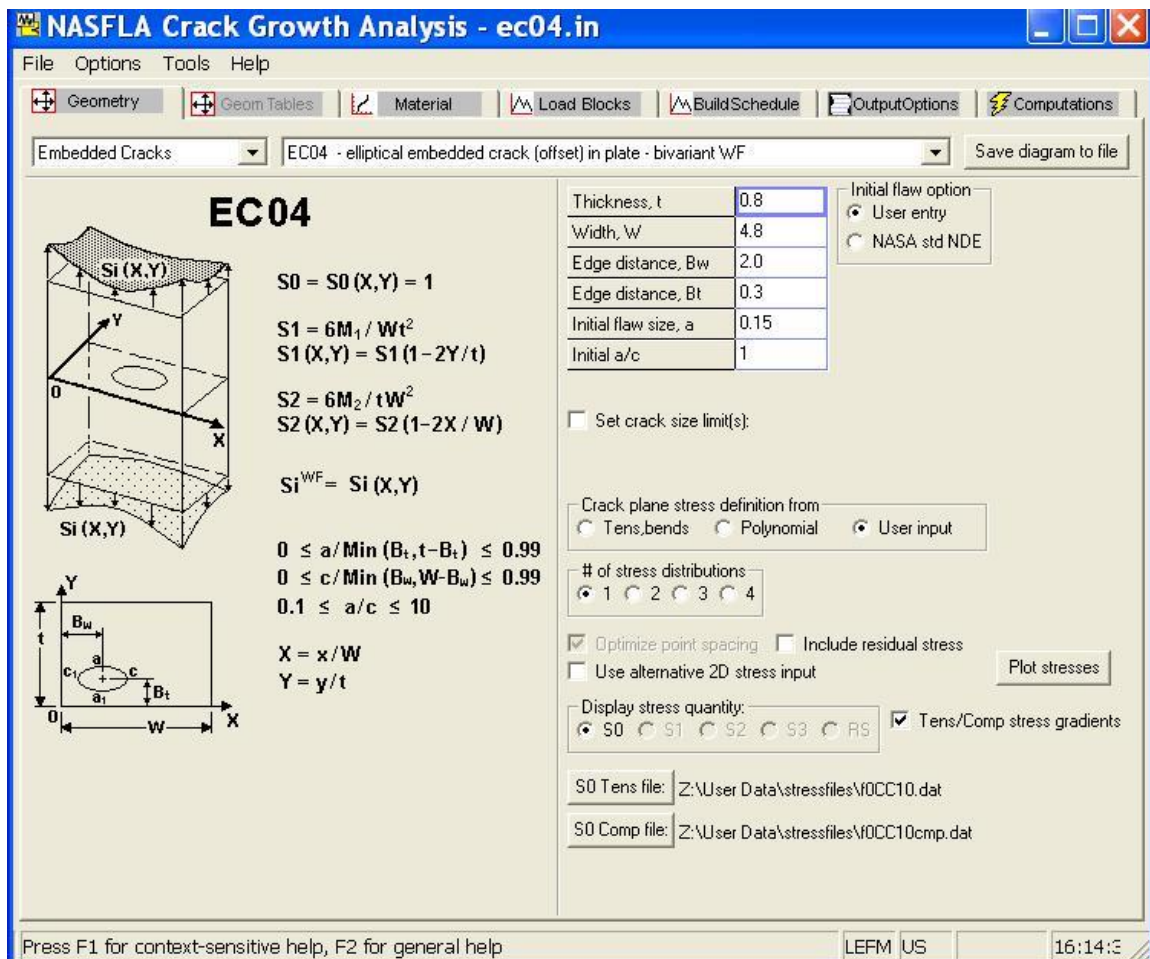
Performing analysis with tension/compression capabilities

To perform NASFLA analysis with tension/compression capabilities, go through the following two additional steps:

- Check “Tens/Comp stress gradients” on Geometry tab to turn on the capabilities.
- Specify stress gradients for both tension and compression either by 1-D tables or by files, as shown in the figures below.



Tension/compression stress gradients specified by 1-D tables



Tension/compression stress gradients specified by files

For bi-varient WF solutions (CC09, CC10, CC12, SC19, and EC04), the OPS checkbox will be automatically checked and grayed out if a user clicks on “Tens/Comp stress gradients”. The OPS operation will be performed commonly on both tension and compression stress gradients if it is activated.

C10.1C The t_1/t_2 Stress Gradients

The capabilities of t_1/t_2 stress gradients is provided for a user to specify two sets of stress gradients in crack growth analysis, one for the time instant t_1 of cyclic loading and the other for the time instant t_2 , as shown in the figure. For a specific fatigue load step, the applied stresses along the crack ligament at t_1 and t_2 are $\sum_i S_i^{t_1} \cdot \sigma_i^{t_1}(X)$ and $\sum_i S_i^{t_2} \cdot \sigma_i^{t_2}(X)$, respectively, where $S_i^{t_1}$ and $\sigma_i^{t_1}$ denote the stress value of the load step and the stress gradient at t_1 ; $S_i^{t_2}$ and $\sigma_i^{t_2}$ are the stress value of the load step and the stress gradient at t_2 . The summation is performed over the stress quantities.

The stress intensity factors at t_1 and t_2 are calculated by using the appropriate stress gradients,

$$K_{t1} = \sum_i S_i^{t_1} F_i^{t_1} \sqrt{\pi a}$$

$$K_{t2} = \sum_i S_i^{t_2} F_i^{t_2} \sqrt{\pi a}$$

where $F_i^{t_1}$ and $F_i^{t_2}$ denote the stress intensity geometry factors caused by the stress gradients at t_1 and t_2 , respectively. The stress intensity factor range and stress ratio are thus obtained by,

$$K_{min} = \min\{K_{t1}, K_{t2}\}$$

$$K_{max} = \max\{K_{t1}, K_{t2}\}$$

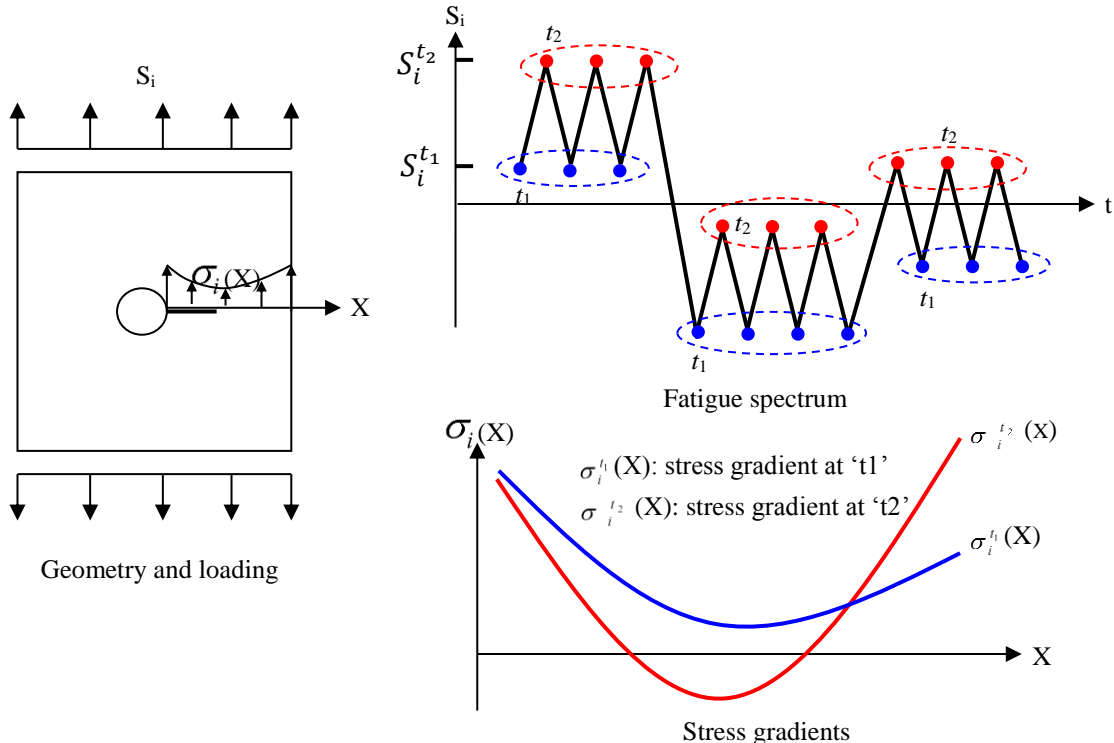
$$\Delta K = K_{max} - K_{min}$$

$$R = K_{min}/K_{max}$$

The shakedown analysis and net section stress calculation are performed by using the appropriate stress gradients.

The t1/t2 capabilities is a feature for NASFLA only. It has been implemented for the following weight function cases:

- Uni-varient weight function cases: TC11, TC12, TC13, TC17, TC18, TC19, CC08, CC11, SC17, SC18, EC02, and EC05.
- Bi-varient weight function cases: CC09, CC10, CC12, SC19, and EC04.



Schematic diagram illustrating t1/t2 stress gradients

To perform NASFLA analysis with the t1/t2 capabilities, go through the following three additional steps:

- Check “t1/t2 stress gradients” on Geometry tab to turn on the capabilities.
- Specify stress gradients for time instants t_1 and t_2 in the similar way as in tension/compression capabilities, either by 1-D tables or by files.
- If limit stress check is enabled, designate stress gradients for limit stresses in Load Blocks tab. The limit stress gradient can be either the stress gradient for t_1 , or the one for t_2 .

C10.2 Optimum Point Spacing

An “Optimum Point Spacing” option is available for many weight function solutions (some univariant and all bivariant solutions) that relaxes some restrictions on data entry. For the univariant mode, the allowable number of points increases from 50 to 500. For the bivariant mode, the allowable size of the matrix increases from 20 x 20 to an unlimited size (within the practical limits of available computer memory), and the positions of the stress values no longer have to be equally spaced.

When the OPS option is invoked, the OPS algorithm evaluates the user-provided stress vs. position points and processes them to create a smooth stress surface that captures the stress variations with a generally smaller number of points needed for an accurate description. Using a Hermite interpolation of the original data as a reference curve, the resulting OPS stress gradient is accurate to within 0.1% of the user-defined stress values. By choosing a smaller number of points needed for adequate accuracy, the OPS algorithm also generally improves the efficiency (speed) of the subsequent stress intensity factor calculation. Stress visualization options in the NASGRO GUI permit the user to evaluate the quality of the resulting OPS description.

C10.3 Stress Visualization

A “Plot Stresses” button on the Geometry tab permits the user to visualize the univariant or bivariant stress field based either on the original user-supplied values or the calculated OPS values.

Figure OPS2 shows the graph generated for a univariant stress distribution based on user-specified point spacing. This distribution was supplied as fifty stress values unequally spaced with a bias towards the steeper region of the stress gradient.

Figure OPS3 shows the graph for the same univariant stress input evaluated using the OPS option. The graph shows the control knots generated from the local slope of the Hermite curve used to determine optimum intervals for the generated points, as well as the points generated from the OPS algorithm that will be used in subsequent stress intensity factor calculations.

For bivariant stresses, multiple plotting options are available. The original user data can be visualized as a surface, employing linear interpolation between given stress values on the rectangular grid (see Figure OPS4). If the OPS option is selected, the generated OPS points can be graphed as a color gradient surface map, with a separate contour map on the base (see Figure OPS5). Also available is a combination plot containing the OPS data plotted as a surface and the original user data as points on that surface (see Figure OPS6).

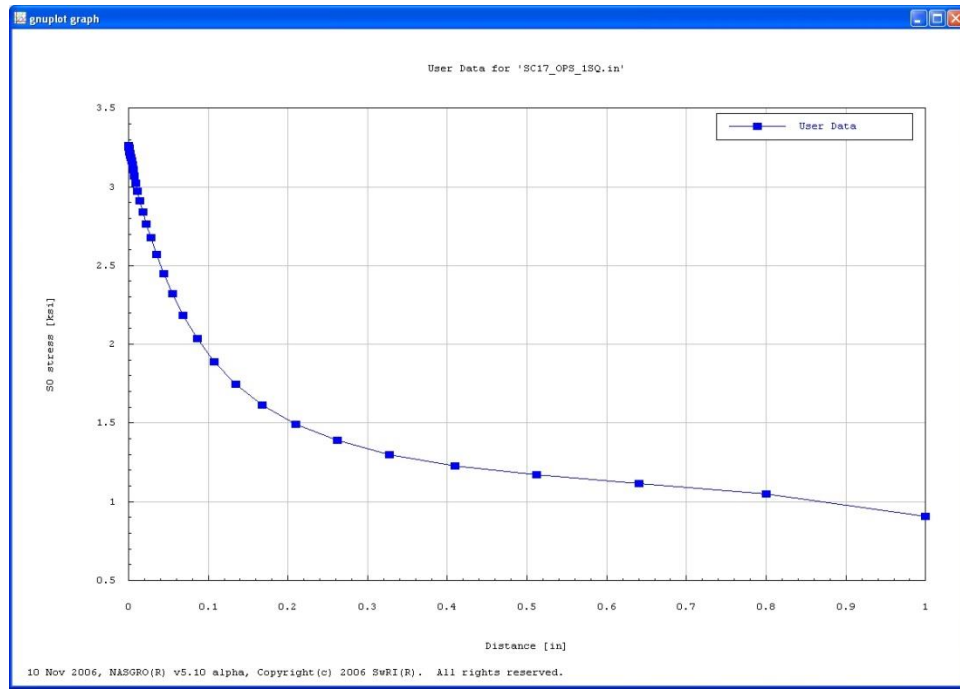


Figure OPS2: Sample NASGRO plot of user-specified point spacing

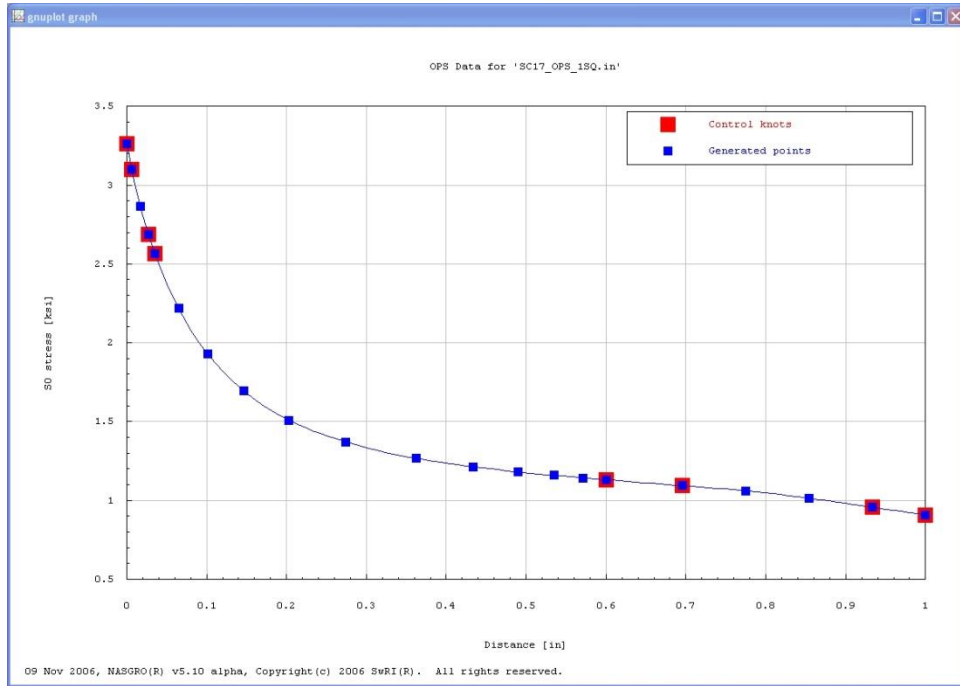


Figure OPS3: Sample NASGRO plot of OPS results for user-specified point spacing shown in Figure OPS2

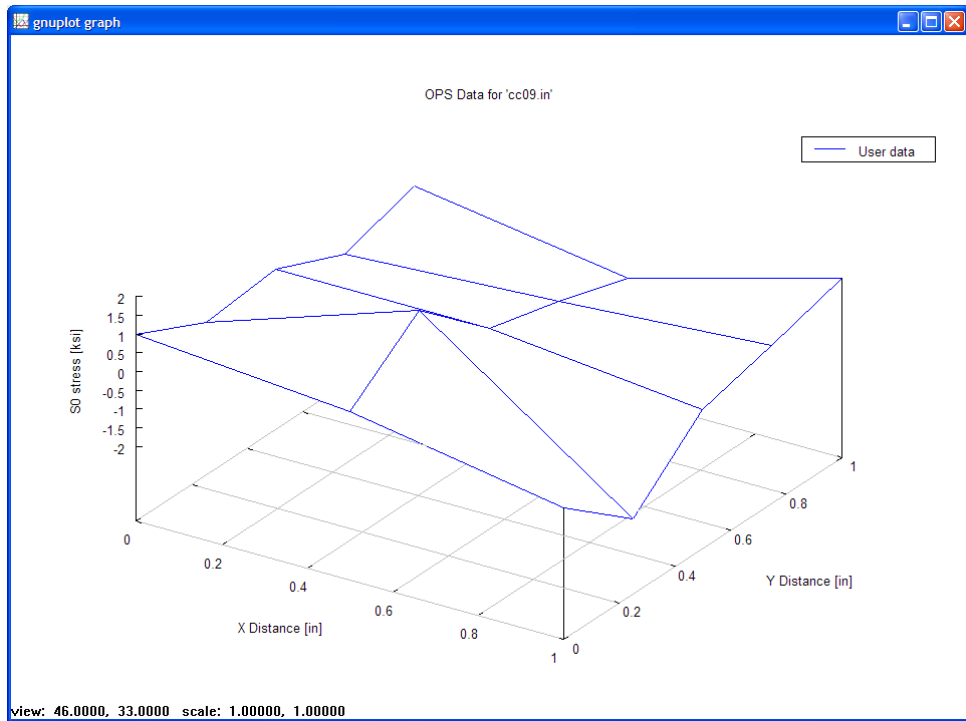


Figure OPS4: User-provided bivariant stress input, plotted as a surface

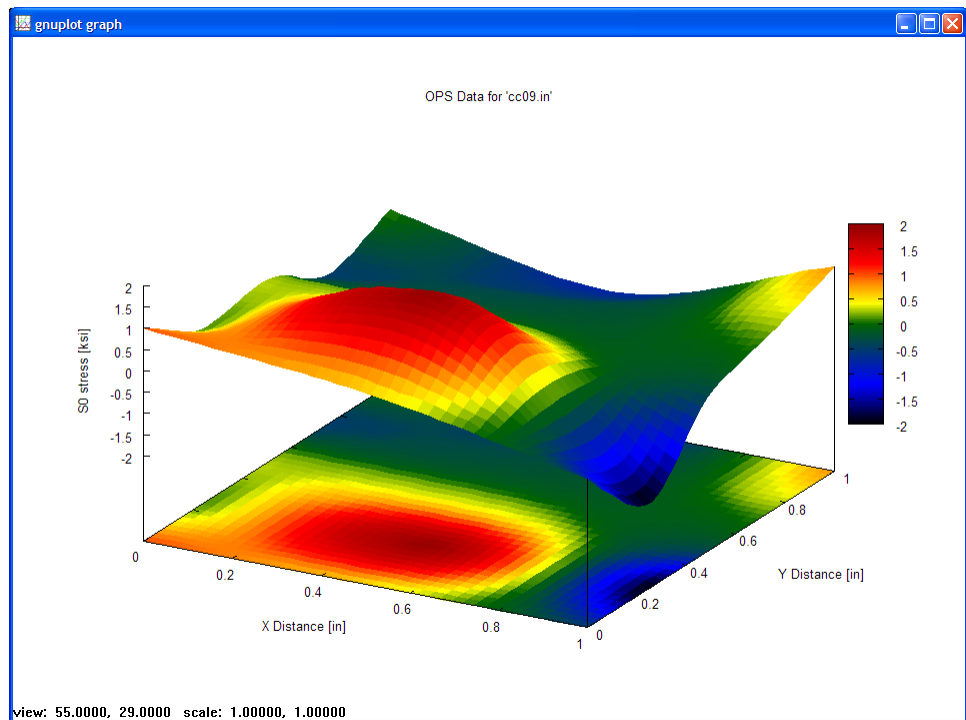


Figure OPS5: OPS generated data, plotted as a surface with color gradient, with an additional contour plot provided at the base.

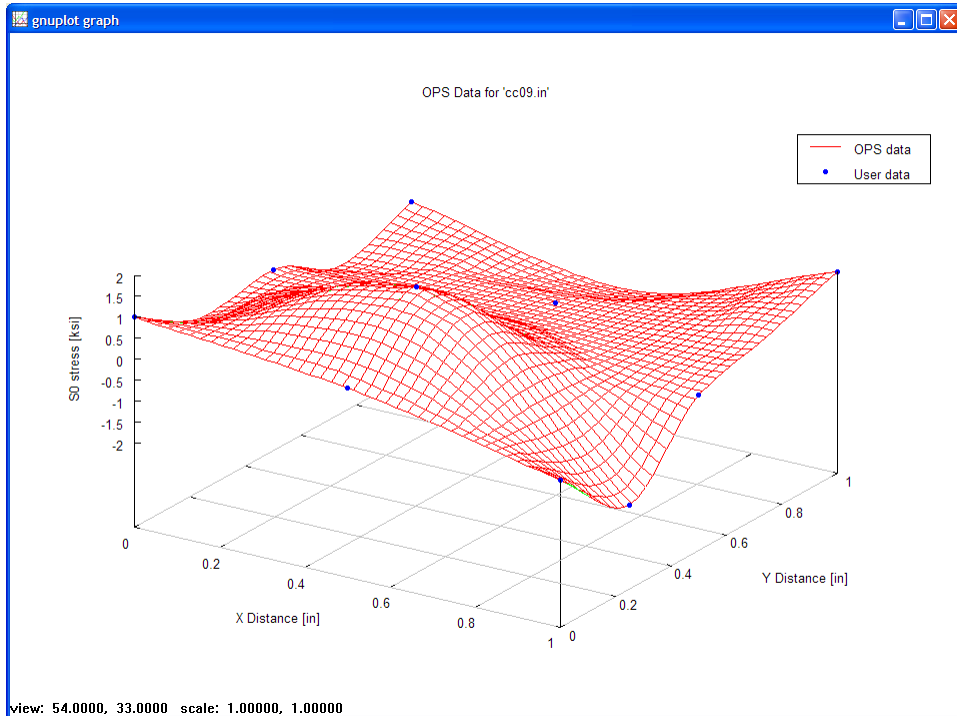


Figure OPS6: Combination plot showing both OPS generated data (surface) and the User-provided data (points on that surface).

C10.4 Residual Stress

An option to superimpose a user-supplied static residual stress is available for many of the univariant and all of the bivariant weight function SIF solutions. Residual stresses cannot currently be included in SIF solutions that are not based on weight functions. The static residual stress defined by the user is applied at each time step (both maximum and minimum turning points) and is not affected by the spectrum scale factors. This residual stress option might be used to account for initial residual stress fields resulting from shot peening, laser shock peening, cold expansion of holes, welding, forging, machining, or other manufacturing processes that cause local plastic deformation. The user would be required to measure or calculate the residual stress fields outside of NASGRO and then input the results into NASGRO as another stress gradient.

Residual stress input follows the same general protocols as regular stress gradient input, although fewer options are available. Residual stress input must be provided in tabular form; polynomial series input is not allowed. For univariant stress intensity factor solutions, residual stresses can be entered directly from the keyboard into the GUI, or they can be entered from a file. For direct keyboard entry, the residual stress table has a blue-grey background to remind the user this is the entry point for the static residual stress gradient, not the regular stress gradient. For file entry, the standard NASGRO file format for univariant stress gradients is applicable, but the univariant full stress tensor file format is not available for residual stress input. For bivariant stress intensity factor solutions, file input is the only input option available for residual stress. Either the historical

NASGRO bivariant format or the alternative bivariant format may be employed. Whichever of these two file formats is selected for the regular (alternating) stress gradient input must also be used for the residual stress input.

The point spacing and number of points for the (static) residual stress gradient does not have to be the same as the point spacing and number of points for the regular (alternating) stress gradient. In order to facilitate the combination of two stress gradients that likely have different length scales, NASGRO will automatically select the Optimum Point Spacing (OPS) option whenever the residual stress input option is selected. This selection of OPS cannot be overridden in this case.

Because the shakedown calculation involves the calculation of a residual stress field based on a simple elastic-plastic model that assumes no initial plasticity, and because the presence of an initial residual stress implies that some prior plastic deformation has occurred, it is not currently possible to select both the shakedown and residual stress input options. The user may choose one or the other, but not both at the same time.

The stress intensity factor is calculated based on linear superposition of the contributions from fatigue (alternating) stresses and (static) residual stresses. However, the contributions of the static residual stress to the net-section stress failure criterion are currently neglected. Although the residual stress will have some influence on the nominal stresses on the net section of the cracked body, it is known that a residual stress does not contribute to plastic collapse (actual net section failure due to yielding), and so this omission is not thought to be significant.

IMPORTANT NOTE: Under some conditions, an initial static residual stress field can change during service, especially under the influence of applied cyclic loading. The most common behavior is for the initial static residual stress field to partially relax and be redistributed. If the initial static residual stresses are compressive and therefore beneficial (reducing the fatigue crack growth rate), then this relaxation and redistribution may reduce or even eliminate the benefit of the residual stresses. These changes in the original residual stress fields are most likely at elevated temperatures, when the superposition of the residual stress and applied stress causes local yielding, or when a crack grows through a regime of tensile residual stress. The NASGRO software does not currently address these potential changes in the residual stress field. Therefore, it is the responsibility of the user to ensure that significant changes in the residual stress field do not occur, or to compensate for these changes through an appropriate selection of the initial residual stress field.

C10.5 Cyclic Shakedown

Theory

In some situations the calculated local elastic stresses in a component may exceed the yield strength of the material, especially near a stress concentration such as a hole or slot. When this happens, the most common result is for yielding to occur locally. This local yielding usually causes a local decrease in the stresses from their calculated elastic values, as well as some local redistribution of stresses to maintain equilibrium (and the stress redistribution may cause some

local stress values to increase). If the calculated local elastic stress range exceeds twice the yield strength (for example, when applied stresses are fully reversed and the maximum stresses exceed the yield strength), then reversed yielding may occur (and may occur repeatedly).

The correct local stress values associated with the load history can generally be computed with elastic-plastic finite element analysis, but this may introduce too much complexity (and time) to the analysis for practical purposes. Furthermore, if the yielding only occurs in at a few isolated locations, then alternative methods may provide acceptable results with substantially less effort.

One such alternative method is a so-called “shakedown” algorithm available in NASGRO. The basic input to this algorithm is the calculated elastic stress distribution in the region of interest. This algorithm uses approximate methods to estimate the local elastic-plastic stress redistribution and relaxation resulting from local yielding. The new stress gradients are then used as input to weight function stress intensity factor solutions. Currently the shakedown algorithm can only be used with univariant weight function stress intensity solutions employing tabular input of stresses. The NASGRO shakedown algorithm can accommodate reversed yielding on subsequent fatigue cycles, and so it is called a “cyclic” shakedown algorithm.

The methodology used in cyclic shakedown analysis is described and illustrated in Appendix M.

Availability

In the current version of NASGRO, the following univariant weight function stress intensity factor solutions allow the use of shakedown: TC13, CC08, CC11, SC17, EC02, and EC05.

The shakedown capability is currently only available in the NASFLA module, and not in the NASSIF or NASCCS modules.

Cyclic Shakedown Model Options

If cyclic shakedown is enabled, two calculation modes are available.

The “automatic” mode will evaluate the elastic stress range associated with each load step and determine if non-negligible yielding will occur locally. If non-negligible yielding is determined to occur, then an appropriate shakedown calculation will be conducted. If non-negligible yielding is not determined to occur, then no shakedown calculation will be conducted.

The “full cyclic” mode will perform a shakedown calculation on every reversal in the history. This mode can substantially increase NASGRO computation time. The “full cyclic” mode should give nearly identical results to the “automatic” mode, but there may be some small differences due to the “automatic” mode neglecting very small amounts of plasticity occurring on some cycles.

Stress Input Options

As noted earlier, several options are available to input the (original elastic) stress gradient information along the crack line. The primary choice is whether the user will input only the stress

values normal to the crack plane along the crack line, or whether the user will input the full stress tensor along the crack line. In some cases, the user only knows the stress values normal to the crack plane. In other cases, the user may have finite element results that provide full stress tensor information.

The shakedown algorithm involves a plasticity calculation incorporating all components of the stress tensor. If only the stress values normal to the crack plane are provided, then NASGRO assumes that the other elastic stresses in the tensor are zero, and proceeds to do the shakedown calculation on this basis. In general, the other values in the stress tensor not normal to the crack plane are usually much smaller than the values normal to the crack plane, but they are still nonzero, and neglecting them will introduce some small error into the shakedown calculation.

When the shakedown option is selected, if the user is providing only the stress values normal to the crack plane along the crack line, then those stress values can either be entered directly from the keyboard into the GUI table, or via a file in standard NASGRO univariant format. If the full stress tensor option is selected, then stress input must be performed through a file. The specific file formats were documented earlier.

Note that in general, the coordinate system defined by the univariant weight function crack geometry bitmaps in NASGRO is

- x – in the crack plane in the width direction
- y – in the crack plane in the thickness direction
- z – normal to the crack plane

The exceptions to this coordinate system are CC11 and SC17, where x denotes the thickness direction in the crack plane, and y denotes the width direction in the crack plane.

In either case (input the crack plane stresses only, or input the full stress tensor, the shakedown algorithm calculates the full elastic-plastic stress tensor but passes only the elastic-plastic S_{zz} component (the stress normal to the crack plane, sometimes called the Mode I opening stress) to the stress intensity factor subroutine to determine K_{\max} and ΔK .

In the absence of plasticity effects, the additional terms in the stress tensor have no effect on the calculation of the stress intensity factor or the fatigue crack growth rate.

Required Material Input

In order to perform the shakedown calculation, NASGRO needs information about the elastic-plastic constitutive behavior of the material, and these data are not contained in the standard NASGRO materials database. NASGRO requires that the constitutive response be characterized by a Ramberg-Osgood type of equation in the general form

$$\frac{\varepsilon}{\varepsilon_0} = \frac{\sigma}{\sigma_0} + \alpha \left(\frac{\sigma}{\sigma_0} \right)^n$$

where

α = Ramberg-Osgood coefficient

n = Ramberg-Osgood exponent

σ_0 = Ramberg-Osgood yield stress

ε_0 = Ramberg-Osgood yield strain, where $\varepsilon_0 = \sigma_0/E$, and E = (Young's) elastic modulus

These values are often determined from a regression of uniaxial tensile data in terms of true stress and true strain. NASGRO also requires input of the Poisson ratio, ν , to support the plasticity calculations.

In some cases, the user may not have sufficient data to determine the Ramberg-Osgood constants. However, if basic tensile information (yield and ultimate strengths) is available, then it is possible to estimate the Ramberg-Osgood constants. It can be shown (Bannantine, et al, 1990) that the Ramberg-Osgood exponent, n , is related approximately to the ratio of yield and ultimate strengths by the expression

$$\frac{\sigma_{ult}}{\sigma_{ys}} = \left\{ \frac{1}{n(0.002)} \right\}^{\frac{1}{n}} \exp\left(-\frac{1}{n}\right)$$

when α is set equal to 1.0 and the yield strength σ_{ys} corresponds to a 0.2 percent (0.002) offset. In this particular expression, σ_{ys} and σ_{ult} are engineering quantities and n is the exponent in a true stress-true strain relationship. Note that direct computation of n from σ_{ult}/σ_{ys} requires an iterative solution (inversion) of the equation. Once n is determined, then σ_0 can be estimated from

$$\sigma_0 = \left\{ \frac{0.002 E}{(\sigma_{ys})^n} \right\}^{\frac{1}{1-n}}$$

and ε_0 is given by $\varepsilon_0 = \sigma_0/E$.

Beginning with NASGRO 6.0, the Ramberg-Osgood material constants are entered on the "Material" tab. These values are only requested when the "Shakedown" option is selected on the "Geometry" tab.

Output from Shakedown Module

The shakedown stress distribution calculated and used by NASGRO is provided in NASGRO output files. A tabular summary is included in the *.out1 file. This tabular summary can be viewed in the output window on the "Computations" tab by selecting "Input: Geometry". The tabular summary includes the following data:

- The original elastic stress gradient values at the original user point spacing
- The calculated shakedown-modified elastic-plastic stress gradient values, and the calculated shakedown residual stress values

- At the uneven point spacing used by NASGRO
- At a common (also uneven) point spacing, to facilitate plotting

All of the stress distribution data are also written to a separate *_stress.csv file that can be opened in Excel (and therefore easily plotted in Excel). The NASGRO GUI does not currently allow direct plotting of the shakedown stresses in the GUI.

Reference:

Bannantine, J. A., Comer, J. J., and Handrock, J. L., *Fundamentals of Metal Fatigue Analysis*, Prentice Hall, 1990.

Section C11: Compounding

1. Introduction

The purpose of this feature is to allow compounding of stress intensity solutions in order to account for other loading or geometry influences, determining total stress intensity factors by multiplying the primary stress intensity factors with compounding factors.

The 1-D and 2-D tabular compounding capabilities are implemented for NASFLA and NASSIF. The 1-D tabular compounding means compounding factors are specified by 1-D tables. For a 2-D crack case, which has two independent crack tips (a-tip and c-tip), the 1-D tables are specified separately in the a- and c-direction. In the 2-D tabular compounding, compounding factors are entered by 2-D tables as a function of two independent variables, crack size and crack aspect ratio. All the through cracks, all corner cracks, and all 1-D/2-D surface cracks are provided with 1-D tabular compounding capabilities:

- Through cracks:
TC01, TC02, TC03, TC04, TC05, TC06, TC07, TC08, TC09, TC10, TC11, TC12, TC13, TC14, TC15, TC16, TC17, TC18, TC19, and TC23.
- Corner cracks:
CC01, CC02, CC03, CC04, CC05, CC07, CC08, CC09, CC10, CC11, CC12, CC13, CC14, CC15, and CC16.
- 1-D/2-D surface cracks:
SC01, SC02, SC03, SC04, SC05, SC06, SC07, SC08, SC09, SC10, SC11, SC12, SC13, SC14, SC15, SC17 (symmetric), SC18 (symmetric), SC26 (symmetric), SC27 (symmetric), and SC28 (symmetric).

Only crack case CC02 is provided now with 2-D tabular compounding; but is extensible to other crack cases if a need develops. Note that net section yield analysis (NSY) will be conducted in the usual manner even if SIF compounding is activated, i.e., with the compounding factors playing no part in the NSY analysis.

Compounding is not available if shakedown or residual stress is enabled.

For each crack tip under each stress quantity, up to four compounding tables, i.e. multiple compounding, are allowed for a user to specify compounding factors. The compounding factor at a given crack size is calculated based on user-specified interpolation scheme. Three interpolation schemes, i.e. piece-wise linear, Hermite, and cubic spline are available for 1-D tabular compounding, while only cubic spline is available for 2-D tabular compounding. The calculated compounding factors are multiplied with the primary SIF-correction factors to obtain the total SIF-correction factors. The primary SIF-correction factors are the SIF-correction factors calculated directly from the geometry model. The total SIF-correction factor ($F_{i,T}$) and total stress intensity factor (K) can be expressed by

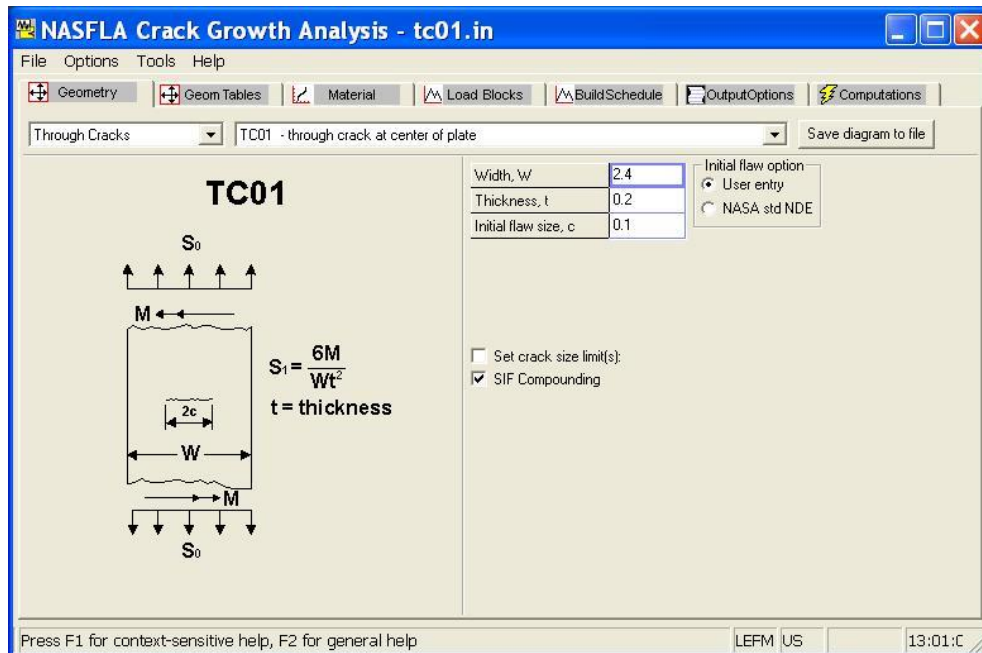
$$F_{i,T} = F_{i,P} \cdot \left(\prod_{j=1}^{n_i} F_{i,j}^c \right)$$

$$K = \sum_{i=1}^n F_{i,T} \cdot S_i \sqrt{\pi a}$$

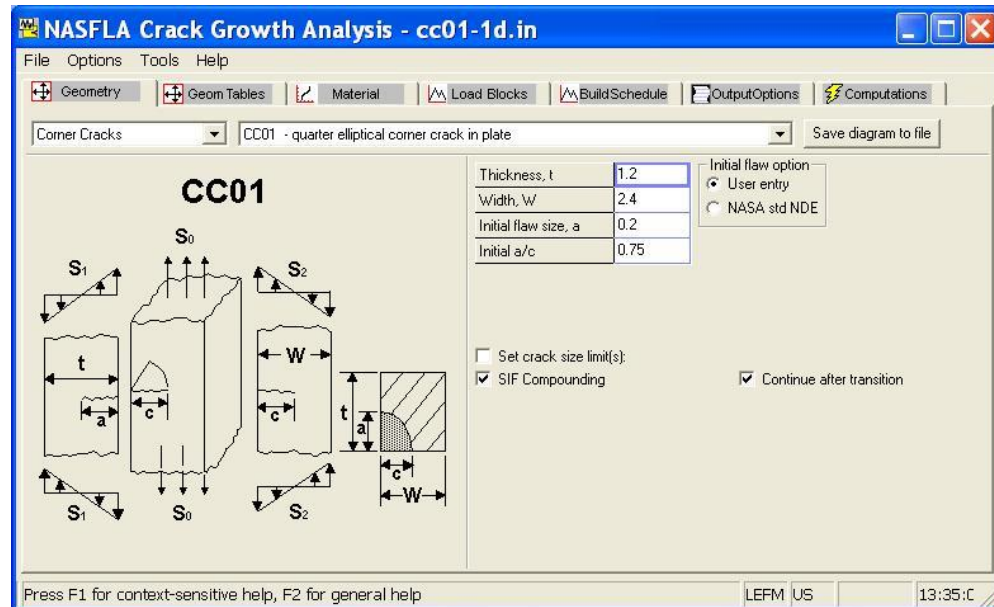
where n_i is the number of compounding tables for the i th stress (S_i). $F_{i,p}$ denotes the primary SIF-correction factors. $F_{i,j}^c$ is the compounding factor calculated by interpolating off the j th compounding table of the i th stress with the current crack size(s), where n is the number of stress quantities.

2. Performing analysis with compounding

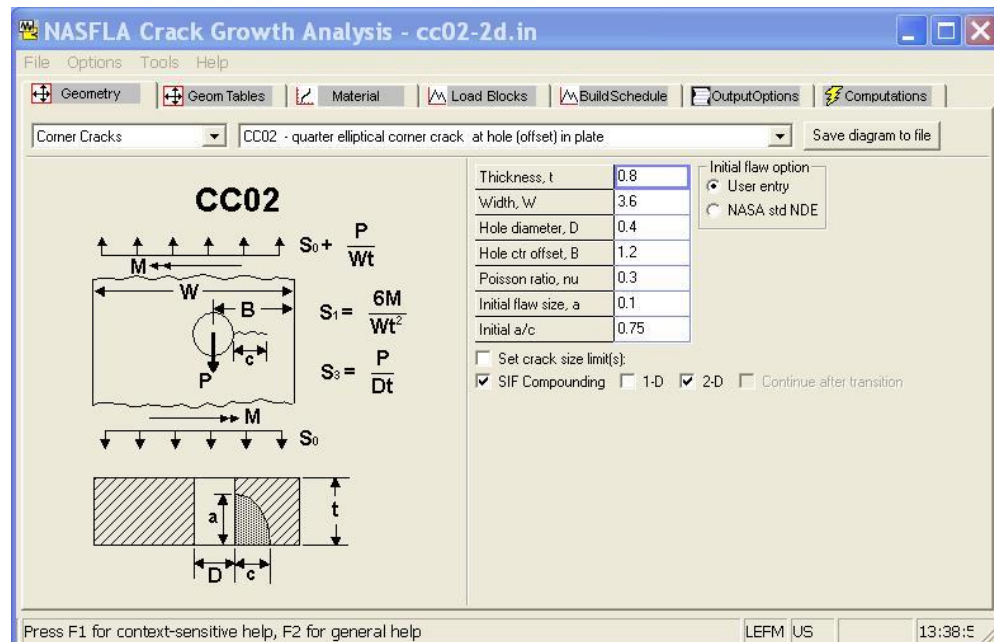
The entry door to specifying compounding is on the Geometry tab of the GUI. A user can turn it on by clicking on the “SIF Compounding” checkbox, as shown in the figure below.



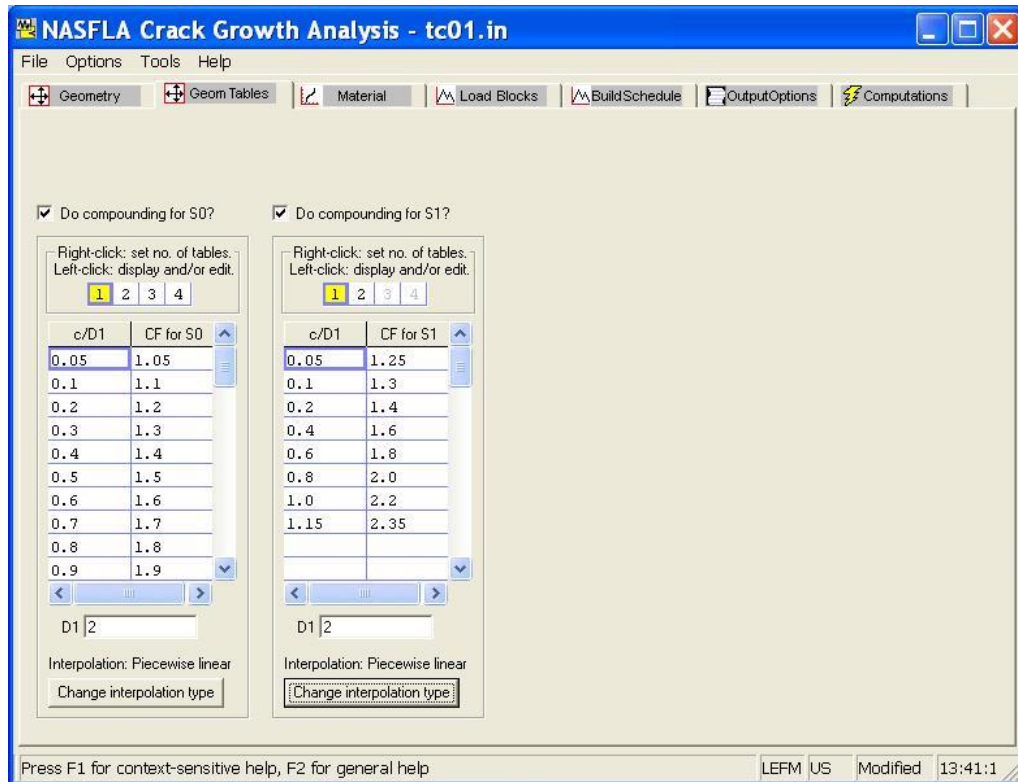
For the crack cases with transition capabilities, when “SIF Compounding” checkbox is checked, another checkbox (“Continue after transition”) will come out, as shown in the figure below. The checkbox is unchecked by default, which means that compounding will be turned off by default after transition. A user can check it to allow compounding to continue for the post-transition model. If the checkbox is checked, a warning window will pop up to let the user confirm that compounding will be performed after transition.



For crack cases with both 1-D and 2-D tabular compounding capabilities, after “SIF Compounding” checkbox is activated, the user can select compounding type by clicking on either 1-D or 2-D checkbox, as shown below. If 2-D tabular compounding is selected, the checkbox “Continue after transition” will be automatically grayed out, which means compounding after transition will be turned off because 2-D tabular compounding does not make sense after transition, and will not be attempted.



Once compounding is activated, a user can specify compounding factors on “Geom Tables” tab by the following steps as shown in the figure below:



- Click checkbox “Do compounding” for each stress quantity if compounding is needed for it. Then, for each stress quantity,
 - Set the number of compounding tables. And for each compounding table:
 - Enter compounding factors. If 1-D tabular compounding is activated, enter compounding factors in 1-D tables. If 2-D tabular compounding is selected, enter compounding factors in 2-D tables. For each compounding table, enter D1, which is the dimension used to define non-dimensional crack size of the table. The default value of D1 is 1.0.
 - Select proper interpolation scheme for each compounding table. For 2-D tabular compounding, skip this step.

If it is a 2-D crack case, which has two independent crack tips (a-tip and c-tip), perform the above steps for each crack tip.

If user-specified crack size is beyond the bounds of the compounding table, an error message will be printed out. If crack size is growing outside of the upper bound of the compounding table, the computation will be terminated.

3. Compounding Output

When an analysis is performed using compounding, an additional plain text output file is created by NASFLA with an “out3” extension. The first few columns of this file are similar to that contained in the “out2” file listing the schedules, steps, cycles,

flights/hours and crack lengths. The remaining columns of the “out3” file summarize all the individual compounding factors (by each stress component and compounding table) along with the total combined compounding factor for each stress component.

Depending on the number of active crack tips, how many stress components are being used, and how many compounding tables are entered for each component, the number of columns in the “out3” file can be quite extensive. The column headings in the “out3” file are defined as follows:

FP_i = stress intensity geometry factor associated with stress S_i before compounding, i.e., the primary correction factor calculated directly from the geometry model

CF_{ij} = compounding factor associated with stress S_i from compounding table “j”

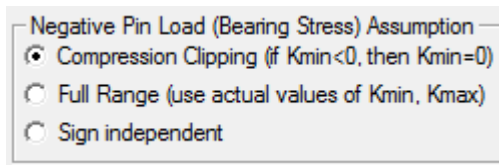
F_i = stress intensity geometry factor associated with stress S_i after compounding

Each of the above quantities is printed in the “out3” file for each crack tip. As with the “out2” file, the “out3” data can be saved to a spreadsheet file by clicking on the “All Calc’d data to csv file” button on the Computations page. They can also be plotted by selecting “Compounding data” in the “Select details to plot” window.

Section C12: Pin Load Options

This section describes options for treatment of negative pin load (Bearing Stress, S3) – implemented in NASGRO v6.2. For crack cases in which pin loads are present, the treatment of negative pin loads was modified in v6.2 to allow the user to specify the option for computing K. While this sub-section refers to and lists pin-load specifiable crack cases below that existed prior to v6.2, all newer crack cases (added post v6.2) in which pin loads are present also allow specification of this option.

These options appear on the Geometry page of the NASFLA GUI as shown below and pertain only to bearing stresses (S3):



This change pertains to the pin-load crack cases: TC03, TC04, TC05, TC10, CC02, CC03, CC04, CC07, SC11 and SC12. The first option (compression clipping) uses only the positive side of the cycle, setting negative Ks equal to zero. *This option was added in v6.2 and is now the default; it is deemed more realistic than the second option.* The second, more conservative option is to use the full range of K (from a negative minimum to a positive maximum K) and it is still available. The third option, which splits the full range into two independent cycles (one from zero to $|K_{min}|$ and the other from zero to K_{max}), is available only for TC03, TC05 and TC09, with TC09 having only this option available.

In NASGRO v6.1 and earlier, some models (the lugs, TC04 and CC03) used compression clipping, others used the full range approach (CC04, CC07, SC11 and SC12), and still others used the two sign-independent cycles approach (TC03, TC05), while TC10 and CC02 used a mixed approach. This caused inconsistencies when comparing results and was confusing. In NASGRO v6.2, the compression clipping option was made the default; however, the full range approach is also available. The capability to use the third option was retained in v6.2 for those models that previously had it: TC03 and TC05. The calculation for TC09, however, remains unchanged from v6.1 and only has the third option available. See the summary table on the next page for additional details. Note that previously existing input files (*nasfla.in*) created with earlier NASGRO versions will be loaded into the v6.2 (and later) versions retaining the previously run option, if available. Otherwise, the default option described herein will be used.

Pin Load Options by Crack Case for NASGRO v6.2 Compared with Previous Approaches

Part Type	Pin-Loaded Crack Cases	Transitions to Pin-Loaded Crack Case	Previous Approach (NASGRO v6.1 & Earlier)	Options Implemented for NASGRO v6.2		
				Compression Clipping	Full Range	Two Sign-Independent Cycles
Plate	TC03	TC02 (a)	Two Sign-Indep Cycles	X	X	X
Lug	TC04	none	Compression Clipped	X	X	
Plate	TC05	none	Two Sign-Indep Cycles	X	X	X
Plate	TC09	none	Two Sign-Indep Cycles			X
Tube	TC10	none	Full Range	X	X	
Plate	CC02	TC03	Mixed (c)	X	X	
Lug	CC03	TC04	Compression Clipped	X	X	
Plate	CC04 (b)	TC03	Mixed (c)	X	X	
Plate	CC07 (b)	TC03	Mixed (c)	X	X	
Plate	SC11	TC03	Mixed (c)	X	X	
Lug	SC12	TC04	Full Range	X	X	

Notes:

- (a) Pin load converted to equivalent Tension + Bending after transition to TC02.
- (b) GUI graphic revised to show wavy bottom of plate to remove impression that these models could be lugs.
- (c) These confusing mixed approaches (details omitted) will no longer be used.

X	Default option
X	Option available
	Option not available

Section C13: Sign-Independent Load Approximation

Mention has already been made in Section C12 about an option under *Negative Pin Load (Bearing Stress) Assumption* called *Sign Independent* which is available to the user for crack cases TC03, TC05 and TC09. This condition of sign independence prevails also for through-the-thickness bending, S_1 , for through-crack cases: TC01, TC02, TC03 and TC09.

In cases where sign-independent loads alone are present, the crack tip experiences two cycles of crack opening for each (nominal) cycle when K_{max} and K_{min} are of equal magnitude and opposite sign. A factor, μ , is used to multiply the crack-growth rate when doing a life calculation to account for the two cycles, with $\Delta K = |K_{max}|$, actually present in this case for each cycle nominally entered for the calculation.

However, when either of the following conditions prevail:

1. Sign-independent loads of stress ratio: $R < 0$ and $R \neq -1$ are alone present [No sign-dependent loads]
2. Sign-independent and sign-dependent loads are both present

the code uses special logic to obtain the value of the crack-growth-rate multiplier, μ . The value of μ ranges between 1 and 2. The value 1 corresponds to the case when sign-independent loads are absent altogether, and the limiting value 2 corresponds to the case when sign-independent loads of stress ratio $R = -1$ are the only loads that are present.

The presence of sign-independent loads almost always results in an increase in the actual (but not nominal output value of the) cycle count experienced by the crack. However, the value of the multiplier, μ , used by the code is an approximation, since it uses the same multiplier on the cycle count as the factor multiplying ΔK of the first cycle (to obtain ΔK during the second cycle). However, the extremal values 1 and 2 of μ may indeed be considered to be “exact”.

Section C14: Surface Crack Closure Correction Factor

As discussed in Section 2.1.2 of the main NASGRO manual, Newman and Raju have shown that for constant amplitude fatigue loading, multiplying ΔK by a crack-closure factor, β_R , produces more accurate crack growth predictions for semi-elliptical surface cracks and quarter-elliptical corner cracks. This β_R factor is only applied at points where the part-through crack front intersects a free surface, and it is a function of the stress ratio. For $R > 0$, β_R is given by:

$$\beta_R = 0.9 + 0.2R^2 - 0.1R^4$$

and for $R \leq 0$, β_R is assumed to have a value of 0.9. In NASGRO, ΔK is multiplied by β_R for many, but not all, corner crack and surface crack models. Note that for some of the advanced crack cases such as CC09, this factor has deliberately been omitted at the present time in order to maintain conservatism until further study can be completed. A complete listing of which crack cases use or do not use the β_R factor is provided in the following table. It is important to be aware that this near-surface correction is applied only in NASFLA (to ΔK for crack growth calculations) and is not used in NASSIF.

Application of Surface Crack Closure Correction Factor to SIF Models

Surface crack models														
Crack case	Crack closure factor (β_R) used				Crack case	Crack closure factor (β_R) used								
	a-tip	c-tip	a1-tip	c1-tip		a-tip	c-tip	a1-tip	c1-tip					
SC01	No	Yes	N.A.	N.A.	SC13	No	N.A.							
SC02	No	Yes			SC14	No	N.A.							
SC03	No	Yes			SC17	No	Yes	N.A.	Yes					
SC04	No	Yes			SC18	Yes	No	Yes	N.A.					
SC05	No	Yes			SC19	No	Yes	N.A.	Yes					
SC06	No	N.A.				SC26	Yes	No	Yes					
SC07	No	SC27			Yes	No	Yes	N.A.						
SC08	No	SC28			Yes	No	Yes							
SC09	No	SC30			No	Yes	N.A.	Yes						
SC10	No	SC31			No	Yes	N.A.	Yes						
SC11	Yes	No	N.A.		SC32	Yes	No	Yes	N.A.					
SC12	Yes	No												
Corner crack models														
Crack case	Crack closure factor (β_R) used				Crack case	Crack closure factor (β_R) used								
	a-tip	c-tip	a1-tip	c1-tip		a-tip	c-tip	a1-tip	c1-tip					
CC01	Yes	Yes	N.A.	N.A.	CC13	No	No	N.A.						
CC02	Yes	Yes			CC14	Yes	Yes							
CC03	Yes	Yes			CC15	No	No							
CC04	Yes	Yes			CC16	Yes	Yes							
CC07	Yes	Yes			CC17	Yes	Yes	Yes	Yes					
CC08	Yes	Yes			CC19	Yes	Yes	N.A.						
CC09	No	No			CC20	Yes	Yes							
CC10	Yes	Yes			CC21	Yes	Yes							
CC11	No	No			CC22	Yes	Yes							
CC12	No	No			CC23	Yes	Yes							
Standard specimens														
Crack case	Crack closure factor (β_R) used				Crack case	Crack closure factor (β_R) used								
	a-tip	c-tip	a1-tip	c1-tip		a-tip	c-tip	a1-tip	c1-tip					
SS08	Yes	No	N.A.		SS11	Yes	Yes	N.A.						
SS09	Yes	Yes												
Boundary element solutions and Hybrid crack model														
Crack case	Crack closure factor (β_R) used													
	a-tip	c-tip	a1-tip	c1-tip										
BE03	Yes	Yes	N.A.											
HC01	Yes	Yes	N.A.											
Color-coded solution type:														
	Uni-variant weight function solution													
	Bi-variant weight function solution													
	Displacement-controlled crack model													

Note: Entries in **bold red font** indicate fixes and changes made in v8.2f.

Section C15: References

- [C1] Fedderson, C. E., Discussion of “Plane Strain Crack Toughness Testing of High Strength Metallic Materials,” by W. F. Brown, Jr., and J. E. Srawley, ASTM STP 410, American Society for Testing and Materials, Philadelphia, 1966, pp. 77-79.
- [C2] Paris, P. C., and Sih, G. C., “Stress Analysis of Cracks,” ASTM STP 381, American Society for Testing and Materials, Philadelphia, 1964, pp. 30-81.
- [C3] Tada, H., Paris, P. C., and Irwin, G. R., *The Stress Analysis of Cracks Handbook*, Del Research Corporation, Hellertown, PA, 1973.
- [C4] Shivakumar, V., and Hsu, Y. C., “Stress Intensity Factors for Cracks Emanating from the Loaded Fastener Hole,” presented at the International Conference on Fracture Mechanics and Technology, Hong Kong, March 1977.
- [C5] Zatz, I. J., Eidinoff, H. L., and Armen, H., Jr., “An Application of the Energy Release Rate Concept to Crack Growth in Attachment Lugs,” AIAA paper No. 81-0491.
- [C6] Isida, M., “Laurent Series Expansion for Internal Crack Problems,” in *Methods of Analysis and Solutions of Crack Problems*, Sih, G. C. (Editor), Noordhoff International Publishing, Leyden, 1973, pp. 56-130.
- [C7] Yeh, F., Mettu, S.R., “Stress Intensity Factors for a through Crack from an Offset Hole in a Finite Plate by Boundary Element Method”, JSC 28935, March 2000.
- [C8] Shivakumar, V., Forman, R. G., and Rosencranz, R., Jr., “Green’s Function Solution and Applications for Cracks Emanating from a Circular Hole in an Infinite Sheet,” *Res Mechanica*, Vol. 9, 1983, pp. 87-104.
- [C9] Newman, J. C., Jr., “Fracture Analysis of Surface and Through Cracks in Cylindrical Pressure Vessels,” NASA TN D-8325, December 1976.
- [C10] Forman, R. G., Hickman, J. C., and Shivakumar, V., “Stress Intensity Factors for Circumferential Through Cracks in Hollow Cylinders Subjected to Combined Tension and Bending Loads,” *Engineering Fracture Mechanics*, Vol. 21, No. 3, 1985, pp. 563-571.
- [C11] Shivakumar, V., and Forman, R. G., “Green’s Function for a Crack Emanating from a Circular Hole in an Infinite Sheet,” *International Journal of Fracture*, Vol. 16, No. 4, August 1980, pp. 305-316.

- [C12] Roberts, R., and Rich, T., "Stress Intensity Factors for Plate Bending," *Trans. ASME, Journal of Applied Mechanics*, Vol. 34, No. 3, September 1967, pp. 777-779.
- [C13] Newman, J. C., Jr., and Raju, I. S., "Stress Intensity Factor Equations for Cracks in Three-Dimensional Finite Bodies Subjected to Tension and Bending Loads," NASA TM 85793.
- [C14] Raju, I. S., Mettu, S. R., and Shivakumar, V., "Stress Intensity Factor Solutions for Surface Cracks in Flat Plates Subjected to Nonuniform Stresses," *Fracture Mechanics: Twenty-Fourth Volume*, ASTM STP 1207, J. D. Landes, D. E. McCabe, and J. A. M. Boulet, Eds., American Society for Testing and Materials, Philadelphia, 1994, pp. 560-580.
- [C15] Forman, R. G., and Shivakumar, V., "Growth Behavior of Surface Cracks in the Circumferential Plane of Solid and Hollow Cylinders," *Fracture Mechanics: Seventeenth Volume*, ASTM STP 905, J. H. Underwood, R. Chait, C. W. Smith, D. P. Wilhelm, W. A. Andrews, and J. C. Newman, Eds., American Society for Testing and Materials, Philadelphia, 1986, pp. 59-74.
- [C16] Newman, J. C., Jr., and Raju, I. S., "Stress Intensity Factors for Internal Surface Cracks in Cylindrical Pressure Vessels," NASA TM 80073, July 1979.
- [C17] Raju, I. S., and Newman, J. C., Jr., "Stress Intensity Factors for Circumferential Surface Cracks in Pipes and Rods under Tension and Bending Loads," *Fracture Mechanics: Seventeenth Volume*, ASTM STP 905, J. H. Underwood, R. Chait, C. W. Smith, D. P. Wilhelm, W. A. Andrews, and J. C. Newman, Eds., American Society for Testing and Materials, Philadelphia, 1986, pp. 789-805.
- [C18] ASTM Designation: E399-83, Standard Test Method for Plane-Strain Fracture Toughness of Metallic Materials, American Society for Testing and Materials, Philadelphia.
- [C19] Dao, X. T., and Mettu, S. R., "Analysis of an Edge-Cracked Specimen Subjected to Rotationally-Constrained End Displacements," JSC Report No. 32171/LESC Report No. 29683, August 1991.
- [C20] Erdogan, F., and Kibler, J. J., "Cylindrical and Spherical Shells with Cracks," *International Journal of Fracture Mechanics*, Vol. 5, No. 3, September 1969, pp. 229-237.
- [C21] Roberts, R., and Kibler, J. J., "Some Aspects of Fatigue Crack Propagation," *Engineering Fracture Mechanics*, Vol. 2, 1971, pp. 243-260.
- [C22] Joseph, P.F. and Erdogan, F., *Journal of Applied Mechanics*, Vol. 58, Sept. 1991, pp.842-846.

- [C23] Raju, I. S., and Newman, J. C., Jr., "Stress Intensity Factors for Corner Cracks in Rectangular Bars," in *Fracture Mechanics: Nineteenth Symposium*, ASTM STP 969, T. A. Cruse, Ed., American Society for Testing and Materials, Philadelphia, 1988, pp. 43-55.
- [C24] Forman, R. G., and Mettu, S. R., "Behavior of Surface and Corner Cracks Subjected to Tensile and Bending Loads in a Ti-6Al-4V Alloy," *Fracture Mechanics: Twenty-Second Symposium (Volume I)*, ASTM STP 1131, H. A. Ernst, A. Saxena and D. L. McDowell, Eds., American Society for Testing and Materials, Philadelphia, 1992, pp. 519-546.
- [C25] Reissner, E., "The Effect of Transverse Shear Deformation on the Bending of Elastic Plates," *Journal of Applied Mechanics*, June 1945, pp. A-69-A-77.
- [C26] Mettu, S. R., and Forman, R. G., "Analysis of Circumferential Cracks in Circular Cylinders using the Weight-Function Method," *Fracture Mechanics: Twenty-Third Symposium*, ASTM STP 1189, Ravinder Chona, Ed., American Society for Testing and Materials, Philadelphia, 1993, pp. 417-440.
- [C27] Mettu, S.R., de Koning, A.U, Lof, C.J., Schra, L., McMahon, J.J., and Forman, R.G., "Stress Intensity Factor Solutions for Fasteners in NASGRO 3.0," *Structural Integrity of Fasteners: Second Volume*, ASTM STP 1391, P.M. Toor, Ed., American Society for Testing and Materials, West Conshohocken, PA, 2000, pp. 133-139.
- [C28] Forman, R. G., Mettu, S. R., and Shivakumar, V., "Fracture Mechanics Evaluation of Pressure Vessels and Pipes in Aerospace Applications," in Fatigue, Fracture, and Risk, Eds., W. H. Banford, H. Mehta, B. A. Bishop, J. H. Phillips, and F. W. Brust, ASME PVP-Vol. 241, Book No. G00676, 1992, pp. 25-36.
- [C29] Mettu, S. R., Raju, I. S., and Forman, R. G., "Stress Intensity Factors for Part-Through Surface Cracks in Hollow Cylinders," JSC Report No. 25685/LESC Report No. 30124, July 1992.
- [C30] Benthem, J. P., and Koiter, W. T., "Asymptotic Approximations to Crack Problems," in Methods of Analysis and Solutions of Crack Problems, Ed., G. C. Sih, Noordhoff International Publishing, Groningen, 1973, pp. 131-178.
- [C31] Yeh, F., Mettu, S. R., and Forman, R. G., "Stress Intensity Factors for Through Cracks from Holes in Cylinders," JSC Report No. 26428A/LESC Report No. 31068A, January 1995.
- [C32] Yeh, F., Mettu, S. R., and Forman, R. G., "Some Further Results for Through Cracks from Holes in Cylinders," JSC Report No. 26618/LESC Report No. 31213, March 1994.

- [C33] Chen, X., and Albrecht, P., "Weight Functions for Eccentric Cracks," *Fracture Mechanics: Twenty-Fourth Volume*, ASTM STP 1207, John D. Landes, Donald E. McCabe, and J.A.M. Boulet, Eds., American Society for Testing and Materials, 1994, pp. 581-614.
- [C34] Wu, X.R. and Carlsson A.J., *Weight Functions and Stress Intensity Factor Solutions*, Pergamon Press, NY, 1991.
- [C35] Newman, J.C., Jr., Wu, X.R., Venneri, S.L., and Li, C.G., "Small-Crack Effects in High Strength Aluminum Alloys," NASA Reference Publication 1309, May 1994.
- [C36] Fujimoto, W.T., "A Computerized Algorithm for Determining Stress Intensity Factor Solutions for Part-Elliptical Radial and Surface Flaws Subjected to Bi-Variant Crack Face Loading," ASTI Report JSC-1999-1, Milford, CT, April 1999.
- [C37] Fujimoto, W.T., Mettu, S.R., "A Weight Function Approach for Tracking the Growth of Surface and Radial Cracks through Residual Stress Fields or Bi-varient Stress Fields," Proceedings of the 2000 USAF Aircraft Structural Integrity Program Conference, San Antonio, Texas, Dec 2000.
- [C38] Tada, H., Paris, P.C., Irwin, G.R., *The Stress Analysis of Cracks Handbook*, 3rd edition, ASME Press.
- [C39] Xiao, L., and Mear, M.E., 1998, *FADD3D User's Manual*, Dept. of Engineering Mechanics, University of Texas at Austin.
- [C40] Li, S., Mear, M.E., and Xiao, L., 1998, "Symmetric Weak-Form Integral Equation Method for Three Dimensional Fracture Analysis," *Computer Methods in Applied Mechanics and Engineering*, **151**, 435-539.
- [C41] Glinka, G., and Shen, G., 1991, "Universal Features of Weight Functions for Cracks in Mode I," *Engineering Fracture Mechanics*, **40**, 1135-1146.
- [C42] Kiciak, A. Glinka, G., and Eman, M., 1998, "Weight Functions and Stress Intensity Factors for Corner Quarter-Elliptical Crack in Finite Thickness Plate subjected to in-Plane Loading," *Engineering Fracture Mechanics*, **60**, 221-238.
- [C43] Shen, G., and Glinka, G., 1991, "Weight Functions for a Surface Semi-Elliptical Crack in a Finite Thickness Plate," *Journal of Theoretical and Applied Fracture Mechanics*, **15**, 247-255.
- [C44] McClung, R. C., Enright, M. P., Lee, Y.-D., Huyse, L., and Fitch, S., "Efficient Fracture Design for Complex Turbine Engine Components," Paper GT-2004-53323, ASME Turbo Expo 2004, Vienna, Austria, June 2004.

- [C45] Orynyak, I.V., Borodii, M.V., and Torop, V.M., 1994, "Approximate Construction of a Weight Function for Quarter-Elliptical, Semi-Elliptical and Elliptical Cracks Subjected to Normal Stresses," *Engineering Fracture Mechanics*, **40**, pp. 143-151.
- [C46] Orynyak, I.V. and Borodii, M.V., 1995, "Point Weight Function Method Application for Semi-Elliptical Mode I Cracks," *International Journal of Fracture*, **70**, pp. 117-124.
- [C47] Kassir, M.K. and Sih, G.C., 1975, "Three-Dimensional Crack Problems," *Mechanics of Fracture*, Vol. II, G.C. Sih Ed., Noordhoff, Holland.
- [C48] Shah, R.C. and Kobayashi, A.S., 1971, "Stress Intensity Factor for an Elliptical Crack under Arbitrary Normal Loading," *Engineering Fracture Mechanics*, **3**, pp. 71-96.
- [C49] ASTM E 647, *Standard Test Method for Measurement of Fatigue Crack Growth Rates*, ASTM International.
- [C50] Swift, T., "Fracture Mechanics", Notes on Fracture Mechanics Lectures Presented at the 1998 USAF Aircraft Structural Integrity Program (ASIP) Conference, San Antonio, USA, November 1998.
- [C51] Swift, T., "Damage Tolerance in Pressurized Fuselage," 11th Plantema Memorial Lecture, 14th Symposium of the International Committee on Aeronautical Fatigue (ICAF), Ottawa, Canada, June 8-12, 1987.
- [C52] Swift, T., "Damage Tolerance Capability," *Fatigue* 1994, Vol 16, Nr 1, pp 75-94, 1994.
- [C53] Chen, D., and Schijve, J., "Bulging of fatigue cracks in a pressurized aircraft fuselage", Proc. 16th ICAF Symp., Tokyo, 22-24 May 1991.
- [C54] Cartwright, D.J., and Rooke, D.P., "Cracks in sheets having stiffeners attached by a single row of rivets," Royal Aircraft Establishment Technical Report TR-80122, UK, 1980.
- [C55] Y. Bombardier, and M. Liao, "A New Stress Intensity Factor Solution for Cracks at An Offset Fastener Hole," 51st AIAA/ASME/ASCE/AHS/ASC structures, Structural Dynamics, and Materials Conference, April 2010, Orlando, Florida.
- [C56] Y. Bombardier, M. Liao, and G. Renaud, "Modeling of Continuing Damage for Damage Tolerance Analysis," 26th ICAF Symposium, Montreal, June, 2011.
- [C57] J. Tweed, and D.P. Rooke, "The Elastic Problem for an Infinite Solid Containing a Circular Hole with a Pair of Radial Edge Cracks of Different Lengths," *International Journal of Engineering Science*, Vol. 14, No. 10, pp. 925-933.

- [C58] Y. Bombardier, G. Renaud, and M. Liao, “Stress Intensity factor Solutions for Cracks at a Hole in an Infinite Sheet,” National Research Council Canada, LTR-SMPL-2010-0117, Ottawa.
- [C59] S.A. Fawaz, and B. Andersson, “Database of Stress Intensity Factor Solutions for One Corner Cracks at a Hole.” DVD provided by Dr. Fawaz for SwRI, 2008.
- [C60] J.C. Newman, Jr, and I.S. Raju, “Stress-Intensity Factor Equations for Cracks in Three-Dimensional Finite Bodies Subjected to Tension and Bending Loads”, Chapter 9, Computational Methods in the Mechanics of Fracture, edited by S.N. Atluri, Elsevier Science Publishers B.V., 1986, p.326.
- [C61] Y.J. Guo, “Finite Width Correction and Hole Offset Correction for One Corner Crack at an Offset Hole in a Finite plate.” NASGRO internal technical report, January, 2013.
- [C62] J.A. Harter, “AFGROW Users Guide and Technical Manual”, AFGROW for Windows XP/VISTA, Version 4.0012.15, July, 2008, pp.73-75.
- [C63] R.C. Shah, “Mechanics of Crack Growth,” ASTM STP 590, pp.429-459, American Society of Testing and Materials, 1976.
- [C64] S.A. Fawaz, and B. Andersson, “Database of Stress Intensity Factor Solutions for Two Unequal Corner Cracks at a Hole.” DVD provided by Dr. Fawaz for SwRI, 2008.
- [C65] Y.J. Guo, “General Finite Width Correction for Two Unequal Corner Cracks at an Offset Hole in a Finite Plate,” NASGRO internal technical report, April, 2013.
- [C66] Y.J. Guo, “Stress Intensity Factor Solution of a Corner Crack and a Through Crack at an Offset Hole in a Finite Plate,” NASGRO internal technical report, October, 2013.
- [C67] R. A. Huls, F. P. Grooteman and R. P. G. Veul, “Stress Intensity Factor for a Center Through Crack in a Finite Width Plate subjected to a Symmetric Remote Displacement Field,” NLR-CR-2012-222, National Aerospace Laboratory, NLR, Amsterdam, The Netherlands, 2012.
- [C68] Y.D. Lee, R.C. McClung and G.G. Chell, ‘An Efficient Stress Intensity Factor Solution Scheme for Corner Cracks at Holes under Bivariant Stressing,’ Fatigue & Fracture of Engineering Materials & Structures, Vol. 31, Issue 11, November 2008, pp. 1004-1016.
- [C69] F. P. Grooteman, “Stress Intensity Factor Solution for a Quarter Elliptical Corner

Crack in a Finite Width Plate subjected to a Bivariant Remote Displacement Field,” NLR-CR-2015-202, National Aerospace Laboratory, NLR, Amsterdam, The Netherlands, 2015.

- [C70] D. P. Crooke and D. J. Cartwright, “Compendium of Stress Intensity Factors”, HMSO, London, 1976.
- [RF1] Herrmann, G. and Sosa, H., 1986, “On Bars with Cracks,” *Engineering Fracture Mechanics*, **24**, pp. 889-894.
- [RF2] Kienzler, R. and Herrmann, 1986, “An Elementary Theory of Defective Beams,” *Acta Mechanica*, **62**, pp.37-46.
- [RF3] Bažant, Z. P., 1990, “Justification and Improvement of Kienzler and Herrmann’s Estimate of Stress Intensity Factors of Cracked Beam,” *Engineering Fracture Mechanics*, **36**, pp. 523-525.
- [RF4] Dunn, M. L., Suwito, W., and Hunter, B., “Stress Intensity Factures for Cracked I-Beams,” *Engineering Fracture Mechanics*, **57**, pp. 609-615.